



THE UNIVERSITY OF QUEENSLAND  
AUSTRALIA

**Quantum effects in non-inertial frames and curved spacetimes**

Daiqin Su

M. S. (Astrophysics), University of Science and Technology of China

*A thesis submitted for the degree of Doctor of Philosophy at  
The University of Queensland in 2017  
School of Mathematics and Physics*

## **Abstract**

Quantum effects in accelerated frames and gravitational fields have been studied for decades. One of the most influential outcomes is the discovery of thermal radiation from a black hole by Hawking in 1975. Other important discoveries include the Unruh effect, dynamical Casimir effect etc.. Although these discoveries are very exciting, experimental verification of them is extremely challenging. Even in the theoretical aspect, not all the issues have been resolved, e.g., the well known black hole information paradox. Quantum information science was developed rapidly during the last thirty years. The well established concepts and tools in quantum information science have been used to explore the quantum effects in gravitational fields and relativistic frames, giving birth to a new research field named relativistic quantum information. This thesis studies quantum effects in accelerated frames and gravitational fields by exploiting the concepts and techniques in quantum information science.

The Unruh effect implies that the state of the fields confined within part of the Minkowski spacetime can appear thermal, and entanglement exists between different spacetime regions. We show that the particle number distribution of the field modes confined within a finite diamond region is also thermal in the Minkowski vacuum, an analogue to the Unruh effect; and there exists entanglement between different diamonds. The vacuum entanglement can be extracted and utilized for some quantum information protocols, e.g., quantum key distribution. Furthermore, we show that the presence of a horizon and the Unruh thermal noise has important consequences to the quantum communication protocols where one of the parties is a uniformly accelerated observer.

Interactions between uniformly accelerated objects and quantum fields are traditionally studied using perturbation theory. The quantum circuit model, a crucial tool in quantum communication and computation, can be exploited to calculate radiations from the uniformly accelerated objects non-perturbatively. By further combining field detection scheme in quantum optics, e.g., homodyne detection, the output field from the uniformly accelerated objects can be fully studied. These techniques help to study decoherence effect in non-inertial frames, which may provide important insights for the black hole information paradox.

Dynamical spacetimes generally create quantum particles. Gravitational perturbations around a black hole oscillate and decay, due to the emission of gravitational waves to spatial infinity and into the black hole. We show that they play the role as a multimode squeezer, squeezing the state of the quantum fields and creating particles.

## **Declaration by author**

This thesis is composed of my original work, and contains no material previously published or written by another person except where due reference has been made in the text. I have clearly stated the contribution by others to jointly-authored works that I have included in my thesis.

I have clearly stated the contribution of others to my thesis as a whole, including statistical assistance, survey design, data analysis, significant technical procedures, professional editorial advice, and any other original research work used or reported in my thesis. The content of my thesis is the result of work I have carried out since the commencement of my research higher degree candidature and does not include a substantial part of work that has been submitted to qualify for the award of any other degree or diploma in any university or other tertiary institution. I have clearly stated which parts of my thesis, if any, have been submitted to qualify for another award.

I acknowledge that an electronic copy of my thesis must be lodged with the University Library and, subject to the policy and procedures of The University of Queensland, the thesis be made available for research and study in accordance with the Copyright Act 1968 unless a period of embargo has been approved by the Dean of the Graduate School.

I acknowledge that copyright of all material contained in my thesis resides with the copyright holder(s) of that material. Where appropriate I have obtained copyright permission from the copyright holder to reproduce material in this thesis.

## Publications during candidature

1. Daiqin Su and Timothy C. Ralph, *Quantum communication in the presence of a horizon*, Phys. Rev. D **90**, 084022 (2014).
2. Daiqin Su and Timothy C. Ralph, *Spacetime diamonds*, Phys. Rev. D **93**, 044023 (2016).
3. \*\* C. T. Marco Ho, Daiqin Su, Robert B. Mann and Timothy C. Ralph, *Black hole field theory with a firewall in two spacetime dimensions*, Phys. Rev. D **94**, 081502(R) (2016).
4. Daiqin Su, C. T. Marco Ho, Robert B. Mann and Timothy C. Ralph, *Quantum circuit model for non-inertial objects: a uniformly accelerated mirror*, New Journal of Physics **19**, 063017 (2017).
5. Daiqin Su, C. T. Marco Ho, Robert B. Mann and Timothy C. Ralph, *Black hole squeezers*, accepted for publication in Phys. Rev. D.

The paper labelled by “\*\*” is not included in this thesis.

## Publications included in this thesis

1. Daiqin Su and Timothy C. Ralph, *Quantum communication in the presence of a horizon*, Phys. Rev. D **90**, 084022 (2014), modified and incorporated as Chapter 6.

Contributor	Statement of contribution
Daiqin Su (Candidate)	Project proposal (20%) Theoretical and numerical calculation (80%) Results analysis and interpretation (50%) Wrote the paper (80%) Edited the paper (40%)
Timothy C. Ralph (Supervisor)	Project proposal (80%) Theoretical and numerical calculation (20%) Results analysis and interpretation (50%) Wrote the paper (20%) Edited the paper (60%)

2. Daiqin Su and Timothy C. Ralph, *Spacetime diamonds*, Phys. Rev. D **93**, 044023 (2016), modified and incorporated in Chapter 5.

Contributor	Statement of contribution
Daiqin Su (Candidate)	Project proposal (15%) Theoretical and numerical calculation (80%) Results analysis and interpretation (50%) Wrote the paper (80%) Edited the paper (40%)
Timothy C. Ralph (Supervisor)	Project proposal (85%) Theoretical and numerical calculation (20%) Results analysis and interpretation (50%) Wrote the paper (20%) Edited the paper (60%)

3. Daiqin Su, C. T. Marco Ho, Robert B. Mann and Timothy C. Ralph, *Quantum circuit model for non-inertial objects: a uniformly accelerated mirror*, New Journal of Physics 19, 063017 (2017), modified and incorporated in Chapter 7.

Contributor	Statement of contribution
Daiqin Su (Candidate)	Project proposal (20%) Theoretical and numerical calculation (70%) Results analysis and interpretation (40%) Wrote the paper (60%) Edited the paper (35%)
C. T. Marco Ho (Collaborator)	Project proposal (5%) Theoretical and numerical calculation (5%) Results analysis and interpretation (5%) Wrote the paper (5%) Edited the paper (10%)
Robert B. Mann (Collaborator)	Project proposal (5%) Theoretical and numerical calculation (5%) Results analysis and interpretation (15%) Wrote the paper (15%) Edited the paper (20%)
Timothy C. Ralph (Supervisor)	Project proposal (70%) Theoretical and numerical calculation (20%) Results analysis and interpretation (40%) Wrote the paper (20%) Edited the paper (35%)

4. Daiqin Su, C. T. Marco Ho, Robert B. Mann and Timothy C. Ralph, *Black hole squeezers*, accepted for publication in Phys. Rev. D, modified and incorporated in Chapter 9.

Contributor	Statement of contribution
Daiqin Su (Candidate)	Project proposal (65%) Theoretical and numerical calculation (80%) Results analysis and interpretation (55%) Wrote the paper (70%) Edited the paper (50%)
C. T. Marco Ho (Collaborator)	Project proposal (5%) Theoretical and numerical calculation (5%) Results analysis and interpretation (5%) Wrote the paper (5%) Edited the paper (5%)
Robert B. Mann (Collaborator)	Project proposal (15%) Theoretical and numerical calculation (10%) Results analysis and interpretation (30%) Wrote the paper (20%) Edited the paper (30%)
Timothy C. Ralph (Supervisor)	Project proposal (15%) Theoretical and numerical calculation (5%) Results analysis and interpretation (10%) Wrote the paper (5%) Edited the paper (15%)

## **Contributions by others to the thesis**

*Chapter 6:* The results in the first part of this chapter have been published in [SR14] by D. Su and T. C. Ralph. The results in the second part of this chapter were contributed by D. Su, R. B. Mann and T. C. Ralph. The original idea came from R. B. Mann. I performed the research under the guidance of R. B. Mann and T. C. Ralph by fortnightly meetings and discussions.

*Chapter 8:* The results in this chapter are available online: arXiv:1705.07432. This project began from an idea by T. C. Ralph and me. I performed the research under the guidance of T. C. Ralph by weekly meetings and discussions. T. C. Ralph and I wrote the manuscript together.

## **Statement of parts of the thesis submitted to qualify for the award of another degree**

None.

## **Acknowledgements**

I would like to express my sincere gratitude to my supervisor Tim Ralph for continuously supporting me during my PhD. Tim has very good physical intuitions and more importantly he can always use simple words to explain his ideas to me. This makes our weekly discussions very stimulating and efficient. By working with Tim, I gradually realize the importance of doing independent research. Thank Tim for proof reading my thesis. I am also very grateful to Gerard Milburn for his willingness to be my associate supervisor. I would like to thank Rob Mann, such an enthusiastic and humorous man. His deep understanding and immense knowledge of physics are really impressive. He always respects my own ideas and treats me as an independent researcher, which makes me more and more confident. I also want to thank Rob for the hospitality when I visited Waterloo and of course the wonderful cottage trip.

I want to thank all members of our group for accompanying me during my PhD. Thanks for Austin's critical thinking and his sense of humour, which make our group meeting very interesting and relaxing. Thank Marco Ho for the collaborations and interesting discussions. I am so happy to share the office with Nathan Walk, Saleh Rahimi-Keshari, Kai Liu, Farid Shahandeh, Josephine Dias and Sebastian Kish. I want to express my especial thanks to Kaerin Gardner for her kindness and accommodating. Thanks for her care about my personal life and my family, and her help to deal with the annoying financial issues.

I enjoyed a wonderful and fruitful life here after working because of a group of friends from physics. They are Bixuan Fan, Changqiu Yu, Shu Zhang, Beibei Li, Yimin Yu, Xin He and Xiuwen Zhou. I agree with Shu that we are like a family. Thank them for organizing amazing outdoor activities like fishing, hiking, BBQ, photography and so on. And more importantly, thanks for sharing the cooking skills and coming to my place to enjoy foods. I think this is the main motivation for me to improve my cooking skills. Additionally, I want to thank my friends outside of physics, Mingchun Guo, Dongjie Wu and Qi Zhang. Thank them for sharing knowledge of Buddhism, experiences of playing piano and their delicious foods.

I would like to thank Jianming Yang, Yiqiu Ma, Ning Jiang, Zheng Cai, Haixing Miao and many others in the department of Astronomy in USTC for their support and

encouragement. Without their help, I could have never started my PhD and lived a completely different life. I also want to thank the members of our discussing group: Qing Chen, Xuewen Liu, Bin Cheng, Manran Zhu and Leihua Liu. It is their contributions and persistence that make the discussion lasts for so many years and I hope it will keep going. I would like to express my special appreciation and thanks to my sisters Freda Yingan Tong, Meizi Guo and Yulan Zheng for giving their hands when I was in trouble.

Last but not the least, I would like to thank my family for their continuous supports, especially my parents. I deeply appreciate my parents' respect to my own decisions and thank them for encouraging me to purchase my own career and life.

## **Keywords**

Quantum information, Quantum communication, Entanglement, Quantum circuit, Homodyne detection, Unruh effect, Hawking effect, Black hole, Gravitational waves

## **Australian and New Zealand Standard Research Classifications (ANZSRC)**

ANZSRC code: 020602, Field theory and String theory, 40%

ANZSRC code: 020603, Quantum Information, Computation and Communication, 30%

ANZSRC code: 020604, Quantum Optics, 30%

## **Fields of Research (FoR) Classification**

FoR code: 0206, Quantum Physics, 100%

# Contents

<b>List of Figures</b>	<b>xxi</b>
<b>List of Tables</b>	<b>xxvii</b>
<b>1 Introduction and Overview</b>	<b>1</b>
1.1 Quantum field theory in flat spacetime . . . . .	4
1.2 Basic concepts in quantum optics . . . . .	4
1.3 Quantum field theory in curved spacetime . . . . .	4
1.4 Spacetime diamonds . . . . .	5
1.5 Quantum communication with accelerated observers . . . . .	5
1.6 Quantum circuit model for non-inertial objects: uniformly accelerated mirror	6
1.7 Quantum circuit model for non-inertial objects: uniformly accelerated squeezer	7
1.8 Particle creation by gravitational perturbations around a Schwarzschild black hole . . . . .	7
<b>2 Introduction to Quantum Field Theory in Flat Spacetime</b>	<b>9</b>
2.1 From harmonic oscillator to atomic chain . . . . .	10
2.1.1 Harmonic oscillator . . . . .	10
2.1.2 Atomic chain model . . . . .	12
2.2 Relativistic quantum fields . . . . .	14
2.2.1 Basics of special relativity . . . . .	15
2.2.2 Hermitian massless scalar fields . . . . .	18

2.2.3	Green's functions . . . . .	20
2.3	Summary and further reading . . . . .	23
<b>3</b>	<b>Basics of Quantum Optics</b>	<b>25</b>
3.1	Quantum states of the electromagnetic field . . . . .	26
3.1.1	Localized wave packet modes . . . . .	26
3.1.2	Number states . . . . .	27
3.1.3	Coherent state . . . . .	28
3.1.4	Squeezed states . . . . .	30
3.1.5	Thermal state . . . . .	34
3.2	Basic optical elements . . . . .	35
3.2.1	Phase shifter . . . . .	36
3.2.2	Beamsplitter . . . . .	36
3.3	Homodyne detection . . . . .	36
3.3.1	Balanced homodyne detection . . . . .	36
3.3.2	Ordinary homodyne detection . . . . .	38
3.3.3	Self-homodyne detection . . . . .	39
3.4	Quantum circuit . . . . .	40
3.5	Summary and further reading . . . . .	41
<b>4</b>	<b>Introduction to Quantum Field Theory in Curved Spacetime</b>	<b>43</b>
4.1	General relativity in a nutshell . . . . .	44
4.2	Rindler space . . . . .	46
4.2.1	Uniformly accelerated observer . . . . .	46
4.2.2	Rindler coordinates . . . . .	47
4.3	Schwarzschild spacetime . . . . .	49
4.3.1	Schwarzschild metric and gravitational redshift . . . . .	49
4.3.2	Maximally extended Schwarzschild spacetime . . . . .	50
4.3.3	Penrose diagram . . . . .	53
4.4	Quantum field theory in curved spacetime . . . . .	53
4.5	Quantum fields in Rindler space . . . . .	58

4.5.1	Rindler modes . . . . .	58
4.5.2	Bogoliubov transformation . . . . .	60
4.5.3	Unruh temperature . . . . .	62
4.5.4	Unruh modes . . . . .	63
4.5.5	Minkowski vacuum as an entangled state . . . . .	66
4.5.6	Unruh-DeWitt detector . . . . .	67
4.6	Quantum fields in Schwarzschild spacetime . . . . .	70
4.6.1	Particle creation from a collapsing star . . . . .	70
4.6.2	Eternal black hole . . . . .	74
4.6.3	Black hole information paradox . . . . .	79
4.7	Summary and further reading . . . . .	80
<b>5</b>	<b>Spacetime Diamonds</b>	<b>81</b>
5.1	Introduction . . . . .	81
5.2	Time-like entanglement . . . . .	83
5.3	Diamond coordinates . . . . .	84
5.4	Thermal radiation . . . . .	88
5.5	Detector response . . . . .	90
5.6	Correlations between different diamonds . . . . .	91
5.7	Summary . . . . .	97
5.8	Appendix . . . . .	98
<b>6</b>	<b>Quantum Communication with Uniformly Accelerated Observers</b>	<b>101</b>
6.1	Introduction . . . . .	101
6.2	Quantum communication between an inertial observer and a uniformly accelerated observer . . . . .	102
6.2.1	Homodyne Detection in an accelerated frame . . . . .	103
6.2.2	Horizon-straddling case . . . . .	110
6.3	Quantum communication between two accelerated observers . . . . .	116
6.3.1	Bogoliubov transformations between Unruh modes . . . . .	118
6.3.2	Bogoliubov transformations between Rindler modes . . . . .	121

6.3.3	Quantum communication protocols . . . . .	124
6.4	Summary . . . . .	129
<b>7</b>	<b>Quantum Circuit Model for Non-inertial Objects: Accelerated Mirror</b>	<b>131</b>
7.1	Introduction . . . . .	131
7.2	Circuit model . . . . .	134
7.2.1	Relations between Rindler modes and Unruh modes . . . . .	134
7.2.2	General circuit for time independent interactions . . . . .	134
7.2.3	Circuit model for a uniformly accelerated mirror . . . . .	138
7.3	Radiation from an eternally accelerated mirror . . . . .	141
7.3.1	Particle number flux . . . . .	141
7.3.2	Total energy flux . . . . .	145
7.4	Squeezing from accelerated mirrors . . . . .	147
7.4.1	Narrow bandwidth detector mode . . . . .	148
7.4.2	Broad bandwidth detector mode . . . . .	150
7.4.3	Ratio of single-mode squeezing . . . . .	152
7.4.4	Origin of single-mode squeezing . . . . .	153
7.5	Squeezed Firewall ? . . . . .	154
7.6	Summary . . . . .	155
<b>8</b>	<b>Quantum Circuit Model for Non-inertial Objects: Accelerated Squeezer</b>	<b>159</b>
8.1	Introduction . . . . .	159
8.2	Accelerated objects acting on narrow bandwidth modes . . . . .	161
8.2.1	Circuit for a single narrow bandwidth mode . . . . .	161
8.2.2	Uniformly accelerated mirror . . . . .	163
8.3	Accelerated objects acting on arbitrary single mode . . . . .	170
8.3.1	Accelerated displacement . . . . .	172
8.3.2	Accelerated phase shifter . . . . .	173
8.3.3	Accelerated single-mode squeezer . . . . .	174
8.4	Decoherence in non-inertial frames . . . . .	175
8.4.1	Detection of the state . . . . .	176

8.4.2	Accelerated self-homodyne detection . . . . .	178
8.4.3	Classical signals . . . . .	180
8.4.4	Quantum signals . . . . .	181
8.4.5	Connetion to black hole information paradox . . . . .	186
8.5	Summary . . . . .	187
<b>9</b>	<b>Particle Creation from Gravitational Perturbations Around Schwarzschild</b>	
	<b>Black Holes</b>	<b>189</b>
9.1	Introduction . . . . .	189
9.2	Scalar field in curved spacetimes . . . . .	191
9.3	Gravitational quasi-normal modes . . . . .	194
9.4	Coupling between scalar field and odd-parity QNMs . . . . .	198
9.4.1	Interaction Hamiltonian from odd-parity QNMs . . . . .	199
9.4.2	Radial integral . . . . .	201
9.4.3	Angular integral . . . . .	206
9.5	QNM as multimode squeezer . . . . .	208
9.6	Coupling between scalar field and even-parity QNMs . . . . .	213
9.7	Summary . . . . .	216
9.8	Appendix . . . . .	218
9.8.1	Appendix A: Radial integrals $\mathcal{I}_{r2}$ , $\mathcal{I}_{r3}$ and $\mathcal{I}_{r4}$ . . . . .	218
9.8.2	Appendix B: Spin-weighted spherical harmonics . . . . .	221
9.8.3	Appendix C: Integrals of the products of three Legendre Functions . . . . .	222
<b>10</b>	<b>Conclusion and Future Outlook</b>	<b>225</b>
10.1	Summary . . . . .	225
10.1.1	Spacetime diamonds . . . . .	225
10.1.2	Quantum communication with accelerated observers . . . . .	226
10.1.3	Quantum circuit model for uniformly accelerated objects . . . . .	226
10.1.4	Squeezed black holes . . . . .	227
10.2	Future work and outlook . . . . .	228
10.2.1	Spacetime diamonds . . . . .	228

10.2.2 Quantum communication with accelerated observers . . . . .	228
10.2.3 Quantum circuit model for uniformly accelerated objects . . . . .	229
10.2.4 Squeezed black holes . . . . .	229

<b>References</b>	<b>231</b>
-------------------	------------

# List of Figures

2.1	(a) A classical harmonic oscillator: a mass confined in a parabolic potential. (b) A quantum harmonic oscillator. The energy level is discrete and the lowest energy $E_0$ is not zero, known as the ground state energy. Jumping between different energy levels is described by the lowering and raising operators. . . . .	11
2.2	One dimensional atomic chain. . . . .	12
2.3	Relation between the principle of Invariant Light Speed and the time dilation, length contraction, relativity of simultaneity. . . . .	16
3.1	Phase space representation of a coherent state with amplitude $\alpha =  \alpha e^{i\theta}$ . For comparison, the vacuum state is also plotted. The vacuum state is centred on the origin and its noise is normalized to one. The coherent state $ \alpha\rangle$ is shifted $2 \alpha $ in the direction $\theta$ and its fluctuation is the same as the vacuum state. . . . .	30
3.2	Phase space representation of a single-mode squeezed vacuum state. The dotted circle represents the vacuum shot noise. . . . .	32
3.3	Phase space representation of an EPR state. The dotted circle represents the vacuum shot noise. (a) and (b) show that the uncertainties of the signal and idler mode are greater than the vacuum shot noise. (c) and (d) show that the correlation and anti-correlation operators are squeezed. The former is squeezed in the quadrature phase $\phi = \frac{\pi}{2}$ and the latter in $\phi = 0$ . . . . .	35
3.4	Schematic diagram of a beamsplitter. . . . .	37
3.5	Schematic diagram of homodyne detection. . . . .	38
3.6	Single-mode quantum gates. . . . .	41

3.7	Two-mode quantum gates. . . . .	41
3.8	An example of a quantum circuit. . . . .	41
4.1	A uniformly accelerated observer Rob follows a hyperbolic worldline, which is confined within the right Rindler wedge formed by the past and future horizon. . . . .	47
4.2	Rindler coordinate system. The whole Minkowski spacetime is divided into four wedges by the past and future horizons: right Rindler wedge (R), left Rindler wedge (L), future wedge (F) and past wedge (P). In the right Rindler wedge, the coordinates are $(\tau, \xi, y, z)$ ; in the left Rindler wedge, the coordinates are $(\bar{\tau}, \bar{\xi}, y, z)$ . . . . .	48
4.3	Kruskal diagram. . . . .	52
4.4	Penrose diagram of the maximally extended Schwarzschild spacetime. . . . .	54
4.5	Integration contour in the complex $V$ plane. . . . .	61
4.6	Penrose diagram of a collapsing star. . . . .	72
4.7	Upcoming and ingoing modes in the maximally extended Schwarzschild spacetime. . . .	77
5.1	Pauli-Jordan function for a massless scalar field in $(1 + 3)$ -dimensional Minkowski spacetime (the three spatial dimensions have been compacted to one). The Pauli-Jordan function is nonzero only on the light cone. . . . .	84
5.2	Schematic diagram of the mapping of left-moving modes in $(1 + 1)$ -dimensional Minkowski spacetime between the past and left Rindler wedges, the future and right Rindler wedges. The detectors $D_3$ and $D_4$ can extract the same entanglement as that extracted by the detectors $D_1$ and $D_2$ . . . . .	85
5.3	Conformal mapping in $(1 + 1)$ -dimensional spacetime: $V' = (1 + V)/(1 - V)$ , $U' = -(1 - U)/(1 + U)$ . A diamond in Minkowski coordinates $(t, x)$ , $ t  +  x  \leq 1$ , is mapped to the right Rindler wedge in the conformal coordinates $(t', x')$ . The regions outside the diamond in Minkowski coordinates $(t, x)$ are together mapped to form the left Rindler wedge in the conformal coordinates $(t', x')$ . . . . .	86
5.4	Diamonds in $(1 + 1)$ -dimensional Minkowski spacetime. Only a chain of diamonds along the $t$ axis is plotted and they are labeled by integers $n = 0, \pm 1, \dots$ . The size of these diamonds are the same, $2/a$ . . . . .	87

5.5 Entanglement between Gaussian modes in the first and zeroth diamond. Left: quadrature phase  $\phi = 0$ , right: quadrature phase  $\phi = 0.2\pi$ . The central frequency of the Gaussian mode in the zeroth diamond is set to be  $\omega_0/a = 1.0$ , the bandwidth and central position are the same,  $\sigma_1/a = \sigma_0/a = 0.02$ ,  $av_1 = av_0 = 0$ . (a) For  $\phi = 0$ , the variances of  $\hat{X}_-^{10}(0)$  and  $\hat{X}_+^{10}(\pi/2)$  are approximately the same and have a minimum which is smaller than 1 when the central frequency  $\omega_1/a = 1$ , while the variances of  $\hat{X}_+^{10}(0)$  and  $\hat{X}_-^{10}(\pi/2)$  have a maximum which is larger than 1 at  $\omega_1/a = 1$ . (b) For  $\phi = 0.2\pi$ , the minimum variance of  $\hat{X}_-^{10}(0.2\pi)$  is also smaller than one, however the corresponding central frequency of the Gaussian wave packet mode in the first diamond is  $\omega_1/a < 1$ . The maximum variance of  $\hat{X}_+^{10}(0.2\pi)$  is greater than one and the corresponding central frequency of the Gaussian wave packet mode in the first diamond is  $\omega_1/a < 1$ . . . . . 95

6.1 Alice (static) sends Rob (accelerated) a Gaussian wave packet which straddles Rob's future horizon. . . . . 103

6.2 Strength of local oscillator for various low frequency cutoffs:  $\Omega_{\text{cut}} = 0.00001$  (top), 0.001 (middle), 0.1 (bottom),  $\delta = \frac{k_\omega}{\sigma} = 10$ . . . . . 111

6.3 Normalized variance for various low frequency cutoffs:  $\Omega_{\text{cut}} = 0.01$  (top), 0.05 (middle), 0.1 (bottom),  $\delta = \frac{k_\omega}{\sigma} = 10$ . . . . . 112

6.4 Signal to noise ratio versus low frequency cutoff for  $k_\omega U_o = n\pi$ ,  $\delta = \frac{k_\omega}{\sigma} = 10$ . The signal to noise ratio decreases when the low frequency cutoff become smaller and larger. The low frequency cutoff that maximizes the signal to noise ratio is between 0.1 and 0.2. . . . . 113

6.5 Signal to noise ratio versus low frequency cutoff for  $k_\omega U_o = (\frac{1}{2} + n)\pi$ ,  $\delta = \frac{k_\omega}{\sigma} = 10$ . The signal to noise ratio first increases and then tends to be a constant when the low frequency cutoff becomes smaller. . . . . 114

6.6 Conditional variance versus low frequency cutoff,  $\delta = \frac{k_\omega}{\sigma} = 10$ . . . . . 116

6.7 Two sets of Rindler observers. World lines of the second set of Rindler observers (red) can be obtained by shifting the world lines of the first set (black). Observer  $O_1$  and  $O_2$  (black) are causally disconnected, as well as  $O_3$  and  $O_4$  (red). While  $O_2$  and  $O_3$ ,  $O_2$  and  $O_4$  are causally connected. . . . . 117

6.8	Strength of local oscillator in the case where an accelerated observer communicates with another accelerated observer. Three low frequency cutoffs are plotted: $\Omega_{\text{cut}} = 0.00001$ (top), 0.001(middle), 0.1(bottom), $\delta = \frac{k_o}{\sigma} = 10$ . . . . .	128
6.9	Normalized variance in the case where an accelerated observer communicates with another accelerated observer. Three low frequency cutoffs are plotted: $\Omega_{\text{cut}} = 0.01$ (top), 0.05(middle), 0.1(bottom), $\delta = \frac{k_o}{\sigma} = 10$ . . . . .	128
7.1	(a) Two-mode squeezer: Unruh modes to Rindler modes. (b) Two-mode antisqueezer: Rindler modes to Unruh modes. . . . .	135
7.2	Unruh modes pass through the squeezers and then become Rindler modes. The Rindler modes in the right Rindler wedge interact with the object ( $U_\omega$ ) and then combine with the Rindler modes from the left Rindler wedge in the antisqueezers, going back to Unruh modes again. . . . .	136
7.3	A uniformly accelerated mirror on the right Rindler wedge. An inertial detector is placed at an appropriate position to detect left-moving particles coming from the uniformly accelerated mirror. . . . .	141
7.4	Particle number versus central position of the Gaussian wave packet: $k_0/a = 20, ag = 10$ . For larger bandwidth (narrower wave packet in time domain), the particle number distribution is narrower, showing that particles are localized around the past event horizon. . . . .	144
7.5	Energy of the wave packets versus the central frequency: $\sigma/a = 1.0, aV_0 = 0, ag = 10$ . The energy is almost constant in the high central frequency limit. . . . .	145
7.6	Minimum variance versus central position of the Gaussian wave packet: $k_0/a = 20, ag = 10$ . Maximum squeezing is achieved when the wave packet centres on the past horizon $V_0 = 0$ . The squeezing is stronger for larger bandwidth wave packets. . . . .	150
7.7	Minimum variance of broad bandwidth wave packet modes (Eq. (7.4.9)) centred on the past horizon: $k_0/a = 20, ag = 10$ . Stronger squeezing is achieved for larger bandwidth wave packet mode. . . . .	152
7.8	Portion of particle number from single-mode squeezing for broad bandwidth wave packet modes (Eq. (7.4.9)) centering on the past horizon: $k_0/a = 20, ag = 10$ . . . . .	153
8.1	Quantum circuit for a narrow bandwidth wave packet mode. . . . .	162

8.2	Particle number versus central position of the detector mode. Central frequency of the detector mode is $k_0/a = 20$ . Parameters for the wave packet $g(\omega)$ are $\omega_0/a = 8.0, \delta/a = 0.2, aV_c = 1.0$ , and $\theta$ is chosen to be $\theta = \pi/2$ . . . . .	168
8.3	Minimal quadrature variance versus central position of the detector mode. Central frequency of the detector mode is $k_0/a = 20$ . Parameters for the wave packet $g(\omega)$ are $\omega_0/a = 8.0, \delta/a = 0.2, aV_c = 1.0$ , and $\theta$ is chosen to be $\theta = \pi/2$ . . . . .	168
8.4	Energy of the fields versus central frequency of the detector mode. Bandwidth of the detector mode is $\sigma/a = 1.0$ . Parameters for the wave packet $g(\omega)$ are $\omega_0/a = 8.0, \delta/a = 0.2, aV_c = 1.0$ , and $\theta$ is chosen to be $\theta = \pi/2$ . . . . .	169
8.5	Circuit for a uniformly accelerated object. Rindler modes in the right Rindler wedge interact with the object, which is represented by the unitary operator $\hat{U}_g$ , while Rindler modes in the left Rindler wedge remain unaffected. The time dependent interactions mix different frequency Rindler modes. . . . .	171
8.6	Penrose diagram of Minkowski spacetime. $I^0$ is the spatial infinity, $I^-$ and $I^+$ are the past and future infinities, $\mathcal{I}^-$ and $\mathcal{I}^+$ are the past and future null infinities. A uniformly accelerated object follows the black worldline. Interactions between the accelerated object and the field are localized in Rindler time, represented by the shaded region. . . . .	177
8.7	Self-homodyne detection. (a) A signal unitary $\hat{S}_g$ generates quantum signals that we are going to analyze. (b) A displacement is added after the signal unitary $\hat{S}_g$ to realize homodyne detection. The mode shape of the displacement is perfectly matched to that of the signal unitary. . . . .	180
8.8	Product of maximum and minimum quadrature variances. . . . .	184
8.9	Phase space representation of quadrature in the final state. The red dashed circle represents the vacuum shot noise, and the blue shaded ellipse represents the quadrature variance of the output state. For fixed single-mode squeezing factor ( $r = 0.5$ ), the minimum quadrature variance is below the vacuum shot noise for small $\mathcal{I}_c$ , indicating the output state is a squeezed state. While for large enough $\mathcal{I}_c$ , the minimum quadrature variance surpasses the vacuum shot noise, showing that squeezing is destroyed. . . . .	185

8.10	Distribution of minimum quadrature variance of the output state as a function of single-mode squeezing factor $r$ and the central frequency $\omega_0$ in the narrow bandwidth limit. A critical curve along which $V_{\min} = 1.0$ separates the squeezing region and no squeezing region. In the squeezing region $V_{\min} < 1.0$ , while in the no squeezing region $V_{\min} > 1.0$ . . . . .	186
9.1	The contour $C$ and branch cut for $\omega_R - \omega - \omega' > 0$ . The two shaded regions are referred to as <i>in</i> (close to the horizon) and <i>out</i> (around $r = \infty$ ) regions, respectively. . . . .	203
9.2	The effective potential for scalar field modes. . . . .	210
9.3	Reflection coefficient for the scalar field modes. . . . .	210
9.4	Modulus of the joint frequency distribution. QNM: $\Omega_R = 0.7474, \Omega_I = 0.178, (l_0, m_0) = (2, 0)$ . Scalar particle one: $(l, m) = (1, 1)$ ; scalar particle two: $(l', m') = (2, -1)$ . . . . .	212
9.5	Density plot of the modulus of the joint frequency distribution. QNM: $\Omega_R = 0.7474, \Omega_I = 0.178, (l_0, m_0) = (2, 0)$ . Scalar particle one: $(l, m) = (1, 1)$ ; scalar particle two: $(l', m') = (2, -1)$ . . . . .	212
9.6	Modulus of the joint frequency distribution for even-parity QNMs. QNM: $\Omega_R = 0.7474, \Omega_I = 0.178, (l_0, m_0) = (2, 0)$ . Scalar particle one: $(l, m) = (1, 1)$ ; scalar particle two: $(l', m') = (3, -1)$ . . . . .	216
9.7	Density plot of the modulus of the joint frequency distribution for even-parity QNMs. QNM: $\Omega_R = 0.7474, \Omega_I = 0.178, (l_0, m_0) = (2, 0)$ . Scalar particle one: $(l, m) = (1, 1)$ ; scalar particle two: $(l', m') = (3, -1)$ . . . . .	217

# List of Tables

4.1	Signs of null coordinates $U$ and $V$ in four regions. Regions I and II are described by the original Schwarzschild coordinates, regions III and IV are the Kruskal extension. . . . .	52
4.2	Meaning of symbols in the Penrose diagram. . . . .	54
9.1	Nonzero $\mathcal{I}_{a4}$ and $\mathcal{I}_{a5}$ for a QNM $(l_0, m_0) = (2, 0)$ and a pair of scalar particles: $(l, m) = (1, 1)$ and $(l', -1)$ . . . . .	215



# 1

## Introduction and Overview

Quantum effects in curved spacetimes have been studied for decades and important progresses have been made. These studies deepen our understanding of both gravity and quantum mechanics. The most important new effects include the Hawking effect [Haw75], Unruh effect [Unr76, Dav75], dynamical Casimir effect [Moo70] and particle creation from an expanding universe [Par68]. However, these effects are very small and are extremely difficult to observe directly. Particle creation by the expanding universe can be observed from astronomical data. In the very early universe, the exponentially expanding universe amplified the quantum fluctuations of curvature and produced curvature perturbations (scalar perturbations and/or gravitational waves), which are subsequently responsible for the anisotropies in the cosmic microwave background (CMB) and the formation of large scale structures. The dynamical Casimir effect was observed in a superconducting circuit recently [WJP<sup>+</sup>11], forty years after its theoretical prediction. The Hawking effect was discovered by Hawking in

1975, which states that a black hole is not ‘black’ but instead emits thermal radiation with temperature proportional to the surface gravity of the black hole. It can be estimated that the Hawking temperature for a solar mass black hole is about  $10^{-8}$  K, which is much lower than the temperature of the CMB ( $\sim 2.7$  K). If there exist primordial black holes with very small mass [CH74], it may be possible to detect Hawking radiation from them. Recently, Hawking radiation in some analogue systems were observed [Ste16], however they are not the true Hawking radiation from a real black hole. Following Hawking’s discovery, Unruh and Davies found that even in flat spacetime, a uniformly accelerated observer experiences a thermal bath with temperature proportional to their proper acceleration. Many attempts have been tried to detect the Unruh effect by electrons in particle detectors [BL83] and penning traps [Rog88], atoms in microwave cavities [SKB<sup>+</sup>03, BKC<sup>+</sup>06] and by ultraintense lasers [CT99, SSH06]. However, the Unruh temperature is so low that it is extremely difficult to detect it. In order to observe Unruh-Davies radiation with 1 K, one needs acceleration about  $10^{20} m/s^2$ , far beyond current technologies in the lab.

In the theoretical aspect, although much progress has been made, some serious issues also arise. The most well known one is the black hole information paradox [Haw76]. As the black hole radiates Hawking particles, its mass gradually decreases. After a sufficiently long time, the black hole may completely evaporate. Since the Hawking radiation is thermal, the complete evaporation of a black hole ends up with a thermal cloud of particles. This results in a non-unitary evolution: a pure initial state (usually a vacuum) evolves into a mixed final state. If this is true, unitary evolution of an isolated system in quantum mechanics is violated and information is lost. In spite of many attempts [STU93, StHW94, Mat05, HPS16, BMT], a completely satisfactory resolution of this issue has not been found.

Quantum information science was developed rapidly during the last thirty years [BB84, Eke91, BW92, BBC<sup>+</sup>93, Sho94, Sho95, Sch95, SW97, Hol98, Llo97], where the importance of concepts like entanglement is emphasized. A modern version of the black hole information paradox is not only concerned with destroying the purity of the state but also destroying the entanglement [HP07]. Quantum information theory thus can provide intuitions and tools

that help to sharpen our understanding of the black hole information paradox. In a broader perspective, quantum information science can also help us to understand other effects in relativistic quantum field theory. The Unruh effect can be understood in this way: the fields in the right Rindler wedge perfectly entangle with that in the left Rindler wedge such that the overall state is pure (vacuum), whilst uniformly accelerated observers restricted to one of the Rindler wedges see a thermal state. This reveals an important fact that the Minkowski vacuum is an entangled state [Unr76, SW85b, SW87]. A large amount of work has been devoted to study whether it is possible to extract the vacuum entanglement in Minkowski spacetime [RRS05, LH10, OR11, SMM15], curved background spacetime [SM09, MMM12], circuit QED [SPdRMM12] and in ion trap systems [RCR05], and utilize it for quantum information science [RW15], e.g., quantum communication. On the other hand, the uniform motion and the acceleration of the observer, as well as the presence of gravity, would have crucial influences to the entanglement [AM03, FSM05, AFSMT06, Dat09, BFSS06, MMGL10, FMMMM10]. Examples like quantum teleportation [AM03, PJ08, FLT<sup>+</sup>13], quantum key distribution [DRW13] in the accelerated frame and gravitational fields have been explored. Quantum metrology [GLM04, GLM06], an important tool in the precise quantum limited measurement, were generalized to relativistic situations [AAF10, MBF14, ABS<sup>+</sup>14, BDU<sup>+</sup>14] where it can be utilized to measure the Unruh temperature [AAF10], parameters of gravitational fields [KR16] etc..

In this thesis, we are going to utilize concepts and tools in quantum information and quantum optics to explore quantum effects in accelerated frames, as well as in the presence of gravity. We try to understand the vacuum entanglement and its potential applications in quantum information science, to study how acceleration and gravity affects quantum communication, to explore decoherence of radiation from a uniformly accelerated quantum source and its possible relation to the black hole information paradox, and to investigate particle creation by gravitational perturbations around a black hole. The main contents of this thesis are summarized in the following.

## 1.1 Quantum field theory in flat spacetime

In Chapter 2, we briefly introduce basic concepts and tools of quantum field theory in flat spacetime. We start from the quantum theory of a simple harmonic oscillator, and then move to discuss a discrete atomic chain, which gives us an intuition of the global properties of quanta, vacuum state *etc.*. In the continuum limit, by taking into account special relativity, we arrive at the standard relativistic quantum field theory in flat spacetime. Without introducing complicated mathematics but being adequate to capture the essential physics, we mainly discuss free scalar fields, in particular, the free massless scalar fields. Important concepts like particles, vacuum state, and Wightman functions are introduced.

## 1.2 Basic concepts in quantum optics

In Chapter 3, we introduce some basic concepts in quantum optics and continuous variable quantum information. The first concept to introduce is the coherent state, which is a good approximation to the light fields coming from a laser. We then discuss various squeezed states, including single-mode, two-mode and multimode squeezed states. The squeezed states are non-classical, containing entanglement which is very useful in quantum communication, e.g., quantum key distribution. Finally, we consider an important field detection model, the homodyne detection. Quantum optics is not a fully relativistic theory because although the electromagnetic field is relativistic, the description of atoms is non-relativistic. However, tools in quantum optics are adequate and useful to study the response of detectors in inertial frame, accelerated frame and even in curved spacetime to the quantum fields.

## 1.3 Quantum field theory in curved spacetime

In Chapter 4, we generalize the quantum field theory in flat spacetime to the curved background spacetime. When considering quantum field theory in curved spacetime or accelerated frame, the concept of particles, as well as the vacuum state of the field, are not unique and are observer dependent. We first formulate a general framework to quantize the fields in

various inequivalent ways and derive the relations between different quantizations. As one of the most important topics of this thesis, we discuss quantum fields in uniformly accelerated frame, and the well known Unruh effect which states that a uniformly accelerated observer experiences a thermal radiation in the Minkowski vacuum with temperature proportional to their acceleration. Another important topic is the thermal radiation from a static, spherically symmetric Schwarzschild black hole, discovered by Hawking forty years ago and named Hawking radiation. The temperature of the Hawking radiation is proportional to the surface gravity of the Schwarzschild black hole. At the end of this chapter we briefly introduce the black hole information paradox.

## 1.4 Spacetime diamonds

The original research in this thesis begins in Chapter 5. In Chapter 5, we study the quantization of a massless scalar field inside a spacetime diamond in Minkowski spacetime. We show that particle number distribution of the diamond modes is thermal in the Minkowski vacuum state. The temperature of the thermal radiation, named diamond temperature, is inversely proportional to the size of the spacetime diamond. We then propose that a two-level Unruh-deWitt detector with energy scaled in a particular way can detect the thermal radiation. Finally, we show that the fields inside different diamonds are entangled.

## 1.5 Quantum communication with accelerated observers

In Chapter 6, we study quantum communication with a uniformly accelerated observer. The standard quantum communication is between two inertial observers Alice and Bob. When one of the observers uniformly accelerates, the quantum communication is affected because of the presence of Unruh thermal noise as well as the event horizon for the accelerated observer. We first consider a protocol where an inertial observer Alice sends a coherent state signal and a local oscillator to a uniformly accelerated observer Rob, who then performs homodyne detection in his own reference frame. We then consider quantum communication between two uniformly accelerated observers: a uniformly accelerated observer sends a coherent state

signal and a local oscillator to another uniformly accelerated observer, who then performs homodyne detection.

## 1.6 Quantum circuit model for non-inertial objects: uniformly accelerated mirror

In Chapter 7, we propose a quantum circuit model to study the interactions between a uniformly accelerated object with the quantum fields. The idea is based on the transformation between the Rindler modes and Unruh modes, which are basically a two-mode squeezing transformation. A uniformly accelerated object is stationary in its own reference frame, so its interactions with the Rindler modes are easy to deal with. We thus start from the inertial frame where the initial state is imposed, usually the Minkowski vacuum; then go to the Rindler frame where the accelerated object couples with the Rindler modes in the corresponding Rindler wedge, leaving the Rindler modes in the other Rindler wedge unchanged; after that we go back to the inertial frame because an inertial detector is used to detect the fields radiated by the accelerated object. The Unruh modes are used as a stepping stone between the accelerated and inertial frames. Finally, in order to model the response of an inertial detector, we transform the Unruh modes to the Minkowski modes.

As the first application of the circuit model, we study an eternally accelerated mirror. We find that a pulse of particles along the horizon is radiated by the mirror and the radiation field is squeezed. The squeezing of the field is related to the fact that the mirror plays a role as a scissor and cuts the correlations across the horizon. The issue for the eternally accelerated mirror is that the total energy of the radiation field is divergent. This divergence problem can be resolved by turning on and off the interactions between the mirror and the fields.

## 1.7 Quantum circuit model for non-inertial objects: uniformly accelerated squeezer

In Chapter 8, we realized the turning on and off the interactions by making the accelerated objects only act on a localised wave packet modes. This resolves the energy divergence problem. As further applications of the circuit model, we focus on a uniformly accelerated single-mode squeezer. Unexpectedly, we find that the output state, as detected by inertial observers, from a uniformly accelerated single-mode squeezer is mixed, even if the input state is pure. The decoherence effect we find is a previously unnoticed consequence of the transformation from the bipartite Hilbert space of the Rindler and Unruh modes, to the single Hilbert space of the Minkowski modes. This unexpected result may indicate new directions in resolving inconsistencies between relativity and quantum theory.

## 1.8 Particle creation by gravitational perturbations around a Schwarzschild black hole

In Chapter 9, we consider particle creation by gravitational perturbations around a Schwarzschild black hole. Quantum particle generation is a general phenomenon in a dynamical spacetimes, e.g., the exponentially expanding universe. However, it was shown that plane gravitational waves can not create particles, analogous to the plane electromagnetic waves case, due to the violation of momentum conservation. It is interesting to see whether this is also true in the black hole background spacetimes. We study the interaction between a massless scalar field and the gravitational quasi-normal modes of a Schwarzschild black hole, and show that scalar particles can be created. The gravitational quasi-normal modes play the role as a multimode squeezer and squeeze any state of the scalar field.



# 2

## Introduction to Quantum Field Theory in Flat Spacetime

In this chapter, we review the fundamental concepts and tools of quantum field theory (QFT) in Minkowski spacetime. For simplicity, we will mainly discuss a massless free scalar field. We will try to develop the QFT step by step from the quantum theory of a simple harmonic oscillator.

## 2.1 From harmonic oscillator to atomic chain

### 2.1.1 Harmonic oscillator

We start from a quantum harmonic oscillator in order to introduce some basic concepts in quantum mechanics, which are very important in quantum field theory. A classical harmonic oscillator is a mass which is tied to a spring and oscillates with a particular frequency  $\omega$ . There are many other models, for example, it can also be considered as a mass confined in a parabolic potential, as shown in Fig. 2.1(a). The total energy of a classical harmonic oscillator is continuous and could be any nonnegative value. The dynamics of a quantum harmonic oscillator is completely different. The Schrödinger equation, instead of the Newtonian equation, needs to be solved with the Hamiltonian [Sak85]

$$\hat{H} = \frac{1}{2}\hat{p}^2 + \frac{1}{2}\omega^2\hat{x}^2, \quad (2.1.1)$$

where we consider an oscillator with unit mass and  $\omega$  is its frequency.  $\hat{x}$  and  $\hat{p}$  are the position and momentum operators, satisfying the commutation relation

$$[\hat{x}, \hat{p}] = i\hbar, \quad (2.1.2)$$

where  $\hbar$  is the reduced Planck constant. After solving the Schrödinger equation one finds that the energy of the quantum harmonic oscillator is discrete, as shown by Fig. 2.1(b), a striking feature that differentiates it from a classical one. The energy eigenvalue of the quantum harmonic oscillator is

$$E_n = \left(n + \frac{1}{2}\right)\hbar\omega, \quad n = 0, 1, 2, \dots \quad (2.1.3)$$

and the corresponding eigenstate is denoted by  $|n\rangle$ . Another important feature is that the energy of the lowest energy state, named ground state, is nonzero,  $E_0 = \hbar\omega/2$ , which means the oscillator cannot be static at the bottom of the potential. This is due to Heisenberg's uncertainty principle,

$$\Delta x \Delta p \geq \frac{\hbar}{2}, \quad (2.1.4)$$

where

$$\begin{aligned} (\Delta x)^2 &= \langle \psi | \hat{x}^2 | \psi \rangle - \langle \psi | \hat{x} | \psi \rangle^2, \\ (\Delta p)^2 &= \langle \psi | \hat{p}^2 | \psi \rangle - \langle \psi | \hat{p} | \psi \rangle^2 \end{aligned} \quad (2.1.5)$$

are the variances of the position and momentum operators for an arbitrary quantum state  $|\psi\rangle$ . For the ground state  $|0\rangle$ , the minimum uncertainty relation is satisfied,  $\Delta x \Delta p = \hbar/2$ .

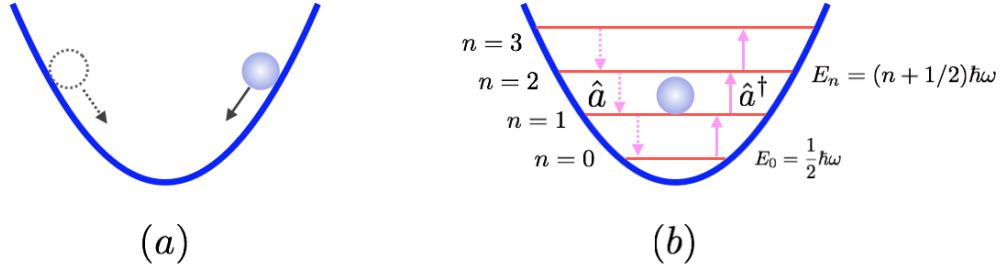


FIGURE 2.1: (a) A classical harmonic oscillator: a mass confined in a parabolic potential. (b) A quantum harmonic oscillator. The energy level is discrete and the lowest energy  $E_0$  is not zero, known as the ground state energy. Jumping between different energy levels is described by the lowering and raising operators.

There exists an algebraic method to describe the quantum harmonic oscillator [Sak85]. Introducing operators

$$\hat{a} = \frac{1}{\sqrt{2\hbar\omega}}(\omega\hat{x} + i\hat{p}), \quad \hat{a}^\dagger = \frac{1}{\sqrt{2\hbar\omega}}(\omega\hat{x} - i\hat{p}) \quad (2.1.6)$$

which satisfy commutation relation

$$[\hat{a}, \hat{a}^\dagger] = 1, \quad (2.1.7)$$

the Hamiltonian Eq. (2.1.1) becomes

$$\hat{H} = \left(\hat{a}^\dagger\hat{a} + \frac{1}{2}\right)\hbar\omega \equiv \left(\hat{N} + \frac{1}{2}\right)\hbar\omega, \quad (2.1.8)$$

where  $\hat{N} = \hat{a}^\dagger\hat{a}$  is the number operator and satisfies  $\hat{N}|n\rangle = n|n\rangle$ . It can be shown that

$$\hat{a}^\dagger|n-1\rangle = \sqrt{n}|n\rangle, \quad \hat{a}|n\rangle = \sqrt{n}|n-1\rangle, \quad n \geq 1. \quad (2.1.9)$$

Therefore the  $\hat{a}^\dagger$  is called raising operator and  $\hat{a}$  is called lowering operator. The action of the raising and lowering operators is pictorially shown in Fig. 2.1(b). In particular, the lowering operator  $\hat{a}$  annihilates the ground state,

$$\hat{a}|0\rangle = 0. \quad (2.1.10)$$

In the following we will consider this as the definition of a ground state (vacuum state).

### 2.1.2 Atomic chain model

We are now going to consider an one-dimension atomic chain model. The chain consists of  $N$  unit mass atoms which are connected by springs with spring constant  $k_s$ , as shown in Fig. 2.2. The distance between neighbouring atoms is  $a_o$ . Here we impose the periodic boundary condition so that in fact it is a closed atomic chain, a ring. When suffering from external perturbations, the atoms would deviate from their equilibrium positions. The classical dynamical equation for these deviations is

$$\ddot{u}_n = k_s(u_{n+1} + u_{n-1} - 2u_n), \quad (2.1.11)$$

where  $u_n(t)$  is the deviation from the equilibrium position for the  $n$ -th atom. At any given

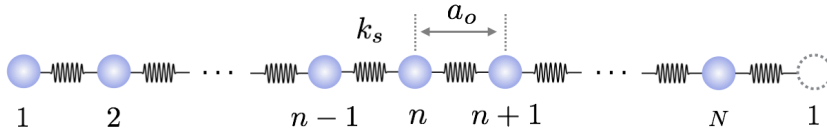


FIGURE 2.2: One dimensional atomic chain.

time,  $u_n(t)$  has to satisfy the periodic boundary condition:  $u_n(t) = u_{n+N}(t)$ . Therefore it can be expanded in terms of a set of complete and orthonormal basis  $\{\phi_{kn}\}$ , which also satisfies the periodic boundary condition. In fact, this is simply a Fourier transformation.  $\phi_{kn}$  is chosen as

$$\phi_{kn} = \frac{1}{\sqrt{N}} e^{ikna_o} \quad (2.1.12)$$

and the periodic boundary condition,  $\phi_{k,N+n} = \phi_{kn}$ , requires that  $k = \frac{2\pi j}{Na_o}$  and  $-N/2 \leq j \leq N/2$  (assume  $N$  is even). It is easy to show that  $\{\phi_{kn}\}$  as chosen is orthonormal and complete,

$$\sum_k \phi_{kn} \phi_{kn'}^* = \delta_{nn'}, \quad \sum_n \phi_{kn} \phi_{k'n}^* = \delta_{kk'}. \quad (2.1.13)$$

Eq. (2.1.11) admits normal modes solutions  $\phi_{kn}(t) = e^{-i\omega_k t} \phi_{kn}$ . By substituting  $\phi_{kn}(t)$  into Eq. (2.1.11) we find the dispersion relation,

$$\omega_k^2 = 4k_s \sin^2(ka_o/2). \quad (2.1.14)$$

When the wavelength of the normal modes is much longer than the distance between neighbouring atoms, that is  $1/k \gg a_o$ ,

$$\omega_k \approx v_s |k|, \quad (2.1.15)$$

where  $v_s = a_o \sqrt{k_s}$  is the velocity of sound waves. The general solutions  $u_n(t)$  is a linear superposition of these normal modes,

$$u_n(t) = \sum_k q_k \phi_{kn}(t), \quad (2.1.16)$$

where  $q_k$  is the expansion coefficients satisfying  $q_k = q_{-k}^*$  because  $u_n(t)$  is real. While  $u_n(t)$  describe the motion of an individual atom, the normal modes  $\phi_{kn}(t)$  describe the collective wave-like excitations of the atomic chain.

Canonical quantization procedure can be used to quantize the the motion of the atomic chain. The classical Lagrangian of the atomic chain is

$$L_{ac} = \sum_n \frac{1}{2} \dot{u}_n^2 - \sum_n \frac{1}{2} k_s (u_{n+1} - u_n)^2. \quad (2.1.17)$$

The canonical momentum is defined as

$$p_n = \frac{\partial L_{ac}}{\partial \dot{u}_n} = \dot{u}_n \quad (2.1.18)$$

so that the classical Hamiltonian of the atomic chain is

$$H_{ac} = p_n \dot{u}_n - L_{ac} = \sum_n \left[ \frac{1}{2} p_n^2 + \frac{1}{2} k_s (u_{n+1} - u_n)^2 \right]. \quad (2.1.19)$$

By replacing  $u_n$  and  $p_n$  in Eq. (2.1.19) by Hermitian operators  $\hat{u}_n$  and  $\hat{p}_n$  we obtain the quantum Hamiltonian for the atomic chain,

$$\hat{H}_{ac} = \sum_n \left[ \frac{1}{2} \hat{p}_n^2 + \frac{1}{2} k_s (\hat{u}_{n+1} - \hat{u}_n)^2 \right]. \quad (2.1.20)$$

The position and momentum operators  $\hat{u}_n$  and  $\hat{p}_n$  satisfy commutation relations

$$[\hat{u}_n, \hat{p}_{n'}] = i\hbar\delta_{nn'}, \quad [\hat{u}_n, \hat{u}_{n'}] = 0, \quad [\hat{p}_n, \hat{p}_{n'}] = 0. \quad (2.1.21)$$

Fourier transform  $\hat{u}_n$  and  $\hat{p}_n$  to define a new set of operators  $\hat{q}_k$  and  $\hat{\pi}_k$ ,

$$\hat{u}_n = \sum_k \hat{q}_k \phi_{kn}, \quad \hat{p}_n = \sum_k \hat{\pi}_k \phi_{kn}^*. \quad (2.1.22)$$

satisfying  $\hat{q}_k^\dagger = \hat{q}_{-k}$  and  $\hat{\pi}_k^\dagger = \hat{\pi}_{-k}$ . Substituting Eq. (2.1.22) into Eq. (2.1.20) we have

$$\hat{H}_{\text{ac}} = \sum_k \left( \frac{1}{2} \hat{\pi}_k \hat{\pi}_{-k} + \frac{1}{2} \omega_k^2 \hat{q}_k \hat{q}_{-k} \right). \quad (2.1.23)$$

We further define the lowering and raising operators as

$$\hat{a}_k = \frac{1}{\sqrt{2\hbar\omega_k}} (\omega_k \hat{q}_k + i\hat{\pi}_{-k}), \quad \hat{a}_k^\dagger = \frac{1}{\sqrt{2\hbar\omega_k}} (\omega_k \hat{q}_{-k} - i\hat{\pi}_k), \quad (2.1.24)$$

which satisfy commutation relations,

$$[\hat{a}_k, \hat{a}_{k'}^\dagger] = \delta_{kk'}, \quad [\hat{a}_k, \hat{a}_{k'}] = 0, \quad [\hat{a}_k^\dagger, \hat{a}_{k'}^\dagger] = 0. \quad (2.1.25)$$

The Hamiltonian now becomes

$$\hat{H}_{\text{ac}} = \sum_k \left( \hat{a}_k^\dagger \hat{a}_k + \frac{1}{2} \right) \hbar\omega_k. \quad (2.1.26)$$

We see that the atomic chain can be considered as a collection of single harmonic oscillators, each of which corresponds to the collective wave-like excitations of the atomic chain, with wave number  $k$  and frequency  $\omega_k$ . These collective excitations are known as phonons. The vacuum state  $|0\rangle$  is defined as

$$\hat{a}_k |0\rangle = 0 \quad (2.1.27)$$

for all  $k$ . Therefore, the vacuum state is global in the sense that it describes the collective motion of the atomic chain.

## 2.2 Relativistic quantum fields

We are now ready to introduce the QFT in flat spacetime. The field is a quantity that distributes continuously over the space and time. A natural generalization to the atomic

chain model discussed in Subsection 2.1.2 is to take the continuum limit, that is,  $a_o \rightarrow 0$  and  $N \rightarrow \infty$ . We thus obtain a non-relativistic QFT in a one-dimension ring. This non-relativistic QFT can be generalized to higher dimensions and open regions, and has been studied and applied extensively in the condensed matter physics [Tsv95]. However in this thesis we are interested in relativistic QFT, which also follows the laws of the special relativity. In a more concrete word, the equation of motion of the fields should be invariant under the Lorentz transformation. The relativistic QFT was developed since 1920s and is now well established, see [Wei95, PS95, IZ06] for example. Another important thing to note is that the phonons discussed in the Subsection 2.1.2 are the excitations of some kind of materials, so they are not fundamental. While quantum fields, e.g., Dirac fields and electromagnetic fields, that we are going to discuss are considered to be fundamental, which means we do not know whether there are even more fundamental “materials”, things like ether for example. From the atomic chain model to a relativistic QFT, we need to take three steps forwards: (1) take the continuum limit; (2) take into account the special relativity; (3) consider the quantum fields as fundamental objects.

### 2.2.1 Basics of special relativity

The special relativity was originally proposed by Albert Einstein in 1905 in the paper “*On the Electrodynamics of Moving Bodies*” [Ein05]. It is based on two postulates:

- **The Principle of Relativity** – the laws of physics are invariant in all inertial systems;
- **The Principle of Invariant Light Speed** – the speed of light in a vacuum is the same for all observers, regardless of the motion of the light source.

Einstein’s special relativity has greatly changed our understanding of space and time. In the Newtonian mechanics, the space and time are absolute and independent of the motion of the objects. While in the special relativity, the principle of invariant light speed leads to completely different notions like the time dilation, length contraction and relativity of simultaneity, see Fig. 2.3.

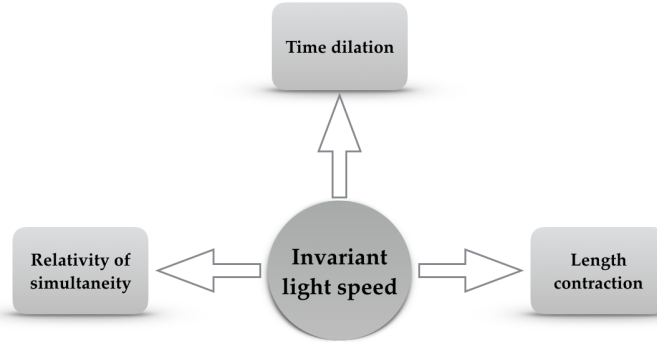


FIGURE 2.3: Relation between the principle of Invariant Light Speed and the time dilation, length contraction, relativity of simultaneity.

In the Newtonian mechanics, coordinates in two different inertial frames are related by the Galilean transformation [Gol65]. In the special relativity, the Galilean transformation is replaced by the Lorentz transformation [Har03]. Suppose that  $x^\mu = (t, x, y, z)$  are the coordinates of a spacetime event in an inertial frame  $K$  and  $x'^\mu = (t', x', y', z')$  are the coordinates of the same event in a different inertial frame  $K'$ . Without loss of generality, we assume the  $K'$  frame moves along the  $x$ -axis with constant velocity  $v$  with respect to the  $K$  frame. The Lorentz transformation relating the coordinates of these two inertial frame is [Har03]

$$\begin{aligned}
 t' &= \gamma(t - vx) \\
 x' &= \gamma(x - vt) \\
 y' &= y \\
 z' &= z,
 \end{aligned}
 \tag{2.2.1}$$

where  $\gamma$  is the Lorentz factor

$$\gamma = \frac{1}{\sqrt{1 - v^2}}.
 \tag{2.2.2}$$

Note that we take the unit where the speed of light is unity,  $c = 1$ . The time dilation, length contraction and relativity of simultaneity can be easily derived from the Lorentz transformation (2.2.1). Although the coordinates are changed in different inertial frames, there are some quantities that are invariant under the Lorentz transformation, known as Lorentz scalar. The spacetime interval between two events is one of the Lorentz scalars. The

spacetime interval between two very close events, with coordinates  $(t, x, y, z)$  and  $(t + dt, x + dx, y + dy, z + dz)$  respectively, is defined as [Har03]

$$ds^2 = -dt^2 + dx^2 + dy^2 + dz^2 = \eta_{\mu\nu} dx^\mu dx^\nu, \quad (2.2.3)$$

where  $\eta_{\mu\nu} = \text{diag}\{-1, +1, +1, +1\}$  is the Minkowski spacetime metric. One specific example of the spacetime interval is the proper time interval of an observer. The proper time  $\tau$  is the time that measured by the clock carried by the observer itself. So in the rest frame of the observer,  $dx = dy = dz = 0$ , one finds  $d\tau^2 = -ds^2$ . Therefore the proper time of any observer is invariant under the Lorentz transformation.

There are three types of causal relations between two spacetime events: time-like, space-like and light-like. When  $ds^2 < 0$ , the two events are time-like, which means slower-than-light signals can be transmitted from the earlier event to the later event. In addition, the temporal order of any pair of time-like events cannot be changed by the Lorentz transformation, implying that causality is preserved. When  $ds^2 = 0$ , the two events are light-like, meaning that these two events are connected by light signals. When  $ds^2 > 0$ , the two events are space-like and there are no signals can connect these two events.

The principle of relativity states that the laws of physics are invariant in all inertial frames, which implies that the dynamical equations that dominate the evolution of physical systems are the same in all inertial frames. Or equivalently, the dynamical equations should be covariant under the Lorentz transformation. To satisfy the above requirement, it is convenient to represent physical quantities by tensors which transform in a particular way under the Lorentz transformation. Here we are going to discuss some examples but not the general case. We have mentioned that a Lorentz scalar (a rank-0 tensor) is invariant under the Lorentz transformation. The transformation for a vector (rank-1 tensor) is the following:

$$V'^\mu = \Lambda^\mu{}_\nu V^\nu, \quad (2.2.4)$$

where  $V^\mu$  is a general vector and  $\Lambda^\mu{}_\nu$  is the general Lorentz transformation matrix which is defined as

$$\Lambda^\mu{}_\nu = \frac{\partial x'^\mu}{\partial x^\nu}. \quad (2.2.5)$$

Examples of vector include the four momentum of a particle  $p^\mu = (E, \mathbf{p}) = (\gamma m_0, \gamma m_0 \mathbf{v})$ , four current  $J^\mu = (\rho, \mathbf{J})$  *etc.*. A rank-2 tensor, denoted by  $V^{\mu\nu}$ , is transformed as

$$V'^{\mu\nu} = \Lambda^\mu_\alpha \Lambda^\nu_\beta V^{\alpha\beta}. \quad (2.2.6)$$

Examples of rank-2 tensor include the energy momentum tensor  $T^{\mu\nu}$ , electromagnetic tensor  $F^{\mu\nu}$  *etc.*. The inner product of two tensors gives a tensor with a lower rank, e.g., the inner product of two vectors is a scalar. It is easy to show that

$$p_\mu p^\mu = -m_0^2 = -E^2 + \mathbf{p} \cdot \mathbf{p}, \quad (2.2.7)$$

which gives the Einstein's mass-energy relation

$$E^2 = m_0^2 + \mathbf{p} \cdot \mathbf{p}. \quad (2.2.8)$$

A dynamical equation represents the relation between different physical quantities. When the physical quantities are represented by tensors that are covariant under the Lorentz transformation, the dynamical equation is also Lorentz covariant. For example the Maxwell's equation can be written as a covariant form [Jac75],

$$\partial_\nu F^{\mu\nu} = 4\pi J^\mu, \quad (2.2.9)$$

implying that the electromagnetic laws are invariant in all inertial frames.

### 2.2.2 Hermitian massless scalar fields

We introduce the quantum theory of an Hermitian massless scalar field  $\hat{\Phi}$  in the (1 + 3)-dimensional Minkowski spacetime. For field theory in lower dimensions, e.g., (1 + 1)-dimensional spacetime, the quantization procedure is similar. The QFT for a massive scalar field can be obtained by introducing a mass term in the Lagrangian density [PS95]. In this section, canonical quantization procedure is adopted. The Lagrangian density of the scalar field  $\hat{\Phi}$  is

$$\hat{\mathcal{L}} = -\frac{1}{2}\eta^{\mu\nu}(\partial_\mu \hat{\Phi})(\partial_\nu \hat{\Phi}) = \frac{1}{2}\dot{\hat{\Phi}}^2 - \frac{1}{2}(\nabla \hat{\Phi})^2 \quad (2.2.10)$$

where the “.” represents derivative with respect to time  $t$  and “ $\nabla$ ” represents the gradient. The conjugate field of  $\hat{\Phi}$  is defined as

$$\hat{\Pi} = \frac{\partial \hat{\mathcal{L}}}{\partial \dot{\hat{\Phi}}} = \dot{\hat{\Phi}}. \quad (2.2.11)$$

The Hamiltonian density of the scalar field is

$$\hat{\mathcal{H}} = \hat{\Pi} \dot{\hat{\Phi}} - \hat{\mathcal{L}} = \frac{1}{2} \hat{\Pi}^2 + \frac{1}{2} (\nabla \hat{\Phi})^2 \quad (2.2.12)$$

The equation of motion for the scalar field can be derived by substituting Eq. (2.2.10) into the Euler-Lagrange equation

$$\partial_\mu \left( \frac{\partial \hat{\mathcal{L}}}{\partial (\partial_\mu \hat{\Phi})} \right) - \frac{\partial \hat{\mathcal{L}}}{\partial \hat{\Phi}} = 0. \quad (2.2.13)$$

We find the Klein-Gordon equation,

$$(\partial_t^2 - \nabla^2) \hat{\Phi} = 0. \quad (2.2.14)$$

In the canonical quantization, the equal-time commutation relations are imposed,

$$[\hat{\Phi}(t, \mathbf{x}), \hat{\Pi}(t, \mathbf{x}')] = i\delta^{(3)}(\mathbf{x} - \mathbf{x}'), \quad [\hat{\Phi}(t, \mathbf{x}), \hat{\Phi}(t, \mathbf{x}')] = [\hat{\Pi}(t, \mathbf{x}), \hat{\Pi}(t, \mathbf{x}')] = 0. \quad (2.2.15)$$

Similar to the atomic chain model, the scalar field  $\hat{\Phi}$  can be expanded in terms of a set of complete and orthonormal bases  $\{\phi_{\mathbf{k}}(t, \mathbf{x}), \phi_{\mathbf{k}}^*(t, \mathbf{x})\}$ , which is defined as

$$\phi_{\mathbf{k}}(t, \mathbf{x}) = \frac{1}{(2\pi)^{3/2} \sqrt{2\omega_{\mathbf{k}}}} e^{-i\omega_{\mathbf{k}}t + i\mathbf{k}\cdot\mathbf{x}}. \quad (2.2.16)$$

Substituting  $\phi_{\mathbf{k}}(t, \mathbf{x})$  into the Klein-Gordon equation (2.2.14) we find

$$\omega_{\mathbf{k}}^2 = |\mathbf{k}|^2. \quad (2.2.17)$$

The bases  $\{\phi_{\mathbf{k}}(t, \mathbf{x}), \phi_{\mathbf{k}}^*(t, \mathbf{x})\}$  are orthonormal in terms of the Klein-Gordon inner product. For any two solutions  $\phi_1$  and  $\phi_2$  of the Klein-Gordon equation, the Klein-Gordon product is defined as [BD82, CHM08]

$$\langle \phi_1, \phi_2 \rangle = i \int d\mathbf{x} (\phi_1^* \partial_t \phi_2 - \phi_2 \partial_t \phi_1^*), \quad (2.2.18)$$

where the spatial integral is on any space-like hypersurface of constant  $t$ . It is straightforward to show that

$$\langle \phi_{\mathbf{k}}, \phi_{\mathbf{k}'} \rangle = -\langle \phi_{\mathbf{k}}^*, \phi_{\mathbf{k}'}^* \rangle = \delta^{(3)}(\mathbf{k} - \mathbf{k}'), \quad \langle \phi_{\mathbf{k}}, \phi_{\mathbf{k}'}^* \rangle = \langle \phi_{\mathbf{k}}^*, \phi_{\mathbf{k}'} \rangle = 0. \quad (2.2.19)$$

The scalar field  $\hat{\Phi}$  is expanded as

$$\hat{\Phi} = \int d\mathbf{k} (\hat{a}_{\mathbf{k}}\phi_{\mathbf{k}} + \hat{a}_{\mathbf{k}}^{\dagger}\phi_{\mathbf{k}}^*), \quad (2.2.20)$$

where  $\hat{a}_{\mathbf{k}}$  and  $\hat{a}_{\mathbf{k}}^{\dagger}$  are known as the annihilation and creation operators (correspond to the lowering and raising operators of the harmonic oscillator), respectively. They satisfy the boson commutation relations,

$$[\hat{a}_{\mathbf{k}}, \hat{a}_{\mathbf{k}'}^{\dagger}] = \delta^{(3)}(\mathbf{k} - \mathbf{k}'), \quad [\hat{a}_{\mathbf{k}}, \hat{a}_{\mathbf{k}'}] = [\hat{a}_{\mathbf{k}}^{\dagger}, \hat{a}_{\mathbf{k}'}^{\dagger}] = 0. \quad (2.2.21)$$

The Hamiltonian of the scalar field can be written in terms of the creation and annihilation operators,

$$\hat{H} = \int d\mathbf{x} \hat{\mathcal{H}} = \int d\mathbf{k} \omega_{\mathbf{k}} \left( \hat{a}_{\mathbf{k}}^{\dagger} \hat{a}_{\mathbf{k}} + \frac{1}{2} \right) \quad (2.2.22)$$

The vacuum state is the lowest energy state and is defined as

$$|0\rangle = |0_{\mathbf{k}_1}\rangle \otimes |0_{\mathbf{k}_2}\rangle \otimes |0_{\mathbf{k}_3}\rangle \otimes \cdots \quad (2.2.23)$$

and satisfies

$$\hat{a}_{\mathbf{k}}|0\rangle = 0 \quad (2.2.24)$$

for all  $\mathbf{k}$ . It is evident that the vacuum state is global since any single-wave-number mode is the global excitation of the field. Although the vacuum state is the lowest energy state, the expectation value of energy is not zero,

$$\langle 0|\hat{H}|0\rangle = \frac{1}{2} \int d\mathbf{k} \omega_{\mathbf{k}} \rightarrow \infty. \quad (2.2.25)$$

The existence of vacuum energy is due to the uncertainty principle. In Minkowski spacetime, the vacuum energy is not observable in most cases and can be disregarded safely. However, it may play very important roles in some special situations, e.g., the Casimir effect [CP48], spontaneous emission of atoms [Dir27].

### 2.2.3 Green's functions

The vacuum expectation values of the products of two field operators are very important in QFT. The most relevant one in this thesis is the positive frequency Wightman function. For

completeness we also briefly introduce other functions, including negative Wightman function, Schwinger function, Hadamard's elementary function, Feynman propagator, retarded and advanced Green functions. Here I follow the definitions and notations by Birrell and Davies [BD82].

The positive frequency Wightman function  $G^+(t, \mathbf{x}; t', \mathbf{x}')$  is defined as

$$G^+(t, \mathbf{x}; t', \mathbf{x}') = \langle 0 | \hat{\Phi}(t, \mathbf{x}) \hat{\Phi}(t', \mathbf{x}') | 0 \rangle \quad (2.2.26)$$

and the negative frequency Wightman function

$$G^-(t, \mathbf{x}; t', \mathbf{x}') = \langle 0 | \hat{\Phi}(t', \mathbf{x}') \hat{\Phi}(t, \mathbf{x}) | 0 \rangle. \quad (2.2.27)$$

The Schwinger and Hadamard functions are related to the commutator and anti-commutator of the scalar field at two spacetime events, respectively.

$$iG(t, \mathbf{x}; t', \mathbf{x}') = \langle 0 | [\hat{\Phi}(t, \mathbf{x}), \hat{\Phi}(t', \mathbf{x}')] | 0 \rangle = G^+(t, \mathbf{x}; t', \mathbf{x}') - G^-(t, \mathbf{x}; t', \mathbf{x}'), \quad (2.2.28)$$

$$G^{(1)}(t, \mathbf{x}; t', \mathbf{x}') = \langle 0 | \{\hat{\Phi}(t, \mathbf{x}), \hat{\Phi}(t', \mathbf{x}')\} | 0 \rangle = G^+(t, \mathbf{x}; t', \mathbf{x}') + G^-(t, \mathbf{x}; t', \mathbf{x}') \quad (2.2.29)$$

The Feynman propagator  $G_F$  is

$$\begin{aligned} G_F(t, \mathbf{x}; t', \mathbf{x}') &= -i \langle 0 | \hat{T} \{ \hat{\Phi}(t, \mathbf{x}) \hat{\Phi}(t', \mathbf{x}') \} | 0 \rangle \\ &= -i\theta(t - t')G^+(t, \mathbf{x}; t', \mathbf{x}') - i\theta(t' - t)G^-(t, \mathbf{x}; t', \mathbf{x}'), \end{aligned} \quad (2.2.30)$$

where  $\hat{T}$  is the time ordering operator and  $\theta(t)$  is the Heaviside step function. The retarded and advanced Green functions are

$$G_R(t, \mathbf{x}; t', \mathbf{x}') = -\theta(t - t')G(t, \mathbf{x}; t', \mathbf{x}'), \quad (2.2.31)$$

$$G_A(t, \mathbf{x}; t', \mathbf{x}') = \theta(t' - t)G(t, \mathbf{x}; t', \mathbf{x}'). \quad (2.2.32)$$

We see that the positive and negative frequency Wightman functions are two fundamental functions from which others can be derived easily.

Substituting Eq. (2.2.20) into the definition of the positive frequency Wightman function, Eq. (2.2.26), we find

$$G^+(t, \mathbf{x}; t', \mathbf{x}') = \int d\mathbf{k} \phi_{\mathbf{k}}(t, \mathbf{x}) \phi_{\mathbf{k}}^*(t', \mathbf{x}') = \frac{1}{2(2\pi)^3} \int d\mathbf{k} \frac{e^{-i\omega_{\mathbf{k}}(t-t') + i\mathbf{k}\cdot(\mathbf{x}-\mathbf{x}')}}{\omega_{\mathbf{k}}}. \quad (2.2.33)$$

For a massless scalar field,  $\omega_{\mathbf{k}} = |\mathbf{k}|$ , the above integral can be calculated analytically,

$$G^+(t, \mathbf{x}; t', \mathbf{x}') = -\frac{1}{4\pi^2} \lim_{\epsilon \rightarrow 0^+} \frac{1}{(t - t' - i\epsilon)^2 - |\mathbf{x} - \mathbf{x}'|^2}. \quad (2.2.34)$$

The limit can be taken after all other calculations have been done, or we can do it right now and find

$$G^+(t, \mathbf{x}; t', \mathbf{x}') = \frac{1}{8\pi i |\mathbf{x} - \mathbf{x}'|} [\delta((t-t') - |\mathbf{x} - \mathbf{x}'|) - \delta((t-t') + |\mathbf{x} - \mathbf{x}'|)] - \frac{1}{4\pi^2} \frac{1}{(t - t')^2 - |\mathbf{x} - \mathbf{x}'|^2}. \quad (2.2.35)$$

The singularity in the last term of Eq. (2.2.35) should be treated as the Cauchy principal value, same for the following equations: (2.2.36) and (2.2.40). The negative frequency Wightman function is basically the complex conjugate of the positive frequency Wightman function,

$$\begin{aligned} G^-(t, \mathbf{x}; t', \mathbf{x}') &= -\frac{1}{4\pi^2} \lim_{\epsilon \rightarrow 0^+} \frac{1}{(t - t' + i\epsilon)^2 - |\mathbf{x} - \mathbf{x}'|^2} \\ &= -\frac{1}{8\pi i |\mathbf{x} - \mathbf{x}'|} [\delta((t - t') - |\mathbf{x} - \mathbf{x}'|) - \delta((t - t') + |\mathbf{x} - \mathbf{x}'|)] \\ &\quad - \frac{1}{4\pi^2} \frac{1}{(t - t')^2 - |\mathbf{x} - \mathbf{x}'|^2}. \end{aligned} \quad (2.2.36)$$

According to the relation between Wightman functions and Schwinger function, we have

$$G(t, \mathbf{x}; t', \mathbf{x}') = -\frac{1}{4\pi |\mathbf{x} - \mathbf{x}'|} [\delta((t - t') - |\mathbf{x} - \mathbf{x}'|) - \delta((t - t') + |\mathbf{x} - \mathbf{x}'|)], \quad (2.2.37)$$

showing that the Schwinger function is nonzero only when  $(t - t') \pm |\mathbf{x} - \mathbf{x}'| = 0$ : the two events are light-like. This means there are no causal connections between space-like and time-like events. This is reasonable because for a massless field all signals travel with the speed of light. The retarded and advanced Green functions are

$$G_R(t, \mathbf{x}; t', \mathbf{x}') = \frac{1}{2\pi} \theta(t - t') \delta((t - t')^2 - |\mathbf{x} - \mathbf{x}'|^2), \quad (2.2.38)$$

$$G_A(t, \mathbf{x}; t', \mathbf{x}') = \frac{1}{2\pi} \theta(t' - t) \delta((t - t')^2 - |\mathbf{x} - \mathbf{x}'|^2), \quad (2.2.39)$$

which are also nonzero on the lightcone and satisfy the corresponding boundary conditions.

Finally, the Feynman propagator is

$$G_F(t, \mathbf{x}; t', \mathbf{x}') = -\frac{1}{4\pi} \delta((t - t')^2 - |\mathbf{x} - \mathbf{x}'|^2) - \frac{i}{4\pi^2} \frac{1}{(t - t')^2 - |\mathbf{x} - \mathbf{x}'|^2}. \quad (2.2.40)$$

## 2.3 Summary and further reading

In this section, we introduce some basic concepts and tools in QFT in flat spacetime. In particular, we discuss the quantization of a massless Hermitian scalar and calculate various Green's functions.

Relativistic QFT in flat spacetime has been developed since 1920s [Dir27]. Many excellent textbooks have been written to introduce the framework of the relativistic quantum field theory. The textbook by Zee [Zee10] gives a very nice introduction to the basic concepts of QFT. The textbook by Peskin and Schroeder [PS95] is more advanced and contains adequate technical details. The one by Weinberg [Wei95] also gives a very excellent introduction and contains technical details.



# 3

## Basics of Quantum Optics

In this chapter, we are going to review some basic concepts and tools in quantum optics, a quantum theory of light. Quantum optics is a research field that studies phenomena involving light and its interactions with matter at submicroscopic level [WM07, SZ97, BR04]. Mature tools and techniques have been developed since 1960s to prepare, manipulate and detect the states of light. These tools and techniques are very important in studying the quantum effects in gravity and accelerated frames. More promisingly, they may help us to conceive some realistic experiments in near future to test the quantum effects in the presence of gravity.

### 3.1 Quantum states of the electromagnetic field

The quantization of a free electromagnetic field can be found in standard quantum optics textbooks [WM07, SZ97, BR04]. The freely propagating electromagnetic field has two polarizations, both of which are perpendicular to its propagation direction. For example, if the electromagnetic wave propagates along the  $z$ -direction, the electric field vector operator can be written as  $\hat{\mathbf{E}} = (\hat{E}_x, \hat{E}_y, 0)$ , where  $\hat{E}_x$  and  $\hat{E}_y$  represent two independent polarizations, respectively. For simplicity, we consider a single polarization electric field, namely, we assume  $\hat{E}(t, z) = \hat{E}_x(t, z)$  without loss of generality. The electric field operator can be expressed as [BLPS90]

$$\hat{E}(t, z) = i \int_0^\infty d\omega \left( \frac{\hbar\omega}{4\pi\epsilon_0 c \mathcal{A}} \right)^{1/2} \left[ \hat{a}_\omega e^{-i\omega(t-z)} - \hat{a}_\omega^\dagger e^{i\omega(t-z)} \right], \quad (3.1.1)$$

where  $\hbar$  is the Planck's constant,  $c$  is the speed of light in vacuum,  $\epsilon_0$  is the free space permittivity,  $\mathcal{A}$  is the cross-sectional area determined by the fibre mode or the geometry of the experiment. The creation and annihilation operators satisfy the boson commutation relations,

$$[\hat{a}_\omega, \hat{a}_{\omega'}^\dagger] = \delta(\omega - \omega'), \quad [\hat{a}_\omega, \hat{a}_{\omega'}] = [\hat{a}_\omega^\dagger, \hat{a}_{\omega'}^\dagger] = 0. \quad (3.1.2)$$

#### 3.1.1 Localized wave packet modes

When discussing quantization of the electromagnetic field in quantum optics, discrete set of modes are usually used. On the one hand, the maths is simpler for the discrete set of modes; on the other hand, the discrete set of modes can be realized when the fields are confined within a finite region, e.g., a cavity. However in the open space, the frequency is continuous and continuum frequency modes should be used, as shown by Eq. (3.1.1). In order to utilize the simplicity and conveniences of the discrete modes, one can define a set of complete and orthonormal discrete modes even in open space [BLPS90]. Assume that  $\{f_i(\omega)\}$  is a set of complete and orthonormal functions, which have support only for  $\omega > 0$  and satisfy

$$\int_0^\infty d\omega f_i(\omega) f_j^*(\omega) = \delta_{ij}, \quad \sum_i f_i(\omega) f_i^*(\omega') = \delta(\omega - \omega'), \quad (3.1.3)$$

where  $i$  and  $j$  label the members of the denumerably infinite set. Correspondingly, we can define localized wave packet mode operators,

$$\hat{a}_i = \int_0^\infty d\omega f_i(\omega) \hat{a}_\omega. \quad (3.1.4)$$

The inverse relation is easy to obtain by using the completeness relation in Eq. (3.1.3),

$$\hat{a}_\omega = \sum_i f_i^*(\omega) \hat{a}_i \quad (3.1.5)$$

The localized wave packet mode operators satisfy commutation relations

$$[\hat{a}_i, \hat{a}_j^\dagger] = \delta_{ij}, \quad [\hat{a}_i, \hat{a}_j] = [\hat{a}_i^\dagger, \hat{a}_j^\dagger] = 0. \quad (3.1.6)$$

Substituting Eq. (3.1.5) into Eq. (3.1.1), we can expand the electric field operator in terms of the localized wave packet modes as

$$\hat{E}(t, z) = i \sum_j [\hat{a}_j f_j(t, z) - \hat{a}_j^\dagger f_j^*(t, z)], \quad (3.1.7)$$

where  $f_j(t, z)$  is the corresponding wave packet in the time domain,

$$f_j(t, z) = \int_0^\infty d\omega \left( \frac{\hbar\omega}{4\pi\epsilon_0 c \mathcal{A}} \right)^{1/2} f_j^*(\omega) e^{-i\omega(t-z)}. \quad (3.1.8)$$

Although  $f_i(\omega)$  is arbitrary, we are mainly concerned with the narrow bandwidth wave packets:  $\omega_0 \gg \sigma$ , where  $\sigma$  is the bandwidth and  $\omega_0$  is the central frequency.

### 3.1.2 Number states

As discussed in Chapter 2, the vacuum state  $|0\rangle$  is a state that contains no excitation in any frequency mode,  $\hat{a}_\omega|0\rangle = 0$ . From the definition of the localized wave packet mode operator (3.1.4), we have  $\hat{a}_i|0\rangle = 0$  for all  $i$ . In the rest of this chapter, we are mostly interested in a particular wave packet mode  $f(\omega)$  and neglect the subscript “ $i$ ” without introducing any confusion. A single photon state can be generated by acting on the vacuum state by the creation operator  $\hat{a}^\dagger$ ,

$$|1\rangle = \hat{a}^\dagger|0\rangle = \int_0^\infty d\omega f^*(\omega) \hat{a}_\omega^\dagger|0\rangle. \quad (3.1.9)$$

This state contains only one particle with frequency distribution  $|f(\omega)|^2$ , and spatiotemporal distribution  $|f(t, z)|^2$ . An  $n$ -photon state is

$$|n\rangle = \frac{(\hat{a}^\dagger)^n}{\sqrt{n!}}|0\rangle, \quad n = 0, 1, 2, \dots \quad (3.1.10)$$

The number states are orthogonal

$$\langle n|m\rangle = \delta_{nm} \quad (3.1.11)$$

and complete

$$\sum_{n=0}^{\infty} |n\rangle\langle n| = 1. \quad (3.1.12)$$

### 3.1.3 Coherent state

A coherent state  $|\alpha\rangle$  can be generated by displacing the vacuum state [WM07],

$$|\alpha\rangle = \hat{D}(\alpha)|0\rangle, \quad (3.1.13)$$

where  $\hat{D}(\alpha)$  is an unitary displacement operator,

$$\hat{D}(\alpha) = \exp(\alpha\hat{a}^\dagger - \alpha^*\hat{a}) \quad (3.1.14)$$

and  $\alpha$  is an arbitrary complex number,  $\alpha = |\alpha|e^{i\theta}$ . Using the Baker-Campbell-Hausdorff formula [Mil72, BK72] one can show that

$$\begin{aligned} \hat{D}^\dagger(\alpha)\hat{a}\hat{D}(\alpha) &= \hat{a} + \alpha, \\ \hat{D}^\dagger(\alpha)\hat{a}^\dagger\hat{D}(\alpha) &= \hat{a}^\dagger + \alpha^*, \end{aligned} \quad (3.1.15)$$

and

$$\hat{a}|\alpha\rangle = \alpha|\alpha\rangle. \quad (3.1.16)$$

So a coherent state  $|\alpha\rangle$  is the eigenstate of the annihilation operator  $\hat{a}$  with a complex eigenvalue  $\alpha$ . The expectation value and variance of the photon number are

$$\begin{aligned} \bar{N} &= \langle\alpha|\hat{N}|\alpha\rangle = |\alpha|^2, \\ (\Delta N)^2 &= \langle\alpha|\hat{N}^2|\alpha\rangle - \langle\alpha|\hat{N}|\alpha\rangle^2 = |\alpha|^2, \end{aligned} \quad (3.1.17)$$

where  $\hat{N} = \hat{a}^\dagger \hat{a}$  is the photon number operator. The relative fluctuation of the photon number is  $\Delta N/\bar{N} = 1/\sqrt{\bar{N}}$ . The coherent state can be written as a linear superposition of the number states,

$$|\alpha\rangle = e^{-|\alpha|^2/2} \sum_{n=0}^{\infty} \frac{\alpha^n}{\sqrt{n!}} |n\rangle, \quad (3.1.18)$$

from which one can easily show that the probability distribution of the photon number is a Poisson distribution,

$$P(n) = |\langle n|\alpha\rangle|^2 = \frac{|\alpha|^{2n} e^{-|\alpha|^2}}{n!}. \quad (3.1.19)$$

We introduce the Hermitian quadrature amplitude as

$$\hat{X}(\phi) = \hat{a} e^{-i\phi} + \hat{a}^\dagger e^{i\phi}, \quad (3.1.20)$$

where  $\phi$  represents the quadrature phase. Two important quadrature amplitudes are the position and momentum operators,

$$\hat{x} = \hat{X}(\phi = 0) = \hat{a} + \hat{a}^\dagger, \quad \hat{p} = \hat{X}(\phi = \pi/2) = -i\hat{a} + i\hat{a}^\dagger. \quad (3.1.21)$$

The commutator between two quadrature amplitudes with  $\pi/2$  phase difference is

$$[\hat{X}(\phi), \hat{X}(\phi + \pi/2)] = 2i. \quad (3.1.22)$$

According to the uncertainty principle [Sak85], the product of the uncertainties of these two quadrature amplitudes satisfy

$$\Delta X(\phi) \Delta X(\phi + \pi/2) \geq 1, \quad (3.1.23)$$

where  $(\Delta X(\phi))^2 = \langle \hat{X}^2(\phi) \rangle - \langle \hat{X}(\phi) \rangle^2$  is the quadrature variance. For a coherent state, the expectation value of the quadrature amplitude is

$$\langle \alpha | \hat{X}(\phi) | \alpha \rangle = \alpha e^{-i\phi} + \alpha^* e^{i\phi} = 2|\alpha| \cos(\theta - \phi) \quad (3.1.24)$$

and the variance is

$$(\Delta X(\phi))^2 = 1. \quad (3.1.25)$$

We can see that the variance of the quadrature observable is unity for all quadrature phase. This means the coherent state satisfies the minimum uncertainty relation,

$$\Delta X(\phi)\Delta X(\phi + \pi/2) = 1. \quad (3.1.26)$$

Fig. 3.1 shows the phase space representation of the coherent state, as well as the vacuum state.

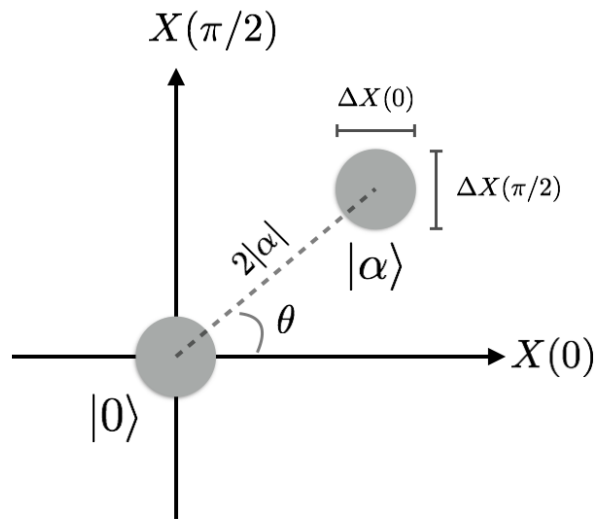


FIGURE 3.1: Phase space representation of a coherent state with amplitude  $\alpha = |\alpha|e^{i\theta}$ . For comparison, the vacuum state is also plotted. The vacuum state is centred on the origin and its noise is normalized to one. The coherent state  $|\alpha\rangle$  is shifted  $2|\alpha|$  in the direction  $\theta$  and its fluctuation is the same as the vacuum state.

### 3.1.4 Squeezed states

In this subsection, we shall introduce two types of squeezed state: the single-mode squeezed vacuum state and two-mode squeezed vacuum state.

*Single-mode squeezed vacuum state* – A single-mode squeezed vacuum state is a minimum-uncertainty state [WM07] with its minimum uncertainty of the quadrature amplitude smaller than unity, that is,  $\Delta X_{\min} < 1$ . According to the uncertainty principle, the uncertainty of its conjugate quadrature amplitude should be greater than unity. The single-mode squeezed

vacuum state can be generated by squeezing the vacuum,

$$|\xi\rangle = \hat{S}(\xi)|0\rangle. \quad (3.1.27)$$

The single-mode squeezing operator  $\hat{S}(\xi)$  is defined as [WM07]

$$\hat{S}(\xi) = \exp\left(\frac{1}{2}\xi^*\hat{a}^2 - \frac{1}{2}\xi\hat{a}^{\dagger 2}\right) \quad (3.1.28)$$

and obeys the relations

$$\hat{S}^\dagger(\xi) = \hat{S}^{-1}(\xi) = \hat{S}(-\xi). \quad (3.1.29)$$

where  $\xi = re^{i\theta}$  is an arbitrary complex number. Using the Baker-Campbell-Hausdorff formula [Mil72, BK72], one can show that

$$\begin{aligned} \hat{S}^\dagger(\xi)\hat{a}\hat{S}(\xi) &= \hat{a}\cosh r - \hat{a}^\dagger e^{i\theta}\sinh r, \\ \hat{S}^\dagger(\xi)\hat{a}^\dagger\hat{S}(\xi) &= \hat{a}^\dagger\cosh r - \hat{a}e^{-i\theta}\sinh r. \end{aligned} \quad (3.1.30)$$

For a single-mode squeezed vacuum state, the expectation value of any quadrature amplitude is vanished,  $\langle\xi|\hat{X}(\phi)|\xi\rangle = 0$ . The variance of the quadrature amplitude is

$$(\Delta X(\phi))^2 = \langle\xi|\hat{X}^2(\phi)|\xi\rangle = \cosh^2 r + \sinh^2 r - 2\cosh r \sinh r \cos(2\phi - \theta). \quad (3.1.31)$$

The minimum and maximum uncertainties are

$$\Delta X(\theta/2) = e^{-r}, \quad \Delta X(\theta/2 + \pi/2) = e^r, \quad (3.1.32)$$

satisfying the minimum-uncertainty relation

$$\Delta X(\theta/2)\Delta X(\theta/2 + \pi/2) = 1. \quad (3.1.33)$$

Note that the minimum uncertainty relation is satisfied only for two conjugate quadrature amplitudes with minimum and maximum uncertainties, respectively. Product of uncertainties of other pairs of conjugate quadrature amplitudes are greater than unity. Fig. 3.2 shows the phase space representation of a single-mode squeezed vacuum state.

*Two-mode squeezed vacuum state* – The two-mode squeezed vacuum state is also known as the Einstein-Podolski-Rosen (EPR) state [WPGP<sup>+</sup>12]. Assume that  $\hat{a}_s$  and  $\hat{a}_i$  are two

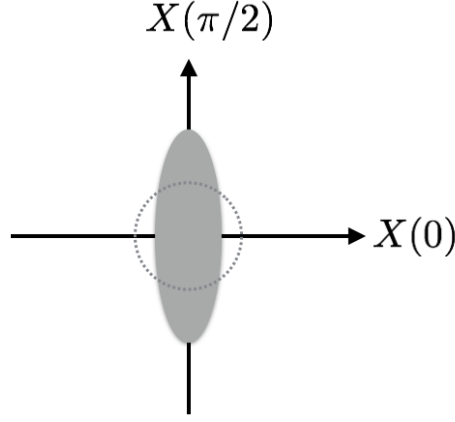


FIGURE 3.2: Phase space representation of a single-mode squeezed vacuum state. The dotted circle represents the vacuum shot noise.

independent modes, which are usually referred to as signal and idler modes, respectively. The EPR state can be generated by squeezing the vacuum state with the two-mode squeezing operator [WM07],

$$|\xi\rangle_{\text{EPR}} = \hat{S}_2(\xi)|0\rangle. \quad (3.1.34)$$

The two-mode squeezing operator is defined as

$$\hat{S}_2(\xi) = \exp(\xi^* \hat{a}_s \hat{a}_i - \xi \hat{a}_s^\dagger \hat{a}_i^\dagger), \quad (3.1.35)$$

and obeys relations

$$\hat{S}_2^\dagger(\xi) = \hat{S}_2^{-1}(\xi) = \hat{S}_2(-\xi), \quad (3.1.36)$$

where  $\xi = r e^{i\theta}$  is an arbitrary complex number. Using the Baker-Campbell-Hausdorff formula [Mil72, BK72], one can show that

$$\begin{aligned} \hat{S}_2^\dagger(\xi) \hat{a}_s \hat{S}_2(\xi) &= \hat{a}_s \cosh r - \hat{a}_i^\dagger e^{i\theta} \sinh r, \\ \hat{S}_2^\dagger(\xi) \hat{a}_i \hat{S}_2(\xi) &= \hat{a}_i \cosh r - \hat{a}_s^\dagger e^{-i\theta} \sinh r. \end{aligned} \quad (3.1.37)$$

According to the disentangling theorem [Tru85],

$$\hat{S}_2(\xi) = \exp[-e^{i\theta} \tanh r \hat{a}_s^\dagger \hat{a}_i^\dagger] \exp[-\ln(\cosh r)(\hat{a}_s^\dagger \hat{a}_s + \hat{a}_i^\dagger \hat{a}_i + 1)] \exp[-e^{i\theta} \tanh r \hat{a}_s \hat{a}_i]. \quad (3.1.38)$$

The EPR state can be expressed in terms of the number states of the signal and idler modes as

$$|\xi\rangle_{\text{EPR}} = \frac{1}{\cosh r} \sum_{n=0}^{\infty} (-1)^n e^{in\theta} \tanh^n r |n\rangle_s |n\rangle_i, \quad (3.1.39)$$

where  $|n\rangle_s$  and  $|n\rangle_i$  are the number states of the signal and idler modes, respectively. Whilst the overall state is pure, the reduced state of each mode is mixed, e.g., the state of the signal mode is

$$\hat{\rho}_s = \text{tr}_i(|\xi\rangle_{\text{EPR}}\langle\xi|) = \frac{1}{\cosh^2 r} \sum_{n=0}^{\infty} \tanh^{2n} r |n\rangle_s \langle n|. \quad (3.1.40)$$

The expectation value and variance of the photon number are

$$\begin{aligned} \bar{N}_s &= \langle\xi|\hat{N}_s|\xi\rangle_{\text{EPR}} = \sinh^2 r, \\ (\Delta N_s)^2 &= \langle\xi|\hat{N}_s^2|\xi\rangle_{\text{EPR}} - \langle\xi|\hat{N}_s|\xi\rangle_{\text{EPR}}^2 = \cosh^2 r \sinh^2 r. \end{aligned} \quad (3.1.41)$$

One can directly read out the probability distribution of the photon number from Eq. (3.1.40),

$$P(n) = \frac{\tanh^{2n} r}{\cosh^2 r} = \frac{\bar{N}_s^n}{(\bar{N}_s + 1)^{n+1}}. \quad (3.1.42)$$

Since the idler and signal modes are symmetric, the above results are also valid for the idler mode.

From Eq. (3.1.37) one can show that the expectation value of the quadrature amplitude of each mode is vanished,

$$\langle\xi|\hat{X}_s(\phi)|\xi\rangle_{\text{EPR}} = \langle\xi|\hat{X}_i(\phi)|\xi\rangle_{\text{EPR}} = 0, \quad (3.1.43)$$

and the variance of the quadrature amplitude is

$$(\Delta X_s(\phi))^2 = (\Delta X_i(\phi))^2 = \cosh(2r). \quad (3.1.44)$$

The uncertainty of the quadrature amplitude of each mode is greater than unity if  $r \neq 0$ . This is consistent with the fact that the reduced state of each mode is mixed. In order to characterize the entanglement between the signal and idler modes, we introduce the correlation (“+”) and anti-correlation (“-”) operators

$$\hat{X}^\pm(\phi) = \frac{1}{\sqrt{2}}(\hat{X}_s(\phi) \pm \hat{X}_i(\phi)). \quad (3.1.45)$$

Without loss of generality, we discuss a special case:  $\theta = 0$ . It is easy to see that

$$\langle \xi | \hat{X}^\pm(\phi) | \xi \rangle_{\text{EPR}} = 0. \quad (3.1.46)$$

The variances of  $\hat{X}^\pm(\phi)$  are

$$(\Delta X^\pm(\phi))^2 = \langle \xi | (\hat{X}^\pm(\phi))^2 | \xi \rangle_{\text{EPR}} = \cosh(2r) \pm \sinh(2r) \cos(2\phi). \quad (3.1.47)$$

The maximum and minimum uncertainties of  $\hat{X}^+(\phi)$  are obtained when  $\phi = 0$  and  $\phi = \pi/2$ ,

$$\Delta X^+(0) = e^r, \quad \Delta X^+(\pi/2) = e^{-r}. \quad (3.1.48)$$

The maximum and minimum uncertainties of  $\hat{X}^-(\phi)$  are obtained when  $\phi = \pi/2$  and  $\phi = 0$ ,

$$\Delta X^-(\pi/2) = e^r, \quad \Delta X^-(0) = e^{-r}. \quad (3.1.49)$$

$\Delta X^-(0)\Delta X^+(\pi/2) = e^{-2r} < 1$  implies that the signal and idler modes are entangled [BR04].

Fig. 3.3 shows the phase space representation of the two-mode squeezed vacuum state.

### 3.1.5 Thermal state

When the electromagnetic field is in equilibrium with a heat bath environment, the field is in a thermal state. The density operator for a thermal state with temperature  $T$  is [SZ97]

$$\hat{\rho}_{\text{th}} = \prod_k \hat{\rho}_k = \prod_k \left\{ \left[ 1 - \exp\left(-\frac{\omega_k}{k_B T}\right) \right] \sum_{n=0}^{\infty} \exp\left(-\frac{n\omega_k}{k_B T}\right) |n\rangle_{\omega_k} \langle n| \right\}, \quad (3.1.50)$$

where  $k_B$  is the Boltzmann constant. For the  $k$ -th mode (with frequency  $\omega_k$ , which we assume to be discrete for convenience), the expectation value and variance of the photon number are

$$\begin{aligned} \bar{N}_k &= \text{tr}(\hat{\rho}_k \hat{N}_k) = \frac{1}{\exp\left(\frac{\omega_k}{k_B T}\right) - 1}, \\ (\Delta N_k)^2 &= \text{tr}(\hat{\rho}_k \hat{N}_k^2) - \bar{N}_k^2 = \frac{\exp\left(\frac{\omega_k}{k_B T}\right)}{\left[\exp\left(\frac{\omega_k}{k_B T}\right) - 1\right]^2} = \bar{N}_k(\bar{N}_k + 1). \end{aligned} \quad (3.1.51)$$

The probability distribution of the photon number can be directly read out from the density operator Eq. (3.1.50) as

$$P_k(n) = \left[ 1 - \exp\left(-\frac{\omega_k}{k_B T}\right) \right] \exp\left(-\frac{n\omega_k}{k_B T}\right) = \frac{\bar{N}_k^n}{(\bar{N}_k + 1)^{n+1}}. \quad (3.1.52)$$

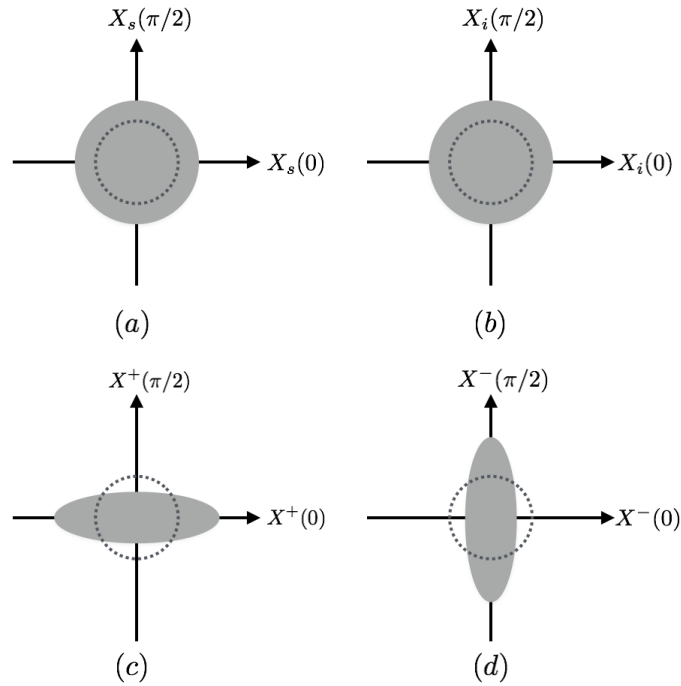


FIGURE 3.3: Phase space representation of an EPR state. The dotted circle represents the vacuum shot noise. (a) and (b) show that the uncertainties of the signal and idler mode are greater than the vacuum shot noise. (c) and (d) show that the correlation and anti-correlation operators are squeezed. The former is squeezed in the quadrature phase  $\phi = \frac{\pi}{2}$  and the latter in  $\phi = 0$ .

By comparing with Eq. (3.1.42) we see that the photon number distribution of the signal or idler mode is the same as the thermal photon number distribution (3.1.52). This implies: on the one hand, the reduced state of the signal or idler mode can be considered as a thermal state with temperature

$$T = \frac{\omega_k}{2k_B \ln(\coth r)}; \quad (3.1.53)$$

on the other hand, a thermal state can be purified by entangling it with another thermal state to form an EPR state.

## 3.2 Basic optical elements

In this section, we introduce two basic optical elements that we will use frequently in the following: the phase shifter and beamsplitter.

### 3.2.1 Phase shifter

A phase shifter added a phase to the field modes. This can be realized by using a delay line or some dielectric materials. The unitary operator for a phase shifter is

$$\hat{U}_\phi = \exp(i\phi\hat{a}^\dagger\hat{a}), \quad (3.2.1)$$

where  $\phi$  is the shifted phase. It can be easily shown that

$$\hat{U}_\phi^\dagger\hat{a}\hat{U}_\phi = \hat{a}e^{i\phi}. \quad (3.2.2)$$

### 3.2.2 Beamsplitter

A beamsplitter is a partially transmitted mirror, with two input and two output modes. Assume that the two input modes are  $\hat{a}_1$  and  $\hat{a}_2$ , respectively. The unitary operator for the beamsplitter is [KMN<sup>+</sup>07]

$$\hat{U}_{\text{BS}} = \exp\left[-i\theta(e^{i\phi}\hat{a}_1^\dagger\hat{a}_2 + e^{-i\phi}\hat{a}_1\hat{a}_2^\dagger)\right], \quad (3.2.3)$$

where  $\theta$  and  $\phi$  characterize the properties of the beamsplitter. The input-output relations for the beamsplitter are

$$\begin{aligned} \hat{a}'_1 &= \hat{U}_{\text{BS}}^\dagger\hat{a}_1\hat{U}_{\text{BS}} = \hat{a}_1 \cos\theta - i\hat{a}_2 e^{i\phi} \sin\theta, \\ \hat{a}'_2 &= \hat{U}_{\text{BS}}^\dagger\hat{a}_2\hat{U}_{\text{BS}} = \hat{a}_2 \cos\theta - i\hat{a}_1 e^{-i\phi} \sin\theta. \end{aligned} \quad (3.2.4)$$

The transmission and reflection coefficients are  $\cos^2\theta$  and  $\sin^2\theta$ , respectively. The relative phase shift  $\phi$  is introduced to ensure that the transformation is unitary. Fig. 7.2.9 shows a schematic diagram of a beamsplitter.

## 3.3 Homodyne detection

### 3.3.1 Balanced homodyne detection

Homodyne detection is a phase sensitive detection scheme that measures the variance of a quadrature amplitude of the optical field [SZ97]. A schematic arrangement for the homodyne

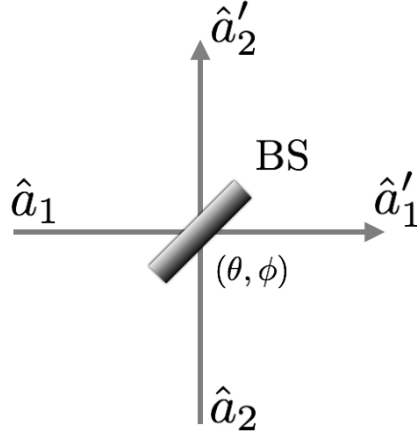


FIGURE 3.4: Schematic diagram of a beamsplitter.

detection is shown in Fig. 3.5. The signal mode,  $\hat{a}_S$ , and the local oscillator mode,  $\hat{a}_L$ , are coherently combined at a lossless 50:50 beamsplitter, then the two output field modes  $\hat{a}_1$  and  $\hat{a}_2$  are detected by two photon detectors  $D_1$  and  $D_2$ , respectively. Finally, the photon numbers registered by these two detectors are subtracted to give the photocurrent. This scheme is known as the balanced homodyne detection. From Eq. (3.2.4), we find

$$\begin{aligned}\hat{a}_1 &= \frac{1}{\sqrt{2}}(\hat{a}_S + \hat{a}_L), \\ \hat{a}_2 &= \frac{1}{\sqrt{2}}(\hat{a}_L - \hat{a}_S),\end{aligned}\quad (3.3.1)$$

where we have chosen  $\cos^2 \theta = \sin^2 \theta = \frac{1}{2}$  and  $\phi = \frac{\pi}{2}$ . The output signal operator is defined as

$$\hat{O} = \hat{N}_1 - \hat{N}_2 = \hat{a}_1^\dagger \hat{a}_1 - \hat{a}_2^\dagger \hat{a}_2. \quad (3.3.2)$$

It can be easily shown that

$$\hat{O} = \hat{a}_S \hat{a}_L^\dagger + \hat{a}_S^\dagger \hat{a}_L. \quad (3.3.3)$$

The local oscillator is usually prepared in a large amplitude coherent state  $|\beta_L\rangle$ , with  $\beta_L = |\beta_L|e^{i\phi_L}$ . The expectation value of the output signal operator is

$$\langle \hat{O} \rangle \equiv \langle \psi_S, \beta_L | \hat{O} | \psi_S, \beta_L \rangle = |\beta_L| \langle \psi_S | (\hat{a}_S e^{-i\phi_L} + \hat{a}_S^\dagger e^{i\phi_L}) | \psi_S \rangle = |\beta_L| \langle \psi_S | \hat{X}(\phi_L) | \psi_S \rangle, \quad (3.3.4)$$

where  $|\psi_S\rangle$  is the state of the signal mode. We can see that the expectation value of the output signal of the balanced homodyne detection is directly related to the expectation value of the quadrature amplitude of the signal mode. The phase of the detected quadrature amplitude is determined by the phase of the local oscillator. The expectation value of the square of the output signal operator is

$$\langle \hat{O}^2 \rangle = \langle (\hat{a}_S \hat{a}_L^\dagger + \hat{a}_S^\dagger \hat{a}_L)^2 \rangle \approx |\beta_L|^2 \langle \hat{X}^2(\phi_L) \rangle, \quad (3.3.5)$$

where we only keep terms in the order of  $|\beta_L|^2$ . This is a good approximation when  $|\beta_L|^2 \gg 1$ . Therefore, the variance of the output signal normalized by the strength of the local oscillator ( $|\beta_L|^2$ ) is the variance of the quadrature amplitude,

$$(\Delta X(\phi_L))^2 = \frac{\langle \hat{O}^2 \rangle - \langle \hat{O} \rangle^2}{|\beta_L|^2}. \quad (3.3.6)$$

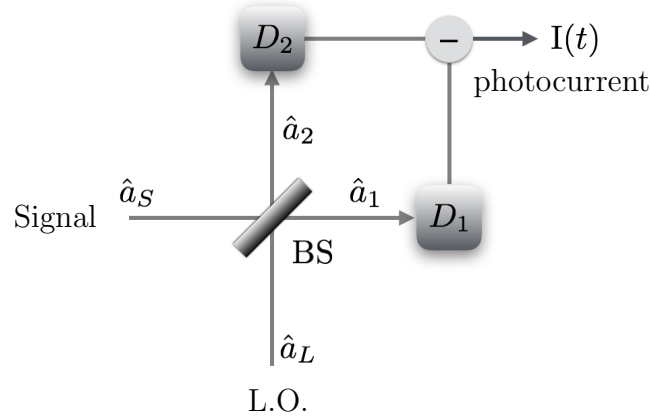


FIGURE 3.5: Schematic diagram of homodyne detection.

### 3.3.2 Ordinary homodyne detection

There is another way of doing homodyne detection: use an almost transparent beamsplitter and detect the photon number of the detector  $D_1$ . This corresponds to the ordinary homodyne detection [SZ97]. Assume that the reflection coefficient  $R = \sin^2 \theta$  is very close to zero. From Eq. (3.2.4) we find

$$\begin{aligned} \hat{a}_1 &= \sqrt{1-R} \hat{a}_S + \sqrt{R} \hat{a}_L, \\ \hat{a}_2 &= \sqrt{1-R} \hat{a}_L - \sqrt{R} \hat{a}_S, \end{aligned} \quad (3.3.7)$$

again we choose the phase as  $\phi = \frac{\pi}{2}$ . The expectation value of the photon number of the detector  $D_1$  is

$$\langle \hat{N}_1 \rangle = (1 - R) \langle \hat{a}_S^\dagger \hat{a}_S \rangle + R |\beta_L|^2 + \sqrt{R(1 - R)} |\beta_L| \langle \hat{X}(\phi_L) \rangle. \quad (3.3.8)$$

Although  $R$  is small, the amplitude of the local oscillator is chosen to be large enough so that the following condition applies,

$$R |\beta_L|^2 \gg (1 - R) \langle \hat{a}_S^\dagger \hat{a}_S \rangle. \quad (3.3.9)$$

Therefore the particle number operator can be approximated as

$$\hat{N}_1 \approx R \hat{a}_L^\dagger \hat{a}_L + \sqrt{R(1 - R)} (\hat{a}_S \hat{a}_L^\dagger + \hat{a}_S^\dagger \hat{a}_L). \quad (3.3.10)$$

To the order of  $|\beta_L|^2$ , the variance of the particle number normalized by the strength of the local oscillator is

$$\frac{(\Delta N_1)^2}{R |\beta_L|^2} \approx R + (1 - R) (\Delta X(\phi_L))^2. \quad (3.3.11)$$

The first term is the shot noise of the local oscillator, attenuated by a factor of  $R$ . The second term is basically the variance of the quadrature amplitude of the signal. In ordinary homodyne detection, the attenuated shot noise of the local oscillator should be subtracted first. If the reflection coefficient  $R$  is much smaller than the minimum variance of the quadrature amplitude, the first term can be neglected. The result then is similar to that of the balanced homodyne detection.

### 3.3.3 Self-homodyne detection

Suppose that an arbitrary quantum state  $|\psi\rangle$  (or  $\hat{\rho}$ ) is displaced by a displacement operator  $\hat{D}(\alpha_L)$ , where  $\alpha_L$  is large,  $|\alpha_L| \gg 1$ . The input mode  $\hat{a}$  is transformed into

$$\hat{a}' = \hat{a} + \alpha_L. \quad (3.3.12)$$

The photon number operator

$$\hat{N} = \hat{a}'^\dagger \hat{a}' = |\alpha_L|^2 + |\alpha_L| \hat{X}(\phi_L) + \hat{a}^\dagger \hat{a}, \quad (3.3.13)$$

and the square of the photon number is

$$\hat{N}^2 \approx |\alpha_L|^4 + 2|\alpha_L|^3 \hat{X}(\phi_L) + |\alpha_L|^2 (\hat{X}(\phi_L))^2 + 2|\alpha_L|^2 \hat{a}^\dagger \hat{a}, \quad (3.3.14)$$

where we only keep terms in the order of  $|\alpha_L|^2$ . Therefore the variance of the photon number normalized by  $|\alpha_L|^2$  is the variance of the quadrature amplitude of the initial state,

$$\frac{(\Delta N)^2}{|\alpha_L|^2} = (\Delta X(\phi_L))^2, \quad (3.3.15)$$

By comparing with the ordinary homodyne detection, we find that this simple scheme can be considered as a way of homodyne detection, called self-homodyne detection. Here  $|\alpha_L|^2$  corresponds to  $R|\beta_L|^2$  in Eq. (3.3.11).

### 3.4 Quantum circuit

Quantum circuit plays an important role in quantum computation, communication and information [Pre98, NC00]. A quantum circuit consists of a collection of quantum gates and lines. In continuous variable quantum computation and quantum information, a line represents a field mode and a quantum gate represents an unitary transformation. In this section, we introduce the pictorial representations of several important quantum gates that were discussed in the previous sections.

The first type of quantum gate is the single-mode quantum gate, which has one input mode and one output mode. Examples include the displacement, single-mode squeezer, phase shifter etc.. Fig. 3.6 show some examples of the single-mode quantum gates.

The second type of quantum gate is the two-mode quantum gate, which has two input modes and two output modes. Examples include the two-mode squeezer, beamsplitter etc.. Fig. 3.7 shows two examples that are frequently used in this thesis.

A combination of these elementary quantum gates forms a general quantum circuit. Fig. 3.8 is a simple example of a quantum circuit which consists of three quantum gates. In principle, any quantum circuit can be decomposed into elementary single-mode and two-mode quantum gates.

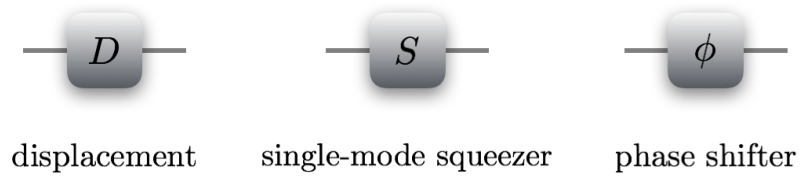


FIGURE 3.6: Single-mode quantum gates.

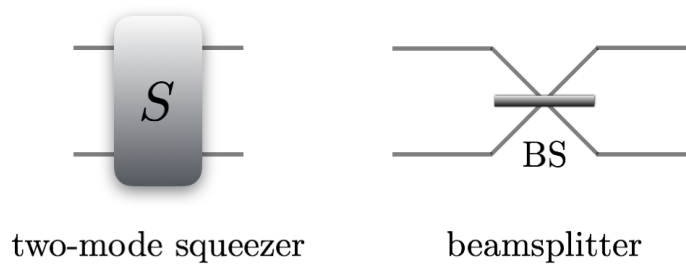


FIGURE 3.7: Two-mode quantum gates.

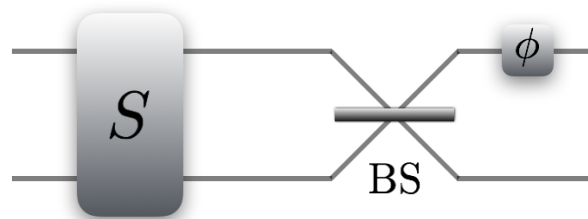


FIGURE 3.8: An example of a quantum circuit.

### 3.5 Summary and further reading

In this chapter, we introduce some basic concepts and tools in quantum optics: some typical quantum states, homodyne detection and quantum circuit. In particular, the homodyne detection is very important and can be used to detect quantum state in the relativistic systems and in the presence of gravity.

The textbooks by Walls and Milburn [WM07], Scully and Zubairy [SZ97] give a very complete

introduction to quantum optics. To learn more about the experimental aspects of quantum optics, one can refer to the textbook by Bachor and Ralph [BR04]. The textbook by Nielsen and Chuang [NC00] contains a comprehensive introduction to quantum information and computation. For Gaussian quantum information, one can refer to the review paper by Weedbrook *et al.* [WPGP<sup>+</sup>12]. For homodyne detection and homodyne tomography, one can refer to an excellent review paper by Lvovsky and Raymer [LR09].

# 4

## Introduction to Quantum Field Theory in Curved Spacetime

In this chapter, we are going to briefly review quantum field theory (QFT) in curved spacetime, which is concerned with the evolution of quantum fields on classical spacetimes. We first briefly introduce general relativity, then discuss the Rindler space and Schwarzschild spacetime. After that QFT in a general curved spacetime is discussed. Finally, we focus on QFT in Rindler space and Schwarzschild spacetime, in particular, the Unruh effect and Hawking effect.

## 4.1 General relativity in a nutshell

General relativity is a geometric theory of gravitation published by Einstein in 1915. It is a generalization of the special relativity and Newton's gravity theory. Let's begin with the Eötvös experiments [Har03] that test the equality of the gravitational and inertial mass. The gravitational mass of an object determines the gravitational force that it experiences in a gravitational field, and the inertial mass determines its acceleration. Eötvös experiments show that the accelerations of two objects made of different materials agree to a very high accuracy better than  $1.5 \times 10^{-13}$  [WND96]. This means the ratio between gravitational mass and inertial mass is the same for all objects, or we can say the gravitational mass and inertial mass are equal. In particular, objects with different compositions follow the same trajectory in a gravitational field.

The equality of gravitational and inertial mass implies that the gravitational field can be eliminated by falling freely. Imagine that there is a freely falling elevator (Einstein's elevator) in a gravitational field and an observer inside the elevator drops some objects. These objects are either at rest or undergo uniform motion (neglecting the resistance) with respect to the observer. The observer inside the freely falling elevator feels no gravity. On the other hand, the equality of gravitational and inertial mass implies that the gravity can be created by acceleration. Imagine that there is a small, closed laboratory that stays static in a gravitational field and the observers inside the laboratory can carry out experiments. Consider a same laboratory in an empty space but instead it uniformly accelerates, and observers inside can carry out experiments. By performing experiments in the laboratory, the observers cannot distinguish whether they are static in a gravitational field or uniformly accelerating in an empty space. The uniform acceleration and a uniform gravitational field are equivalent. This can be summarized as the Einstein's Equivalence Principle (EEP) [Car04]:

- **In a small enough region of spacetime, the law of physics reduce to those of special relativity; it is impossible to detect the existence of a gravitational field by means of local experiments.**

The EEP implies that gravitation can be described in terms of a geometry. Suppose that a coordinate system  $\{x^\mu\}$  is chosen to label the events in a spacetime. The metric tensor  $g_{\mu\nu}$  fully characterizes the properties of the spacetime. The spacetime interval between two very close spacetime events, with coordinates  $x^\mu$  and  $x^\mu + dx^\mu$ , is

$$ds^2 = g_{\mu\nu} dx^\mu dx^\nu. \quad (4.1.1)$$

A freely falling body follows a geodesic in the spacetime geometry, which is determined by the geodesic equation,

$$\frac{d^2 x^\mu}{d\lambda^2} + \Gamma_{\rho\sigma}^\mu \frac{dx^\rho}{d\lambda} \frac{dx^\sigma}{d\lambda} = 0, \quad (4.1.2)$$

where  $\lambda$  is the proper time of the massive body or an affine parameter for a massless body, and  $\Gamma_{\rho\sigma}^\mu$  is the Christoffel symbol [Car04],

$$\Gamma_{\rho\sigma}^\mu = \frac{1}{2} g^{\mu\alpha} (g_{\rho\alpha,\sigma} + g_{\sigma\alpha,\rho} - g_{\rho\sigma,\alpha}). \quad (4.1.3)$$

As emphasized by the EEP, the motion of one body cannot detect the presence of gravity. In order to detect the presence of gravity, one has to observe the relative motion between two bodies, which is described by the geodesic deviation equation, where the Riemann curvature tensor  $R_{\nu\rho\sigma}^\mu$  appears [Har03]. The Riemann curvature tensor  $R_{\nu\rho\sigma}^\mu$  is defined as

$$R_{\nu\rho\sigma}^\mu = \partial_\rho \Gamma_{\sigma\nu}^\mu - \partial_\sigma \Gamma_{\rho\nu}^\mu + \Gamma_{\rho\beta}^\mu \Gamma_{\sigma\nu}^\beta - \Gamma_{\sigma\beta}^\mu \Gamma_{\rho\nu}^\beta \quad (4.1.4)$$

and contains full information about the gravity.

We have discussed briefly how to describe gravity in terms of geometry and its influence on matter. On the other hand, the matter also influences the curvature of spacetime, which is described by the Einstein's equation. Suppose  $T_{\mu\nu}$  is the energy momentum tensor of the matter, the Einstein equation is

$$G_{\mu\nu} = 8\pi G T_{\mu\nu}, \quad (4.1.5)$$

where  $G_{\mu\nu}$  is the Einstein tensor constructed from the Riemann curvature tensor [Har03].

## 4.2 Rindler space

### 4.2.1 Uniformly accelerated observer

A uniformly accelerated observer moves with a constant proper acceleration in the Minkowski spacetime. Their proper acceleration is measured in their own reference frame. The worldline of a uniformly accelerated observer who accelerates along the  $x$ -axis is [Har03]

$$\begin{aligned} t &= a^{-1} \sinh(a\tau), \\ x &= a^{-1} \cosh(a\tau), \\ y &= \text{const.}, \\ z &= \text{const.}, \end{aligned} \tag{4.2.1}$$

where  $\tau$  is the proper time of the accelerated observer,  $a$  is the proper acceleration. Without loss of generality, we can set  $y = z = 0$ . The four velocity  $u^\mu$  of the uniformly accelerated observer can be easily derived from Eq. (4.2.1),

$$u^t = \frac{dt}{d\tau} = \cosh(a\tau), \quad u^x = \frac{dx}{d\tau} = \sinh(a\tau), \quad u^y = u^z = 0, \tag{4.2.2}$$

and the four acceleration  $a^\mu$  is

$$a^t = \frac{du^t}{d\tau} = a \sinh(a\tau), \quad a^x = \frac{du^x}{d\tau} = a \cosh(a\tau), \quad a^y = a^z = 0. \tag{4.2.3}$$

Therefore we have

$$\eta_{\mu\nu} a^\mu a^\nu = \eta_{tt} (a^t)^2 + \eta_{xx} (a^x)^2 = a^2. \tag{4.2.4}$$

This is consistent with the fact that the observer is uniformly accelerated. By looking carefully at the four velocity we note that there exist horizons for uniformly accelerated observers. When  $\tau \rightarrow -\infty$ ,  $u^\mu$  becomes asymptotically parallel to  $(-1, 1, 0, 0)$  but never go beyond the light ray  $(-1, 1, 0, 0)$ . When  $\tau \rightarrow +\infty$ ,  $u^\mu$  becomes asymptotically parallel to  $(1, 1, 0, 0)$  but never go beyond the light ray  $(1, 1, 0, 0)$ . Therefore there exist a past and a future horizon for the accelerated observers. The horizon can be clearly illustrated in the  $(1+1)$ -dimensional flat spacetime (or one can suppress the other two spatial dimensions in the figure), see Fig. 4.1.

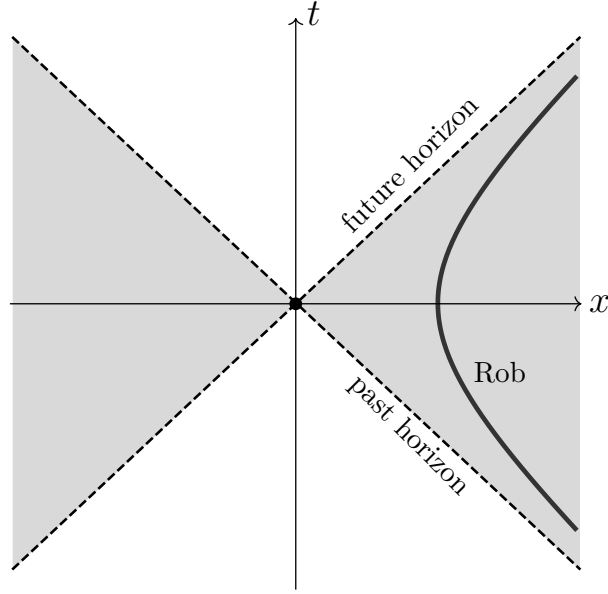


FIGURE 4.1: A uniformly accelerated observer Rob follows a hyperbolic worldline, which is confined within the right Rindler wedge formed by the past and future horizon.

### 4.2.2 Rindler coordinates

Instead of using Minkowski coordinates, accelerated observers can use a new coordinate system to describe the spacetime events in the Rindler space. The new coordinate system is called Rindler coordinate system, denoted as  $(\tau, \xi, y, z)$ . The proper time  $\tau$  of a particular accelerated observer is chosen as the global time, and  $\xi$  is a new spatial coordinate. The coordinate transformations between the Minkowski and Rindler coordinates are

$$\begin{aligned} t &= a^{-1}e^{a\xi} \sinh(a\tau), \\ x &= a^{-1}e^{a\xi} \cosh(a\tau), \end{aligned} \quad (4.2.5)$$

and  $y, z$  are the same. The line element can be written in terms of the Rindler coordinates as

$$ds^2 = -e^{2a\xi}(d\tau^2 - d\xi^2) + dy^2 + dz^2. \quad (4.2.6)$$

There is a corresponding Rindler coordinate system  $(\bar{\tau}, \bar{\xi}, y, z)$  in the left Rindler wedge, as shown in Fig. 4.2. The coordinate transformations are

$$\begin{aligned} t &= -a^{-1}e^{a\bar{\xi}} \sinh(a\bar{\tau}), \\ x &= -a^{-1}e^{a\bar{\xi}} \cosh(a\bar{\tau}). \end{aligned} \quad (4.2.7)$$

Note that we have used the prescription that  $\partial_{\bar{\tau}}$  is past directed. The line element is

$$ds^2 = -e^{2a\bar{\xi}}(d\bar{\tau}^2 - d\bar{\xi}^2) + dy^2 + dz^2. \quad (4.2.8)$$

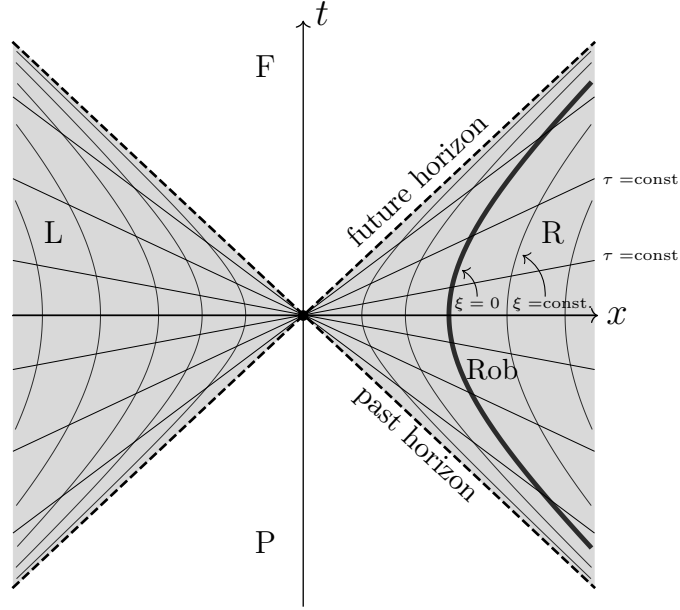


FIGURE 4.2: Rindler coordinate system. The whole Minkowski spacetime is divided into four wedges by the past and future horizons: right Rindler wedge (R), left Rindler wedge (L), future wedge (F) and past wedge (P). In the right Rindler wedge, the coordinates are  $(\tau, \xi, y, z)$ ; in the left Rindler wedge, the coordinates are  $(\bar{\tau}, \bar{\xi}, y, z)$ .

It is evident from Eq. (4.2.6) that the global time  $\tau$  is also the proper time of the accelerated observer with  $\xi = 0$ . Clocks of different stationary observers (with  $\xi = \xi_0 = \text{const.}$ ) in the accelerated frame tick at different rate. From the line element Eq. (4.2.6) it is easy to show that  $d\tau_0 = e^{a\xi_0}d\tau$ . So the the clock ticks slower when it is closer to the horizon ( $\xi_0 \rightarrow -\infty$ ). In fact, a stationary observer in accelerated frame is a uniformly accelerated observer with proper acceleration  $a_0 = ae^{-a\xi_0}$ . Their acceleration is huge when they are close to the horizon and is tiny when they are far away from the horizon.

## 4.3 Schwarzschild spacetime

The Schwarzschild metric was discovered by Schwarzschild in 1916 [Sch16]. It describes an empty, static, spherically symmetric and asymptotically flat spacetime. Examples include the spacetime outside a static and spherical star, a Schwarzschild black hole etc.. In this thesis we are interested in a Schwarzschild black hole, a peculiar spacetime region that one can fall in but can never come out. The interface between this region and the outside world is called the event horizon. An astrophysical, stellar mass black hole is believed to be formed from the collapse of a star [Tol39, OV39].

### 4.3.1 Schwarzschild metric and gravitational redshift

In terms of Schwarzschild coordinates  $(t, r, \theta, \phi)$ , the line element for the Schwarzschild spacetime is

$$ds^2 = -\left(1 - \frac{2M}{r}\right)dt^2 + \frac{1}{1 - \frac{2M}{r}}dr^2 + r^2(d\theta^2 + \sin^2\theta d\phi^2), \quad (4.3.1)$$

where  $M$  is the mass of the black hole and geometric unit has been used:  $G = c = 1$ . Static observers in the Schwarzschild spacetime are those observers with constant  $r, \theta$  and  $\phi$ . We can see from Eq. (4.3.1) that when a static observer is very far away from the black hole ( $r \rightarrow \infty$ ), their proper time coincides with the coordinate time  $t$ . Therefore we can consider  $t$  as the proper time of static observers at spatial infinity. When a static observer is close to the black hole, their clock ticks slower than that at spatial infinity. This is known as the gravitational redshift. Suppose that a static observer is at  $r = r_0, \theta = \phi = 0$ . From Eq. (4.3.1) we have

$$d\tau_0 = \sqrt{1 - \frac{2M}{r_0}}dt, \quad (4.3.2)$$

where  $\tau_0$  is proper time of the static observer at  $r_0$ . We note that as the static observer gets closer and closer to  $2M$ , their clock ticks slower and slower as compared to those at spatial infinity.

Imagine that if a static observer close to the horizon holds a source of light and sends a light signal radially toward spatial infinity, then the frequency of the light signal received by a

static observer at spatial infinity would be lower than when it was initially sent. We can verify this by a rigorous calculation. A light ray follows a null geodesic in a curved spacetime. If  $\mathbf{K}$  is a Killing vector of the spacetime, then its inner product with the four momentum of the light,  $\mathbf{p} \cdot \mathbf{K}$ , is a conserved quantity [Har03]. Since the Schwarzschild spacetime is static, it has a time-like Killing vector  $\mathbf{K}_t = (1, 0, 0, 0)$ . It can be shown that the four velocity of a static observer is proportional to the Killing vector  $\mathbf{K}_t$ , that is,  $\mathbf{u}_{\text{obs}} = \mathbf{K}_t / \sqrt{1 - \frac{2M}{r}}$ . Therefore we have  $\sqrt{1 - \frac{2M}{r}} \mathbf{p} \cdot \mathbf{u}_{\text{obs}}$  is a constant. Note that the quantity  $\mathbf{p} \cdot \mathbf{u}_{\text{obs}}$  is the frequency of the light as measured by the static observer [Har03]. The relation between the frequencies as measured by two static observers at  $r_1$  and  $r_0$  is

$$\omega_1 = \frac{\sqrt{1 - \frac{2M}{r_0}}}{\sqrt{1 - \frac{2M}{r_1}}} \omega_0. \quad (4.3.3)$$

This represents a gravitational redshift or blueshift, depending on the relative position of these two observers. If  $r_1 \rightarrow \infty$ , then we have

$$\omega_\infty = \sqrt{1 - \frac{2M}{r_0}} \omega_0. \quad (4.3.4)$$

This represents the gravitational redshift we mentioned before. A particular interesting limit is  $r_0 \rightarrow 2M$ . From Eq. (4.3.3), the frequency as measured by any static observer tends to be zero (this result can be generalized to any observer outside the black hole). It seems that the light is trapped at  $r = 2M$  and can never escape. This light-like surface is known as the event horizon of the Schwarzschild black hole. Nothing can escape from it even for light.

### 4.3.2 Maximally extended Schwarzschild spacetime

If we look more closely at the metric of the Schwarzschild spacetime, Eq. (4.3.1), we would find that the metric is divergent at  $r = 2M$ , the event horizon. However the Riemann curvature tensor at the horizon is finite [Har03]. This suggests that the singularity at the horizon is superficial and is due to the silliness of the Schwarzschild coordinates at the horizon. A choice of a different coordinate system, e.g., Eddington-Finkelstein coordinate system [Har03], can remove the coordinate singularity at the horizon. Another option is the Kruskal-Szekeres coordinate system [Har03], which is more relevant to this thesis. The

Kruskal-Szekeres coordinate are denoted by  $(T, R, \theta, \phi)$ , where  $\theta, \phi$  coordinates are the same as the Schwarzschild polar angles. The transformations between  $(T, R)$  and  $(t, r)$  are

$$\begin{cases} T = \left(\frac{r}{2M} - 1\right)^{1/2} e^{r/4M} \sinh\left(\frac{t}{4M}\right), \\ R = \left(\frac{r}{2M} - 1\right)^{1/2} e^{r/4M} \cosh\left(\frac{t}{4M}\right) \end{cases} \quad (4.3.5)$$

for  $r > 2M$  and

$$\begin{cases} T = \left(1 - \frac{r}{2M}\right)^{1/2} e^{r/4M} \cosh\left(\frac{t}{4M}\right), \\ R = \left(1 - \frac{r}{2M}\right)^{1/2} e^{r/4M} \sinh\left(\frac{t}{4M}\right) \end{cases} \quad (4.3.6)$$

for  $r < 2M$ . The line element of the Schwarzschild spacetime in terms of the new coordinates becomes

$$ds^2 = -\frac{32M^3}{r} e^{-r/2M} (dT^2 - dR^2) + r^2 (d\theta^2 + \sin^2 \theta d\phi^2), \quad (4.3.7)$$

where  $r$  should be considered as a function of  $T$  and  $R$ ,

$$r = 2M \left[ 1 + W\left(\frac{R^2 - T^2}{e}\right) \right], \quad (4.3.8)$$

where  $W(z)$  is the Lambert W function [CGH<sup>+</sup>96]. It is clear that the metric is regular at  $r = 2M$ . It is convenient to introduce null coordinates  $U$  and  $V$ ,

$$\begin{aligned} \bar{U} &= T - R, \\ \bar{V} &= T + R. \end{aligned} \quad (4.3.9)$$

The line element in terms of  $U$  and  $V$  is

$$ds^2 = -\frac{32M^3}{r} e^{-r/2M} dU dV + r^2 (d\theta^2 + \sin^2 \theta d\phi^2) \quad (4.3.10)$$

where  $r$  is the function of  $U$  and  $V$ ,

$$r = 2M [1 + W(-UV/e)]. \quad (4.3.11)$$

We denote the region outside the event horizon,  $r > 2M$ , as region I; and the region inside the horizon,  $r < 2M$ , as region II. In region I,

$$\begin{cases} U = -\exp\left\{-\frac{1}{4M}\left[t - r - 2M \ln\left(\frac{r}{2M} - 1\right)\right]\right\}, \\ V = \exp\left\{\frac{1}{4M}\left[t + r + 2M \ln\left(\frac{r}{2M} - 1\right)\right]\right\}. \end{cases} \quad (4.3.12)$$

TABLE 4.1: Signs of null coordinates  $U$  and  $V$  in four regions. Regions I and II are described by the original Schwarzschild coordinates, regions III and IV are the Kruskal extension.

	I	II	III	IV
U	-	+	+	-
V	+	+	-	-

In region II,

$$\begin{cases} U = \exp \left\{ -\frac{1}{4M} \left[ t - r - 2M \ln \left( 1 - \frac{r}{2M} \right) \right] \right\}, \\ V = \exp \left\{ \frac{1}{4M} \left[ t + r + 2M \ln \left( 1 - \frac{r}{2M} \right) \right] \right\}. \end{cases} \quad (4.3.13)$$

Thus  $U = \text{const.}$  represents a radially outgoing light ray, and  $V = \text{const.}$  represents a radially ingoing light ray. In addition, if we look at the signs of  $U$  and  $V$ , as summarized in Table 4.1, we note that in region I and II,  $V$  is positive. Mathematically, it is possible to extend the value of  $V$  to negative values. We thus obtain another two regions, III and IV, as summarized in Table 4.1. This is known as the Kruskal extension of the Schwarzschild geometry.

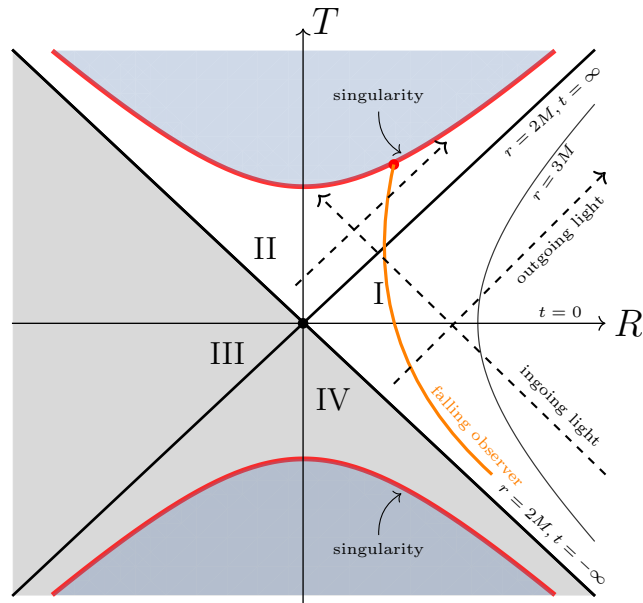


FIGURE 4.3: Kruskal diagram.

The four regions can be nicely illustrated in the Kruskal diagram, Fig. 4.3. Region I is the outside world (where we live) of the black hole and region II is the inside of the black hole. The shaded part, including regions III and IV, is the Kruskal extension. In the Kruskal diagram, the worldline of a light ray is represented by a  $45^\circ$  ( $U = \text{const.}$  or  $V = \text{const.}$ ) straight line. The future horizon is  $r = 2M, t = \infty$  (or  $U = 0$ ); the past horizon is  $r = 2M, t = -\infty$  (or  $V = 0$ ). Falling observers or ingoing light rays in region I will cross the future horizon and eventually hit the singularity. Outgoing light rays in region I will go to spatial infinity, while outgoing light rays in region II cannot escape and will hit the singularity. Note that there is no way of sending signals from region I to region III, and vice versa. So these two regions are causally disconnected.

### 4.3.3 Penrose diagram

By doing a conformal transformation, which preserves the angles of light rays, the Kruskal diagram can be drawn in a compact way. This is known as the Penrose diagram of the maximally extended Schwarzschild spacetime. The new null coordinates are  $(U', V')$  [Car04],

$$\begin{cases} U' = \tan^{-1}(U), \\ V' = \tan^{-1}(V). \end{cases} \quad (4.3.14)$$

The transformation maps the infinities of  $U$  and  $V$  to finite values of  $U'$  and  $V'$ . A typical Penrose diagram of the Schwarzschild spacetime is shown in Fig. 8.6. A few symbols are introduced in Fig. 8.6, the meanings of which are listed in Table 4.2.

## 4.4 Quantum field theory in curved spacetime

QFT in curved spacetime is concerned with the dynamics of quantum fields in curved background spacetimes. The background spacetime is considered to be classical and plays the role as a stage on which the quantum fields evolve. This is obviously not a complete theory because the back action of the quantum fields toward the spacetimes should also be taken



general covariance requires that the laws of physics are the same in any reference frame. Therefore the scalar field equation in curved spacetimes should be written in a generally covariant form. For a minimally coupled and massless scalar field  $\hat{\Phi}$ , the field equation is assumed to be [BD82]

$$\square\hat{\Phi} = 0, \quad (4.4.1)$$

where the d' Alembertian  $\square \equiv (\sqrt{-g})^{-1}\partial_\mu(\sqrt{-g}g^{\mu\nu}\partial_\nu)$  and  $g_{\mu\nu}$  is the metric of the background spacetime. This is known as the Klein-Gordon equation.

For a space-like hypersurface  $\Sigma$  with induced metric  $g_{\Sigma ij}$  and unit normal vector  $n^\mu$ , the Klein-Gordon inner product Eq. (2.2.18) is generalized to [BD82, CHM08]

$$\langle\phi_1, \phi_2\rangle = i \int_\Sigma (\phi_1^* \partial_\mu \phi_2 - \phi_2 \partial_\mu \phi_1^*) n^\mu \sqrt{g_\Sigma} d\Sigma, \quad (4.4.2)$$

where  $g_\Sigma$  is the determinant of the induced metric  $g_{\Sigma ij}$  and  $d\Sigma$  is the volume element of the space-like hypersurface  $\Sigma$ . The Klein-Gordon product is independent of the choice of  $\Sigma$  [HE73]. We can find a complete set of mode solutions  $\phi_i$  to the Klein-Gordon Eq. (4.4.1) that are orthonormal in terms of the Klein-Gordon product (4.4.2), namely,

$$\langle\phi_i, \phi_j\rangle = \delta_{ij}, \quad \langle\phi_i^*, \phi_j^*\rangle = -\delta_{ij}, \quad \langle\phi_i, \phi_j^*\rangle = 0. \quad (4.4.3)$$

Here  $i$  or  $j$  is to be understood as a collection of several indexes, including continuous and discrete indexes. The scalar field  $\hat{\Phi}$  can be expanded as

$$\hat{\Phi} = \sum_i (\hat{a}_i \phi_i + \hat{a}_i^\dagger \phi_i^*). \quad (4.4.4)$$

The annihilation and creation operators satisfy the standard boson commutation relations,

$$[\hat{a}_i, \hat{a}_j^\dagger] = \delta_{ij}, \quad [\hat{a}_i, \hat{a}_j] = [\hat{a}_i^\dagger, \hat{a}_j^\dagger] = 0. \quad (4.4.5)$$

The vacuum state  $|0\rangle_a$ , named  $a$ -vacuum, is defined as

$$\hat{a}_i |0\rangle_a = 0, \quad \forall i. \quad (4.4.6)$$

All other states can be generated from the  $a$ -vacuum and the creation operators  $\hat{a}_i^\dagger$ .

There is an essential difference between the QFT in the Minkowski spacetime and that in the curved spacetime. A natural set of modes, Eq. (4.5.10), can be chosen in the Minkowski spacetime, however the choice of modes in a general curved spacetime is ambiguous. The Minkowski spacetime is invariant under the translations in time and space, rotations in space, and Lorentz boosts, which consist of the elementary actions of the Poincaré group. In the Cartesian coordinates  $(t, x, y, z)$ , the Minkowski line element is invariant under the actions of the Poincaré group. Therefore, the Cartesian coordinates are the natural coordinates that manifest all the symmetries of the Minkowski spacetime. In particular, the vector  $\partial_t$  is a time-like Killing vector of the Minkowski spacetime and the modes Eq. (4.5.10) are the eigenfunctions of  $\partial_t$ . Furthermore, the Minkowski vacuum is invariant under the actions of the Poincaré group. In a general curved spacetime, there exist less symmetries or even no symmetry. Therefore no coordinate system is preferred in a curved spacetime. In addition, the principle of general covariance states that the coordinate systems are physically irrelevant. This implies in principle we are free to choose any coordinate system, and an arbitrary set of complete and orthonormal modes. Consequently, the definition of the vacuum state is ambiguous.

In this thesis, we focus on spacetimes that possess time-like Killing vectors so that positive and negative frequency modes can be defined; or spacetimes that are asymptotically flat in the distant past and distant future, so that a natural *in* and *out* vacuum are well defined. Suppose we have two sets of complete and orthonormal modes,  $\phi_i$  and  $\psi_i$ , e.g., they could be the *in* and *out* modes, respectively. The scalar field can be expanded in terms of the second set of modes as

$$\hat{\Phi} = \sum_i (\hat{b}_i \psi_i + \hat{b}_i^\dagger \psi_i^*), \quad (4.4.7)$$

where  $\hat{b}_i$  and  $\hat{b}_i^\dagger$  are the corresponding creation and annihilation operators. The vacuum state  $|0\rangle_b$ , named *b*-vacuum, is defined as

$$\hat{b}_i |0\rangle_b = 0, \quad \forall i. \quad (4.4.8)$$

All other states can be generated from the  $b$ -vacuum and the creation operators  $\hat{b}_i^\dagger$ . Since these two sets of modes are complete and orthonormal, one can expand  $\psi_i$  in terms of  $\phi_i$ ,

$$\psi_i = \sum_j (\alpha_{ij} \phi_j + \beta_{ij} \phi_j^*). \quad (4.4.9)$$

Conversely,

$$\phi_j = \sum_i (\alpha_{ij}^* \psi_i - \beta_{ij} \psi_i^*). \quad (4.4.10)$$

These relations are known as the Bogoliubov transformations [BD82].  $\alpha_{ij}$  and  $\beta_{ij}$  are the Bogoliubov coefficients, which can be obtained by using Eq. (4.4.3),

$$\begin{aligned} \alpha_{ij} &= \langle \phi_j, \psi_i \rangle, \\ \beta_{ij} &= -\langle \phi_j^*, \psi_i \rangle. \end{aligned} \quad (4.4.11)$$

Using the two ways of expansion of the scalar field  $\hat{\Phi}$ , Eqs. (4.4.4) and (4.4.7), one can derive the relations between the operators  $\hat{a}_i$  and  $\hat{b}_i$ ,

$$\hat{a}_i = \sum_j (\alpha_{ji} \hat{b}_j + \beta_{ji}^* \hat{b}_j^\dagger), \quad (4.4.12)$$

$$\hat{b}_j = \sum_i (\alpha_{ji}^* \hat{a}_i - \beta_{ji} \hat{a}_i^\dagger). \quad (4.4.13)$$

The Bogoliubov coefficients satisfy the following relations in order to preserve the commutation relations of  $\hat{a}_i$  and  $\hat{b}_i$ ,

$$\sum_k (\alpha_{ki} \alpha_{kj}^* - \beta_{ki}^* \beta_{kj}) = \delta_{ij}, \quad \sum_k (\alpha_{ki} \beta_{kj}^* - \beta_{ki}^* \alpha_{kj}) = 0, \quad (4.4.14)$$

$$\sum_k (\alpha_{ik} \alpha_{jk}^* - \beta_{ik} \beta_{jk}^*) = \delta_{ij}, \quad \sum_k (\alpha_{ik} \beta_{jk} - \beta_{ik} \alpha_{jk}) = 0. \quad (4.4.15)$$

If the Bogoliubov coefficients  $\beta_{ij} \neq 0$ , the  $a$ -vacuum and  $b$ -vacuum are not equivalent. In particular, the  $a$ -vacuum contains  $b$  particles,

$${}_a \langle 0 | \hat{b}_j^\dagger \hat{b}_j | 0 \rangle_a = \sum_k |\beta_{jk}|^2. \quad (4.4.16)$$

This is the ambiguity of the vacuum state that we mentioned before. A given time-like Killing vector field corresponds to a set of physical observers. If  $\phi_i$  and  $\psi_i$  are the eigenfunctions of

two different time-like Killing vector fields, then we can conclude that the notion of particles and vacuum are observer dependent. In particular, if  $\phi_i$  and  $\psi_i$  correspond to modes in the distant past and the distant future of an asymptotically flat spacetime, then an initial vacuum  $|0\rangle_a$  contains  $b$  particles if  $\beta_{ij} \neq 0$ . This process can be considered as particle creation from the evolution of the spacetime.

## 4.5 Quantum fields in Rindler space

In this section, we introduce QFT in Rindler space and the Unruh effect. Although Rindler space is not a curved spacetime, the studies of QFT in it give very important insights to the QFT in curved spacetime.

### 4.5.1 Rindler modes

In the Minkowski spacetime  $\partial_t$  is a time-like Killing vector field, the integral curves of which correspond to the worldlines of inertial observers. There exists another Killing vector field in the Minkowski spacetime:  $x\partial_t + t\partial_x = (x, t, 0, 0)$ . It is time-like when  $|x| > |t|$ , namely, in the right or left Rindler wedge. It turns out that the integral curves of  $x\partial_t + t\partial_x$  in the right or left Rindler wedge are associated with the worldlines of uniformly accelerated observers. As we have discussed in Section 4.2, the uniformly accelerated observers are stationary and the metric Eq. (4.2.6) is static in the Rindler coordinates. According to the general theory we discussed in Section 4.4, there exist a natural set of complete and orthonormal modes, and a corresponding vacuum. They are known as the Rindler modes and Rindler vacuum, respectively.

The Unruh effect is better illustrated in the QFT in  $(1+1)$ -dimensional Rindler space. We thus study an Hermitian massless scalar field  $\hat{\Phi}$  in  $(1+1)$ -dimensional Rindler space in this section. Generalization to higher dimensions can be found in [BD82, CHM08]. In the right Rindler wedge ( $x > |t|$ ), the Klein-Gordon equation in terms of the Rindler coordinates is

$$\left(-\frac{\partial}{\partial\tau^2} + \frac{\partial}{\partial\xi^2}\right)\hat{\Phi} = 0. \quad (4.5.1)$$

The positive frequency solutions should be proportional to  $e^{-i\omega\tau}$ , where  $\omega$  is a positive constant. The spatial part of the solutions can be a linear combination of  $e^{i\omega\xi}$  and  $e^{-i\omega\xi}$ . We choose normalized solutions as

$$g_{1\omega}^R(\tau, \xi) = \frac{1}{\sqrt{4\pi\omega}} e^{-i\omega(\tau+\xi)} = \frac{1}{\sqrt{4\pi\omega}} e^{-i\omega v}, \quad (4.5.2)$$

$$g_{2\omega}^R(\tau, \xi) = \frac{1}{\sqrt{4\pi\omega}} e^{-i\omega(\tau-\xi)} = \frac{1}{\sqrt{4\pi\omega}} e^{-i\omega u}, \quad (4.5.3)$$

where  $v = \tau + \xi$ ,  $u = \tau - \xi$  are null coordinates.  $g_{1\omega}^R(v)$  and  $g_{2\omega}^R(u)$  represent left-moving and right-moving modes, respectively. Note that the right Rindler modes are only defined in the right Rindler wedge, and should vanish in the left Rindler wedge if they are extended to the whole Minkowski spacetime. Therefore a more complete definition of the right Rindler modes is

$$g_{1\omega}^R(v) = \begin{cases} \frac{1}{\sqrt{4\pi\omega}} e^{-i\omega v}, & x > |t|; \\ 0, & x < -|t|. \end{cases} \quad (4.5.4)$$

$$g_{2\omega}^R(u) = \begin{cases} \frac{1}{\sqrt{4\pi\omega}} e^{-i\omega u}, & x > |t|; \\ 0, & x < -|t|. \end{cases} \quad (4.5.5)$$

These Rindler modes are orthonormal in terms of the Klein-Gordon inner product Eq. (4.4.2). The left-moving and right-moving right Rindler modes are decoupled for a massless scalar field. The Rindler modes in the left Rindler wedge can be obtained by simply replacing  $v, u$  by  $\bar{v} = -\bar{\tau} - \bar{\xi}$  and  $\bar{u} = -\bar{\tau} + \bar{\xi}$ .

$$g_{1\omega}^L(\bar{v}) = \begin{cases} 0, & x > |t|; \\ \frac{1}{\sqrt{4\pi\omega}} e^{-i\omega\bar{v}}, & x < -|t|. \end{cases} \quad (4.5.6)$$

$$g_{2\omega}^L(\bar{u}) = \begin{cases} 0, & x > |t|; \\ \frac{1}{\sqrt{4\pi\omega}} e^{-i\omega\bar{u}}, & x < -|t|. \end{cases} \quad (4.5.7)$$

By combining the right and left Rindler modes, we have an alternative set of complete and orthonormal modes for a massless scalar field in the (1+1)-dimensional Minkowski spacetime.

The scalar field  $\hat{\Phi}$  can be expanded in terms of the Rindler modes as

$$\hat{\Phi} = \int d\omega [\hat{b}_{1\omega}^R g_{1\omega}^R(v) + \hat{b}_{2\omega}^R g_{2\omega}^R(u) + \hat{b}_{1\omega}^L g_{1\omega}^L(\bar{v}) + \hat{b}_{2\omega}^L g_{2\omega}^L(\bar{u}) + \text{h.c.}], \quad (4.5.8)$$

where h.c. represents the Hermitian conjugate.  $\hat{b}_{m\omega}^R$  and  $\hat{b}_{m\omega}^L$  ( $m=1, 2$ ) are the Rindler annihilation operators. The Rindler vacuum state  $|0_R\rangle$  is defined as

$$\hat{b}_{m\omega}^R|0_R\rangle = \hat{b}_{m\omega}^L|0_R\rangle = 0, \quad \forall m, \omega. \quad (4.5.9)$$

### 4.5.2 Bogoliubov transformation

In  $(1+1)$ -dimensional Minkowski spacetime, the positive frequency eigenfunctions of the time-like Killing vector  $\partial_t$  are chosen as

$$\begin{aligned} u_{1k}(V) &= \frac{1}{\sqrt{4\pi k}} e^{-ikV}, \\ u_{2k}(U) &= \frac{1}{\sqrt{4\pi k}} e^{-ikU}, \end{aligned} \quad (4.5.10)$$

where  $V = t+x$ ,  $U = t-x$  and  $k$  is a positive constant, representing the Minkowski frequency. The scalar field  $\hat{\Phi}$  can be expanded in the standard way,

$$\hat{\Phi} = \int dk (\hat{a}_{1k} u_{1k} + \hat{a}_{2k} u_{2k} + \text{h.c.}), \quad (4.5.11)$$

where  $\hat{a}_{1k}, \hat{a}_{2k}, \hat{a}_{1k}^\dagger, \hat{a}_{2k}^\dagger$  are the Minkowski annihilation and creation operators satisfying the boson commutation relations,

$$[\hat{a}_{mk}, \hat{a}_{nk'}^\dagger] = \delta_{mn} \delta(k - k'), \quad [\hat{a}_{mk}, \hat{a}_{nk'}] = [\hat{a}_{mk}^\dagger, \hat{a}_{nk'}^\dagger] = 0,$$

with  $m, n = 1, 2$ . The Minkowski vacuum state  $|0_M\rangle$  is defined as

$$\hat{a}_{mk}|0_M\rangle = 0, \quad \forall m, k. \quad (4.5.12)$$

We are now going to derive the Bogoliubov transformations between the Minkowski modes and the Rindler modes. Since the left-moving and right-moving modes are independent, we first consider left-moving modes. The Rindler modes can be written in terms of the Minkowski modes as

$$g_{1\omega}^R(v) = \int_0^\infty dk [\alpha_{1\omega k}^R u_{1k}(V) + \beta_{1\omega k}^R u_{1k}^*(V)], \quad (4.5.13)$$

$$g_{1\omega}^L(\bar{v}) = \int_0^\infty dk [\alpha_{1\omega k}^L u_{1k}(V) + \beta_{1\omega k}^L u_{1k}^*(V)]. \quad (4.5.14)$$

The Bogoliubov coefficients can be calculated directly using the Klein-Gordon inner product. However, due to the special form of the Minkowski modes, an easier way to find  $\alpha_{1\omega k}^R$  is to multiply Eq. (4.5.13) by  $e^{ikV}/2\pi$  with  $k > 0$ , and integrate over  $V$ . We find

$$\alpha_{1\omega k}^R = \frac{1}{2\pi} \sqrt{\frac{k}{\omega}} \int_0^\infty dV (aV)^{-i\omega/a} e^{ikV}. \quad (4.5.15)$$

We have used the relation  $aV = e^{av}$ , so that  $g_{1\omega}^R(v) \propto (aV)^{-i\omega/a}$ . The integral Eq. (4.5.15) is convergent if we shift the integration path from the real axis to  $V + i\epsilon$ , with  $\epsilon \rightarrow 0^+$ . Since the integrand is analytic, according to the Cauchy theorem, the contour integral along  $C_1 + C_2 + C_3$ , as shown in Fig. 4.5, is vanishing. Furthermore, the integrand along the path  $C_2$  goes to zero when  $|V| \rightarrow \infty$ . We thus can shift the integration path  $C_1$  to the positive imaginary axis  $C_3$ . According to the definition of Gamma's function [AS72], we find

$$\alpha_{1\omega k}^R = \frac{ie^{\pi\omega/2a}}{2\pi\sqrt{\omega k}} \left(\frac{k}{a}\right)^{i\omega/a} \Gamma(1 - i\omega/a), \quad (4.5.16)$$

where  $\Gamma(z)$  is the Gamma function.

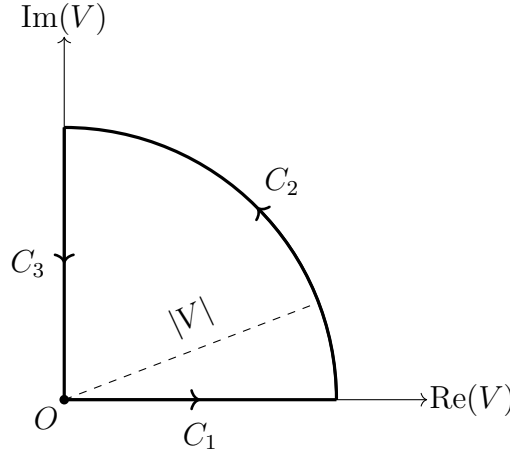


FIGURE 4.5: Integration contour in the complex  $V$  plane.

The coefficient  $\beta_{1\omega k}^R$  can be calculated in a similar way. The phase  $e^{ikV}$  in Eq. (4.5.15) is replaced by  $e^{-ikV}$  and the integration path should be shifted to the negative imaginary axis.

We find

$$\beta_{1\omega k}^R = -\frac{ie^{-\pi\omega/2a}}{2\pi\sqrt{\omega k}} \left(\frac{k}{a}\right)^{i\omega/a} \Gamma(1 - i\omega/a). \quad (4.5.17)$$

The derivation of  $\alpha_{1\omega k}^L$  and  $\beta_{1\omega k}^L$  proceeds similarly. We find

$$\alpha_{1\omega k}^L = \alpha_{1\omega k}^{R*} = -\frac{ie^{\pi\omega/2a}}{2\pi\sqrt{\omega k}} \left(\frac{k}{a}\right)^{-i\omega/a} \Gamma(1 + i\omega/a), \quad (4.5.18)$$

$$\beta_{1\omega k}^L = \beta_{1\omega k}^{R*} = \frac{ie^{-\pi\omega/2a}}{2\pi\sqrt{\omega k}} \left(\frac{k}{a}\right)^{-i\omega/a} \Gamma(1 + i\omega/a). \quad (4.5.19)$$

The right-moving Rindler modes can be written as

$$g_{2\omega}^R(u) = \int_0^\infty dk [\alpha_{2\omega k}^R u_{2k}(U) + \beta_{2\omega k}^R u_{2k}^*(U)], \quad (4.5.20)$$

$$g_{2\omega}^L(\bar{u}) = \int_0^\infty dk [\alpha_{2\omega k}^L u_{2k}(U) + \beta_{2\omega k}^L u_{2k}^*(U)]. \quad (4.5.21)$$

The Bogoliubov transformation coefficients  $\alpha_{2\omega k}^R$ ,  $\beta_{2\omega k}^R$ ,  $\alpha_{2\omega k}^L$  and  $\beta_{2\omega k}^L$  can be shown to be

$$\alpha_{2\omega k}^R = \alpha_{1\omega k}^L, \quad \beta_{2\omega k}^R = \beta_{1\omega k}^L, \quad (4.5.22)$$

$$\alpha_{2\omega k}^L = \alpha_{1\omega k}^R, \quad \beta_{2\omega k}^L = \beta_{1\omega k}^R. \quad (4.5.23)$$

### 4.5.3 Unruh temperature

We have shown explicitly that the Bogoliubov coefficients  $\beta_{m\omega k}^{R,L}$  are not vanishing. This means the Minkowski vacuum is inequivalent to the Rindler vacuum. The Minkowski vacuum is empty of Minkowski particles but not Rindler particles. The expectation value of the Rindler particle number in the Minkowski vacuum is

$$\langle 0_M | \hat{b}_{m\omega}^{R\dagger} \hat{b}_{m\omega}^R | 0_M \rangle = \langle 0_M | \hat{b}_{m\omega}^{L\dagger} \hat{b}_{m\omega}^L | 0_M \rangle = \frac{\delta(0)}{e^{2\pi\omega/a} - 1}. \quad (4.5.24)$$

The formally divergent quantity  $\delta(0)$  appears because we consider a space with infinite volume. We can see that the Rindler particle number distribution is a thermal distribution with temperature  $T_U = a/2\pi$ , which is known as the Unruh temperature [Unr76]. The Rindler particles can be understood as particles observed by a uniformly accelerated observer. This means a uniformly accelerated observer experiences a thermal bath with the Unruh temperature in the Minkowski vacuum.

The Unruh temperature is proportional to the acceleration of the accelerated observer. If we recover all the physical constants we find

$$T_U = \frac{\hbar a}{2\pi c k_B}, \quad (4.5.25)$$

where  $\hbar$  is the reduced Plank constant,  $c$  is the speed of light in vacuum and  $k_B$  is the Boltzmann constant. In order to observe temperature  $T_U \sim 1K$ , one has to accelerate with acceleration  $a \sim 10^{20} \text{ kg} \cdot \text{m}/\text{s}^2$ , a huge acceleration. It is therefore extremely difficult to detect the Unruh effect with the state-of-art technologies.

#### 4.5.4 Unruh modes

It is very useful to introduce Unruh modes [Unr76] that are linear combinations of only positive frequency Minkowski modes, and thus share the same vacuum state with the Minkowski modes. In Unruh's original paper [Unr76], the Unruh modes are defined through analytically extending the Rindler modes to the whole spacetime region. The left-moving Rindler mode in the right Rindler wedge,  $g_{1\omega}^R = (4\pi\omega)^{-1/2}(aV)^{-i\omega/a}$  for  $V > 0$ , is extended to the negative real axis along a small circle centred on  $V = 0$  and in the lower-half complex plane, leading to  $(4\pi\omega)^{-1/2}e^{-\pi\omega/a}(-aV)^{-i\omega/a} = e^{-\pi\omega/a}g_{1\omega}^{L*}$  for  $V < 0$ . The corresponding normalized Unruh mode is thus defined as

$$G_{1\omega}(V) = \cosh(r_\omega)g_{1\omega}^R(v) + \sinh(r_\omega)g_{1\omega}^{L*}(\bar{v}), \quad (4.5.26)$$

where the factor  $r_\omega$  satisfies  $\tanh(r_\omega) = e^{-\pi\omega/a}$ . Since  $G_{1\omega}(V)$  is analytic and bounded in the lower-half complex plane, it thus can be expressed purely in terms of  $u_{1k}(V)$ , which are also analytic and bounded in the lower-half complex plane. This means  $G_{1\omega}(V)$  contains only positive frequency Minkowski modes. The left-moving Rindler mode in the left Rindler wedge,  $g_{1\omega}^L = (4\pi\omega)^{-1/2}(-aV)^{i\omega/a}$  for  $V < 0$ , is extended to the positive real axis along a small circle centred on  $V = 0$  and in the lower half complex plane, leading to  $(4\pi\omega)^{-1/2}e^{-\pi\omega/a}(aV)^{i\omega/a} = e^{-\pi\omega/a}g_{1\omega}^{R*}$  for  $V > 0$ . The corresponding normalized Unruh mode is thus defined as

$$\bar{G}_{1\omega}(V) = \cosh(r_\omega)g_{1\omega}^L(\bar{v}) + \sinh(r_\omega)g_{1\omega}^{R*}(v). \quad (4.5.27)$$

The Unruh mode  $\bar{G}_{1\omega}(V)$  is also analytic in the lower-half complex plane and can be expressed purely in terms of positive Minkowski modes.

The above argument is from the perspective of analyticity. In fact, one can straightforwardly show that the Unruh modes Eqs. (4.5.26) and (4.5.27) are linear combinations of positive frequency modes  $e^{-ikV}$ . Substituting the Bogoliubov transformations, Eqs. (4.5.13) and (4.5.14), into the definition of  $G_{1\omega}$ , we find

$$G_{1\omega} = \frac{1}{\sqrt{1 - e^{-2\pi\omega/a}}} \int dk [(\alpha_{1\omega k}^R + e^{-\pi\omega/a} \beta_{1\omega k}^{L*}) u_{1k} + (\beta_{1\omega k}^R + e^{-\pi\omega/a} \alpha_{1\omega k}^{L*}) u_{1k}^*]. \quad (4.5.28)$$

From the explicit expressions of the Bogoliubov coefficients, Eqs. (4.5.16)-(4.5.19),

$$\alpha_{1\omega k}^R + e^{-\pi\omega/a} \beta_{1\omega k}^{L*} = \frac{ie^{\pi\omega/2a}(1 - e^{-2\pi\omega/a})}{2\pi\sqrt{\omega k}} \left(\frac{k}{a}\right)^{i\omega/a} \Gamma(1 - i\omega/a), \quad (4.5.29)$$

$$\beta_{1\omega k}^R + e^{-\pi\omega/a} \alpha_{1\omega k}^{L*} = 0. \quad (4.5.30)$$

Therefore we have

$$G_{1\omega}(V) = \int dk A_{k\omega} u_{1k}(V) \quad (4.5.31)$$

where

$$A_{k\omega} = \frac{i\sqrt{2 \sinh(\pi\omega/a)}}{2\pi\sqrt{\omega k}} \left(\frac{k}{a}\right)^{i\omega/a} \Gamma(1 - i\omega/a). \quad (4.5.32)$$

It is clear that the Unruh mode  $G_{1\omega}(V)$  contains purely positive frequency Minkowski modes.

Similarly, using the Bogoliubov transformations, Eqs. (4.5.13) and (4.5.14), we find

$$\bar{G}_{1\omega} = \frac{1}{\sqrt{1 - e^{-2\pi\omega/a}}} \int dk [(\alpha_{1\omega k}^L + e^{-\pi\omega/a} \beta_{1\omega k}^{R*}) u_{1k} + (\beta_{1\omega k}^L + e^{-\pi\omega/a} \alpha_{1\omega k}^{R*}) u_{1k}^*]. \quad (4.5.33)$$

From the explicit expressions of the Bogoliubov coefficients, Eqs. (4.5.16)-(4.5.19),

$$\alpha_{1\omega k}^L + e^{-\pi\omega/a} \beta_{1\omega k}^{R*} = -\frac{ie^{\pi\omega/2a}(1 - e^{-2\pi\omega/a})}{2\pi\sqrt{\omega k}} \left(\frac{k}{a}\right)^{-i\omega/a} \Gamma(1 + i\omega/a), \quad (4.5.34)$$

$$\beta_{1\omega k}^L + e^{-\pi\omega/a} \alpha_{1\omega k}^{R*} = 0. \quad (4.5.35)$$

Therefore we have

$$\bar{G}_{1\omega}(V) = \int dk B_{k\omega} u_{1k}(V) \quad (4.5.36)$$

where

$$B_{k\omega} = -\frac{i\sqrt{2 \sinh(\pi\omega/a)}}{2\pi\sqrt{\omega k}} \left(\frac{k}{a}\right)^{-i\omega/a} \Gamma(1 + i\omega/a). \quad (4.5.37)$$

It is clear that the Unruh mode  $\bar{G}_{1\omega}(V)$  contains purely positive frequency Minkowski modes. Note that  $B_{k\omega} = A_{k\omega}^*$ .

Right-moving Unruh modes are defined as

$$G_{2\omega}(U) = \cosh(r_\omega)g_{2\omega}^R(u) + \sinh(r_\omega)g_{2\omega}^{L*}(\bar{u}), \quad (4.5.38)$$

$$\bar{G}_{2\omega}(U) = \cosh(r_\omega)g_{2\omega}^L(\bar{u}) + \sinh(r_\omega)g_{2\omega}^{R*}(u). \quad (4.5.39)$$

It can be similarly shown that

$$G_{2\omega}(U) = \int dk B_{k\omega} u_{2k}(U), \quad \bar{G}_{2\omega}(U) = \int dk A_{k\omega} u_{2k}(U). \quad (4.5.40)$$

Therefore the right-moving Unruh modes are linear combinations of positive frequency modes  $e^{-ikU}$ . The Unruh modes can be written in a compact way,

$$\begin{aligned} G_{1\omega}(V) &= F(\omega, a)(aV)^{-i\omega/a}, \\ \bar{G}_{1\omega}(V) &= F(\omega, a)(-aV)^{i\omega/a}, \\ G_{2\omega}(U) &= F(\omega, a)(-aU)^{i\omega/a}, \\ \bar{G}_{2\omega}(U) &= F(\omega, a)(aU)^{-i\omega/a}, \end{aligned} \quad (4.5.41)$$

with  $F(\omega, a) \equiv \frac{e^{\pi\omega/2a}}{\sqrt{4\pi\omega}\sqrt{2\sinh(\pi\omega/a)}}$ .  $G_{1\omega}(V)$ ,  $\bar{G}_{1\omega}(V)$ ,  $G_{2\omega}(U)$  and  $\bar{G}_{2\omega}(U)$  are all analytic in the lower-half complex plane.

The Unruh modes form a set of complete and orthonormal modes. The scalar field can be expanded in terms of the Unruh modes,

$$\hat{\Phi} = \int d\omega (\hat{c}_{1\omega}G_{1\omega} + \hat{d}_{1\omega}\bar{G}_{1\omega} + \hat{c}_{2\omega}G_{2\omega} + \hat{d}_{2\omega}\bar{G}_{2\omega} + \text{h.c.}), \quad (4.5.42)$$

where  $\hat{c}_{1\omega}$ ,  $\hat{d}_{1\omega}$ ,  $\hat{c}_{2\omega}$  and  $\hat{d}_{2\omega}$  are the corresponding Unruh annihilation operators. These operators satisfy boson commutation relations,

$$[\hat{c}_{m\omega}, \hat{c}_{n\omega'}^\dagger] = \delta_{mn}\delta(\omega - \omega'), \quad [\hat{d}_{m\omega}, \hat{d}_{n\omega'}^\dagger] = \delta_{mn}\delta(\omega - \omega'), \quad (4.5.43)$$

with all others vanishing. The relations between the Unruh and Rindler operators can be derived as

$$\begin{aligned}\hat{c}_{m\omega} &= \cosh(r_\omega)\hat{b}_{m\omega}^R - \sinh(r_\omega)\hat{b}_{m\omega}^{L\dagger}, \\ \hat{d}_{m\omega} &= \cosh(r_\omega)\hat{b}_{m\omega}^L - \sinh(r_\omega)\hat{b}_{m\omega}^{R\dagger}.\end{aligned}\quad (4.5.44)$$

Conversely,

$$\begin{aligned}\hat{b}_{m\omega}^R &= \cosh(r_\omega)\hat{c}_{m\omega} + \sinh(r_\omega)\hat{d}_{m\omega}^\dagger, \\ \hat{b}_{m\omega}^L &= \cosh(r_\omega)\hat{d}_{m\omega} + \sinh(r_\omega)\hat{c}_{m\omega}^\dagger.\end{aligned}\quad (4.5.45)$$

We can see that the Rindler modes  $(\hat{b}_{m\omega}^R, \hat{b}_{m\omega}^L)$  and Unruh modes  $(\hat{c}_{m\omega}, \hat{d}_{m\omega})$  are related by a two-mode squeezing transformation with a frequency dependent squeezing parameter  $r_\omega$ .

The relations between Unruh modes and Minkowski modes can be derived as

$$\hat{a}_{1k} = \int d\omega (A_{k\omega}\hat{c}_{1\omega} + B_{k\omega}\hat{d}_{1\omega}), \quad (4.5.46)$$

$$\hat{a}_{2k} = \int d\omega (B_{k\omega}\hat{c}_{2\omega} + A_{k\omega}\hat{d}_{2\omega}). \quad (4.5.47)$$

Conversely,

$$\hat{c}_{1\omega} = \int dk B_{k\omega}\hat{a}_{1k}, \quad \hat{d}_{1\omega} = \int dk A_{k\omega}\hat{a}_{1k}, \quad (4.5.48)$$

$$\hat{c}_{2\omega} = \int dk A_{k\omega}\hat{a}_{2k}, \quad \hat{d}_{2\omega} = \int dk B_{k\omega}\hat{a}_{2k}. \quad (4.5.49)$$

It is thus clear that the Unruh modes and Minkowski modes share the same vacuum,

$$\hat{c}_{m\omega}|0_M\rangle = \hat{d}_{m\omega}|0_M\rangle = 0. \quad (4.5.50)$$

#### 4.5.5 Minkowski vacuum as an entangled state

From the transformations between Unruh modes and Rindler modes, Eq. (4.5.45), we can see that the Minkowski vacuum is a two-mode squeezed state of the left and right Rindler modes. In the discrete-frequency limit, the Minkowski vacuum can be written as [Unr76]

$$\begin{aligned}|0_M\rangle &= \prod_i C_i \sum_{n_i=0}^{\infty} \frac{e^{-\pi n_i \omega_i / a}}{n_i!} (\hat{b}_{1\omega_i}^{R\dagger} \hat{b}_{1\omega_i}^{L\dagger})^{n_i} |0_R\rangle \\ &= \prod_i \left( C_i \sum_{n_i=0}^{\infty} e^{-\pi n_i \omega_i / a} |n_i, R\rangle \otimes |n_i, L\rangle \right),\end{aligned}\quad (4.5.51)$$

where  $C_i = \sqrt{1 - e^{-2\pi\omega_i/a}}$  is the normalization factor. Here  $|n_i, R\rangle$  and  $|n_i, L\rangle$  are the  $n_i$ -particle states with Rindler frequency  $\omega_i$  in the right and left Rindler wedge, respectively. A similar expression to Eq. (4.5.51) also holds for the right moving modes. If one only has access to the fields in the right Rindler wedge, then he (or she) traces out the state in the left Rindler wedge, obtaining

$$\hat{\rho}_R = \prod_i \left( C_i^2 \sum_{n_i=0}^{\infty} e^{-\pi n_i \omega_i / a} |n_i, R\rangle \langle n_i, R| \right). \quad (4.5.52)$$

This is a density matrix for the system of free bosons with Unruh temperature  $T_U = a/2\pi$ . Therefore the Minkowski vacuum state looks like a thermal state with Unruh temperature  $T_U = a/2\pi$  as viewed by a uniformly accelerated observer with acceleration  $a$  in the right (or left) Rindler wedge.

#### 4.5.6 Unruh-DeWitt detector

In the previous subsections, we have shown that the Minkowski vacuum looks like a thermal state if the observer is restricted either to the right or left Rindler wedge. A uniformly accelerated observer with acceleration  $a$  experiences a thermal bath with the Unruh temperature  $T_U = a/2\pi$ . It is thus expected that a uniformly accelerated detector would respond to the thermal radiation, e.g., being excited from its ground state to excited states. In this subsection, we introduce a simple particle detector model, the Unruh-DeWitt detector [Unr76, DeW79], that responds to the quantum fields and discuss the response of a uniformly accelerated Unruh-DeWitt detector in the Minkowski vacuum.

Assume that an Unruh-DeWitt detector moves along a world line described by  $x^\mu(\tau)$ , where  $\tau$  is the proper time of the detector. The detector couples to the scalar field  $\hat{\Phi}$  through the interaction Hamiltonian

$$\hat{H}_I = \lambda \chi(\tau) \hat{m}(\tau) \hat{\Phi}(x^\mu(\tau)), \quad (4.5.53)$$

where  $\lambda$  is a small coupling constant,  $\chi(\tau)$  is the switching function that characterizes he turning on and off of the interaction, and  $\hat{m}(\tau)$  is the monopole of the detector. Suppose

that the initial state of the scalar field is the Minkowski vacuum  $|0_M\rangle$ , and the initial state for the detector is its ground state  $|E_0\rangle$ . When the detector moves and interacts with the scalar field, it may not remain in its ground state and could be excited to a higher energy eigenstate  $|E\rangle$ . Meanwhile, the scalar field may make a transition to a new state  $|\psi\rangle$ . If the coupling constant  $\lambda$  is sufficiently small, perturbation theory can be used to calculate the transition probability of the detector from its ground state to a higher energy state. To first order, the transition amplitude is

$$i\lambda\langle E, \psi | \int_{-\infty}^{+\infty} d\tau \chi(\tau) \hat{m}(\tau) \hat{\Phi}(x^\mu(\tau)) | E_0, 0_M \rangle. \quad (4.5.54)$$

The time evolution of the monopole is

$$\hat{m}(\tau) = e^{i\hat{H}_0\tau} \hat{m}(0) e^{-i\hat{H}_0\tau}, \quad (4.5.55)$$

where  $\hat{H}_0$  is the free Hamiltonian of the internal dynamics of the detector,  $\hat{H}_0|E\rangle = E|E\rangle$ . Substituting Eq. (4.5.55) into Eq. (4.5.54), the transition amplitude becomes

$$i\lambda\langle E | \hat{m}(0) | E_0 \rangle \int_{-\infty}^{+\infty} d\tau \chi(\tau) e^{i(E-E_0)\tau} \langle \psi | \hat{\Phi}(x^\mu(\tau)) | 0_M \rangle. \quad (4.5.56)$$

By squaring the modulus of the transition amplitude Eq. (4.5.56) and summing over all the final states of the scalar field, we obtain the transition probability of the detector from its ground state  $|E_0\rangle$  to an excited state  $|E\rangle$ ,

$$P(E_0 \rightarrow E) = |\lambda|^2 |\langle E | \hat{m}(0) | E_0 \rangle|^2 \mathcal{F}(E - E_0), \quad (4.5.57)$$

where the response function  $\mathcal{F}(E)$ , which does not depend on the internal structure of the detector, is

$$\mathcal{F}(E) = \int_{-\infty}^{+\infty} d\tau \int_{-\infty}^{+\infty} d\tau' \chi(\tau) \chi(\tau') e^{-iE(\tau-\tau')} G^+(x^\mu(\tau), x^\mu(\tau')), \quad (4.5.58)$$

with  $G^+(x^\mu(\tau), x^\mu(\tau')) = \langle 0_M | \hat{\Phi}(x^\mu(\tau)) \hat{\Phi}(x^\mu(\tau')) | 0_M \rangle$  the positive frequency Wightman function. If the world line of the detector is along the orbit of a time-like Killing vector and the Minkowski vacuum  $|0_M\rangle$  is invariant under the isometry generated by the time-like Killing vector, the Wightman function is invariant under the time translation along the

world line. It is then convenient to consider the transition probability per unit proper time (transition rate), which is proportional to [BD82]

$$\dot{\mathcal{F}}(E) = \int_{-\infty}^{+\infty} ds e^{-iEs} G^+(s). \quad (4.5.59)$$

Note that  $\dot{\mathcal{F}}(E)$  is basically the Fourier transform of the positive frequency Wightman function.

We discuss two examples: the responses of a static detector and a uniformly accelerated detector interacting with a massless scalar field in the Minkowski vacuum. The Wightman function is given by Eq. (2.2.34). For a static inertial detector, the Wightman function becomes

$$G_{\text{static}}^+(\tau - \tau') = -\frac{1}{4\pi^2} \frac{1}{(\tau - \tau' - i\epsilon)^2}. \quad (4.5.60)$$

The transition rate is proportional to

$$\dot{\mathcal{F}}_{\text{static}}(E) = -\frac{1}{4\pi^2} \int_{-\infty}^{+\infty} ds \frac{e^{-iEs}}{(s - i\epsilon)^2} = 0. \quad (4.5.61)$$

Note that we have assumed  $E > 0$ . Therefore, if the scalar field is in the Minkowski vacuum state, the static inertial detector cannot be excited from its ground state to a higher energy state.

For a uniformly accelerated detector with acceleration  $a$ , the world line is given by Eq. (4.2.1). The Wightman function for an accelerated trajectory can be derived as [BD82]

$$G_{\text{acc}}^+(\tau - \tau') = -\frac{1}{16\pi^2} \frac{a^2}{\sinh^2(a(\tau - \tau')/2 - ia\epsilon)}. \quad (4.5.62)$$

Using the identity

$$\frac{1}{\sinh^2(\pi x)} = \frac{1}{\pi^2} \sum_{k=-\infty}^{+\infty} \frac{1}{(x - k)^2}, \quad (4.5.63)$$

we can write the Wightman function for the accelerated trajectory as

$$G_{\text{acc}}^+(\tau - \tau') = -\frac{1}{4\pi^2} \sum_{k=-\infty}^{+\infty} \frac{1}{(\tau - \tau' - 2i\epsilon + 2\pi ik/a)^2}. \quad (4.5.64)$$

Substituting this into Eq. (4.5.59), we find

$$\begin{aligned}\dot{\mathcal{F}}_{\text{acc}}(E) &= -\frac{1}{4\pi^2} \sum_{k=-\infty}^{+\infty} \int_{-\infty}^{+\infty} ds \frac{e^{-iEs}}{(s - 2i\epsilon + 2\pi ik/a)^2} = \frac{E}{2\pi} \sum_{k=1}^{+\infty} e^{-2\pi kE/a} \\ &= \frac{E}{2\pi} \frac{1}{e^{2\pi E/a} - 1}.\end{aligned}\tag{4.5.65}$$

We have used the residue theorem in the second equality. The appearance of the Planck factor  $(e^{2\pi E/a} - 1)^{-1}$  in the transition rate Eq. (4.5.65) indicates that the response of a uniformly accelerated Unruh-DeWitt detector in the Minkowski vacuum  $|0_M\rangle$  is thermal. The temperature of the thermal response is the Unruh temperature  $T_U = a/2\pi$ . This is consistent with the results obtained via a different way, i.e., the Bogoliubov transformation of field modes.

## 4.6 Quantum fields in Schwarzschild spacetime

### 4.6.1 Particle creation from a collapsing star

The well known Hawking radiation from a black hole was discovered by Hawking when he studied the quantum fields on the geometry of a collapsing star [Haw75]. Here we briefly summarize the essential physics of particle creation from a collapsing star without going into technical details. The details of explicit calculations can be found in [Haw75, Wal75, Par75].

At the final evolution stage of a massive star, no other forces can balance the self gravity of the star and it collapses to form a black hole [Tol39, OV39]. We consider a simplified model of the star collapsing: a spherically symmetric matter ball collapses to form a Schwarzschild black hole. In the exterior of the matter ball the space is empty, so the spacetime is described by the Schwarzschild metric Eq. (4.3.1). During the process of collapsing and even after the formation of the event horizon, the exterior spacetime is not affected according to the Birkhoff's theorem [Bir23]. Here the exact metric inside the matter ball is irrelevant. The essential point is that the quantum fields propagating through the matter ball are distorted when the matter ball is collapsing. It is evident that the whole spacetime of the collapsing star is dynamical (time-dependent). According to the general discussions of QFT in curved

spacetime in Section 4.4, there exists intrinsic ambiguity in defining field modes and vacuum state. Fortunately, there are well defined *in* region and *out* region for the spacetime of the collapsing star. In the remote past, if the matter ball is sufficiently distended or at region that is far away from the surface of the star, the spacetime is approximately flat, one thus can construct the standard Minkowski space quantum vacuum. This is called the *in* region. The *in*-vacuum is empty of particles as observed by static observers far away from the surface of the star in the past. After the black hole was formed and at the region very far away from the event horizon, the spacetime is also approximately flat, so that we can define a new quantum vacuum. This is called the *out* region and the corresponding vacuum is known as the Boulware vacuum [Bou75]. The Boulware vacuum (*out*-vacuum) is empty of particles as observed by static observers far away from the event horizon in the future.

Consider a massless scalar field  $\hat{\Phi}$  in the spacetime of the collapsing star. In the *in*-region, the mode solutions to the Klein-Gordon equation (4.4.1) are proportional to

$$r^{-1}Y_{lm}e^{-i\omega u}, \quad (4.6.1)$$

and

$$r^{-1}Y_{lm}e^{-i\omega v}, \quad (4.6.2)$$

where  $Y_{lm}(\theta, \phi)$  is the spherical harmonic,  $u = t - r - 2M \ln(r/2M - 1)$ ,  $v = t + r + 2M \ln(r/2M - 1)$ . These two sets of mode solutions represent outgoing and ingoing modes in the *in*-region, respectively. An ingoing mode propagates toward the star, with part of it is reflected by the curvature around the star, and part of it propagates through the star and becomes an outgoing mode. To simplify the analysis, we take the geometric optics approximation and neglect the scattering by the curvature. When the ingoing mode propagates from spatial infinity to the surface of the matter ball, it is blue shifted. We assume that the ingoing quanta do not interact with the matter inside the matter ball. After passing through the matter ball, it propagates to spatial infinity and is red shifted. If the matter ball is static, the blueshift and redshift cancels with each other so that the ingoing mode becomes the exact outgoing mode Eq. (4.6.1). However, if the star is collapsing, during the

period that the mode transits through the matter ball, the radius of the matter ball has become smaller so that the blueshift and redshift cannot cancel with each other. The net effect is that the ingoing mode is red shifted when it emerges from the other side of the matter ball. The redshift effect becomes more and more significant when the surface of the matter ball is closer and closer to the gravitational radius. There is a critical moment at which the redshift becomes infinity.

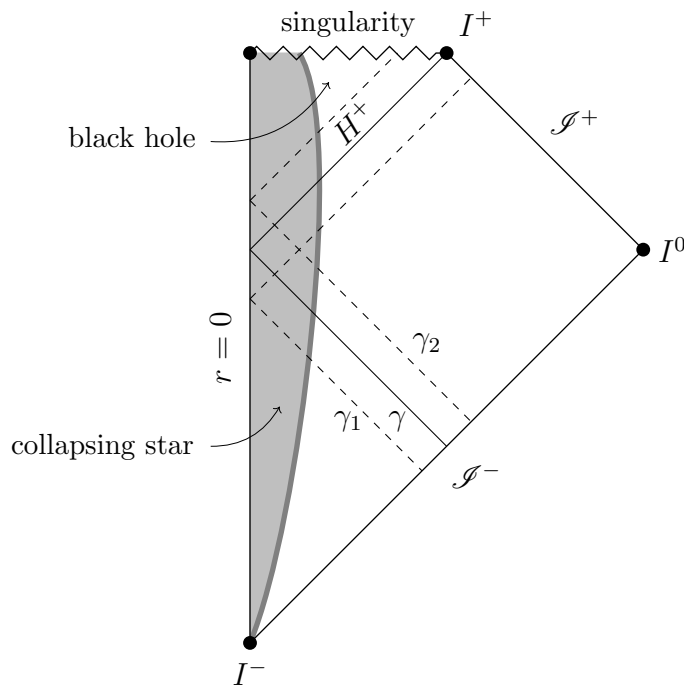


FIGURE 4.6: Penrose diagram of a collapsing star.

This process is depicted schematically by Fig. 4.6, which shows the matter ball collapsing to form a black hole. The null ray  $\gamma$  passes through the matter ball and emerges from the surface of the matter ball when the surface is crossing the gravitational radius. Therefore the null ray  $\gamma$  stays on the event horizon. Null rays advanced to  $\gamma$ , for example  $\gamma_1$ , can escape to future null infinity  $\mathcal{I}^+$  after passing through the matter ball. However null rays retarded to  $\gamma$ , for example  $\gamma_2$ , cannot escape to future null infinity  $\mathcal{I}^+$  but instead fall into the singularity. If one traces the propagation of an ingoing mode, Eq. (4.6.2), originated from the past null infinity  $\mathcal{I}^-$ , one would find that the part retarded to the null ray  $\gamma$  falls

into the event horizon and eventually hits the singularity, while the part advanced to the null ray  $\gamma$  escapes to future null infinity and can be detected by outside observers. Therefore, the outside observers after the black hole was formed cannot have full information about the ingoing modes in the *in* region. In addition, the part that escapes to future null infinity is red shifted. The redshift is more and more significant as closer and closer to the event horizon.

As we have shown, the positive frequency modes as observed by static observers in the *out* region are dramatically different from that as observed by static observers in the *in* region. The Bogoliubov transformations between the *in* modes and *out* modes were first calculated by Hawking [Haw75]. He showed that the *in*-vacuum is inequivalent to the *out*-vacuum. If the initial state of the quantum field is the *in*-vacuum, the state as observed by static observers in the *out* region is a thermal state with temperature (in the unit  $G = c = \hbar = k_B = 1$ )

$$T_H = \frac{\kappa}{2\pi}, \quad (4.6.3)$$

known as the Hawking temperature [Haw75]. Here  $\kappa$  is the surface gravity of the black hole, e.g.,  $\kappa = 1/4M$  for a Schwarzschild black hole. This is a rather surprising result. A classical black hole absorbs everything and nothing can escape from it. When quantum mechanics is considered, the black hole is not “black ” but instead radiates particles. It can be estimated that the characteristic wavelength of the Hawking particle is at the same order of magnitude as the size of the black hole. Therefore the Hawking radiation can be understood in terms of the Heisenberg’s uncertainty principle: a black hole cannot trap a particle with wavelength at the same size as the black hole. Hawking proposed a heuristic picture for the production of Hawking particles. Vacuum fluctuations around the event horizon produce virtual particle and antiparticle pairs. Due to the gravity around the black hole, the antiparticle falls into the black hole while the particle escapes to spatial infinity.

The temperature of an astrophysical black hole is so low that it is extremely challenging to directly detect the Hawking radiation. If we recover all the physical constants in Eq. (4.6.3),

we have

$$T_H = \frac{\hbar c^3}{8\pi G M k_B} \approx 6.169 \times 10^{-8} \times \left( \frac{M_\odot}{M} \right) \text{ K}, \quad (4.6.4)$$

where  $G$  is the gravitational constant,  $M_\odot$  is the solar mass. The Hawking temperature of a solar mass black hole is about  $10^{-8}$  K, which is much lower than the temperature of the Cosmic Microwave Background radiation ( $\sim 2.73$  K).

### 4.6.2 Eternal black hole

In the previous subsection, we have introduced the Hawking radiation created by a collapsing star. One can also obtain the Hawking radiation by studying quantum fields in an eternal Schwarzschild black hole, the maximally extended Schwarzschild spacetime. Although it is not clear whether an eternal black hole exists in the real world, it is instructive to study quantum fields in it and make comparison with quantum fields in Rindler space.

**Boulware vacuum**—The exterior Schwarzschild spacetime is static and possesses a time-like Killing vector  $\partial_t = (1, 0, 0, 0)$ . We can quantize a massless scalar field  $\hat{\Phi}$  in terms of the eigenfunctions of the time-like Killing vector  $\partial_t$ . Since  $t$  can be considered as the proper time of static observers at spatial infinity, the excitations of these field modes are particles as observed by static observers at spatial infinity. We consider a Hermitian massless field  $\hat{\Phi}$  that satisfies the Klein-Gordon equation (4.4.1). The normal-mode solutions to Eq. (4.4.1) can be decomposed as

$$u_{\omega lm}(t, r, \theta, \phi) = \frac{1}{\sqrt{4\pi\omega}} e^{-i\omega t} Y_{lm}(\theta, \phi) R_{\omega l}(r)/r \quad (4.6.5)$$

where  $\omega > 0$  is the frequency of the mode,  $Y_{lm}(\theta, \phi)$  is the spherical harmonic that represents the angular momentum of the mode. The radial function  $R_{\omega l}(r)$  satisfies

$$-\frac{d^2 R_{\omega l}}{dr_*^2} + V_l^{(s)}(r) R_{\omega l} = \omega^2 R_{\omega l}, \quad (4.6.6)$$

where  $V_l^{(s)}(r)$  is the effective potential

$$V_l^{(s)}(r) = f(r) \left[ \frac{l(l+1)}{r^2} + \frac{2M}{r^3} \right], \quad (4.6.7)$$

with  $f(r) \equiv 1 - 2M/r$ . Here  $r_*$  is the tortoise coordinate,

$$dr_* = dr/f(r), \quad r_* = r + 2M \ln(r/2M - 1), \quad (4.6.8)$$

and the event horizon corresponds to  $r_* \rightarrow -\infty$ . An implicit relation  $r = r(r_*)$  can be derived and substituted into the effective potential  $V_l^{(s)}$ , Eq. (4.6.7), so that the effective potential can be considered as a function of  $r_*$ .

In region I (the world we live in), two types of modes form a complete and orthonormal set of basis: the upcoming modes and ingoing modes, denoted as  $u_{\omega lm}^{\text{up}}$  and  $u_{\omega lm}^{\text{in}}$  respectively. The asymptotic behaviour for the radial part of the upcoming mode,  $R_{\omega l}^{\text{up}}$ , is

$$R_{\omega l}^{\text{up}} \sim \begin{cases} B_{\omega l}^{\text{up}} e^{i\omega r_*}, & r_* \rightarrow +\infty; \\ e^{i\omega r_*} + A_{\omega l}^{\text{up}} e^{-i\omega r_*}, & r_* \rightarrow -\infty, \end{cases} \quad (4.6.9)$$

and for the radial part of the ingoing mode,  $R_{\omega l}^{\text{in}}$ , is

$$R_{\omega l}^{\text{in}} \sim \begin{cases} e^{-i\omega r_*} + A_{\omega l}^{\text{in}} e^{i\omega r_*}, & r_* \rightarrow +\infty; \\ B_{\omega l}^{\text{in}} e^{-i\omega r_*}, & r_* \rightarrow -\infty. \end{cases} \quad (4.6.10)$$

Here  $A_{\omega l}^{\text{up}}$  ( $A_{\omega l}^{\text{in}}$ ) and  $B_{\omega l}^{\text{up}}$  ( $B_{\omega l}^{\text{in}}$ ) are the reflection and transmission amplitudes of the upcoming (ingoing) modes, respectively. They satisfy the following Wronskian relations [HLO14],

$$\begin{aligned} |A_{\omega l}^{\text{up}}|^2 &= 1 - |B_{\omega l}^{\text{up}}|^2, \\ |A_{\omega l}^{\text{in}}|^2 &= 1 - |B_{\omega l}^{\text{in}}|^2, \\ |A_{\omega l}^{\text{up}}| &= |A_{\omega l}^{\text{in}}|, \quad B_{\omega l}^{\text{up}} = B_{\omega l}^{\text{in}}. \end{aligned} \quad (4.6.11)$$

The upcoming modes  $u_{\omega lm}^{\text{up}}$  and ingoing modes  $u_{\omega lm}^{\text{in}}$  are chosen to satisfy the orthonormality

relations,

$$\begin{aligned}
\langle u_{\omega lm}^{\text{up}}, u_{\omega' l' m'}^{\text{up}} \rangle &= \delta(\omega - \omega') \delta_{ll'} \delta_{mm'}, \\
\langle u_{\omega lm}^{\text{up}*}, u_{\omega' l' m'}^{\text{up}*} \rangle &= -\delta(\omega - \omega') \delta_{ll'} \delta_{mm'}, \\
\langle u_{\omega lm}^{\text{in}}, u_{\omega' l' m'}^{\text{in}} \rangle &= \delta(\omega - \omega') \delta_{ll'} \delta_{mm'}, \\
\langle u_{\omega lm}^{\text{in}*}, u_{\omega' l' m'}^{\text{in}*} \rangle &= -\delta(\omega - \omega') \delta_{ll'} \delta_{mm'}. \\
\langle \phi_{\omega lm}^{\text{up}}, \phi_{\omega' l' m'}^{\text{in}} \rangle &= 0, \\
\langle \phi_{\omega lm}^{\text{up}*}, \phi_{\omega' l' m'}^{\text{in}*} \rangle &= 0.
\end{aligned} \tag{4.6.12}$$

Here  $\langle , \rangle$  represents the Klein-Gordon inner product [BD82], which is defined on a spacelike hypersurface  $t = \text{const.}$  as

$$\langle \varphi, \chi \rangle = i \int_{2M}^{\infty} dr \frac{r^2}{f(r)} \int_{4\pi} d\Omega (\varphi^* \partial_t \chi - \chi \partial_t \varphi^*) \tag{4.6.13}$$

for any two solutions  $\varphi$  and  $\chi$  of the Klein-Gordon equation (4.4.1) in the Schwarzschild background spacetime.

A corresponding set of upcoming and ingoing modes in region III (the extended Schwarzschild spacetime) can be similarly defined, which are denoted as  $v_{\omega lm}^{\text{up}}$  and  $v_{\omega lm}^{\text{in}}$  respectively. They form a set of complete and orthonormal modes in the region III and are independent of those modes in region I. The upcoming and ingoing modes in region I and III are schematically shown in Fig. 4.7.

The scalar field operator  $\hat{\Phi}$  can be expanded as

$$\hat{\Phi} = \sum_{lm} \int d\omega (\hat{a}_{\omega lm}^{\text{I}} u_{\omega lm}^{\text{up}} + \hat{b}_{\omega lm}^{\text{I}} u_{\omega lm}^{\text{in}} + \hat{a}_{\omega lm}^{\text{III}} v_{\omega lm}^{\text{up}} + \hat{b}_{\omega lm}^{\text{III}} v_{\omega lm}^{\text{in}} + \text{h.c.}), \tag{4.6.14}$$

where  $\hat{a}_{\omega lm}^{\text{I}}$  and  $\hat{b}_{\omega lm}^{\text{I}}$  are the upcoming and ingoing annihilation operators in region I,  $\hat{a}_{\omega lm}^{\text{III}}$  and  $\hat{b}_{\omega lm}^{\text{III}}$  are the upcoming and ingoing annihilation operators in region III. The corresponding vacuum is known as the Boulware vacuum [Bou75],

$$\hat{a}_{\omega lm}^{\text{I}} |0_{\text{B}}\rangle = \hat{b}_{\omega lm}^{\text{I}} |0_{\text{B}}\rangle = \hat{a}_{\omega lm}^{\text{III}} |0_{\text{B}}\rangle = \hat{b}_{\omega lm}^{\text{III}} |0_{\text{B}}\rangle = 0, \quad \forall \omega, l, m. \tag{4.6.15}$$

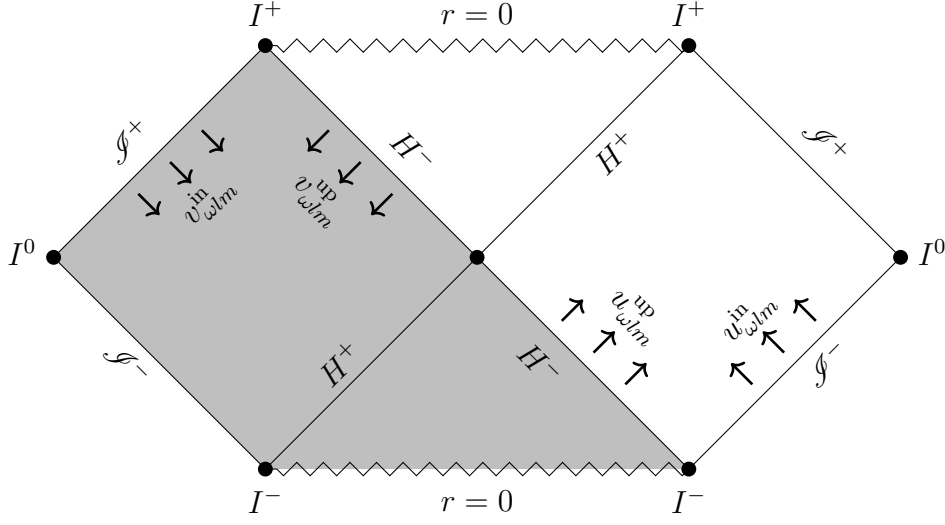


FIGURE 4.7: Upcoming and ingoing modes in the maximally extended Schwarzschild spacetime.

The Boulware vacuum is empty of particles as observed by static observers at spatial infinity.

**Unruh vacuum**—There exists another Killing vector,  $\partial_U$ , on the past horizon  $H^-$ . One can quantize the scalar field in terms of the eigenfunctions of the Killing vector  $\partial_U$  [Unr76]. The normalized positive frequency modes with respect to  $\partial_U$  are defined as [CF77]

$$w_{\omega lm}^{\text{up}} = \frac{1}{\sqrt{2 \sinh(4\pi M\omega)}} (e^{2\pi M\omega} u_{\omega lm}^{\text{up}} + e^{-2\pi M\omega} v_{\omega lm}^{\text{up}*}), \quad (4.6.16)$$

$$\bar{w}_{\omega lm}^{\text{up}} = \frac{1}{\sqrt{2 \sinh(4\pi M\omega)}} (e^{2\pi M\omega} v_{\omega lm}^{\text{up}} + e^{-2\pi M\omega} u_{\omega lm}^{\text{up}*}). \quad (4.6.17)$$

Note that the definitions of  $w$  and  $\bar{w}$  modes are very similar to the definitions of Unruh modes from the Rindler modes, Eqs. (4.5.26) and (4.5.27). The scalar field operator  $\hat{\Phi}$  can be expanded as

$$\hat{\Phi} = \sum_{lm} \int d\omega (\hat{c}_{\omega lm} w_{\omega lm}^{\text{up}} + \hat{\bar{c}}_{\omega lm} \bar{w}_{\omega lm}^{\text{up}} + \hat{b}_{\omega lm}^{\text{I}} u_{\omega lm}^{\text{in}} + \hat{b}_{\omega lm}^{\text{III}} v_{\omega lm}^{\text{in}} + \text{h.c.}), \quad (4.6.18)$$

where  $\hat{c}_{\omega lm}$  and  $\hat{\bar{c}}_{\omega lm}$  are the upcoming Unruh annihilation operators. The corresponding vacuum state is known as the Unruh vacuum [Unr76],

$$\hat{c}_{\omega lm} |0_U\rangle = \hat{\bar{c}}_{\omega lm} |0_U\rangle = \hat{b}_{\omega lm}^{\text{I}} |0_U\rangle = \hat{b}_{\omega lm}^{\text{III}} |0_U\rangle = 0, \quad \forall \omega, l, m. \quad (4.6.19)$$

It can be easily shown that

$$\hat{a}_{\omega lm}^{\text{I}} = \frac{1}{\sqrt{2 \sinh(4\pi M\omega)}} (e^{2\pi M\omega} \hat{c}_{\omega lm} + e^{-2\pi M\omega} \hat{c}_{\omega lm}^\dagger), \quad (4.6.20)$$

$$\hat{a}_{\omega lm}^{\text{III}} = \frac{1}{\sqrt{2 \sinh(4\pi M\omega)}} (e^{2\pi M\omega} \hat{c}_{\omega lm} + e^{-2\pi M\omega} \hat{c}_{\omega lm}^\dagger). \quad (4.6.21)$$

If the state of the scalar field is the Unruh vacuum  $|0_{\text{U}}\rangle$ , we have

$$\begin{aligned} \langle 0_{\text{U}} | \hat{a}_{\omega lm}^{\text{I}\dagger} \hat{a}_{\omega lm}^{\text{I}} | 0_{\text{U}} \rangle &= \frac{\delta(0)}{e^{8\pi M\omega} - 1}, \\ \langle 0_{\text{U}} | \hat{b}_{\omega lm}^{\text{I}\dagger} \hat{b}_{\omega lm}^{\text{I}} | 0_{\text{U}} \rangle &= 0. \end{aligned} \quad (4.6.22)$$

The formally divergent quantity  $\delta(0)$  appears because we consider an infinite space outside the black hole. This implies static observers at spatial infinity see a thermal flux coming out from the black hole. The temperature of the thermal flux is the Hawking temperature  $T_H = 1/8\pi M$ . The specification of the Unruh vacuum in an external black hole reproduces the Hawking radiation from a collapsing star at late times.

**Hartle-Hawking vacuum**—In addition to Eqs. (4.6.16) and (4.6.17), we further introduce

$$w_{\omega lm}^{\text{in}} = \frac{1}{\sqrt{2 \sinh(4\pi M\omega)}} (e^{2\pi M\omega} u_{\omega lm}^{\text{in}} + e^{-2\pi M\omega} v_{\omega lm}^{\text{in}*}), \quad (4.6.23)$$

$$\bar{w}_{\omega lm}^{\text{in}} = \frac{1}{\sqrt{2 \sinh(4\pi M\omega)}} (e^{2\pi M\omega} v_{\omega lm}^{\text{in}} + e^{-2\pi M\omega} u_{\omega lm}^{\text{in}*}). \quad (4.6.24)$$

The scalar field operator  $\hat{\Phi}$  can be expanded as

$$\hat{\Phi} = \sum_{lm} \int d\omega (\hat{c}_{\omega lm} w_{\omega lm}^{\text{up}} + \hat{c}_{\omega lm} \bar{w}_{\omega lm}^{\text{up}} + \hat{d}_{\omega lm} w_{\omega lm}^{\text{in}} + \hat{d}_{\omega lm} \bar{w}_{\omega lm}^{\text{in}} + \text{h.c.}), \quad (4.6.25)$$

where  $\hat{d}_{\omega lm}$  and  $\hat{\bar{d}}_{\omega lm}$  are the ingoing Unruh annihilation operators. The corresponding vacuum state is known as the Hartle-Hawking vacuum [HH76],

$$\hat{c}_{\omega lm} |0_{\text{U}}\rangle = \hat{\bar{c}}_{\omega lm} |0_{\text{U}}\rangle = \hat{d}_{\omega lm} |0_{\text{U}}\rangle = \hat{\bar{d}}_{\omega lm} |0_{\text{U}}\rangle = 0, \quad \forall \omega, l, m. \quad (4.6.26)$$

Similarly, we have

$$\hat{b}_{\omega lm}^{\text{I}} = \frac{1}{\sqrt{2 \sinh(4\pi M\omega)}} (e^{2\pi M\omega} \hat{d}_{\omega lm} + e^{-2\pi M\omega} \hat{d}_{\omega lm}^\dagger), \quad (4.6.27)$$

$$\hat{b}_{\omega lm}^{\text{III}} = \frac{1}{\sqrt{2 \sinh(4\pi M\omega)}} (e^{2\pi M\omega} \hat{\bar{d}}_{\omega lm} + e^{-2\pi M\omega} \hat{\bar{d}}_{\omega lm}^\dagger). \quad (4.6.28)$$

If the state of the scalar field is the Hartle-Hawking vacuum  $|0_U\rangle$ , we have

$$\langle 0_U | \hat{a}_{\omega lm}^{\dagger} \hat{a}_{\omega lm}^{\dagger} | 0_U \rangle = \langle 0_U | \hat{b}_{\omega lm}^{\dagger} \hat{b}_{\omega lm}^{\dagger} | 0_U \rangle = \frac{\delta(0)}{e^{8\pi M\omega} - 1}. \quad (4.6.29)$$

This implies static observers at spatial infinity see a thermal flux coming out from the black hole as well as a thermal flux coming into the black hole. The black hole is in equilibrium with the environment at the Hawking temperature.

### 4.6.3 Black hole information paradox

It was shown by Hawking that when a star collapses to form a black hole, there is a thermal flux coming out from the black hole. The temperature of the Hawking radiation is proportional to the surface gravity of the black hole. The Hawking temperature is very low for large black hole, e.g., about  $10^{-8}$  K for a solar mass black hole. Nevertheless, the black hole loses mass when it emits Hawking particles. The energy flux was estimated to be [Pag76]

$$P = \frac{\hbar c^6}{15360\pi G^2 M^2}, \quad (4.6.30)$$

where we have restored all the physical constants. This is known as the Stefan-Boltzmann-Schwarzschild-Hawking power law. The power for a black hole with one solar mass is about  $10^{-29}W$ , which is extremely small as expected. As the black hole loses mass, it gradually evaporates. After a sufficiently long time, the black hole could completely evaporate and disappear. The lifetime of a black hole with initial mass  $M_0$  is about [Pag76]

$$t_{\text{ev}} = \frac{5120\pi G^2 M_0^3}{\hbar c^4}. \quad (4.6.31)$$

The lifetime for a black hole with one solar mass is about  $10^{74}s$ , which is much longer than the age of the universe ( $\sim 10^{17}s$ ). However, for a Planck mass quantum black hole, the lifetime is about  $10^{-40}s$ .

If a black hole evaporated completely, the leftover is a cloud of Hawking particles. Since the Hawking radiation is thermal, there are no correlations between different Hawking particles. The state of the Hawking particles cloud is thus mixed. Without loss of generality, the initial state of the quantum fields can be a vacuum, which is a pure state. This implies that

the process of formation and evaporation of a black hole is not unitary: a pure initial state evolved into a mixed final state. This is the information paradox first proposed by Hawking [Haw76].

## 4.7 Summary and further reading

In this chapter, we introduce QFT in curved spacetime. In particular, we discuss the Unruh effect and the Hawking effect, which are the striking results of exploring QFT in Rindler space and Schwarzschild spacetime, respectively.

There are many excellent textbooks that introduce general relativity. For a basic introduction with more emphasis on basic concepts, one can refer to the textbook by Hartle [Har03]. For more technical details, one can refer to the textbook by Weinberg [Wei72]. The textbook by Carroll [Car04] tries to introduce general relativity in the language of differential geometry. The most comprehensive textbook of general relativity would be the well known “MTW” [MTW73]. The standard textbook for quantum field theory in curved spacetime was written by Birrell and Davies [BD82] in 1982. A more recent one is written by Parker and Toms [PT09]. The textbooks by Wald [Wal94], and Haag [Haa12] describe the quantum field theory in curved spacetime using the algebraic method.

# 5

## Spacetime Diamonds

### 5.1 Introduction

A key result of relativistic quantum field theory is that the restriction of observers to partial regions of spacetime leads to the observation of particles, even if the total spacetime is in the vacuum state (see Ref. [PT04] and references therein). Key examples are Hawking radiation [Haw75], where the observers are cut off from the inside of a black hole by its event horizon, and Unruh-Davies radiation [Unr76, Dav75, CHM08], where uniform acceleration of the observer restricts them to a Rindler wedge through the formation of a virtual horizon. Both Hawking and Unruh-Davies radiation are thermal and their temperatures are proportional to the surface gravity of the black hole and the acceleration of a uniformly accelerated observer, respectively. The thermal character of the radiation is closely related to entanglement of the observed field modes with others hidden behind the horizon [BD82]. More recently, it has

been predicted that particles should also be observed when a detector is restricted to the future or past light cone [OR11].

In all these cases, the region the observer is restricted to is unbounded. A natural question is whether an observer restricted to a bound region of spacetime can see thermal radiation. Using the thermal time hypothesis [CR94], Martinetti and Rovelli found that an accelerated observer with a finite lifetime can experience an effective temperature, a generalization to the Unruh-Davies temperature [MR03]. For the special case of an inertial observer with a finite lifetime, the temperature at the middle of their lifetime is nonzero. This so-called “diamond temperature” is given by [MR03]

$$T_D = \frac{2}{\pi\mathcal{T}}, \quad (5.1.1)$$

where  $\mathcal{T}$  is the lifetime of the inertial observer. The diamond temperature arises because an observer with a finite lifetime does not have access to all the degrees of freedom of the quantum field. However, the temperature discovered by Martinetti and Rovelli is time dependent. Also, it was unclear what type of physical system could observe the diamond temperature. In [OR11], an Unruh-DeWitt detector [Unr76, DeW79] with an energy scaling that effectively restricts it to the future or past light cone was shown to register a thermal response identical to that of a uniformly accelerated Unruh-DeWitt detector. In this chapter, we show that an Unruh-DeWitt detector with an energy scaling which effectively gives it a finite lifetime, or equivalently, confines it within one diamond, also registers a thermal response. The temperature that the detector sees is exactly the diamond temperature (5.1.1) discovered by Martinetti and Rovelli. We thus find a physical meaning for the diamond temperature: it is the temperature observed by a particular type of energy-scaled detector. Note that a similar version of these diamonds on the static  $(1+1)$ -dimensional Minkowski cylinder has been encountered in the context of the gauge-gravity correspondence, leading to the thermal effects on the conformal boundary of the Bañados-Teitelboim-Zanelli black hole [MS98, LM99].

This chapter is organized as follows. Section 5.2 briefly reviews the time-like entanglement.

Section 5.3 reviews the diamond coordinates and derives the Minkowski metric in terms of the diamond coordinates. In Section 5.4, we explicitly calculate the Bogoliubov transformation between the diamond modes and the Minkowski modes, and show that the particle-number distribution of the diamond modes is thermal in the Minkowski vacuum. In Section 5.5, we calculate the response of an energy scaled Unruh-DeWitt detector in  $(1 + 3)$ -dimensional spacetime and show that the response is thermal. Section 5.6 studies the entanglement between different diamonds. The results in this chapter have been published as “*Spacetime diamonds*” in [SR16].

## 5.2 Time-like entanglement

The concept of entanglement between the left and right Rindler wedge rests on the fact that the fields within can be considered as independent systems. In particular, no signal can be sent from the left Rindler wedge to the right Rindler wedge and vice versa. This is evidently illustrated by the vanishing of the Pauli-Jordan function (or Schwinger function) for space-like intervals [PS95],  $iG(t, \mathbf{r}; t', \mathbf{r}') = \langle 0 | [\hat{\Phi}(t, \mathbf{r}), \hat{\Phi}(t', \mathbf{r}')] | 0 \rangle = 0$ . This is true for both massive and massless fields. For a massless field in  $(3 + 1)$ -dimensional Minkowski spacetime, the Pauli-Jordan function is also vanishing for time-like intervals, as can be seen from Eq. (2.2.37). The Pauli-Jordan function for a massless scalar field is shown in Figure 5.1. Therefore, the fields in the future and past region can be considered as independent systems. No light signal can be sent from the past region to the future region and vice versa. However, for massless scalar fields in  $(1 + 1)$ -dimensional (and  $2 + 1$  and other even+1) Minkowski spacetime, the strong Huygens principle is violated. This means the massless scalar fields propagate not only on but also into the future lightcone [JMMK15]. Nevertheless, one can still calculate the distribution of field modes in the past or future wedge, and the entanglement between the past and future wedges in the Minkowski vacuum. These calculations are independent of whether the strong Huygens principle is violated or not. In the case where the strong Huygens principle is violated, the origin of the time-like entanglement may be different from that of the space-like entanglement which is assumed to be preexistent.

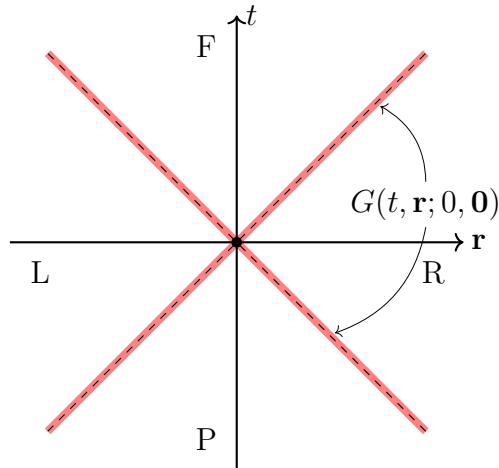


FIGURE 5.1: Pauli-Jordan function for a massless scalar field in  $(1 + 3)$ -dimensional Minkowski space-time (the three spatial dimensions have been compacted to one). The Pauli-Jordan function is nonzero only on the light cone.

It was shown that there exists a direct mapping between the fields in past and future wedges, to the fields in the right and left Rindler wedges [OR11]. The mapping in  $(1 + 1)$ -dimensional space-time is schematically illustrated in Figure 5.2. An inertial observer who is localized only in the past or future, and uses appropriate energy scaling detector can detect a thermal radiation, an analogue to the Unruh radiation. According to the dimensional analysis, the observation of this effect is within the range of current technology [OR11]. The space-like entanglement between the right and left Rindler wedges can be extracted by using two detectors ( $D_1$  and  $D_2$ ), which detect localized wave packet modes, in the right and left Rindler wedges, respectively [RRS05]. According to the mapping, two detectors ( $D_3$  and  $D_4$ ), with appropriate scaled energy, in the past and future wedges can extract exactly the same entanglement [OR12]. Note that the detectors  $D_3$  and  $D_4$  operate in past and future wedges, we thus name the entanglement extracted by them as time-like entanglement.

### 5.3 Diamond coordinates

A static observer with a finite lifetime stays at  $\mathbf{r} = 0$ . The overlap of the future light cone of their birth and the past light cone of their death is called a diamond, satisfying

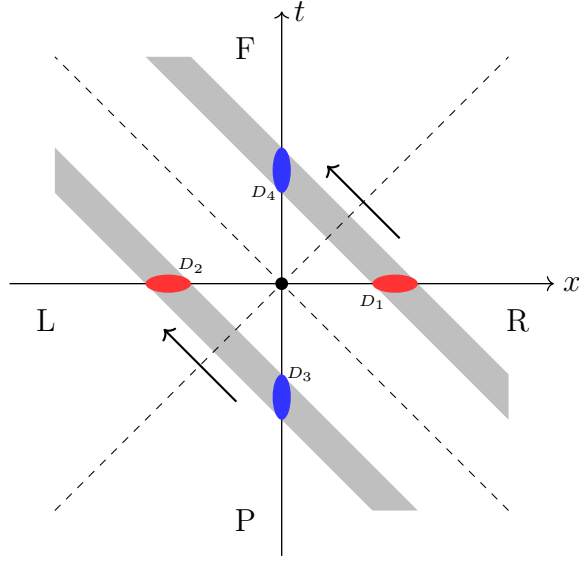


FIGURE 5.2: Schematic diagram of the mapping of left-moving modes in  $(1+1)$ -dimensional Minkowski spacetime between the past and left Rindler wedges, the future and right Rindler wedges. The detectors  $D_3$  and  $D_4$  can extract the same entanglement as that extracted by the detectors  $D_1$  and  $D_2$ .

$|t| + |\mathbf{r}| < 2/a$ , where  $2/a$  is the size of the diamond or  $\mathcal{T} = 4/a$  is the lifetime of the static observer. There exists a conformal transformation which maps the diamond (bounded) to a Rindler wedge (unbounded) [MR03]. Assume that  $(t, x, y, z)$  are the Minkowski coordinates and  $(t', x', y', z')$  are the conformal coordinates. The conformal transformation is defined as

$$\frac{at'}{2} = \frac{at}{f_-(t, \mathbf{r}; a)}, \quad \frac{ax'}{2} = \frac{1 + (at/2)^2 - (ar/2)^2}{f_-(t, \mathbf{r}; a)}, \quad \frac{ay'}{2} = \frac{ay}{f_-(t, \mathbf{r}; a)}, \quad \frac{az'}{2} = \frac{az}{f_-(t, \mathbf{r}; a)}, \quad (5.3.1)$$

and the inverse transformation is

$$\frac{at}{2} = \frac{at'}{f_+(t', \mathbf{r}'; a)}, \quad \frac{ax}{2} = \frac{1 + (at'/2)^2 - (ar'/2)^2}{f_+(t', \mathbf{r}'; a)}, \quad \frac{ay}{2} = \frac{ay'}{f_+(t', \mathbf{r}'; a)}, \quad \frac{az}{2} = \frac{az'}{f_+(t', \mathbf{r}'; a)}, \quad (5.3.2)$$

where  $f_{\pm}(t, \mathbf{r}; a) = 1 - (at/2)^2 + (ar/2)^2 \pm ax$ , and  $r = \sqrt{x^2 + y^2 + z^2}$ . It can be shown by straightforward calculation that the line element in terms of the conformal coordinates is

$$\begin{aligned} ds^2 &= -dt^2 + dx^2 + dy^2 + dz^2 \\ &= \frac{4}{f_+^2(t', \mathbf{r}'; a)} (-dt'^2 + dx'^2 + dy'^2 + dz'^2), \end{aligned} \quad (5.3.3)$$

which is consistent with the assumption that this is a conformal transformation. The conformal mapping from a diamond in Minkowski coordinates to the right Rindler wedge in the

conformal coordinates can be clearly illustrated in (1 + 1)-dimensional spacetime, see Figure 5.3.

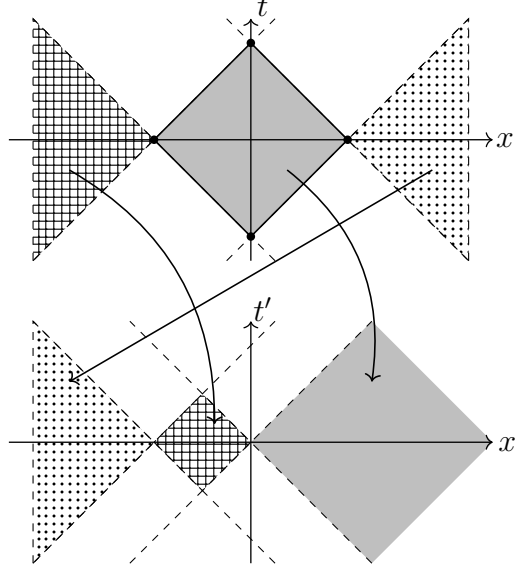


FIGURE 5.3: Conformal mapping in (1 + 1)-dimensional spacetime:  $V' = (1 + V)/(1 - V)$ ,  $U' = -(1 - U)/(1 + U)$ . A diamond in Minkowski coordinates  $(t, x)$ ,  $|t| + |x| \leq 1$ , is mapped to the right Rindler wedge in the conformal coordinates  $(t', x')$ . The regions outside the diamond in Minkowski coordinates  $(t, x)$  are together mapped to form the left Rindler wedge in the conformal coordinates  $(t', x')$ .

This motivates us to introduce a new coordinate system  $(\eta, \xi, \zeta, \rho)$ , called diamond coordinates, to describe spacetime events and field modes inside the diamond.

$$at'/2 = e^{a\xi} \sinh(a\eta), \quad ax'/2 = e^{a\xi} \cosh(a\eta), \quad \zeta = y', \quad \rho = z'. \quad (5.3.4)$$

The relationship between the diamond coordinates and Minkowski coordinates can be easily derived by using Eq. (5.3.1),

$$\begin{aligned} \eta &= \frac{1}{a} \tanh^{-1} \left\{ \frac{at}{1 + a^2t^2/4 - a^2r^2/4} \right\}, \\ \xi &= \frac{1}{a} \ln \left\{ \frac{\sqrt{(1 + a^2t^2/4 - a^2r^2/4)^2 - a^2t^2}}{f_-(t, \mathbf{r}; a)} \right\}, \\ \zeta &= \frac{2y}{f_-(t, \mathbf{r}; a)}, \\ \rho &= \frac{2z}{f_-(t, \mathbf{r}; a)}, \end{aligned} \quad (5.3.5)$$

Inside the diamond, the line element written in terms of the diamond coordinates is

$$ds^2 = \frac{4(-d\eta^2 + d\xi^2) + e^{-2a\xi}(d\zeta^2 + d\rho^2)}{[\cosh(a\eta) + \cosh(a\xi) + \frac{a^2}{2}e^{-a\xi}(\zeta^2 + \rho^2)]^2}. \quad (5.3.6)$$

Although the  $x$  direction appears special in the coordinate transformation (5.3.5), no direction is preferred due to the rotational invariance of the diamond. In fact, the same conformal transformation [MR03] maps the region outside the diamond to another Rindler wedge, e.g., see Fig 5.3. This nice property can help us to intuitively understand correlations between field modes inside and outside the diamond.

It can be shown that  $\zeta = \rho = 0$ ,  $\xi = \text{const.}$  are worldlines of uniformly accelerated observers with acceleration  $\frac{a}{2}|\sinh(a\xi)|$  in the perspective of inertial observers. The most interesting one is  $\zeta = \rho = \xi = 0$ , which is exactly the worldline of the static observer. Along the static worldline,  $t = \frac{2}{a}\tanh(\frac{1}{2}a\eta)$ , or  $dt = d\eta/\cosh^2(a\eta/2)$ . That means the diamond clock ticks at the same rate as the inertial clock at  $\eta = 0$ , while the former ticks much faster than the latter when  $\eta \rightarrow \pm\infty$ .

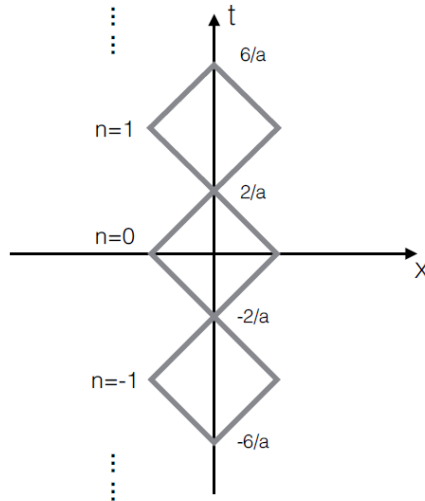


FIGURE 5.4: Diamonds in  $(1 + 1)$ -dimensional Minkowski spacetime. Only a chain of diamonds along the  $t$  axis is plotted and they are labeled by integers  $n = 0, \pm 1, \dots$ . The size of these diamonds are the same,  $2/a$ .

## 5.4 Thermal radiation

As a concrete example, we first consider a massless Hermitian scalar field  $\hat{\Phi}$  in the  $(1+1)$ -dimensional Minkowski spacetime and directly calculate the Bogoliubov transformation between the diamonds modes and Minkowski plane wave modes. We show that the Minkowski vacuum looks like a thermal state in the diamond and the temperature of the thermal state is inversely proportional to the lifetime of the static observer.

A chain of diamonds along the  $t$  axis is shown in Fig. 5.4. Other diamonds are not plotted, but one can imagine that the  $(1+1)$ -dimensional Minkowski spacetime is in fact a network of such diamonds. Without loss of generality, we first consider the zeroth diamond in Fig. 5.4. By simply setting  $\zeta = \rho = 0$  in Eq. (5.3.6), we can directly read out the metric inside the diamond in terms of  $\eta$  and  $\xi$ , which turns out to be conformal to the Minkowski metric (note that this is only true for  $(1+1)$ -dimensional spacetime). It is thus very easy to derive the Klein-Gordon equation by utilizing the conformal invariance of the massless scalar field in  $(1+1)$ -dimensional Minkowski spacetime.

Since the left-moving modes and right-moving modes are decoupled, we only discuss the left-moving modes in the following. Results for the right-moving modes can be obtained similarly. The Minkowski annihilation operators and positive frequency mode functions are  $\hat{a}_k$  and  $u_k(V) = e^{-ikV}/\sqrt{4\pi k}$ , with  $V = t + x$ . While in the zeroth diamond they are  $\hat{b}_\omega^{(0)}$  and  $g_\omega^{(0)}(v) = e^{-i\omega v}/\sqrt{4\pi\omega}$ , with  $v = \eta + \xi$ . Meanwhile,  $g_\omega^{(0)}(v)$  can be rewritten in terms of Minkowski null coordinate  $V$ ,

$$g_\omega^{(0)}(V) = \frac{1}{\sqrt{4\pi\omega}} \left( \frac{1 + aV/2}{1 - aV/2} \right)^{-i\omega/a}, \quad (5.4.1)$$

where  $V \in (-2/a, 2/a)$  and the mode functions vanish outside the zeroth diamond.

We now have two ways to quantize the scalar field and it is straightforward to find the Bogoliubov transformation between operators  $(\hat{b}_\omega^{(0)}, \hat{b}_\omega^{(0)\dagger})$  and  $(\hat{a}_k, \hat{a}_k^\dagger)$ ,

$$\hat{b}_\omega^{(0)} = \int dk \left( \alpha_{\omega k}^{(0)} \hat{a}_k + \beta_{\omega k}^{(0)} \hat{a}_k^\dagger \right). \quad (5.4.2)$$

Direct calculation shows that  $\beta_{\omega k}^{(0)} \neq 0$ , which means these two ways of quantization are inequivalent; in particular, the Minkowski vacuum is not a vacuum in the diamond and vice versa. The Bogoliubov transformation coefficients  $\alpha_{\omega k}^{(0)}$  and  $\beta_{\omega k}^{(0)}$  can be calculated using the Klein-Gordon inner product [BD82]; we have

$$\begin{aligned}\alpha_{\omega k}^{(0)} &= \langle g_{\omega}^{(0)}(V), u_k(V) \rangle = \frac{1}{\pi a} \sqrt{\frac{\kappa}{\Omega}} \int_{-1}^{+1} ds \left( \frac{1+s}{1-s} \right)^{i\Omega} e^{-2i\kappa s} \\ &= \frac{1}{a} \frac{\sqrt{\Omega\kappa}}{\sinh(\pi\Omega)} e^{2i\kappa} M(1+i\Omega, 2, -4i\kappa),\end{aligned}\tag{5.4.3}$$

$$\begin{aligned}\beta_{\omega k}^{(0)} &= \langle g_{\omega}^{(0)}(V), u_k^*(V) \rangle = -\frac{1}{\pi a} \sqrt{\frac{\kappa}{\Omega}} \int_{-1}^{+1} ds \left( \frac{1+s}{1-s} \right)^{i\Omega} e^{2i\kappa s} \\ &= -\frac{1}{a} \frac{\sqrt{\Omega\kappa}}{\sinh(\pi\Omega)} e^{-2i\kappa} M(1+i\Omega, 2, 4i\kappa),\end{aligned}\tag{5.4.4}$$

where  $M(a, b, z)$  is the Kummer's function [AS72] and  $\Omega \equiv \omega/a$ ,  $\kappa \equiv k/a$ . In the Minkowski vacuum state, the particle-number distribution in the diamond is

$$\langle 0_M | \hat{b}_{\omega}^{(0)\dagger} \hat{b}_{\omega'}^{(0)} | 0_M \rangle = \int dk \beta_{\omega k}^{(0)*} \beta_{\omega' k}^{(0)} = \frac{\delta(\omega - \omega')}{e^{2\pi\omega/a} - 1},\tag{5.4.5}$$

which is exactly a thermal distribution with temperature

$$T_D = \frac{a}{2\pi} = \frac{2}{\pi\mathcal{T}}.\tag{5.4.6}$$

The temperature  $T_D$  derived here is the same as the diamond temperature derived from the thermal time hypothesis [MR03]. The same thermal particle-number distribution was obtained by Ida *et al.* [IOS13] through a different way. However, they use it as an intermediate result to derive the time-dependent temperature as proposed by Martinetti and Rovelli instead of interpreting it as the diamond temperature. We emphasize that  $T_D$  is exactly the diamond temperature and will show that this thermal radiation could be detected by an energy-scaled Unruh-DeWitt detector.

In principle, the above result can be generalized to (1 + 3)-dimensional spacetime. One can define diamond modes, calculate the Bogoliubov transformation coefficients and show that the particle-number distribution is thermal in the Minkowski vacuum. However instead of

doing the long mathematical calculation, we propose a detector model in  $(1+3)$ -dimensional spacetime and show that it responds to the diamond temperature, which is more physically relevant.

## 5.5 Detector response

We now turn to  $(1+3)$ -dimensional Minkowski spacetime. In [OR11], an inertial detector switched on at  $t = 0$  and sensitive to energy  $E$  with respect to conformal time is proved to register a thermal response. We now show that a similar inertial detector, which is switched on at  $t = -\frac{2}{a}$  and switched off at  $t = \frac{2}{a}$ , detects thermal radiation with diamond temperature in the Minkowski vacuum. Because we require the energy difference of the two-level detector at  $\mathbf{r} = 0$  to be constant with respect to diamond time  $\eta$ , the free Hamiltonian of the detector in the inertial frame should be

$$\frac{d\eta}{dt} H_0 = \frac{H_0}{1 - a^2 t^2 / 4}. \quad (5.5.1)$$

We then take the complete Hamiltonian to be  $H = H_0 / (1 - a^2 t^2 / 4) + H_I$ , where  $H_I$  is the standard interaction term for an Unruh-DeWitt detector,  $\lambda \hat{m} \hat{\Phi}$ . Converting to diamond time  $\eta$ , the Schrödinger equation is

$$i \frac{\partial \Psi}{\partial \eta} = \left[ H_0 + \frac{1}{\cosh^2(a\eta/2)} H_I \right] \Psi, \quad (5.5.2)$$

where  $\Psi$  is the wave function of the detector. In contrast to Ref. [OR11] where perturbation theory breaks down at sufficiently late time, the perturbation theory is always valid here provided  $|H_I| \ll |H_0|$  at  $\eta = 0$ .

To first order perturbation theory, the detector response function can be obtained in a standard way,

$$\mathcal{F}(E) = \int_{-\infty}^{\infty} d\eta \int_{-\infty}^{\infty} d\eta' \frac{e^{-iE(\eta-\eta')} G^+(\eta, \eta')}{\cosh^2(a\eta/2) \cosh^2(a\eta'/2)}, \quad (5.5.3)$$

where  $G^+(\eta, \eta') = \langle 0_M | \hat{\Phi}(\eta) \hat{\Phi}(\eta') | 0_M \rangle$  is the positive-frequency Wightman function in the Minkowski vacuum state. In terms of Minkowski coordinates  $t$  and  $\mathbf{r}$ , the general expression of the Wightman function is given by Eq. (2.2.34). Taking into account that the inertial

detector is at  $\mathbf{r} = 0$ , and the relation between the Minkowski time and diamond time is  $t = \frac{2}{a} \tanh(\frac{1}{2}a\eta)$ , we find

$$\frac{G^+(\eta, \eta')}{\cosh^2(a\eta/2)\cosh^2(a\eta'/2)} = -\frac{1}{16\pi^2} \frac{a^2}{\sinh^2(\frac{a}{2}(\eta - \eta'))}. \quad (5.5.4)$$

Now, consider an accelerated trajectory  $t = a^{-1} \sinh(a\tau)$ ,  $x = a^{-1} \cosh(a\tau)$ ,  $y = z = 0$ , with  $a$  and  $\tau$  the proper acceleration and proper time of the accelerated observer; in this case, the Wightman function is given by Eq. (4.5.62). Comparing Eqs. (5.5.4) and (4.5.62), it is clear that the response function  $\mathcal{F}(E)$  is the same as that of a uniformly accelerated detector, showing that an inertial Unruh-DeWitt detector with energy scaled as  $\frac{1}{1-a^2t^2/4}$  detects thermal radiation with temperature  $T_D = \frac{a}{2\pi}$  in the Minkowski vacuum.

Energy-scaled detectors are physically realizable; e.g., by applying a time-dependent external electric field or magnetic field to an atom one can realize a time-dependent Stark effect or Zeeman splitting. However, an order-of-magnitude estimate shows that for current technology the change of the electric field or the magnetic field is not large and fast enough to detect the diamond temperature. More promising candidates might be artificial atoms such as the superconducting qubits and quantum dots [RW15].

## 5.6 Correlations between different diamonds

In Minkowski vacuum state, a mode localized in the right Rindler wedge is perfectly entangled with a corresponding mode in the left Rindler wedge [BD82]. Similarly, a mode localized in the past light cone is perfectly entangled with a corresponding mode in the future light cone [OR11]. As we have mentioned before, there exists a conformal transformation that maps a diamond into a Rindler wedge, and the region outside the diamond to another Rindler wedge [MR03]. Therefore, if the dynamics of the scalar field is conformally invariant and also the vacuum state, then a mode inside the diamond should be perfectly entangled with a corresponding mode outside the diamond. A pair of entangled modes inside and outside the diamond has been calculated in the  $(1+1)$ -dimensional spacetime [IOS13]. Here, we are interested in the timelike entanglement between diamonds along the  $t$  axis, which is

now not bipartite entanglement but multipartite entanglement. In this case, it is convenient to consider localized modes and introduce Gaussian formalism [WPGP<sup>+</sup>12] to describe the entanglement between various diamonds.

As shown in Fig. 5.4, orthonormal mode functions in the  $n$ th diamond can be easily obtained by shifting those of the zeroth diamond,

$$g_\omega^{(n)}(V) = g_\omega^{(0)}(V - 4n/a), \quad (5.6.1)$$

where  $V \in (2(2n-1)/a, 2(2n+1)/a)$ . The Bogoliubov transformation coefficients  $\alpha_{\omega k}^{(n)}$  and  $\beta_{\omega k}^{(n)}$  are

$$\alpha_{\omega k}^{(n)} = e^{-4in\kappa} \alpha_{\omega k}^{(0)}, \quad \beta_{\omega k}^{(n)} = e^{4in\kappa} \beta_{\omega k}^{(0)}. \quad (5.6.2)$$

It is obvious that the temperature in every diamond is the same, owing to the translational invariance of the Minkowski vacuum. Notice that the modes  $g_\omega^{(n)}(V)$  are orthonormal and form a complete set of modes with which the scalar field  $\hat{\Phi}$  can be expanded.

$$\hat{\Phi} = \sum_{n=-\infty}^{+\infty} \int_0^\infty d\omega [\hat{b}_\omega^{(n)} g_\omega^{(n)}(V) + \hat{b}_\omega^{(n)\dagger} g_\omega^{(n)*}(V)], \quad (5.6.3)$$

where  $\hat{b}_\omega^{(n)}$  and  $\hat{b}_\omega^{(n)\dagger}$  are the annihilation and creation operators in the  $n$ -th diamond. Another orthonormal and complete set of modes was introduced in [IOS13], the modes inside the zeroth diamond,  $g_\omega^{(0)}(V)$ , and that outside,

$$g_\omega^{(\text{ex})}(V) = \frac{1}{\sqrt{4\pi\omega}} \left( \frac{aV/2 + 1}{aV/2 - 1} \right)^{i\omega/a} \theta(|V| - 2/a), \quad (5.6.4)$$

which is perfectly correlated with  $g_\omega^{(0)}(V)$ . One can expand the scalar field  $\hat{\Phi}$  as

$$\hat{\Phi} = \int_0^\infty d\omega [\hat{b}_\omega^{(0)} g_\omega^{(0)}(V) + \hat{b}_\omega^{(\text{ex})} g_\omega^{(\text{ex})}(V) + \hat{b}_\omega^{(0)\dagger} g_\omega^{(0)*}(V) + \hat{b}_\omega^{(\text{ex})\dagger} g_\omega^{(\text{ex})*}(V)], \quad (5.6.5)$$

where  $\hat{b}_\omega^{(\text{ex})}$  and  $\hat{b}_\omega^{(\text{ex})\dagger}$  are the annihilation and creation operators outside the 0-th diamond. Similar to constructing the Unruh modes, one can construct modes that cover the whole Minkowski spacetime from  $g_\omega^{(0)}(V)$  and  $g_\omega^{(\text{ex})}(V)$ . Define a new set of operators ( $\hat{c}_\omega^{(0)}, \hat{c}_\omega^{(\text{ex})}$ ) as

$$\begin{aligned} \hat{c}_\omega^{(0)} &= \cosh(r_\omega) \hat{b}_\omega^{(0)} - \sinh(r_\omega) \hat{b}_\omega^{(\text{ex})\dagger}, \\ \hat{c}_\omega^{(\text{ex})} &= \cosh(r_\omega) \hat{b}_\omega^{(\text{ex})} - \sinh(r_\omega) \hat{b}_\omega^{(0)\dagger}. \end{aligned} \quad (5.6.6)$$

The new operators  $\hat{c}_\omega^{(0)}$  and  $\hat{c}_\omega^{(\text{ex})}$  annihilate the Minkowski vacuum,

$$\hat{c}_\omega^{(0)}|0_M\rangle = \hat{c}_\omega^{(\text{ex})}|0_M\rangle = 0. \quad (5.6.7)$$

The inverse transformation of Eq. (5.6.6) is

$$\begin{aligned} \hat{b}_\omega^{(0)} &= \cosh(r_\omega)\hat{c}_\omega^{(0)} + \sinh(r_\omega)\hat{c}_\omega^{(\text{ex})\dagger}, \\ \hat{b}_\omega^{(\text{ex})} &= \cosh(r_\omega)\hat{c}_\omega^{(\text{ex})} + \sinh(r_\omega)\hat{c}_\omega^{(0)\dagger}. \end{aligned} \quad (5.6.8)$$

Based on the inverse transformation Eq. (5.6.8), one can calculate the correlations between  $\hat{b}_\omega^{(0)}$  and  $\hat{b}_\omega^{(\text{ex})}$ ,

$$\begin{aligned} \langle 0_M|\hat{b}_\omega^{(0)}\hat{b}_{\omega'}^{(\text{ex})}|0_M\rangle &= \langle 0_M|\hat{b}_\omega^{(0)\dagger}\hat{b}_{\omega'}^{(\text{ex})\dagger}|0_M\rangle^* = \cosh(r_\omega)\sinh(r_\omega)\delta(\omega - \omega'), \\ \langle 0_M|\hat{b}_\omega^{(0)}\hat{b}_{\omega'}^{(\text{ex})\dagger}|0_M\rangle &= \langle 0_M|\hat{b}_\omega^{(0)\dagger}\hat{b}_{\omega'}^{(\text{ex})}|0_M\rangle^* = 0. \end{aligned} \quad (5.6.9)$$

From Eqs. (5.6.3) and (5.6.5), the operator  $\hat{b}_\omega^{(n)}$  ( $n \neq 0$ ) can be expressed in terms of  $\hat{b}_\omega^{(\text{ex})}$  and  $\hat{b}_\omega^{(\text{ex})\dagger}$ ,

$$\begin{aligned} \hat{b}_\omega^{(n)} &= \int_0^\infty d\omega' \left[ \langle g_\omega^{(n)}, g_{\omega'}^{(\text{ex})} \rangle \hat{b}_{\omega'}^{(\text{ex})} + \langle g_\omega^{(n)}, g_{\omega'}^{(\text{ex})*} \rangle \hat{b}_{\omega'}^{(\text{ex})\dagger} \right] \\ &\equiv \int_0^\infty d\omega' \left[ A_{\omega\omega'}^{(n)} \hat{b}_{\omega'}^{(\text{ex})} + B_{\omega\omega'}^{(n)} \hat{b}_{\omega'}^{(\text{ex})\dagger} \right]. \end{aligned} \quad (5.6.10)$$

By using this property and the Bogoliubov transformation between  $g_\omega^{(\text{ex})}(V)$  and  $g_\omega^{(n)}(V)$  with  $n \neq 0$ , one can easily find

$$\begin{aligned} \langle 0_M|\hat{b}_\omega^{(n)}\hat{b}_{\omega'}^{(0)}|0_M\rangle &= \langle 0_M|\hat{b}_\omega^{(n)\dagger}\hat{b}_{\omega'}^{(0)\dagger}|0_M\rangle^* = \frac{A_{\omega\omega'}^{(n)}}{2\sinh(\pi\Omega')}, \\ \langle 0_M|\hat{b}_\omega^{(n)\dagger}\hat{b}_{\omega'}^{(0)}|0_M\rangle &= \langle 0_M|\hat{b}_\omega^{(n)}\hat{b}_{\omega'}^{(0)\dagger}|0_M\rangle^* = \frac{B_{\omega\omega'}^{(n)}}{2\sinh(\pi\Omega')}. \end{aligned} \quad (5.6.11)$$

From Eqs. (5.6.1) and (5.6.4), we can derive the integral representations of  $A_{\omega\omega'}^{(n)}$  and  $B_{\omega\omega'}^{(n)}$ ,

$$\begin{aligned} A_{\omega\omega'}^{(n)} &= \frac{1}{\pi a} \sqrt{\frac{\Omega'}{\Omega}} \int_{-1}^{+1} ds \frac{1}{(s+2n-1)(s+2n+1)} \left(\frac{1+s}{1-s}\right)^{i\Omega} \left(\frac{s+2n+1}{s+2n-1}\right)^{i\Omega'}, \\ B_{\omega\omega'}^{(n)} &= -\frac{1}{\pi a} \sqrt{\frac{\Omega'}{\Omega}} \int_{-1}^{+1} ds \frac{1}{(s+2n-1)(s+2n+1)} \left(\frac{1+s}{1-s}\right)^{i\Omega} \left(\frac{s+2n+1}{s+2n-1}\right)^{-i\Omega'}. \end{aligned} \quad (5.6.12)$$

For the  $n = 1$  case (adjacent diamonds), the coefficients  $A_{\omega\omega'}^{(1)}$  and  $B_{\omega\omega'}^{(1)}$  can be calculated analytically:

$$A_{\omega\omega'}^{(1)} = \frac{2^{-i(\Omega-\Omega')}}{2\pi a} \sqrt{\frac{\Omega'}{\Omega}} \frac{\Gamma(1-i\Omega)\Gamma(i(\Omega-\Omega'))}{\Gamma(1-i\Omega')}, \quad (5.6.13)$$

$$B_{\omega\omega'}^{(1)} = -\frac{2^{-i(\Omega+\Omega')}}{2\pi a} \sqrt{\frac{\Omega'}{\Omega}} \frac{\Gamma(1-i\Omega)\Gamma(i(\Omega'+\Omega))}{\Gamma(1+i\Omega')}. \quad (5.6.14)$$

When  $\omega = \omega'$ ,  $A_{\omega\omega'}^{(1)}$  is divergent, which means the correlation between same-frequency modes is dominant. The divergence causes no problem, because it should be understood in the sense of a distribution and disappears when a wave packet mode is considered. It is obvious that  $A_{\omega\omega'}^{(1)}$  and  $B_{\omega\omega'}^{(1)}$  are finite and nonzero when  $\omega \neq \omega'$ , indicating different-frequency modes are also correlated. For  $n > 1$ , there are no analytic expressions for  $A_{\omega\omega'}^{(n)}$  and  $B_{\omega\omega'}^{(n)}$ . However, for large  $n$ , we can find asymptotic results:

$$\langle 0_M | \hat{b}_\omega^{(n)} \hat{b}_{\omega'}^{(0)} | 0_M \rangle \approx \frac{1}{4an^2} \frac{\sqrt{\Omega\Omega'}}{\sinh(\pi\Omega) \sinh(\pi\Omega')}, \quad (5.6.15)$$

$$\langle 0_M | \hat{b}_\omega^{(n)\dagger} \hat{b}_{\omega'}^{(0)} | 0_M \rangle \approx -\frac{1}{4an^2} \frac{\sqrt{\Omega\Omega'}}{\sinh(\pi\Omega) \sinh(\pi\Omega')}. \quad (5.6.16)$$

The correlation decays as  $\frac{1}{n^2}$  for large  $n$  but does not vanish. Contrary to the adjacent diamonds, the correlation between same-frequency modes is not dominant.

We proceed to consider localized modes instead of single-frequency modes. In each diamond, we construct Gaussian wave packet modes,

$$\hat{b}^{(n)} = \int_0^\infty d\omega g_n(\omega; \omega_n, \sigma_n, v_n) \hat{b}_\omega^{(n)}, \quad (5.6.17)$$

where  $g_n(\omega; \omega_n, \sigma_n, v_n)$  is a Gaussian wave packet

$$g_n(\omega; \omega_n, \sigma_n, v_n) = \left( \frac{1}{2\pi\sigma_n^2} \right)^{1/4} \exp\left\{ -\frac{(\omega - \omega_n)^2}{4\sigma_n^2} \right\} e^{-i\omega v_n},$$

where  $\omega_n$  is the central frequency,  $\sigma_n$  is the bandwidth,  $v_n$  is the central position of the wave packet, and we assume  $\omega_n \gg \sigma_n$ . The quadrature observable of the Gaussian mode is defined as

$$\hat{X}^{(n)}(\phi) = \hat{b}^{(n)} e^{-i\phi} + \hat{b}^{(n)\dagger} e^{i\phi}, \quad (5.6.18)$$

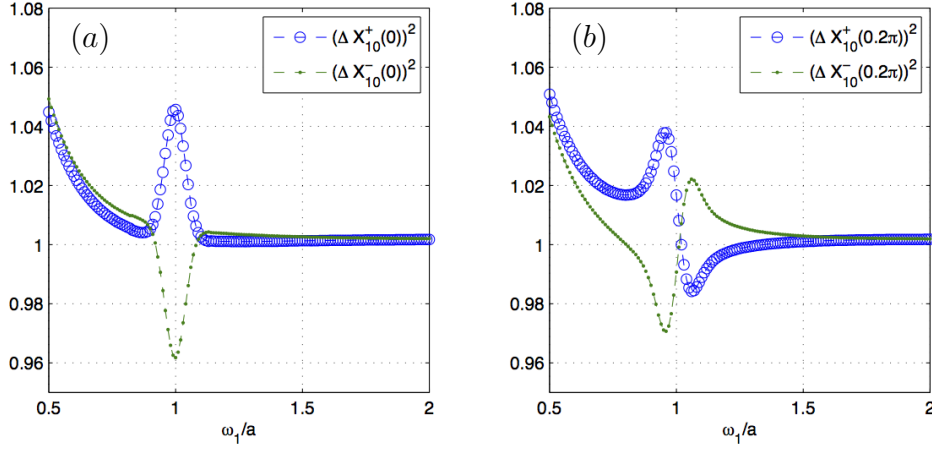


FIGURE 5.5: Entanglement between Gaussian modes in the first and zeroth diamond. Left: quadrature phase  $\phi = 0$ , right: quadrature phase  $\phi = 0.2\pi$ . The central frequency of the Gaussian mode in the zeroth diamond is set to be  $\omega_0/a = 1.0$ , the bandwidth and central position are the same,  $\sigma_1/a = \sigma_0/a = 0.02$ ,  $av_1 = av_0 = 0$ . (a) For  $\phi = 0$ , the variances of  $\hat{X}_-^{10}(0)$  and  $\hat{X}_+^{10}(\pi/2)$  are approximately the same and have a minimum which is smaller than 1 when the central frequency  $\omega_1/a = 1$ , while the variances of  $\hat{X}_+^{10}(0)$  and  $\hat{X}_-^{10}(\pi/2)$  have a maximum which is larger than 1 at  $\omega_1/a = 1$ . (b) For  $\phi = 0.2\pi$ , the minimum variance of  $\hat{X}_-^{10}(0.2\pi)$  is also smaller than one, however the corresponding central frequency of the Gaussian wave packet mode in the first diamond is  $\omega_1/a < 1$ . The maximum variance of  $\hat{X}_+^{10}(0.2\pi)$  is greater than one and the corresponding central frequency of the Gaussian wave packet mode in the first diamond is  $\omega_1/a < 1$ .

where  $\phi$  is the quadrature phase. With  $\phi = 0$  and  $\phi = \frac{\pi}{2}$ , the quadrature  $\hat{X}^{(n)}$  are analogous to the position operator and momentum operator, respectively. Correlations between diamonds can be characterised by the variances of the correlation (“+”) and anti-correlation (“-”) observables,  $\hat{X}_{nm}^\pm \equiv (\hat{X}^{(n)} \pm \hat{X}^{(m)})/\sqrt{2}$ . For example, for two-mode squeezing,  $V(\hat{X}_{nm}^-(0)) < 1$  and  $V(\hat{X}_{nm}^+(\frac{\pi}{2})) < 1$ , indicating that the correlations between the quadratures of the two modes beat the quantum shot noise and are entangled.

In Minkowski vacuum state,  $\langle 0_M | \hat{b}_\omega^{(n)} | 0_M \rangle = 0$ , therefore  $\langle 0_M | \hat{X}^{(n)}(\phi) | 0_M \rangle = 0$ . The variance of the quadrature observable is

$$\begin{aligned}
 (\Delta X^{(n)}(\phi))^2 &= \langle 0_M | (\hat{X}^{(n)}(\phi))^2 | 0_M \rangle \\
 &= 1 + 2\langle 0_M | \hat{b}^{(n)\dagger} \hat{b}^{(n)} | 0_M \rangle + \langle 0_M | \hat{b}^{(n)} \hat{b}^{(n)} | 0_M \rangle e^{-2i\phi} + \langle 0_M | \hat{b}^{(n)\dagger} \hat{b}^{(n)\dagger} | 0_M \rangle e^{2i\phi} \\
 &= 1 + 2\langle 0_M | \hat{b}^{(n)\dagger} \hat{b}^{(n)} | 0_M \rangle.
 \end{aligned} \tag{5.6.19}$$

In the last equality we used the fact that  $\langle 0_M | \hat{b}_\omega^{(n)} \hat{b}_{\omega'}^{(n)} | 0_M \rangle = 0$ . The variance of the quadrature observable is independent of phase and greater than unity, indicating that the state within

a diamond appears mixed. This is consistent with previous result that the particle number distribution of diamond modes is thermal in the Minkowski vacuum. The expectation value of the product of two quadrature observables belonging to two different diamonds is

$$\begin{aligned}
\langle 0_M | \hat{X}^{(n)}(\phi) \hat{X}^{(m)}(\phi) | 0_M \rangle &= \langle 0_M | \hat{b}^{(n)\dagger} \hat{b}^{(m)} | 0_M \rangle + \langle 0_M | \hat{b}^{(m)\dagger} \hat{b}^{(n)} | 0_M \rangle + \langle 0_M | \hat{b}^{(n)} \hat{b}^{(m)} | 0_M \rangle e^{-2i\phi} \\
&\quad + \langle 0_M | \hat{b}^{(n)\dagger} \hat{b}^{(m)\dagger} | 0_M \rangle e^{2i\phi} \\
&= 2 \operatorname{Re} \{ \langle 0_M | \hat{b}^{(n)\dagger} \hat{b}^{(m)} | 0_M \rangle \} + 2 \operatorname{Re} \{ \langle 0_M | \hat{b}^{(n)} \hat{b}^{(m)} | 0_M \rangle e^{-2i\phi} \},
\end{aligned} \tag{5.6.20}$$

where

$$\begin{aligned}
\langle 0_M | \hat{b}^{(n)\dagger} \hat{b}^{(m)} | 0_M \rangle &= \int d\omega \int d\omega' g_n^*(\omega) g_m(\omega') \langle 0_M | \hat{b}_\omega^{(n)\dagger} \hat{b}_{\omega'}^{(m)} | 0_M \rangle \\
&= \int d\omega \int d\omega' g_n^*(\omega) g_m(\omega') \langle 0_M | \hat{b}_\omega^{(n-m)\dagger} \hat{b}_{\omega'}^{(0)} | 0_M \rangle \\
&= \int d\omega \int d\omega' \frac{g_n^*(\omega) g_m(\omega') B_{\omega\omega'}^{(n-m)}}{2 \sinh(\pi\omega'/a)},
\end{aligned} \tag{5.6.21}$$

$$\begin{aligned}
\langle 0_M | \hat{b}^{(n)} \hat{b}^{(m)} | 0_M \rangle &= \int d\omega \int d\omega' g_n(\omega) g_m(\omega') \langle 0_M | \hat{b}_\omega^{(n)} \hat{b}_{\omega'}^{(m)} | 0_M \rangle \\
&= \int d\omega \int d\omega' g_n(\omega) g_m(\omega') \langle 0_M | \hat{b}_\omega^{(n-m)} \hat{b}_{\omega'}^{(0)} | 0_M \rangle \\
&= \int d\omega \int d\omega' \frac{g_n(\omega) g_m(\omega') A_{\omega\omega'}^{(n-m)}}{2 \sinh(\pi\omega'/a)}.
\end{aligned} \tag{5.6.22}$$

We have assumed that  $n \neq m$  and the phases of the two localized modes are the same. Based on Eqs. (5.6.19) and (5.6.20), the variances of the correlation and anti-correlation observables are

$$\begin{aligned}
(\Delta X_{nm}^\pm(\phi))^2 &= \frac{1}{2} (\Delta X^{(n)}(\phi))^2 + \frac{1}{2} (\Delta X^{(m)}(\phi))^2 \pm \langle 0_M | \hat{X}^{(n)}(\phi) \hat{X}^{(m)}(\phi) | 0_M \rangle \\
&= 1 + \langle 0_M | \hat{b}^{(n)\dagger} \hat{b}^{(n)} | 0_M \rangle + \langle 0_M | \hat{b}^{(m)\dagger} \hat{b}^{(m)} | 0_M \rangle \pm \langle 0_M | \hat{X}^{(n)}(\phi) \hat{X}^{(m)}(\phi) | 0_M \rangle.
\end{aligned} \tag{5.6.23}$$

For  $\phi = 0$ , Fig. 5.5(a),  $(\Delta X_{10}^-)^2 < 1$  for two Gaussian modes in adjacent diamonds with the same central frequency, bandwidth and central position. The correlation between the two Gaussian modes beat the quantum shot noise, that is, they are entangled. In fact, since

the bandwidth is so small that the mode distributes across almost the whole diamond, the central position of the Gaussian mode is not so relevant. For nonzero  $\phi$ , e.g.,  $\phi = 0.2\pi$  (Fig. 5.5(b)), correlation between two Gaussian modes with different central frequency can beat the quantum shot noise. These properties are different from the Rindler entanglement which only exists between same-frequency modes and is independent of the quadrature phase. In the next nearby diamonds, correlation between Gaussian modes with much broader bandwidth still can beat the quantum shot noise, although the entanglement is very small. That implies entanglement is stored between Gaussian modes localized in position rather than in frequency. For further away diamonds, it is hard to see entanglement. Although Eq. (5.6.15) shows that the correlation has not vanished, it is very small.

In (1+3)-dimensional Minkowski spacetime, although we know that a mode inside a diamond is perfectly correlated with a corresponding mode outside the diamond, explicit expressions for these modes have not yet been found. In addition, the diamond modes are not complete in the whole Minkowski spacetime. This can be seen by noticing that at  $t = 0$ , the diamonds can not cover the whole space. However, if we only consider timelike entanglement between diamonds along the  $t$  axis, the method used in this section is still valid. In realistic quantum optics experiments, a detector often detects a localized mode, e.g., a Gaussian beam with very narrow transverse size travelling along the  $x$  axis, then the (1 + 1)-dimensional calculation provides a very good approximation to the (1 + 3)-dimensional case.

## 5.7 Summary

By directly calculating the Bogoliubov transformation between the diamond modes and the Minkowski modes, we show that the particle-number distribution in the diamond is thermal in the Minkowski vacuum. The temperature of the thermal distribution is identical to the diamond temperature (that observed by an inertial observer at the middle of their lifetime) discovered by Martinetti and Rovelli [MR03]. We interpret this temperature as the diamond temperature and show that a particular type of energy-scaled detector responds to the diamond temperature. The temperature is constant with respect to diamond time,

but varies with respect to lab time. It is, therefore, clear that the diamond temperature is real and detectable. An order-of-magnitude calculation shows that  $T_D \sim 1K$  corresponds to  $\mathcal{T} \sim 10^{-11}s$ , which is challenge but potentially accessible in the lab in near future. We further study the timelike entanglement between various diamonds and show that entanglement between adjacent diamonds is dominant.

## 5.8 Appendix

In this appendix, we derive in details the particle number distribution of diamond modes in Minkowski vacuum. From Eq. (5.4.4),

$$\begin{aligned} N_{\omega\omega'} &\equiv \int_0^\infty dk \beta_{\omega k}^{(0)*} \beta_{\omega' k}^{(0)} \\ &= \frac{1}{\pi^2 a \sqrt{\Omega\Omega'}} \int_{-1}^{+1} ds \int_{-1}^{+1} ds' \left(\frac{1+s}{1-s}\right)^{-i\Omega} \left(\frac{1+s'}{1-s'}\right)^{i\Omega'} \int_0^\infty d\kappa \kappa e^{-2i\kappa(s-s')} \\ &= -\frac{1}{4\pi^2 a \sqrt{\Omega\Omega'}} \int_{-1}^{+1} ds \int_{-1}^{+1} ds' \frac{1}{(s-s'-i\epsilon)^2} \left(\frac{1+s}{1-s}\right)^{-i\Omega} \left(\frac{1+s'}{1-s'}\right)^{i\Omega'}, \end{aligned}$$

where in the last equality we have used the integration  $\int_0^\infty d\kappa \kappa e^{-i\kappa z} = -\frac{1}{(z-i\epsilon)^2}$ . Define new integration variables  $t$  and  $t'$  as

$$\begin{aligned} t &= \frac{1}{2} \ln \left( \frac{1+s}{1-s} \right), \quad \text{or } s = \tanh t, \\ t' &= \frac{1}{2} \ln \left( \frac{1+s'}{1-s'} \right), \quad \text{or } s' = \tanh t', \end{aligned}$$

we have

$$N_{\omega\omega'} = -\frac{1}{4\pi^2 a \sqrt{\Omega\Omega'}} \int_{-\infty}^{+\infty} dt \int_{-\infty}^{+\infty} dt' \frac{e^{-2i(\Omega t - \Omega' t')}}{\sinh^2(t - t' - i\epsilon)}.$$

By further introducing integration variables  $p$  and  $q$ ,

$$p = t + t', \quad q = t - t',$$

we find

$$\begin{aligned} N_{\omega\omega'} &= -\frac{1}{8\pi^2 a \sqrt{\Omega\Omega'}} \int_{-\infty}^{+\infty} dp e^{-i(\Omega - \Omega')p} \int_{-\infty}^{+\infty} dq \frac{e^{-i(\Omega + \Omega')q}}{\sinh^2(q - i\epsilon)} \\ &= -\frac{1}{4\pi^2 a \Omega} \delta(\Omega - \Omega') \int_{-\infty}^{+\infty} dq \frac{e^{-2i\Omega q}}{\sinh^2(q - i\epsilon)}. \end{aligned}$$

Utilizing the trick that we used to calculate the transition rate of a uniformly accelerated Unruh-DeWitt detector in Minkowski vacuum, Eq. (4.5.65), we finally obtain

$$N_{\omega\omega'} = \frac{1}{e^{2\pi\omega/a} - 1} \delta(\omega - \omega').$$

Therefore the particle number distribution of diamond modes in the Minkowski vacuum is thermal, with temperature  $a/2\pi$ .



# 6

## Quantum Communication with Uniformly Accelerated Observers

### 6.1 Introduction

One important task of relativistic quantum information [PT04] is to investigate how relativistic motion and gravitational fields affect the storage, transfer and processing of quantum information. Early works mainly studied global states of quantum fields, for example, the effects of acceleration on the entanglement of global states [AM03, FSM05]. Recently, a general framework for projective measurements on a localized single mode of the quantum field was proposed [DDMMB13]. This formalism was used to study the effect of relativistic acceleration on continuous variable quantum teleportation and dense coding [GRKD17]. In reference [GRKD17], the authors assume that accelerated observers only have access to a

single mode in the accelerated frame, which results in larger mode mismatch as the acceleration increases. In this chapter, we are study mode mismatch due to the presence of a horizon, which causes intrinsic loss of information about the state as viewed by inertial observers.

As a specific realization of localized projective measurements, homodyne detection was proposed as a way to model efficient, directional quantum communication between two localized parties in a relativistic quantum field theory scenario [DRW13]. An interesting case is the quantum communication with a uniformly accelerated partner, in which the Unruh effect [Unr76] is expected to play an important role.

In this chapter, we are going to discuss two quantum communication protocols with accelerated observers. In Section 6.2, we study the quantum communication between an inertial observer and a uniformly accelerated observer. In Section 6.3, we investigate the quantum communication between two uniformly accelerated observers. In particular, we are interested in cases where the localized wave packet sent by the sender straddles the future horizon of the receiver. The results in Section 6.2 have been published in [SR14]. The result of Section 6.3 is the joint research effort by Robert Mann, Timothy Ralph and myself.

## 6.2 Quantum communication between an inertial observer and a uniformly accelerated observer

This section discusses the first protocol: quantum communication between an inertial observer and a uniformly accelerated observer. In this protocol, an inertial sender, Alice, sends a coherent state signal and a local oscillator to an accelerated receiver, Rob, who then performs homodyne detection in his own frame. Approximate analytic solutions were obtained in the case the wave packet sent by Alice is well localized in the right Rindler wedge. We generalize this work to the case where the wave packet straddles the future horizon of Rob. Similar scenario was considered to study quantum entanglement through the event horizon [DDMM13]. As a result, Rob can only access part of the signal and local oscillator.

Generally, the signal and noise received by Rob are divergent if Rob’s detector can detect arbitrarily low frequency particles. This is because in the horizon-straddling case Rob can still detect particles at late times when his velocity approaches the speed of light, resulting in large redshift of the signal and local oscillator. While, under some special conditions, the signal and local oscillator received by Rob remain finite no matter what low frequency cutoff he chooses. In order to get finite results generally, and to correspond with physical detectors, we introduce a low frequency cutoff. We find that there exists a low frequency cutoff that maximizes the signal to noise ratio. Interestingly, this low frequency cutoff approximately corresponds to the Unruh temperature, and we thus call it the Unruh frequency. In addition, we calculate the conditional variance and find that the low frequency cutoff that minimizes the conditional variance is also approximately equal to the Unruh frequency.

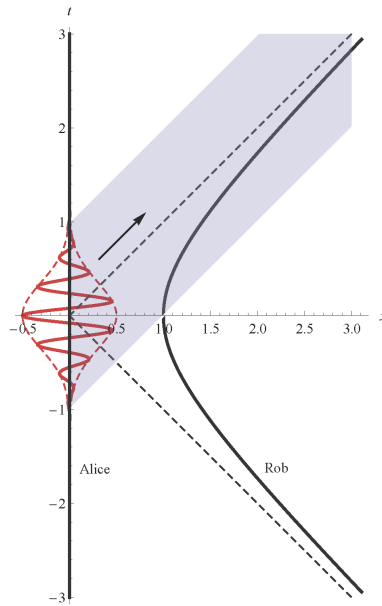


FIGURE 6.1: Alice (static) sends Rob (accelerated) a Gaussian wave packet which straddles Rob’s future horizon.

### 6.2.1 Homodyne Detection in an accelerated frame

For simplicity, we consider the massless scalar field in  $(1 + 1)$ -dimensional Minkowski spacetime. Generalization to  $(3 + 1)$ -dimensional Minkowski spacetime is straightforward by making the paraxial approximation and taking into account the expansion of the transverse

shape of the wave packet during its propagation. There are two inequivalent ways to quantize the massless scalar field in Minkowski spacetime [Ful73], one for inertial observers and the other for uniformly accelerated observers.

In the inertial frame, the massless scalar field is quantized in the usual way,

$$\hat{\Phi}(t, x) = \int_0^\infty dk [\hat{a}_k u_k(U) + \hat{a}_k^\dagger u_k^*(U)] + (\text{left-moving parts}), \quad (6.2.1)$$

where  $u_k(U) = \frac{1}{\sqrt{4\pi k}} e^{-ikU}$ , with  $U = t - x$ , are positive frequency right-moving Minkowski plane wave mode functions,  $u_k^*$  are negative frequency mode functions, and  $\hat{a}_k$  ( $\hat{a}_k^\dagger$ ) are annihilation(creation) operators of single frequency Minkowski modes. In this chapter, we only consider right-moving modes and neglect the subscript “2”, which characterizes right-moving modes, without introducing confusions. In terms of Rindler coordinates and Rindler modes,  $\hat{\Phi}(\tau, \xi)$  can be expanded as

$$\hat{\Phi}(\tau, \xi) = \int_0^\infty d\Omega [\hat{b}_\Omega g_\Omega^R(u) + \hat{b}_\Omega^\dagger g_\Omega^{R*}(u)] + (\text{left-moving parts}), \quad (6.2.2)$$

where  $g_\Omega^R(u) = \frac{1}{\sqrt{4\pi\Omega a}} e^{-i\Omega a u}$  are positive frequency right-moving Rindler plane wave mode functions,  $g_\Omega^{R*}(u)$  are negative mode functions,  $\hat{b}_\Omega$  ( $\hat{b}_\Omega^\dagger$ ) are annihilation(creation) operators of single frequency Rindler modes obeying boson commutation relation

$$[\hat{b}_\Omega, \hat{b}_{\Omega'}^\dagger] = \delta(\Omega - \Omega'). \quad (6.2.3)$$

Here  $\Omega$  is defined as a dimensionless Rindler frequency, which is related to the physical frequency  $\omega$  by  $\Omega = \omega/a$ . The subscript “2” is also neglected for the Rindler modes. In addition, we only consider Rindler modes in the right Rindler wedge, we thus neglect the superscript “R” in the Rindler annihilation and creation operators.

We consider the scenario that a uniformly accelerated observer, Rob, with proper acceleration  $a$  travels along  $\xi = 0$  in the right Rindler wedge and an inertial observer, Alice, stays at spatial origin  $x = 0$ , as shown in Figure 6.1. Alice sends a right-moving signal, a coherent state with amplitude  $\alpha$ , and a local oscillator to Rob. The local oscillator is also a coherent state, but with very large amplitude  $\beta \in \mathbb{R}$ ,  $\beta \gg |\alpha|$ . Rob then performs homodyne detection

on the signal using the local oscillator as seen in his own reference frame. The homodyne detector is formed from two identical photodetectors that detect distinct modes  $S$  and  $L$  after they have been mixed on a beam splitter. The photocurrents from the photodetectors are subtracted to give the output signal. As a result the output of Rob's homodyne detector at some time  $\tau$  (as measured in Rob's frame) is represented by the following operator [BR04]:

$$\hat{O}(\tau, \phi) = \hat{b}_S(\tau)\hat{b}_L^\dagger(\tau)e^{i\phi} + \hat{b}_S^\dagger(\tau)\hat{b}_L(\tau)e^{-i\phi}, \quad (6.2.4)$$

where  $\hat{b}_K$  ( $\hat{b}_K^\dagger$ ) are boson annihilation(creation) operators with  $K = S, L$ . The subscripts  $S, L$  refer to the signal and local oscillator modes, respectively. The relative phase  $\phi$  determines the quadrature angle detected. Here  $\hat{b}_K(\tau)$  are temporally and spatially localized single mode annihilation operators in the perspective of Rob. They can be constructed from the single frequency Rindler annihilation operators  $\hat{b}_\Omega$ ,

$$\hat{b}_K(\tau) = \int_0^\infty d\Omega f_K(\Omega, \tau)\hat{b}_\Omega, \quad (6.2.5)$$

where  $f_K(\Omega, \tau)$  is Rob's detector mode function. In an experiment, Rob would integrate the photocurrent from his detector over a time long compared to the inverse of the frequency being analyzed (as will be determined by the frequency of the local detector). For later convenience, we define the integrated output signal operator  $\hat{X}(\phi)$ ,

$$\hat{X}(\phi) \equiv \int d\tau \hat{O}(\tau, \phi) = \int d\tau [\hat{b}_S(\tau)\hat{b}_L^\dagger(\tau)e^{i\phi} + \hat{b}_S^\dagger(\tau)\hat{b}_L(\tau)e^{-i\phi}]. \quad (6.2.6)$$

The expectation value of the output signal received by Rob is

$$X_\phi = \langle \hat{X}(\phi) \rangle, \quad (6.2.7)$$

and the variance is

$$V_\phi = \langle \hat{X}^2(\phi) \rangle - \langle \hat{X}(\phi) \rangle^2. \quad (6.2.8)$$

Alice prepares coherent states (signal and local oscillator) by displacing the Minkowski vacuum  $|0_M\rangle$  using the displacement operators  $\hat{D}_K(\gamma) = \exp(\gamma\hat{a}_K^\dagger - \gamma^*\hat{a}_K)$ , with  $\gamma = \alpha, \beta$ , and

$$\hat{a}_K = \int dk f_{D_K}(k, t, x)\hat{a}_k, \quad (6.2.9)$$

where  $f_{D_K}(k, t, x)$  is a normalized displacement mode function satisfying  $\int dk |f_{D_K}(k, t, x)|^2 = 1$ . Therefore,  $\hat{a}_K$  are also temporally and spatially localized annihilation operators in the perspective of Alice. The state that Alice prepares can be written in a compact form,

$$|\alpha, \beta, t\rangle = \hat{D}_S(\alpha)\hat{D}_L(\beta)|0_M\rangle. \quad (6.2.10)$$

The expectation value of the signal becomes

$$X_\phi = \langle 0_M | \hat{D}_L^\dagger(\beta)\hat{D}_S^\dagger(\alpha)\hat{X}(\phi)\hat{D}_S(\alpha)\hat{D}_L(\beta) | 0_M \rangle. \quad (6.2.11)$$

In order to explicitly calculate the expectation value and variance of the signal, we need to know the Bogolyubov transformation between the Rindler modes and Minkowski modes, which are already given by [Tak86, CHM08]

$$\hat{b}_\Omega = \int dk (\alpha_{\Omega k}\hat{a}_k + \beta_{\Omega k}\hat{a}_k^\dagger), \quad (6.2.12)$$

where

$$\begin{aligned} \alpha_{\Omega k} &= \frac{ie^{\pi\Omega/2}}{2\pi\sqrt{\Omega k}}\Gamma(1-i\Omega)\left(\frac{k}{a}\right)^{i\Omega}, \\ \beta_{\Omega k} &= \frac{ie^{-\pi\Omega/2}}{2\pi\sqrt{\Omega k}}\Gamma(1-i\Omega)\left(\frac{k}{a}\right)^{i\Omega} \end{aligned} \quad (6.2.13)$$

are the Bogolyubov coefficients for right-moving waves. Taking into account Eq. (6.2.12), we can find the identity

$$\begin{aligned} \hat{D}_K^\dagger(\gamma)\hat{b}_K(\tau)\hat{D}_K(\gamma) &= \hat{b}_K(\tau) + \gamma \int d\Omega \int dk f_K(\Omega, \tau) [\alpha_{\Omega k}f_{D_K}^*(k) + \beta_{\Omega k}f_{D_K}(k)] \\ &\equiv \hat{b}_K(\tau) + \gamma F_K(\tau). \end{aligned} \quad (6.2.14)$$

The expressions for  $X_\phi$  and  $V_\phi$  can be expanded via Eq.(6.2.14).

Although the amplitude of the local oscillator sent by Alice is  $\beta$ , it is not so when viewed by Rob due to Doppler shift and Rob's inability to access the whole wave packet. The latter effect is more important in the horizon-straddling case. However, one has to bear in mind that this does not mean the amplitude of the local oscillator must be attenuated. In fact, it sometimes can be amplified. Homodyne detection only measures the amplitude without

caring about the frequency of the mode. So it is possible that Rob detects a large amount of low frequency particles but the total energy of these particles is still smaller than the energy of the original wave packet. If Rob performs homodyne detection without knowing the amplitude of the local oscillator sent by Alice, he has to measure the strength of the local oscillator by adding the photocurrents of the two photodetectors. We define the strength of the local oscillator as seen by Rob as

$$I \equiv \int d\tau \langle \hat{b}_L^\dagger \hat{b}_L \rangle = \int d\tau \langle 0_M | \hat{D}_L^\dagger(\beta) \hat{D}_S^\dagger(\alpha) \hat{b}_L^\dagger \hat{b}_L \hat{D}_S(\alpha) \hat{D}_L(\beta) | 0_M \rangle. \quad (6.2.15)$$

Both the expectation value  $X_\phi$  and variance  $V_\phi$  of the signal should be normalized by the strength of the local oscillator. Since the Bogolyubov transformation (6.2.12) is a linear transformation, it is obvious that  $\langle 0_M | \hat{b}_K | 0_M \rangle = \langle 0_M | \hat{b}_K^\dagger | 0_M \rangle = 0$ . Taking into account the fact that  $\beta \gg |\alpha|$ , we have

$$\begin{aligned} X_\phi &\approx \beta \alpha e^{i\phi} \int d\tau F_S(\tau) F_L^*(\tau) + \beta \alpha^* e^{-i\phi} \int d\tau F_S^*(\tau) F_L(\tau), \\ V_\phi &\approx \beta^2 \int d\tau \int d\tau' F_L^*(\tau) F_L(\tau') \langle 0_M | \{ \hat{b}_S(\tau), \hat{b}_S^\dagger(\tau') \} | 0_M \rangle, \\ I &\approx \beta^2 \int d\tau F_L(\tau) F_L^*(\tau), \end{aligned} \quad (6.2.16)$$

where  $\{\hat{A}, \hat{B}\} = \hat{A}\hat{B} + \hat{B}\hat{A}$  represents anticommutation of two operators. If we further require that the detector mode function for signal and local oscillator are the same and the displacement mode function for signal and local oscillator are also the same, then  $F_S(\tau) = F_L(\tau)$ . The normalized output signal becomes

$$\bar{X}_\phi = \frac{X_\phi}{\sqrt{I}} \approx \sqrt{\int d\tau F_L(\tau) F_L^*(\tau)} (\alpha e^{i\phi} + \alpha^* e^{-i\phi}) \approx \frac{\sqrt{I}}{\beta} (\alpha e^{i\phi} + \alpha^* e^{-i\phi}), \quad (6.2.17)$$

and the normalized variance becomes

$$\bar{V}_\phi = \frac{V_\phi}{I} \approx \frac{\int d\tau \int d\tau' F_L^*(\tau) F_L(\tau') \langle 0_M | \{ \hat{b}_S(\tau), \hat{b}_S^\dagger(\tau') \} | 0_M \rangle}{\int d\tau F_L(\tau) F_L^*(\tau)}. \quad (6.2.18)$$

In order to proceed, we need to introduce explicit forms for Rob's detector mode function and Alice's displacement mode function. The detector mode function can be written as

$$f_K(\Omega, \tau) = e^{-i\Omega a \tau} f_K(\Omega). \quad (6.2.19)$$

It is important that the detector mode function should be well localized spatially and temporally; otherwise, its interpretation as a detector following a particular spacetime trajectory is compromised. Thus we consider a detector mode function that is very broad in  $\Omega$ ; in particular, we take  $f_K(\Omega) \approx \sqrt{a/2\pi}$  for  $\Omega \geq \Omega_{\text{cut}} > 0$  and zero otherwise, where  $\Omega_{\text{cut}}$  is some low frequency cutoff. We will see that if we do not introduce a low frequency cutoff,  $\bar{X}_\phi$  and  $\bar{V}_\phi$  may be divergent. That means if Rob's detector is accurate enough so that it responds to any low frequency particles, he will detect very large amounts of low frequency particles. However, in practice, there is always some low frequency below which Rob's detector cannot detect. From Figure 6.1 we can see that, in the horizon-straddling case, the wave packet overlaps with Rob's whole future worldline. That is to say, Rob can detect particles even when  $\tau \rightarrow +\infty$ . Therefore, the integrals over  $\tau$  in Eqs.(6.2.17) and (6.2.18) go from  $-\infty$  to  $+\infty$  and we have the simplification  $\int d\tau \frac{a}{2\pi} e^{-i(\Omega-\Omega')a\tau} \approx \delta(\Omega - \Omega')$ .

We assume that the displacement mode function is peaked at a large wave number  $k_o > 0$ , much larger than the bandwidth  $\sigma$ , although  $\sigma$  is also broad on the wavelength scale. Hence we write  $k = k_o + \bar{k}$ , where  $k_o \gg |\bar{k}|$  for the region of wave numbers for which the mode function is nonzero. These are typical approximations used for nonrelativistic quantum communication systems. The displacement mode function thus can be written as

$$f_{D_K}(k; t_o, x_o) = e^{-ikU_o} f_D(k), \quad (6.2.20)$$

where  $U_o = t_o - x_o$  represents the central position of the wave packet. In particular, we choose  $f_D(k)$  as a Gaussian form,

$$f_D(k) = \left( \frac{1}{2\pi\sigma^2} \right)^{1/4} \exp \left\{ -\frac{(k - k_o)^2}{4\sigma^2} \right\}, \quad (6.2.21)$$

satisfying  $k_o/\sigma \gg 1$ . One term in Eq.(6.2.13) can be approximated as

$$\left( \frac{k}{a} \right)^{i\Omega} \approx e^{ik(\frac{\Omega}{k_o})} e^{i\Omega[\ln(k_o/a)-1]}, \quad (6.2.22)$$

and using the identity

$$|\Gamma(1 - i\Omega)|^2 = \frac{\pi\Omega}{\sinh(\pi\Omega)},$$

we have

$$\begin{aligned}
 \alpha_{\Omega k} \alpha_{\Omega k'}^* &\approx \frac{1}{2\pi k_o (1 - e^{-2\pi\Omega})} e^{ik(\frac{\Omega}{k_o})} e^{-ik'(\frac{\Omega}{k_o})}, \\
 \alpha_{\Omega k} \beta_{\Omega k'}^* &\approx \frac{e^{-\pi\Omega}}{2\pi k_o (1 - e^{-2\pi\Omega})} e^{ik(\frac{\Omega}{k_o})} e^{-ik'(\frac{\Omega}{k_o})}, \\
 \beta_{\Omega k} \alpha_{\Omega k'}^* &\approx \frac{e^{-\pi\Omega}}{2\pi k_o (1 - e^{-2\pi\Omega})} e^{ik(\frac{\Omega}{k_o})} e^{-ik'(\frac{\Omega}{k_o})}, \\
 \beta_{\Omega k} \beta_{\Omega k'}^* &\approx \frac{e^{-2\pi\Omega}}{2\pi k_o (1 - e^{-2\pi\Omega})} e^{ik(\frac{\Omega}{k_o})} e^{-ik'(\frac{\Omega}{k_o})}.
 \end{aligned} \tag{6.2.23}$$

The strength of the local oscillator received by Rob can be calculated as

$$\begin{aligned}
 I &\approx \beta^2 \int d\Omega \int dk \int d\Omega' \int dk' \int d\tau f_L(\Omega, \tau) f_L^*(\Omega', \tau) \left[ \alpha_{\Omega k} f_{D_L}^*(k) + \beta_{\Omega k} f_{D_L}(k) \right] \\
 &\quad \times \left[ \alpha_{\Omega' k'}^* f_{D_L}(k') + \beta_{\Omega' k'}^* f_{D_L}^*(k') \right] \\
 &\approx \beta^2 \int d\Omega \int dk \int dk' \left[ \alpha_{\Omega k} \alpha_{\Omega k'}^* f_{D_L}^*(k) f_{D_L}(k') + \alpha_{\Omega k} \beta_{\Omega k'}^* f_{D_L}^*(k) f_{D_L}^*(k') \right. \\
 &\quad \left. + \beta_{\Omega k} \alpha_{\Omega k'}^* f_{D_L}(k) f_{D_L}(k') + \beta_{\Omega k} \beta_{\Omega k'}^* f_{D_L}(k) f_{D_L}^*(k') \right] \\
 &\approx \beta^2 \sqrt{\frac{2}{\pi}} \frac{\sigma}{k_o} \int d\Omega \frac{1}{1 - e^{-2\pi\Omega}} \left[ e^{-2\sigma^2(\Omega+k_o U_o)^2/k_o^2} + e^{-2\pi\Omega} e^{-2\sigma^2(\Omega-k_o U_o)^2/k_o^2} \right. \\
 &\quad \left. + 2 \cos(2k_o U_o) e^{-\pi\Omega} e^{-\sigma^2(\Omega+k_o U_o)^2/k_o^2} e^{-\sigma^2(\Omega-k_o U_o)^2/k_o^2} \right].
 \end{aligned} \tag{6.2.24}$$

Substituting Eq. (6.2.24) into Eq. (6.2.17), we have a general expression for the expectation value of the signal.

If  $U_o < 0$  and  $|k_o U_o| \gg k_{so}/\sigma$ , then only the first term in Eq.(6.2.24) survives. In addition, the Gaussian part of the integrand can be approximated as a delta function, that is,  $\sqrt{\frac{2}{\pi}} \frac{\sigma}{k_o} e^{-2\sigma^2(\Omega+k_o U_o)^2/k_o^2} \approx \delta(\Omega + k_o U_o)$ . We can recover the analytic expression for the normalized output signal found in [DRW13],

$$\bar{X}_\phi \approx \frac{\alpha e^{i\phi} + \alpha^* e^{-i\phi}}{\sqrt{1 - e^{-2\pi k_o |U_o|}}}. \tag{6.2.25}$$

In this case, Rob can access nearly the whole wave packet because  $|k_o U_o| \gg k_o/\sigma$  implies  $|U_o| \gg 1/\sigma \approx l_c$ , where  $l_c$  is the characteristic spread of the wave packet in position space. The approximate expression of  $\bar{X}_\phi$  shows that the output signal is amplified due to the

Unruh thermalization. However, this amplification is quite small. Since we initially assume that  $k_o/\sigma \gg 1$ , so  $|k_o U_o| \gg 1$ , then  $e^{-2\pi k_o |U_o|}$  must be a very small number. This can be verified in our numerical integration of Eq. (6.2.24) below.

Next, we would like to calculate the variance of the signal. Using Eq.(6.2.13) and the identity

$$\int_0^\infty \frac{dk}{2\pi k} k^{i(\Omega - \Omega')} = \delta(\Omega - \Omega'), \quad (6.2.26)$$

we find

$$\begin{aligned} \langle 0_M | \hat{b}_\Omega \hat{b}_{\Omega'}^\dagger | 0_M \rangle &= \int dk \alpha_{\Omega k} \alpha_{\Omega' k}^* = \frac{1}{1 - e^{-2\pi\Omega}} \delta(\Omega - \Omega'), \\ \langle 0_M | \hat{b}_{\Omega'}^\dagger \hat{b}_\Omega | 0_M \rangle &= \int dk \beta_{\Omega k} \beta_{\Omega' k}^* = \frac{e^{-2\pi\Omega}}{1 - e^{-2\pi\Omega}} \delta(\Omega - \Omega'), \end{aligned} \quad (6.2.27)$$

and therefore,

$$\begin{aligned} \langle 0_M | \{ \hat{b}_S(\tau), \hat{b}_S^\dagger(\tau') \} | 0_M \rangle &= \int d\Omega \int d\Omega' f_S(\Omega, \tau) f_S^*(\Omega', \tau') \langle 0_M | \{ \hat{b}_\Omega, \hat{b}_{\Omega'}^\dagger \} | 0_M \rangle \\ &= \int d\Omega f_S(\Omega, \tau) f_S^*(\Omega, \tau') \frac{1 + e^{-2\pi\Omega}}{1 - e^{-2\pi\Omega}}. \end{aligned} \quad (6.2.28)$$

Taking into account  $f_S(\Omega, \tau) = f_L(\Omega, \tau)$ , we have

$$\begin{aligned} V_\phi &= \beta^2 \sqrt{\frac{2}{\pi}} \frac{\sigma}{k_o} \int d\Omega \left[ e^{-2\sigma^2(\Omega + k_o U_o)^2 / k_o^2} + 2 \cos(2k_o U_o) e^{-\pi\Omega} e^{-\sigma^2(\Omega + k_o U_o)^2 / k_o^2} e^{-\sigma^2(\Omega - k_o U_o)^2 / k_o^2} \right. \\ &\quad \left. + e^{-2\pi\Omega} e^{-2\sigma^2(\Omega - k_o U_o)^2 / k_o^2} \right] \frac{1 + e^{-2\pi\Omega}}{(1 - e^{-2\pi\Omega})^2}. \end{aligned} \quad (6.2.29)$$

Substituting Eq. (6.2.29) into Eq. (6.2.18), we finally get a general expression for the normalized variance of the output signal. Again, in the case where  $U_o < 0$  and  $|k_o U_o| \gg k_o/\sigma$ , we can recover the analytic expression found in [DRW13],

$$\bar{V}_\phi \approx \frac{1 + e^{-2\pi k_o |U_o|}}{1 - e^{-2\pi k_o |U_o|}}. \quad (6.2.30)$$

However, the Unruh thermalization effect is still very small because  $|k_o U_o| \gg 1$  so  $\bar{V}_\phi \approx 1$ .

## 6.2.2 Horizon-straddling case

We would like to explore the horizon-straddling case where  $U_o \approx 0$ . The approximation made in [DRW13] is no longer valid because contributions of the second and third terms

in Eqs. (6.2.24) and (6.2.29) are significant and important. Since there is no analytic expression for the integration, we numerically integrate Eqs. (6.2.24) and (6.2.29) for various parameters. It turns out that in most cases  $I$  and  $\bar{V}_\phi$  are divergent if we integrate over an arbitrarily low frequency. Physically, this means if Rob's detector is strong enough such that it can detect arbitrarily low frequency particles, then Rob will observe a large expectation value and fluctuation of the number of low frequency particles. This is reasonable because when the wave packet straddles Rob's future horizon, most of these particles are greatly redshifted as seen by Rob, especially at late times when Rob's velocity approaches the speed of light. In realistic situations, Rob's detector cannot detect arbitrarily low frequency particles. Therefore, we introduce a low frequency cutoff  $\Omega_{\text{cut}}$  for the detector mode function. One might expect that the low frequency cutoff depends on the specific detector Rob carries. That is true, but we do not want to discuss specific models of Rob's detector. We can find a natural low frequency cutoff by other considerations.

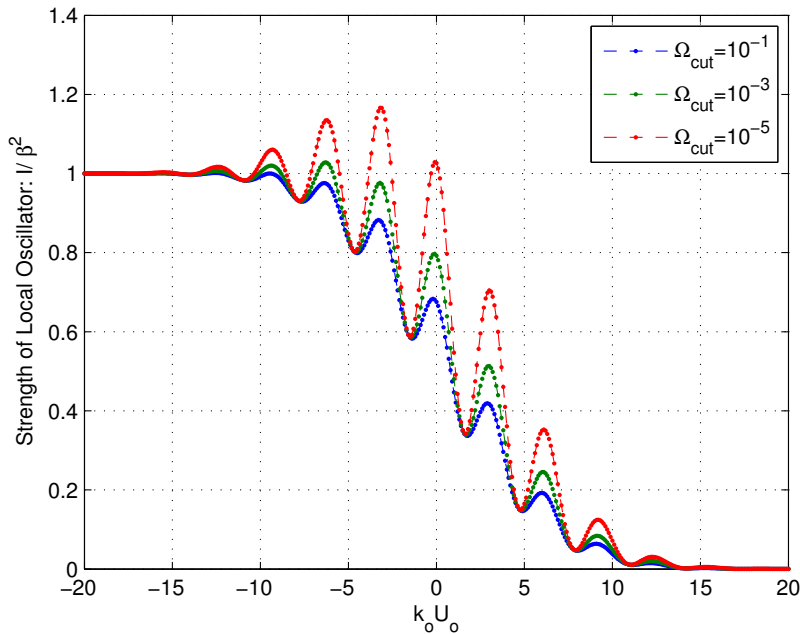


FIGURE 6.2: Strength of local oscillator for various low frequency cutoffs:  $\Omega_{\text{cut}} = 0.00001$  (top),  $0.001$  (middle),  $0.1$  (bottom),  $\delta = \frac{k_\sigma}{\sigma} = 10$ .

Figs. 6.2 and 6.3 show the strength of the local oscillator and the variance of the output

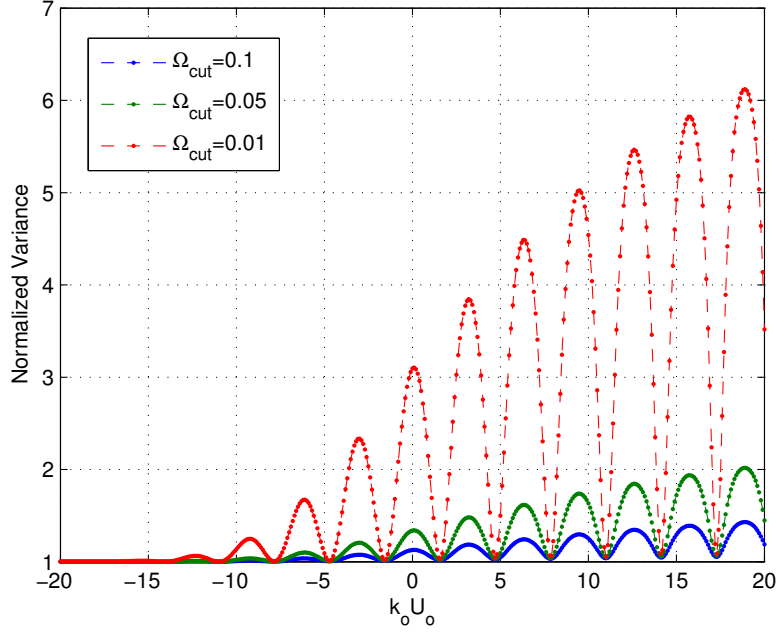


FIGURE 6.3: Normalized variance for various low frequency cutoffs:  $\Omega_{\text{cut}} = 0.01$  (top), 0.05 (middle), 0.1 (bottom),  $\delta = \frac{k_o}{\sigma} = 10$ .

signal received by Rob for various parameters. According to Eq. (6.2.17), the strength of the local oscillator  $I/\beta^2$  also characterizes the amplitude of the expectation value of the output signal for a given relative phase  $\phi$ . Thus Fig. 6.2 also indirectly shows the amplitude of the expectation value of the output signal. We can see that they depend on when Alice sends the signal and local oscillator if the central wave number  $k_o$  is fixed. If Alice sends the signal and local oscillator early enough then  $I \approx \beta^2$ ,  $\bar{V}_\phi \approx 1$ , and thus  $\bar{X}_\phi \approx \alpha e^{i\phi} + \alpha^* e^{-i\phi}$ . Rob sees the original coherent state signal. The Unruh thermalization effect is not significant, as we have argued before. If Alice sends them later so that the wave packet straddles Rob's future horizon, the strength of the local oscillator decreases with some characteristic oscillation, while the variance increases with similar oscillation. The Unruh thermalization becomes significant in this horizon-straddling case. Interestingly, if we choose lower frequency cutoff, for some specific values of  $k_o U_o$  the strength of the local oscillator and the variance remain unchanged, while for other  $k_o U_o$  they increase dramatically. These particular values of  $k_o U_o$  can be determined by  $k_o U_o \approx (\frac{1}{2} + n)\pi$ ,  $n = 0, \pm 1, \pm 2, \dots$ , and at these points the variances are approximately one. From Eq. (6.2.24), the local oscillator received by Rob is quite different

from that sent by Alice in the horizon-straddling case. Since Rob still can see the wave packet at late times when his velocity approaches the speed of light, one expects that the wave packet is greatly redshifted as seen by Rob. Therefore, Rob's effective local oscillator consists of large amounts of low frequency components, resulting in large expectation value and variance in the homodyne detection, implying an amplification of the original coherent state. However, for some specific values of  $k_o U_o$ , the low frequency components in the local oscillator are strongly suppressed. This can easily be verified by substituting  $k_o U_o = (\frac{1}{2} + n)\pi$  into the integrand in Eq. (6.2.24). Consequently, the strength of the local oscillator and the variance do not significantly depend on the low frequency cutoff for these values of  $k_o U_o$ .

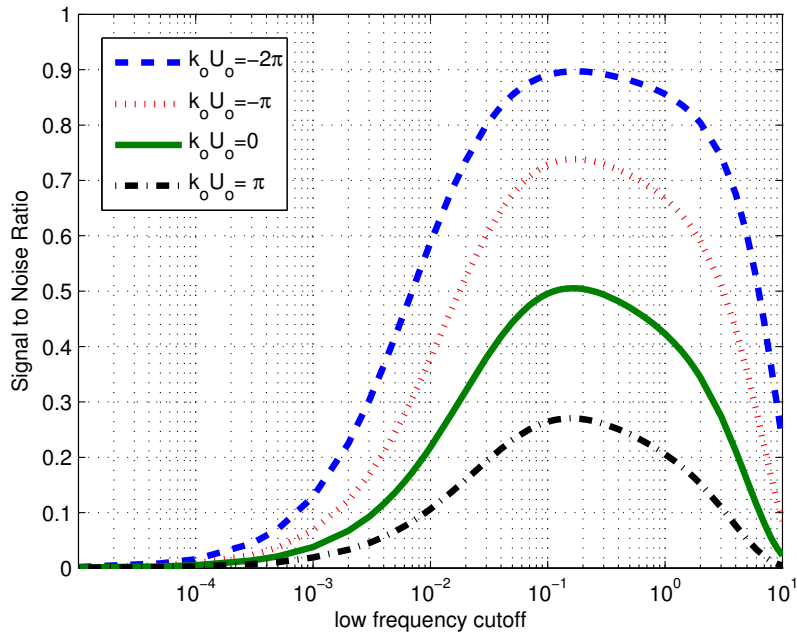


FIGURE 6.4: Signal to noise ratio versus low frequency cutoff for  $k_o U_o = n\pi$ ,  $\delta = \frac{k_o}{\sigma} = 10$ . The signal to noise ratio decreases when the low frequency cutoff become smaller and larger. The low frequency cutoff that maximizes the signal to noise ratio is between 0.1 and 0.2.

Fig. 6.4 shows Rob's signal to noise ratio for  $k_o U_o = n\pi$ . These values approximately correspond to peaks of the oscillation of the expectation value and variance of the output signal, as shown in Figs. 6.2 and 6.3. The signal to noise ratio decreases and goes to zero when the low frequency cutoff becomes smaller. This is because the variance increases faster than the expectation value as the low frequency cutoff approaches zero. On the other side, when the low frequency cutoff becomes larger, the signal to noise ratio also decreases. Since the

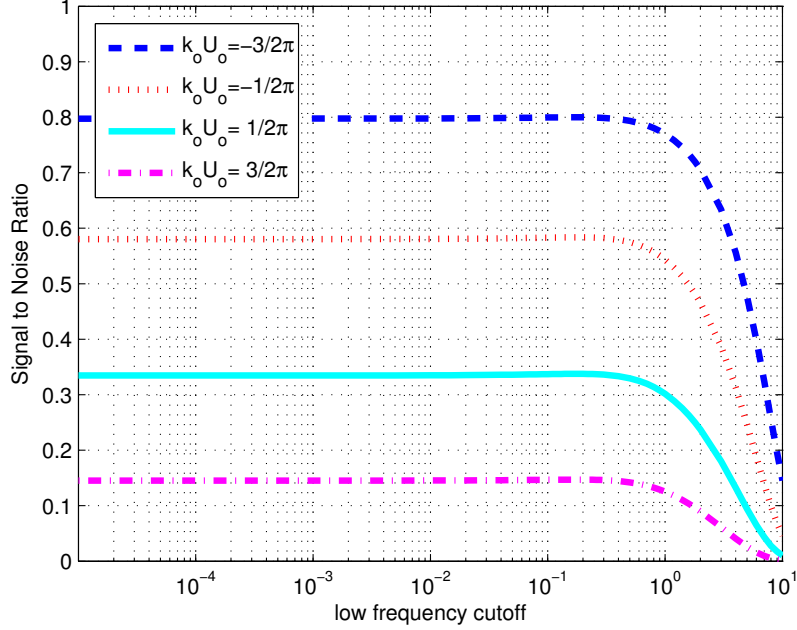


FIGURE 6.5: Signal to noise ratio versus low frequency cutoff for  $k_o U_o = (\frac{1}{2} + n)\pi$ ,  $\delta = \frac{k_o}{\sigma} = 10$ . The signal to noise ratio first increases and then tends to be a constant when the low frequency cutoff becomes smaller.

variance tends to one in the large low frequency cutoff limit, this means the expectation value of the output signal decreases. There is a maximum when the low frequency cutoff is between 0.1 and 0.2. The behavior of the signal to noise implies that the signal and local oscillator Rob receives mainly contain low frequency particles. However, when  $k_o U_o = (n + 1/2)\pi$  where troughs of the oscillation of the expectation value and variance of the signal locate, the behaviour of the signal to noise ratio is a bit different. Instead of going to zero, it tends to be constant when the low frequency cutoff is smaller than some particular value, which is also between 0.1 and 0.2, as can be seen from Fig. 6.5. This is closely related to the fact that for these values of  $k_o U_o$  the low frequency components in the local oscillator are strongly suppressed. For those values of  $k_o U_o$  between peaks and troughs, the signal to noise ratio behaves more like those at the peaks, because both the expectation value and variance increase but the variance increases faster than the expectation value in the low frequency limit. Therefore, we can see that there exists a low frequency cutoff  $\Omega_{cm}$  which maximizes the signal to noise ratio for various  $k_o U_o$  and  $\Omega_{cm} \approx 0.15$ . An interesting observation is that the low frequency cutoff that maximizes the signal to noise ratio is approximately corresponding

to the Unruh temperature

$$\omega_{cm} = k_{cm}a \approx \frac{a}{2\pi}, \tag{6.2.31}$$

where  $a$  is the proper acceleration of Rob. In communication of classical information using quantum states, the best strategy is to have a maximal signal to noise ratio. Therefore, the Unruh frequency provides a natural low frequency cutoff if Alice tries to send classical information to Rob via her quantum states.

However, if Alice wants to send quantum information to Rob, it is also important to minimize the amount of noise added such that the states remain close to the quantum limit. This can be quantified via the conditional variance between the input and output [RL98], which for this system can be defined as

$$V_C = \left(1 - \frac{\text{SNR}_{\text{out}}}{\text{SNR}_{\text{in}}}\right) V_{\text{out}} = \left(1 - \frac{I^2}{\beta^2 V}\right) \bar{V}, \tag{6.2.32}$$

where  $\text{SNR}_{\text{in}}$  represents the signal to noise ratio of input state, in our case it is the coherent state signal  $|\alpha\rangle$  sent by Alice; while  $\text{SNR}_{\text{out}}$  represents the signal to noise ratio of output state, in our case it is the state received by Rob.

Fig. 6.6 shows that for a given  $k_o U_o \leq \delta$  (horizon-straddling case), the conditional variance has a minimum. However, the location of the minimum slightly changes for various  $k_o U_o$ . Comparing with Fig. 6.4 one can see that locations of the minimum of the conditional variance do not exactly coincide with locations of the maximum of the signal to noise ratio. The former are a bit larger than the latter, approximately ranging from 0.1 to 0.4. Nevertheless, they are still in the same order of magnitude, approximately equal to the Unruh frequency. Therefore, we conclude that the Unruh frequency provides a natural low frequency cutoff to optimize the communication of both classical and quantum information between an inertial partner and uniformly accelerated partner using coherent states.

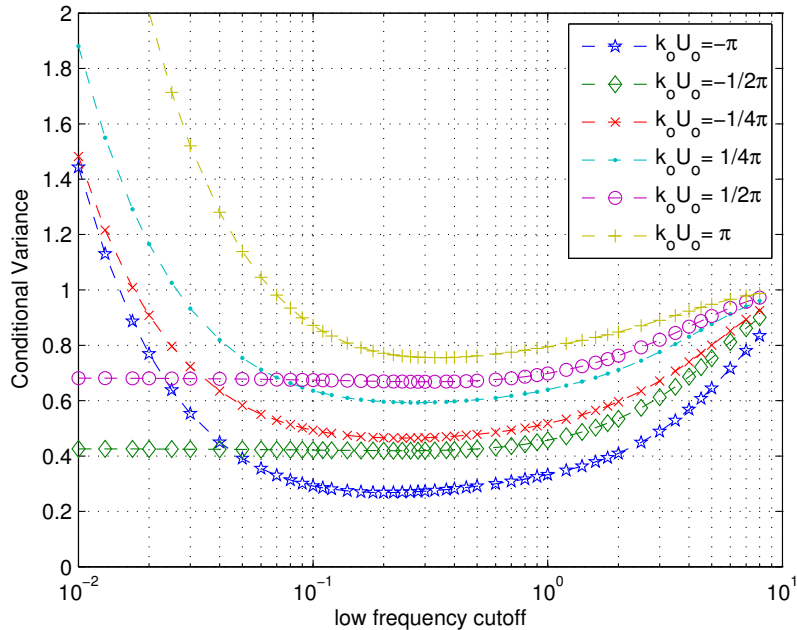


FIGURE 6.6: Conditional variance versus low frequency cutoff,  $\delta = \frac{k_a}{\sigma} = 10$ .

### 6.3 Quantum communication between two accelerated observers

In previous sections we have considered quantum communication between an inertial partner and a uniformly accelerated partner. An inertial partner, Alice, sends a coherent state signal  $|\alpha\rangle$  and a local oscillator  $|\beta\rangle$  to a uniformly accelerated partner, Rob, who then performs homodyne detection. We found some interesting results when the wave packet sent by Alice straddles Rob's future horizon: 1) the expectation value and variance of the signal could be amplified; 2) the signal to noise ratio is maximized and the conditional variance is minimized if the low frequency cut off is chosen to be the Unruh frequency. A question arises as to whether these results are only due to the presence of a horizon. If Alice is not an inertial observer, for example she is another uniformly accelerated observer, can we still get the same conclusions? To answer these questions we need to study quantum communication between two Rindler observers.

For any uniformly accelerated observer, there exist a past horizon and a future horizon. It is possible that one accelerated observer is beyond the horizons of another accelerated observer so that communication between them is impossible. If a set of Rindler observers share the same future and past horizon, those in the right Rindler wedge and those in the left Rindler wedge are causally disconnected. For example in Fig. 6.7, observer  $O_1$  cannot send signal to  $O_2$ , and vice versa. If we shift this set of Rindler observers along the  $x$ -axis in the space-time diagram, we get a new set of Rindler observers (red curves). For the new set of Rindler observers, those in the right Rindler wedge and those in the left Rindler wedge are also causally disconnected. For example, observer  $O_3$  cannot send signal to observer  $O_4$ , and vice versa. However, observer  $O_2$  and  $O_3$ ,  $O_2$  and  $O_4$  are causally connected so communication between them is possible. We can propose two communication protocols in which signal can straddle the future horizon of the receiver: 1) observer  $O_2$  sends a left-moving coherent state signal and local oscillator to observer  $O_3$ , who then performs homodyne detection; 2) observer  $O_2$  sends a right-moving coherent state signal and local oscillator to observer  $O_4$ , who then performs homodyne detection.

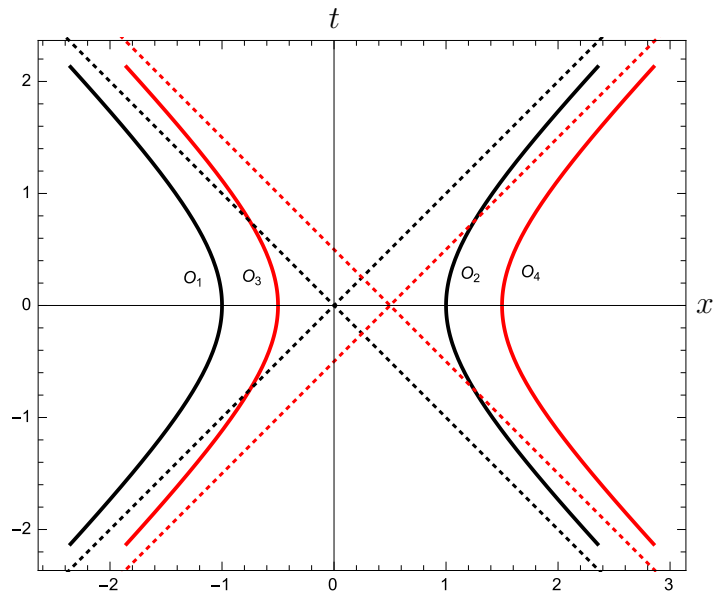


FIGURE 6.7: Two sets of Rindler observers. World lines of the second set of Rindler observers (red) can be obtained by shifting the world lines of the first set (black). Observer  $O_1$  and  $O_2$  (black) are causally disconnected, as well as  $O_3$  and  $O_4$  (red). While  $O_2$  and  $O_3$ ,  $O_2$  and  $O_4$  are causally connected.

We should keep in mind that quantization of fields for different observers could be very different. One of the typical examples is the quantization of fields for inertial observers and uniformly accelerated observers, as we have discussed in Chapter 4. Each observer prepares and detects quantum states in accordance with their own field modes. In order to investigate quantum communication, which basically involves preparing and detecting quantum states, between two observers, we need to know the Bogoliubov transformations between field modes of the two observers. For example when we discuss quantum communication between an inertial partner and a uniformly accelerated partner, we need to know the Bogoliubov transformations between Minkowski modes and Rindler modes. Similarly, if we want to study quantum communication between two uniformly accelerated observers, we have to find out Bogoliubov transformations between two sets of Rindler modes.

Due to the time translation and space translation invariance of the Minkowski space-time, the local observations of uniformly accelerated observers whose world lines are connected by parallel transportation are the same if the state is also translational invariant. For example they see Unruh radiation with the same temperature in the Minkowski vacuum state. However, the field modes they can detect are very different in the perspective of inertial observers. We are going to derive the Bogoliubov transformations between different Rindler modes corresponding to different uniformly accelerated observers. We do it by two steps: 1) find the Bogoliubov transformations between Unruh modes; 2) use the relations between Rindler modes and Unruh modes to derive the Bogoliubov transformations between Rindler modes.

### 6.3.1 Bogoliubov transformations between Unruh modes

For a massless scalar field in  $(1 + 1)$ -dimensional Minkowski space-time, the left-moving modes and right-moving modes are independent so they can be treated separately. In this chapter we only consider left-moving modes and neglect the subscript “1”. Generalization to right-moving modes is straightforward. To make notations clearer, we introduce Heaviside step function  $\theta(V)$  in the definition of Rindler modes. Suppose that  $\theta(V)g_{\omega}^R(v), \theta(-V)g_{\omega}^L(\bar{v})$

are the Rindler modes in the right and left Rindler wedges, respectively. The left-moving Unruh modes are defined by Eqs. (4.5.26) and (4.5.27). The inverse transformations can be easily found to be

$$\begin{aligned}\theta(V)g_\omega^R(v) &= \cosh(r_\omega)G_\omega(V) - \sinh(r_\omega)\bar{G}_\omega^*(V), \\ \theta(-V)g_\omega^L(\bar{v}) &= \cosh(r_\omega)\bar{G}_\omega(V) - \sinh(r_\omega)G_\omega^*(V).\end{aligned}\quad (6.3.1)$$

The explicit expressions for Unruh modes,  $G_\omega(V)$  and  $\bar{G}_\omega(V)$ , are given by Eq. (4.5.41). When we shift the world lines of this set of Rindler observers along the  $x$ -axis in the space-time diagram, we get world lines of another set of Rindler observers. The corresponding Rindler modes and Unruh modes are denoted as  $\{\theta(V \pm s/a)h_\omega^R(\zeta), \theta(-V \mp s/a)h_\omega^L(\bar{\zeta})\}$  and  $\{G_\omega(V \pm s/a), \bar{G}_\omega(V \pm s/a)\}$ , respectively. Here  $s$  is a positive, dimensionless parameter characterizing the shift distance. From Eq. (4.5.41), it is easy to see that

$$\begin{aligned}G_\omega(V \pm s/a) &= F(\omega, a)(aV \pm s)^{-i\omega/a}, \\ \bar{G}_\omega(V \pm s/a) &= F(\omega, a)(-aV \mp s)^{i\omega/a},\end{aligned}\quad (6.3.2)$$

where  $F(\omega, a) = \frac{e^{\pi\omega/2a}}{\sqrt{4\pi\omega}\sqrt{2\sinh(\pi\omega/a)}}$ .

The Unruh modes  $\{G_\omega(V), \bar{G}_\omega(V)\}$  form a set of orthonormal and complete modes, as well as  $\{G_\omega(V + s/a), \bar{G}_\omega(V + s/a)\}$  and  $\{G_\omega(V - s/a), \bar{G}_\omega(V - s/a)\}$ . One can express  $G_\omega(V \pm s/a)$  and  $\bar{G}_\omega(V \pm s/a)$  in terms of the Unruh modes  $\{G_\omega(V), \bar{G}_\omega(V)\}$ .

$$\begin{aligned}G_{\omega'}(V \pm s/a) &= \int d\omega [A_{\omega'\omega}(\pm s)G_\omega(V) + B_{\omega'\omega}(\pm s)\bar{G}_\omega(V)], \\ \bar{G}_{\omega'}(V \pm s/a) &= \int d\omega [C_{\omega'\omega}(\pm s)G_\omega(V) + D_{\omega'\omega}(\pm s)\bar{G}_\omega(V)],\end{aligned}\quad (6.3.3)$$

where the transformation coefficients are

$$\begin{aligned}A_{\omega'\omega}(\pm s) &= \langle G_\omega(V), G_{\omega'}(V \pm s/a) \rangle, \\ B_{\omega'\omega}(\pm s) &= \langle \bar{G}_\omega(V), G_{\omega'}(V \pm s/a) \rangle, \\ C_{\omega'\omega}(\pm s) &= \langle G_\omega(V), \bar{G}_{\omega'}(V \pm s/a) \rangle, \\ D_{\omega'\omega}(\pm s) &= \langle \bar{G}_\omega(V), \bar{G}_{\omega'}(V \pm s/a) \rangle.\end{aligned}\quad (6.3.4)$$

Note that all these Unruh modes are positive frequency modes with respect to the Minkowski time, so there is no mixing of negative frequency modes in the above Bogoliubov transformations. The inverse transformations can be found to be

$$\begin{aligned} G_\omega(V) &= \int d\omega' [A_{\omega'\omega}^*(\pm s)G_{\omega'}(V \pm s/a) + C_{\omega'\omega}^*(\pm s)\bar{G}_{\omega'}(V \pm s/a)], \\ \bar{G}_\omega(V) &= \int d\omega' [B_{\omega'\omega}^*(\pm s)G_{\omega'}(V \pm s/a) + D_{\omega'\omega}^*(\pm s)\bar{G}_{\omega'}(V \pm s/a)]. \end{aligned} \quad (6.3.5)$$

From the explicit expressions for the Unruh modes, Eqs. (4.5.41) and (6.3.2), we can directly calculate the Klein-Gordon products and obtain the Bogoliubov transformation coefficients  $A_{\omega'\omega}(\pm s)$ ,  $B_{\omega'\omega}(\pm s)$ ,  $C_{\omega'\omega}(\pm s)$  and  $D_{\omega'\omega}(\pm s)$ . We find

$$\begin{aligned} A_{\omega'\omega}(s) &= \frac{\pi}{2\sqrt{\omega\omega'}} \frac{e^{-\pi(\Omega-\Omega')/2}}{\sqrt{\sinh(\pi\Omega)\sinh(\pi\Omega')}} \\ &\quad \times \frac{s^{i(\Omega-\Omega')}}{(\Omega-\Omega'+i\epsilon)\sinh(\pi(\Omega-\Omega'))\Gamma(-i\Omega)\Gamma(i\Omega')\Gamma(i(\Omega-\Omega'))}, \\ B_{\omega'\omega}(s) &= \frac{\pi}{2\sqrt{\omega\omega'}} \frac{e^{\pi(\Omega+\Omega')/2}}{\sqrt{\sinh(\pi\Omega)\sinh(\pi\Omega')}} \\ &\quad \times \frac{s^{-i(\Omega+\Omega')}}{(\Omega+\Omega')\sinh(\pi(\Omega+\Omega'))\Gamma(i\Omega)\Gamma(i\Omega')\Gamma(-i(\Omega+\Omega'))}, \\ C_{\omega'\omega}(s) &= \frac{\pi}{2\sqrt{\omega\omega'}} \frac{e^{-\pi(\Omega+\Omega')/2}}{\sqrt{\sinh(\pi\Omega)\sinh(\pi\Omega')}} \\ &\quad \times \frac{s^{i(\Omega+\Omega')}}{(\Omega+\Omega')\sinh(\pi(\Omega+\Omega'))\Gamma(-i\Omega)\Gamma(-i\Omega')\Gamma(i(\Omega+\Omega'))}, \\ D_{\omega'\omega}(s) &= \frac{\pi}{2\sqrt{\omega\omega'}} \frac{e^{\pi(\Omega-\Omega')/2}}{\sqrt{\sinh(\pi\Omega)\sinh(\pi\Omega')}} \\ &\quad \times \frac{s^{-i(\Omega-\Omega')}}{(\Omega-\Omega'-i\epsilon)\sinh(\pi(\Omega-\Omega'))\Gamma(i\Omega)\Gamma(-i\Omega')\Gamma(-i(\Omega-\Omega'))}, \end{aligned} \quad (6.3.6)$$

where  $\Omega = \omega/a$  and  $\Gamma(z)$  is the Gamma's function. Here  $\epsilon$  is a small positive regularization parameter and has to be taken to be zero:  $\epsilon \rightarrow 0^+$ . It is easy to verify the following equalities,

$$A_{\omega'\omega}(s) = e^{-\pi(\Omega-\Omega')}D_{\omega'\omega}^*(s), \quad B_{\omega'\omega}(s) = e^{\pi(\Omega+\Omega')}C_{\omega'\omega}^*(s). \quad (6.3.7)$$

The Klein-Gordon products between  $\{G_\omega(V), \bar{G}_\omega(V)\}$  and  $\{G_\omega(V-s/a), \bar{G}_\omega(V-s/a)\}$  can be calculated following the same procedure. By doing the explicit calculation, we find that

the following trick applies: replace  $s$  in Eq. (6.3.6) by  $-s$ , and then let  $(-1)^i = e^\pi$ . We have

$$\begin{aligned}
A_{\omega'\omega}(-s) &= e^{\pi(\Omega-\Omega')}A_{\omega'\omega}(s) = D_{\omega'\omega}^*(s), \\
B_{\omega'\omega}(-s) &= e^{-\pi(\Omega+\Omega')}B_{\omega'\omega}(s) = C_{\omega'\omega}^*(s), \\
C_{\omega'\omega}(-s) &= e^{\pi(\Omega+\Omega')}C_{\omega'\omega}(s) = B_{\omega'\omega}^*(s), \\
D_{\omega'\omega}(-s) &= e^{-\pi(\Omega-\Omega')}D_{\omega'\omega}(s) = A_{\omega'\omega}^*(s).
\end{aligned} \tag{6.3.8}$$

### 6.3.2 Bogoliubov transformations between Rindler modes

We have built up relations between the shifted Unruh modes  $\{G_\omega(V \pm s/a), \bar{G}_\omega(V \pm s/a)\}$  and the original Unruh modes  $\{G_\omega(V), \bar{G}_\omega(V)\}$ . The relations between the shifted Rindler modes and the shifted Unruh modes are basically the same as that between the original modes and the original Unruh modes, Eq. (6.3.1). Namely,

$$\begin{aligned}
\theta(V \pm s/a)g_\omega^R(v) &= \cosh(r_\omega)G_\omega(V \pm s/a) - \sinh(r_\omega)\bar{G}_\omega^*(V \pm s/a), \\
\theta(-V \mp s/a)g_\omega^L(\bar{v}) &= \cosh(r_\omega)\bar{G}_\omega(V \pm s/a) - \sinh(r_\omega)G_\omega^*(V \pm s/a).
\end{aligned} \tag{6.3.9}$$

Using Eqs. (6.3.5), (4.5.26) and (4.5.27), we can relate the shifted Rindler modes and the original Rindler modes.

$$\begin{aligned}
&\theta(V + s/a)h_{\omega'}^R(\zeta) \\
= &\int d\omega \left\{ \sqrt{\frac{\sinh(\pi\Omega')}{\sinh(\pi\Omega)}} \left[ e^{\pi(\Omega-\Omega')/2}A_{\omega'\omega}(s)\theta(V)g_\omega^R(v) + e^{-\pi(\Omega+\Omega')/2}B_{\omega'\omega}(s)\theta(V)g_\omega^{R*}(v) \right] \right. \\
&+ \frac{1}{\sqrt{\sinh(\pi\Omega')\sinh(\pi\Omega)}} \left[ e^{-\pi(\Omega+\Omega')/2}\sinh(\pi(\Omega + \Omega'))B_{\omega'\omega}(s)\theta(-V)g_\omega^L(\bar{v}) \right. \\
&\left. \left. - e^{\pi(\Omega-\Omega')/2}\sinh(\pi(\Omega - \Omega'))A_{\omega'\omega}(s)\theta(-V)g_\omega^{L*}(\bar{v}) \right] \right\}.
\end{aligned} \tag{6.3.10}$$

$$\begin{aligned}
&\theta(-V - s/a)h_{\omega'}^L(\bar{\zeta}) \\
= &\int d\omega \sqrt{\frac{\sinh(\pi\Omega)}{\sinh(\pi\Omega')}} \left\{ e^{-\pi(\Omega-\Omega')/2}D_{\omega'\omega}(s)\theta(-V)g_\omega^L(\bar{v}) - e^{\pi(\Omega+\Omega')/2}C_{\omega'\omega}(s)\theta(-V)g_\omega^{L*}(\bar{v}) \right\}.
\end{aligned} \tag{6.3.11}$$

$$\begin{aligned}
& \theta(V - s/a)h_{\omega'}^R(\zeta) \\
= & \int d\omega \sqrt{\frac{\sinh(\pi\Omega)}{\sinh(\pi\Omega')}} \left\{ e^{-\pi(\Omega-\Omega')/2} A_{\omega'\omega}(-s)\theta(V)g_{\omega}^R(v) - e^{\pi(\Omega+\Omega')/2} B_{\omega'\omega}(-s)\theta(V)g_{\omega}^{R*}(v) \right\}.
\end{aligned} \tag{6.3.12}$$

$$\begin{aligned}
& \theta(-V + s/a)h_{\omega'}^L(\bar{\zeta}) \\
= & \int d\omega \left\{ \frac{1}{\sqrt{\sinh(\pi\Omega')\sinh(\pi\Omega)}} \left[ e^{-\pi(\Omega+\Omega')/2} \sinh(\pi(\Omega + \Omega')) C_{\omega'\omega}(-s)\theta(V)g_{\omega}^R(v) \right. \right. \\
& \left. \left. - e^{\pi(\Omega-\Omega')/2} \sinh(\pi(\Omega - \Omega')) D_{\omega'\omega}(-s)\theta(V)g_{\omega}^{R*}(v) \right] \right. \\
& \left. + \sqrt{\frac{\sinh(\pi\Omega')}{\sinh(\pi\Omega)}} \left[ e^{\pi(\Omega-\Omega')/2} D_{\omega'\omega}(-s)\theta(-V)g_{\omega}^L(\bar{v}) + e^{-\pi(\Omega+\Omega')/2} C_{\omega'\omega}(-s)\theta(-V)g_{\omega}^{L*}(\bar{v}) \right] \right\}.
\end{aligned} \tag{6.3.13}$$

Since  $\{\theta(V)g_{\omega}^R(v), \theta(-V)g_{\omega}^L(\bar{v})\}$  form a set of orthonormal and complete modes, the scalar field  $\hat{\Phi}$  can be expanded by them and the corresponding operators  $\{\hat{b}_{\omega}^R, \hat{b}_{\omega}^L\}$ . Meanwhile, the Rindler modes  $\{\theta(V \pm s/a)h_{\omega'}^R(\zeta), \theta(-V \mp s/a)h_{\omega'}^L(\bar{\zeta})\}$  also form a set of orthonormal and complete modes, and we denote the corresponding operators as  $\{\hat{b}_{\omega'}^R(\pm s), \hat{b}_{\omega'}^L(\pm s)\}$ . The scalar field can be expanded as

$$\begin{aligned}
\hat{\Phi} &= \int d\omega \left[ \hat{b}_{\omega}^R \theta(V)g_{\omega}^R(v) + \hat{b}_{\omega}^{R\dagger} \theta(V)g_{\omega}^{R*}(v) + \hat{b}_{\omega}^L \theta(-V)g_{\omega}^L(\bar{v}) + \hat{b}_{\omega}^{L\dagger} \theta(-V)g_{\omega}^{L*}(\bar{v}) \right] \\
&= \int d\omega' \left[ \hat{b}_{\omega'}^R(\pm s) \theta(V \pm s/a)h_{\omega'}^R(\zeta) + \hat{b}_{\omega'}^{R\dagger}(\pm s) \theta(V \pm s/a)h_{\omega'}^{R*}(\zeta) \right. \\
&\quad \left. + \hat{b}_{\omega'}^L(\pm s) \theta(-V \mp s/a)h_{\omega'}^L(\bar{\zeta}) + \hat{b}_{\omega'}^{L\dagger}(\pm s) \theta(-V \mp s/a)h_{\omega'}^{L*}(\bar{\zeta}) \right].
\end{aligned} \tag{6.3.14}$$

The Bogoliubov transformations between the shifted and original Rindler operators are

$$\begin{aligned}
\hat{b}_{\omega'}^R(\pm s) &= \int d\omega \left[ \alpha_{\omega'\omega}^R(\pm s) \hat{b}_{\omega}^R + \beta_{\omega'\omega}^R(\pm s) \hat{b}_{\omega}^{R\dagger} + \gamma_{\omega'\omega}^R(\pm s) \hat{b}_{\omega}^L + \delta_{\omega'\omega}^R(\pm s) \hat{b}_{\omega}^{L\dagger} \right], \\
\hat{b}_{\omega'}^L(\pm s) &= \int d\omega \left[ \alpha_{\omega'\omega}^L(\pm s) \hat{b}_{\omega}^R + \beta_{\omega'\omega}^L(\pm s) \hat{b}_{\omega}^{R\dagger} + \gamma_{\omega'\omega}^L(\pm s) \hat{b}_{\omega}^L + \delta_{\omega'\omega}^L(\pm s) \hat{b}_{\omega}^{L\dagger} \right].
\end{aligned} \tag{6.3.15}$$

The Bogoliubov transformation coefficients can be obtained from the relations between the shifted Rindler modes and original Rindler modes, Eqs. (6.3.10)–(6.3.13).

$$\begin{aligned}\alpha_{\omega'\omega}^R(s) &= \gamma_{\omega'\omega}^{L*}(-s) = \langle \theta(V + s/a)h_{\omega'}^R(\zeta), \theta(V)g_{\omega}^R(v) \rangle \\ &= \frac{\pi}{2\sqrt{\omega\omega'}} \frac{1}{\sinh(\pi\Omega)} \frac{1}{(\Omega - \Omega' + i\epsilon)\sinh(\pi(\Omega - \Omega'))\Gamma(i\Omega)\Gamma(-i\Omega')\Gamma(-i(\Omega - \Omega'))},\end{aligned}\quad (6.3.16)$$

$$\begin{aligned}\beta_{\omega'\omega}^R(s) &= \delta_{\omega'\omega}^{L*}(-s) = \langle \theta(V + s/a)h_{\omega'}^R(\zeta), \theta(V)g_{\omega}^{R*}(v) \rangle \\ &= -\frac{\pi}{2\sqrt{\omega\omega'}} \frac{1}{\sinh(\pi\Omega)} \frac{1}{(\Omega + \Omega')\sinh(\pi(\Omega + \Omega'))\Gamma(-i\Omega)\Gamma(-i\Omega')\Gamma(i(\Omega + \Omega'))},\end{aligned}\quad (6.3.17)$$

$$\begin{aligned}\gamma_{\omega'\omega}^R(s) &= \alpha_{\omega'\omega}^{L*}(-s) = \langle \theta(V + s/a)h_{\omega'}^R(\zeta), \theta(-V)g_{\omega}^L(\bar{v}) \rangle \\ &= \frac{\pi}{2\sqrt{\omega\omega'}} \frac{1}{(\Omega + \Omega')\sinh(\pi\Omega)\sinh(\pi\Omega')\Gamma(-i\Omega)\Gamma(-i\Omega')\Gamma(i(\Omega + \Omega'))},\end{aligned}\quad (6.3.18)$$

$$\begin{aligned}\delta_{\omega'\omega}^R(s) &= \beta_{\omega'\omega}^{L*}(-s) = \langle \theta(V + s/a)h_{\omega'}^R(\zeta), \theta(-V)g_{\omega}^{L*}(\bar{v}) \rangle \\ &= \frac{\pi}{2\sqrt{\omega\omega'}} \frac{1}{(\Omega - \Omega' + i\epsilon)\sinh(\pi\Omega)\sinh(\pi\Omega')\Gamma(i\Omega)\Gamma(-i\Omega')\Gamma(-i(\Omega - \Omega'))}.\end{aligned}\quad (6.3.19)$$

$$\alpha_{\omega'\omega}^L(s) = \gamma_{\omega'\omega}^{R*}(-s) = \langle \theta(-V - s/a)h_{\omega'}^L(\zeta), \theta(V)g_{\omega}^R(v) \rangle = 0, \quad (6.3.20)$$

$$\beta_{\omega'\omega}^L(s) = \delta_{\omega'\omega}^{R*}(-s) = \langle \theta(-V - s/a)h_{\omega'}^L(\zeta), \theta(V)g_{\omega}^{R*}(v) \rangle = 0, \quad (6.3.21)$$

$$\begin{aligned}\gamma_{\omega'\omega}^L(s) &= \alpha_{\omega'\omega}^{R*}(-s) = \langle \theta(-V - s/a)h_{\omega'}^L(\zeta), \theta(-V)g_{\omega}^L(\bar{v}) \rangle \\ &= \frac{\pi}{2\sqrt{\omega\omega'}} \frac{1}{\sinh(\pi\Omega')} \frac{1}{(\Omega - \Omega' - i\epsilon)\sinh(\pi(\Omega - \Omega'))\Gamma(-i\Omega)\Gamma(i\Omega')\Gamma(i(\Omega - \Omega'))},\end{aligned}\quad (6.3.22)$$

$$\begin{aligned}\delta_{\omega'\omega}^L(s) &= \beta_{\omega'\omega}^{R*}(-s) = \langle \theta(-V - s/a)h_{\omega'}^L(\zeta), \theta(-V)g_{\omega}^{L*}(\bar{v}) \rangle \\ &= \frac{\pi}{2\sqrt{\omega\omega'}} \frac{1}{\sinh(\pi\Omega')} \frac{1}{(\Omega + \Omega')\sinh(\pi(\Omega + \Omega'))\Gamma(i\Omega)\Gamma(i\Omega')\Gamma(-i(\Omega + \Omega'))}.\end{aligned}\quad (6.3.23)$$

### 6.3.3 Quantum communication protocols

We restrict ourselves to quantum communication between two uniformly accelerated observers with the same proper acceleration. In this case, there are two kinds of communication protocols between two Rindler observers. One is between two Rindler observers undergoing anti-parallel uniform acceleration and the other is between two Rindler observers undergoing parallel uniform acceleration. We are interested in scenarios where signal and local oscillator sent by the sender may straddle the receiver's future horizon, for example in Fig. 6.7, observer  $O_2$  sends signal and local oscillator to observer  $O_3$  or vice versa. For concreteness, we first consider the case that observer  $O_2$  sends signal and local oscillator to observer  $O_3$  who then performs homodyne detection.

The following calculation is similar to the case where the sender Alice is an inertial observer. Observer  $O_2$  prepares the signal and local oscillator in his own reference frame by displacing the Minkowski vacuum with amplitude  $\alpha$  and  $\beta$ . That is, the state prepared by observer  $O_2$  is

$$|\alpha, \beta, \tau_2\rangle = \hat{D}_S(\alpha)\hat{D}_L(\beta)|0_M\rangle, \quad (6.3.24)$$

where  $|0_M\rangle$  is the Minkowski vacuum state and  $\tau_2$  is the proper time of observer  $O_2$ . The displacement operator is  $\hat{D}_K(\gamma) = \exp(\gamma\hat{b}_K^{R\dagger} - \gamma^*\hat{b}_K^R)$ , with  $\gamma = \alpha, \beta$  and  $K = L, S$ . The spatiotemporally localized Rindler operator  $\hat{b}_K^R$  is defined as

$$\hat{b}_K^R = \int d\omega f_{D_K}(\omega; \omega_0, \sigma, v_0)\hat{b}_\omega^R, \quad (6.3.25)$$

where  $f_{D_K}(\omega)$  is a normalized displacement mode function satisfying  $\int d\omega |f_{D_K}(\omega)|^2 = 1$ . We choose the normalized displacement mode function to be a Gaussian wave packet in the perspective of observer  $O_2$ ,

$$f_{D_K}(\omega; \omega_0, \sigma, v_0) = \left(\frac{1}{2\pi\sigma^2}\right)^{1/4} \exp\left\{-\frac{(\omega - \omega_0)^2}{4\sigma^2}\right\} e^{-i\omega v_0}, \quad (6.3.26)$$

where  $\omega_0, \sigma$  are the central frequency and bandwidth of the wave packet satisfying  $\omega_0/\sigma \gg 1$ ,  $v_0 = \tau_{20} + \xi_0$  is the central position of the wave packet. The integrated output signal operator

of observer  $O_3$ 's homodyne detection is [SR14]

$$\hat{X}(\phi) = \int d\tau_3 [\hat{b}_S^L(-s, \tau_3) \hat{b}_L^{L\dagger}(-s, \tau_3) e^{i\phi} + \hat{b}_S^{L\dagger}(-s, \tau_3) \hat{b}_L^L(-s, \tau_3) e^{-i\phi}], \quad (6.3.27)$$

where  $\tau_3$  is the proper time of the observer  $O_3$ .  $\hat{b}_K^L(-s, \tau_3)$  are spatiotemporally localized operators,

$$\hat{b}_K^L(-s, \tau_3) = \int d\omega f_K(\omega, \tau_3) \hat{b}_\omega^L(-s), \quad (6.3.28)$$

where  $f_K(\omega, \tau_3)$  is a broadband detector mode function which can be written as

$$f_K(\omega, \tau_3) = e^{-i\omega\tau_3} f_K(\omega).$$

In order to have a localized detector, we take  $f_K(\omega) = \sqrt{a/2\pi}$  for  $\omega > \omega_{\text{cut}} > 0$  and zero otherwise, where  $\omega_{\text{cut}}$  is a low frequency cut off. The expectation value of the signal is

$$X_\phi = \langle 0_M | \hat{D}_L^\dagger(\beta) \hat{D}_S^\dagger(\alpha) \hat{X}(\phi) \hat{D}_S(\alpha) \hat{D}_L(\beta) | 0_M \rangle \quad (6.3.29)$$

and the variance is

$$V_\phi = \langle 0 | \hat{D}_L^\dagger(\beta) \hat{D}_S^\dagger(\alpha) \hat{X}^2(\phi) \hat{D}_S(\alpha) \hat{D}_L(\beta) | 0_M \rangle - X_\phi^2. \quad (6.3.30)$$

Using the Bogoliubov transformation (6.3.15) and (6.3.16), we can derive the identity

$$\begin{aligned} \hat{D}_K^\dagger(\gamma) \hat{b}_K^L(-s, \tau_3) \hat{D}_K(\gamma) &= \hat{b}_K^L(-s, \tau_3) + \gamma \int d\omega' \int d\omega f_K(\omega', \tau_3) \left[ \alpha_{\omega'\omega}^L(-s) f_{D_K}^*(\omega, v_0) \right. \\ &\quad \left. + \beta_{\omega'\omega}^L(-s) f_{D_K}(\omega, v_0) \right] \\ &\equiv \hat{b}_K^L(-s, \tau_3) + \gamma F_K(\tau_3). \end{aligned} \quad (6.3.31)$$

The expressions for  $X_\phi$  and  $V_\phi$  can be expanded via Eq. (6.3.31). The local oscillator sent by observer  $O_2$  will be distorted as viewed by observer  $O_3$  due to the Doppler shift and observer  $O_3$ 's inability to access the whole wave packet. If observer  $O_3$  performs homodyne detection without knowing the amplitude of the local oscillator, he has to measure the strength of the local oscillator by adding the photocurrents of the two photodetectors. We define the strength of the local oscillator as seen by observer  $O_3$  as

$$\begin{aligned} I &= \int d\tau_3 \langle \alpha, \beta, \tau_2 | \hat{b}_K^{L\dagger}(-s, \tau_3) \hat{b}_K^L(-s, \tau_3) | \alpha, \beta, \tau_2 \rangle \\ &= \int d\tau_3 \langle 0_M | \hat{D}_L^\dagger(\beta) \hat{D}_S^\dagger(\alpha) \hat{b}_K^{L\dagger}(-s, \tau_3) \hat{b}_K^L(-s, \tau_3) \hat{D}_S(\alpha) \hat{D}_L(\beta) | 0_M \rangle. \end{aligned} \quad (6.3.32)$$

Both the expectation value  $X_\phi$  and variance  $V_\phi$  of the signal should be normalized by the strength of the local oscillator. Since the Bogoliubov transformation(6.3.15) is linear, it is obvious that  $\langle 0_M | \hat{b}_K^L(-s, \tau_3) | 0_M \rangle = \langle 0_M | \hat{b}_K^{L\dagger}(-s, \tau_3) | 0_M \rangle = 0$ . Taking into account the fact that  $\beta \gg |\alpha|$ , we have

$$\begin{aligned} X_\phi &= \beta \alpha e^{i\phi} \int d\tau_3 F_S(\tau_3) F_L^*(\tau_3) + \text{c.c.}, \\ V_\phi &\approx \beta^2 \int d\tau_3 \int d\tau'_3 F_L^*(\tau_3) F_L(\tau'_3) \langle 0_M | \{ \hat{b}_S^L(-s, \tau_3), \hat{b}_S^{L\dagger}(-s, \tau'_3) \} | 0_M \rangle, \\ I &\approx \beta^2 \int d\tau_3 F_L(\tau_3) F_L^*(\tau_3). \end{aligned} \quad (6.3.33)$$

If we further require that the detector mode function for signal and local oscillator are the same and the displacement mode function for signal and local oscillator are also the same, then  $F_S(\tau_3) = F_L(\tau_3)$ . The normalized output signal becomes

$$\bar{X}_\phi = \frac{X_\phi}{\sqrt{I}} \approx \sqrt{\int d\tau_3 F_L(\tau_3) F_L^*(\tau_3)} (\alpha e^{i\phi} + \alpha^* e^{-i\phi}) \approx \frac{\sqrt{I}}{\beta} (\alpha e^{i\phi} + \alpha^* e^{-i\phi}), \quad (6.3.34)$$

and the normalized variance becomes

$$\bar{V}_\phi = \frac{V_\phi}{I} \approx \frac{\int d\tau_3 \int d\tau'_3 F_L^*(\tau_3) F_L(\tau'_3) \langle 0_M | \{ \hat{b}_S^L(-s, \tau_3), \hat{b}_S^{L\dagger}(-s, \tau'_3) \} | 0_M \rangle}{\int d\tau_3 F_L(\tau_3) F_L^*(\tau_3)}. \quad (6.3.35)$$

It is convenient to introduce two quantities  $\mathcal{A}_{\omega'}$  and  $\mathcal{B}_{\omega'}$  as

$$\begin{aligned} \mathcal{A}_{\omega'} &= \int d\omega \alpha_{\omega'\omega}^L(-s) f_{DK}^*(\omega, v_0) = \left( \frac{1}{2\pi\sigma^2} \right)^{1/4} \frac{\pi e^{-i\Omega'\ln(s)}}{2\sqrt{\Omega'} \sinh(\pi\Omega') \Gamma(i\Omega')} I_1(\Omega'; \Omega_0, v_0, \sigma, s), \\ \mathcal{B}_{\omega'} &= \int d\omega \beta_{\omega'\omega}^L(-s) f_{DK}(\omega, v_0) = \left( \frac{1}{2\pi\sigma^2} \right)^{1/4} \frac{\pi e^{-i\Omega'\ln(s)}}{2\sqrt{\Omega'} \sinh(\pi\Omega') \Gamma(i\Omega')} I_2(\Omega'; \Omega_0, v_0, \sigma, s), \end{aligned} \quad (6.3.36)$$

where

$$\begin{aligned} I_1(\Omega'; \Omega_0, v_0, \sigma, s) &= \int_0^\infty \frac{d\Omega}{\sqrt{\Omega}} \frac{e^{i\Omega(av_0 - \ln(s))}}{(\Omega + \Omega') \sinh(\pi\Omega) \Gamma(i\Omega) \Gamma(-i(\Omega + \Omega'))} \exp\left\{ -\frac{(\Omega - \Omega_0)^2}{4(\sigma/a)^2} \right\}, \\ I_2(\Omega'; \Omega_0, v_0, \sigma, s) &= \int_0^\infty \frac{d\Omega}{\sqrt{\Omega}} \frac{e^{-i\Omega(av_0 - \ln(s))}}{(\Omega - \Omega' - i\epsilon) \sinh(\pi\Omega) \Gamma(-i\Omega) \Gamma(i(\Omega - \Omega'))} \exp\left\{ -\frac{(\Omega - \Omega_0)^2}{4(\sigma/a)^2} \right\}. \end{aligned} \quad (6.3.37)$$

Substituting  $\mathcal{A}_{\omega'}$  and  $\mathcal{B}_{\omega'}$  into (6.3.33), we find

$$\begin{aligned} I &= \beta^2 \int d\omega \left( |\mathcal{A}_\omega|^2 + |\mathcal{B}_\omega|^2 + \mathcal{A}_\omega \mathcal{B}_\omega^* + \mathcal{A}_\omega^* \mathcal{B}_\omega \right) \\ &= \beta^2 \frac{\pi}{4\sqrt{2\pi}(\sigma/a)} \int_{\Omega_{\text{cut}}}^{\infty} \frac{d\Omega}{\sinh(\pi\Omega)} \left[ |I_1(\Omega)|^2 + |I_2(\Omega)|^2 + I_1^*(\Omega)I_2(\Omega) + I_1(\Omega)I_2^*(\Omega) \right], \end{aligned} \quad (6.3.38)$$

and

$$\begin{aligned} V_\phi &= \beta^2 \int d\omega \left( |\mathcal{A}_\omega|^2 + |\mathcal{B}_\omega|^2 + \mathcal{A}_\omega \mathcal{B}_\omega^* + \mathcal{A}_\omega^* \mathcal{B}_\omega \right) \frac{e^{2\pi\Omega} + 1}{e^{2\pi\Omega} - 1} \\ &= \beta^2 \frac{\pi}{4\sqrt{2\pi}(\sigma/a)} \int_{\Omega_{\text{cut}}}^{\infty} \frac{d\Omega}{\sinh(\pi\Omega)} \left[ |I_1(\Omega)|^2 + |I_2(\Omega)|^2 + I_1^*(\Omega)I_2(\Omega) + I_1(\Omega)I_2^*(\Omega) \right] \\ &\quad \times \frac{e^{2\pi\Omega} + 1}{e^{2\pi\Omega} - 1}, \end{aligned} \quad (6.3.39)$$

where  $\Omega_{\text{cut}} = \omega_{\text{cut}}/a$  represents the low frequency cutoff.

In the high central frequency and narrow bandwidth limit, namely,  $\Omega_0 \gg 1$  and  $\Omega_0 \gg \sigma/a$ , the integrals  $I_1(\Omega'; \Omega_0, v_0, \sigma, s)$  and  $I_2(\Omega'; \Omega_0, v_0, \sigma, s)$  can be evaluated approximately. This is due to the fact that the Gamma's function can be approximated as

$$\Gamma(z) \sim \sqrt{2\pi} z^{z-1/2} e^{-z} \quad (6.3.40)$$

when  $|z|$  is large. The only issue here comes from  $\Gamma(i(\Omega - \Omega'))$ . When  $\Omega'$  is close to  $\Omega$ ,  $i(\Omega - \Omega') \sim 0$ , the above approximation is not valid. However, numerical calculation shows that  $\mathcal{B}_{\omega'}$  rapidly decays when  $\Omega'$  increases. Therefore it is reasonable to only consider small  $\Omega'$ , so that  $\Omega - \Omega' \gg 1$  and Eq. (6.3.40) can be applied to  $\Gamma(i(\Omega - \Omega'))$ .

We take the high central frequency and narrow bandwidth limit, evaluate the strength of the local oscillator and the normalized variance, Eq. (6.3.35). The results are shown in Figs. 6.8 and 6.9. By comparing Figs. 6.8 and 6.2, we can see that the strengths of local oscillator received by the accelerated observer in two different scenarios are almost the same. This is also true for the normalized variances, if one compares Figs. 6.9 and 6.3. This implies that, in the high central frequency and narrow bandwidth limit, the output of the homodyne detection as performed by an accelerated observer does not depend on the motion of the senders. Instead, it reflects the unique properties of the horizon of the receiver.

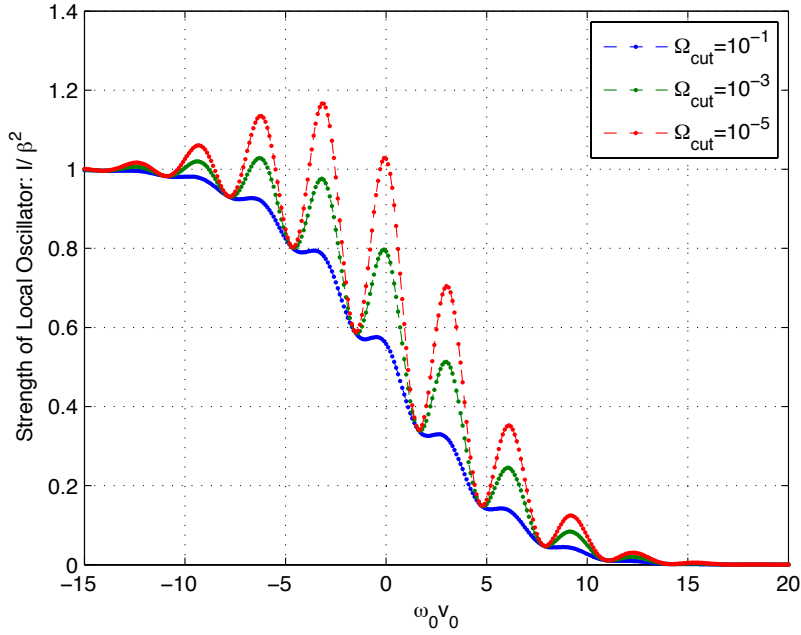


FIGURE 6.8: Strength of local oscillator in the case where an accelerated observer communicates with another accelerated observer. Three low frequency cutoffs are plotted:  $\Omega_{\text{cut}} = 0.00001$ (top),  $0.001$ (middle),  $0.1$ (bottom),  $\delta = \frac{k_\sigma}{\sigma} = 10$ .

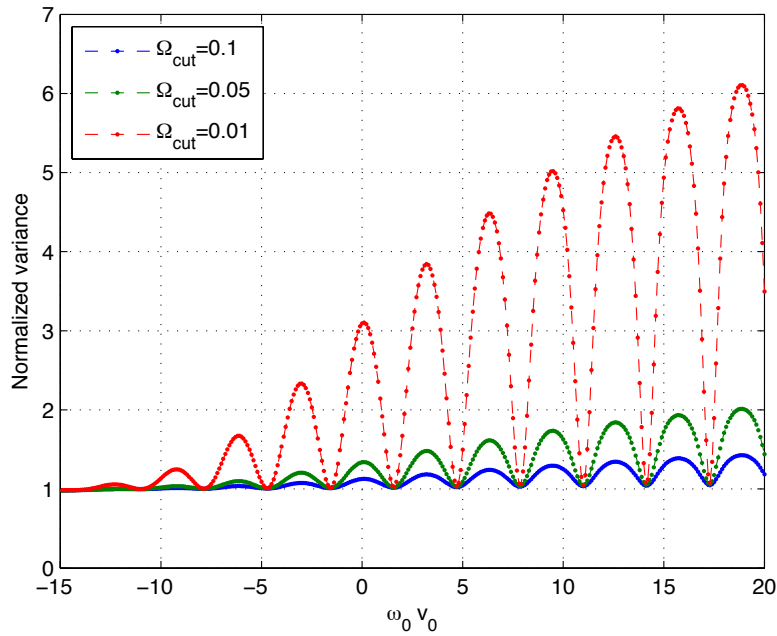


FIGURE 6.9: Normalized variance in the case where an accelerated observer communicates with another accelerated observer. Three low frequency cutoffs are plotted:  $\Omega_{\text{cut}} = 0.01$ (top),  $0.05$ (middle),  $0.1$ (bottom),  $\delta = \frac{k_\sigma}{\sigma} = 10$ .

## 6.4 Summary

In this chapter, we discuss quantum communication using coherent states and homodyne detection with a uniformly accelerated observer in the horizon-straddling case in which the sender sends both the signal and local oscillator. Two different protocols are studied: the sender is either an inertial observer or a uniformly accelerated observer. In the case that the sender is inertial, we find that under some special conditions the accelerated observer cannot detect substantial low frequency particles regardless of his proper acceleration, in contrast with the general viewpoint that the accelerated observer sees large amounts of low frequency particles if their acceleration is large. We also show that the Unruh frequency provides a natural low frequency cutoff both for quantum limited classical communication and quantum communication between the inertial observer and uniformly accelerated observer.

In the case that the sender is another uniformly accelerated observer, we derived the general expressions for the expectation value of the quadrature amplitude and the variance. In the high central frequency and narrow bandwidth limit, we explicitly calculated the the normalized output signal and the normalized variance. It is surprising that they are almost the same as that in the case where the sender is inertial. We thus conclude that the output of the homodyne detection as performed by an accelerated observer does not depend on the motion of the senders. Instead, it reflects the unique properties of the horizon of the receiver.



# 7

## Quantum Circuit Model for Non-inertial Objects: Accelerated Mirror

### 7.1 Introduction

It has been well known since the 1970s that a moving mirror can radiate particles [Moo70, FD76]. A perfect moving mirror acts as a moving boundary and thus changes the states, especially the vacuum, of the quantum fields. For an appropriately chosen accelerated trajectory the radiation flux is thermal, and an analogy [DF77, Wal85, CW87] can be drawn with Hawking radiation from a collapsing star [Haw75] that eventually forms a black hole. Since the thermal fluxes are correlated with the final vacuum fluctuations, some authors [Wil93, HSU15] have proposed that the emission of the large amounts of information left in the black hole need not be accompanied by the eventual emission of a large amount of energy,

providing a new perspective to the solution of the black hole information paradox [Haw76]. Recently, experiments have been performed to mimic the moving mirrors by changing the properties of the materials, e.g., the inductance of a superconducting quantum interference device [WJP<sup>+</sup>11, LPHH13].

When the mirror is uniformly accelerating, its trajectory is a hyperbola in spacetime, and both the energy flux and particle flux are zero away from the event horizon [FD76, DF77, BD82, Gro86]. Particles and energy are only radiated when the acceleration of the mirror changes. In the case that the mirror eternally accelerates, the energy flux along the horizon is divergent [FS79, FS80, FS99, Kay15, KL16]. This divergence is evidently related to the ideal assumption that the mirror accelerates for infinitely long time. One way to get rid of the divergence is to turn on and off the mirror so that effectively it interacts with the fields for a finite time [OP01, OP03a, OP03b].

In this chapter, we develop a quantum circuit model to describe unitary interactions between quantum fields and a uniformly accelerated object (such as a mirror, cavity, squeezer *etc.*). This allows one to straightforwardly calculate the radiation produced by such objects as observed by a localized Minkowski (inertial) observer. We concentrate on a uniformly accelerated object because the transformations between Minkowski modes, Rindler modes and Unruh modes are well known [Unr76, Tak86, CHM08] and can be represented by some simple quantum optical elements, like two-mode squeezers, beamsplitters *etc.* As an application of our circuit model, we revisit the uniformly accelerated mirror problem with variable reflection coefficient  $R_\omega$  in  $(1+1)$ -dimensional Minkowski spacetime. Our approach has a number of advantages. It allows inclusion of general unitary interactions (including nonlinear interactions), generalizing the formalism developed for linear scattering [MP96]. It is also non-perturbative in the reflection coefficient  $R_\omega$ , unlike the self-interaction model proposed by Obadia and Parentani [OP01], which requires a perturbative expansion in this quantity and so is valid only for low reflection coefficients.

For the eternally accelerated mirror, the radiation flux detected in a localized Minkowski

wave packet mode is divergent. We can regularize this infrared divergence by introducing a low-frequency cutoff for the mirror, which means the mirror is transparent for the low-frequency field modes (to some extent, this is physically equivalent to having the mirror interact with the field for a finite period of time). After infrared regularization the particle number in a localized wave packet mode is finite.

We further study the properties of the radiation flux and find that the radiation field is locally squeezed. That is, the variance of the field quadrature observable at a particular angle is lower than the quantum vacuum noise. This local squeezing effect has gone unnoticed up to now, but in our circuit model it is a very straightforward result. We show that the generation of local squeezing is closely related to cutting the correlations across the horizon, somewhat reminiscent of destroying coherences by allowing an accelerated thermal bath (or an accelerated detector) to equilibrate with the traced out Minkowski vacuum state [Unr92]. This mechanism of transferring correlations to local squeezing may have important implications for black hole firewalls [AMPS13, BP13], as we shall discuss. It is known that two-mode squeezing between the outgoing left-moving and right-moving modes is also generated by an accelerating mirror [OP03b]. This means that the correlations between the quadratures of these field modes are below the quantum vacuum noise, and implies the presence of bipartite entanglement [WPGP<sup>+</sup>12]. While the presence of entanglement between left-moving and right-moving modes is obvious in our circuit model, we choose to focus here on the properties of the left-moving modes alone. Henceforth, by ‘local squeezing’ we shall mean specifically the squeezing within the left-moving modes.

This chapter is organized as follows. Section 7.2 constructs a general circuit model for a uniformly accelerated object with time independent interactions, and derives input-output relations for a uniformly accelerated mirror. Section 7.3 calculates the radiation flux from a uniformly accelerated mirror. Section 7.4 investigates local squeezing in the radiation field. Section 7.5 discusses possible connections with black hole firewalls. The results in this chapter have been published in [SHMR17b].

## 7.2 Circuit model

### 7.2.1 Relations between Rindler modes and Unruh modes

In Chapter 4 we have introduced the relations between Rindler modes and Unruh modes. These relations act as the foundation of our quantum circuit model. For simplicity, we focus on a massless scalar field  $\hat{\Phi}$  in  $(1+1)$ -dimensional Minkowski spacetime. There exists three ways of quantizing the massless scalar field and the corresponding operators are known as the Minkowski mode operators  $(\hat{a}_{mk})$ , Rindler mode operators  $(\hat{b}_{m\omega}^R, \hat{b}_{m\omega}^L)$  and Unruh mode operators  $(\hat{c}_{m\omega}, \hat{d}_{m\omega})$ . One can directly derive the Bogoliubov transformation between the Minkowski modes and the Rindler modes to show the Unruh effect, or use the Unruh modes as the stepping stone to link the Minkowski modes and Rindler modes. The utilization of Unruh modes is proved to be very convenient because the relation between the Rindler modes and Unruh modes is simply a two-mode squeezing transformation, as given by Eqs. (4.5.44) and (4.5.45).

In terms of concepts in quantum optics, the transformation from Unruh modes to Rindler modes, Eq. (4.5.45), can be represented by a two-mode squeezer, as shown in Fig. 7.1(a). The two output modes of the two-mode squeezer are the right and left Rindler modes, which are spatially separated and independent. For a uniformly accelerated object in the right Rindler wedge, it only interacts with the right Rindler modes and leaves the left Rindler modes unchanged. So the accelerated object can be represented by a unitary connected to the right Rindler modes. After the interaction, Rindler modes are transformed back to the Unruh modes, which is described by Eq. (4.5.44). This transformation can be represented by a two-mode antisqueezer, as shown by Fig. 7.1(b).

### 7.2.2 General circuit for time independent interactions

How are the states of a quantum field affected by an object (such as a beamsplitter) that is uniformly accelerated in the right Rindler wedge? This is the question of central interest in this chapter. A straightforward way to study this problem is to work in the accelerated

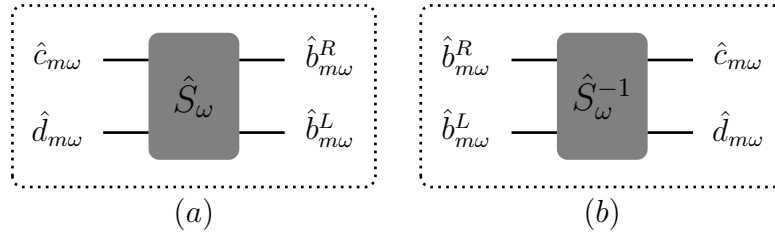


FIGURE 7.1: (a) Two-mode squeezer: Unruh modes to Rindler modes. (b) Two-mode antisqueezer: Rindler modes to Unruh modes.

frame in which the object is static. As we have mentioned before, the object only interacts with Rindler modes in the right Rindler wedge and the Rindler modes in the left Rindler wedge remain unaffected. The most general unitary interactions between the object and the field not only couples the left-moving and right-moving Rindler modes, but also Rindler modes with different frequencies. Together with Eqs. (4.5.44) and (4.5.45), we can construct a quantum circuit model (or input-output formalism) for the uniformly accelerated object. We start from the inertial frame in which Unruh modes are used instead of Minkowski modes. This makes the model simpler although we still need to transform the Minkowski modes to the Unruh modes and vice versa.

First, based on Eq. (4.5.45), the Unruh modes pass through a collection of two-mode squeezers each of which couples a pair of Unruh modes  $(\hat{c}_{m\omega}, \hat{d}_{m\omega})$  with frequency dependent squeezing parameter  $r_\omega$ . Second, the output right Rindler modes  $\hat{b}_{m\omega}^R$  interact with the object and are transformed to  $\hat{b}'_{m\omega}{}^R$  which could be a function of other Rindler frequency modes  $\hat{b}_{m\omega'}^R$ . The left Rindler modes  $\hat{b}_{m\omega}^L$  remain unchanged. Finally, based on Eq. (4.5.44), the Rindler modes pass through a collection of two-mode antisqueezers and are transformed to output Unruh modes  $(\hat{c}'_{m\omega}, \hat{d}'_{m\omega})$ . If we use an inertial detector to detect the radiation field from the accelerated object, then the final step is to compute the response of the inertial detector, which is most conveniently done by transforming the Unruh modes  $(\hat{c}'_{m\omega}, \hat{d}'_{m\omega})$  to Minkowski modes.

We focus on time independent interactions in this chapter and discuss time dependent interactions in the next chapter. If the interaction is time independent, the unitary does not

couple Rindler modes with different frequencies, so that the input-output formalism is substantially simplified. Since modes with different frequencies are independent, we can draw a quantum circuit for each single frequency. The quantum circuit is shown in Fig. 7.2. A pair of left-moving Unruh modes  $(\hat{c}_{1\omega}, \hat{d}_{1\omega})$  and a pair of right-moving Unruh modes  $(\hat{c}_{2\omega}, \hat{d}_{2\omega})$  pass through the two-mode squeezers  $S_\omega$ , from which emerge left-moving Rindler modes  $(\hat{b}_{1\omega}^R, \hat{b}_{1\omega}^L)$  and right-moving Rindler modes  $(\hat{b}_{2\omega}^R, \hat{b}_{2\omega}^L)$ , respectively.  $\hat{b}_{1\omega}^R$  and  $\hat{b}_{2\omega}^R$  interact with each other when passing through the object (symbolized by the black dot in Fig. 7.2) and emerge as  $\hat{b}'_{1\omega}^R$  and  $\hat{b}'_{2\omega}^R$ ,

$$\hat{b}'_{m\omega} = \hat{U}_\omega \hat{b}_{m\omega} \hat{U}_\omega \quad (7.2.1)$$

where the operator  $\hat{U}_\omega$  represents a general unitary transformation which includes nonlinear interactions. For example,  $\hat{U}_\omega = \exp\{i\chi_\omega(\hat{b}_{1\omega}^{R\dagger}\hat{b}_{1\omega}^R)^2\}$  describes the nonlinear Kerr effect. After that, the Rindler modes are combined by two-mode antisqueezers  $S_\omega^{-1}$ , ending up with Unruh modes again.

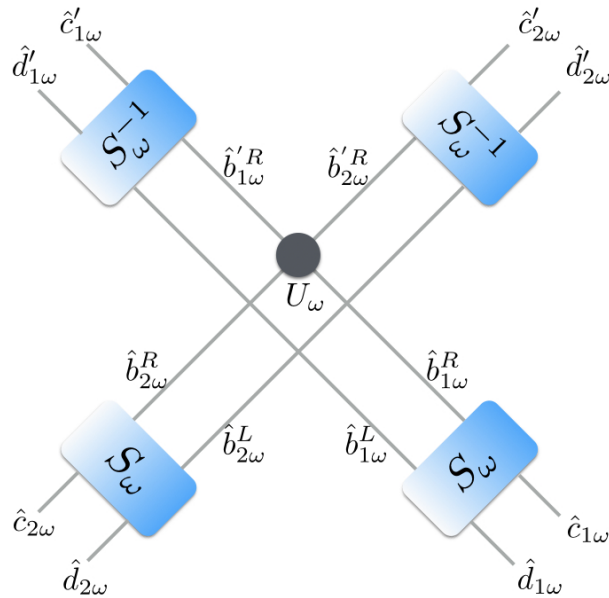


FIGURE 7.2: Unruh modes pass through the squeezers and then become Rindler modes. The Rindler modes in the right Rindler wedge interact with the object ( $U_\omega$ ) and then combine with the Rindler modes from the left Rindler wedge in the antisqueezers, going back to Unruh modes again.

If we restrict the unitary functions of up to quadratic power of the mode operators then a linear input-output relation can be written. In particular,

$$\hat{b}_{m\omega}^{R\dagger} = \alpha_{\omega\omega}^{m1} \hat{b}_{1\omega}^R + \beta_{\omega\omega}^{m1} \hat{b}_{1\omega}^{R\dagger} + \alpha_{\omega\omega}^{m2} \hat{b}_{2\omega}^R + \beta_{\omega\omega}^{m2} \hat{b}_{2\omega}^{R\dagger}. \quad (7.2.2)$$

Note that this describes not only linear scattering but also active linear processes such as squeezing (represented by the dagger terms). For computational purposes, we introduce operator vectors  $\hat{\mathbf{c}}_\omega$ ,  $\hat{\mathbf{d}}_\omega$ ,  $\hat{\mathbf{b}}_\omega^R$  and  $\hat{\mathbf{b}}_\omega^L$ , which are defined as

$$\hat{\mathbf{c}}_\omega = \begin{pmatrix} \hat{c}_\omega \\ \hat{c}_\omega^\dagger \end{pmatrix}, \quad \hat{\mathbf{d}}_\omega = \begin{pmatrix} \hat{d}_\omega \\ \hat{d}_\omega^\dagger \end{pmatrix}, \quad \hat{\mathbf{b}}_\omega^R = \begin{pmatrix} \hat{b}_\omega^R \\ \hat{b}_\omega^{R\dagger} \end{pmatrix}, \quad \hat{\mathbf{b}}_\omega^L = \begin{pmatrix} \hat{b}_\omega^L \\ \hat{b}_\omega^{L\dagger} \end{pmatrix}.$$

Then Eqs. (4.5.44) and (4.5.45) can be rewritten as

$$\begin{pmatrix} \hat{\mathbf{c}}_{m\omega} \\ \hat{\mathbf{d}}_{m\omega} \end{pmatrix} = S_\omega^{-1} \begin{pmatrix} \hat{\mathbf{b}}_{m\omega}^R \\ \hat{\mathbf{b}}_{m\omega}^L \end{pmatrix}, \quad \begin{pmatrix} \hat{\mathbf{b}}_{m\omega}^R \\ \hat{\mathbf{b}}_{m\omega}^L \end{pmatrix} = S_\omega \begin{pmatrix} \hat{\mathbf{c}}_{m\omega} \\ \hat{\mathbf{d}}_{m\omega} \end{pmatrix}, \quad (7.2.3)$$

with

$$S_\omega \equiv \begin{pmatrix} I \cosh(r_\omega) & \sigma_x \sinh(r_\omega) \\ \sigma_x \sinh(r_\omega) & I \cosh(r_\omega) \end{pmatrix} \quad (7.2.4)$$

where  $I = \begin{pmatrix} 1 & 0 \\ 0 & 1 \end{pmatrix}$  is the identity matrix and  $\sigma_x = \begin{pmatrix} 0 & 1 \\ 1 & 0 \end{pmatrix}$  is one of the Pauli matrices. The transformation between the input Unruh modes  $(\hat{\mathbf{c}}_{1\omega}, \hat{\mathbf{d}}_{1\omega}, \hat{\mathbf{c}}_{2\omega}, \hat{\mathbf{d}}_{2\omega})^T$  and the output Unruh modes  $(\hat{\mathbf{c}}'_{1\omega}, \hat{\mathbf{d}}'_{1\omega}, \hat{\mathbf{c}}'_{2\omega}, \hat{\mathbf{d}}'_{2\omega})^T$  can be represented as

$$\begin{pmatrix} \hat{\mathbf{c}}'_{1\omega} \\ \hat{\mathbf{d}}'_{1\omega} \\ \hat{\mathbf{c}}'_{2\omega} \\ \hat{\mathbf{d}}'_{2\omega} \end{pmatrix} = S_\omega^{-1} \mathcal{U}_\omega S_\omega \begin{pmatrix} \hat{\mathbf{c}}_{1\omega} \\ \hat{\mathbf{d}}_{1\omega} \\ \hat{\mathbf{c}}_{2\omega} \\ \hat{\mathbf{d}}_{2\omega} \end{pmatrix}. \quad (7.2.5)$$

$S_\omega$  characterizes the transformation from Unruh modes to Rindler modes

$$S_\omega = \begin{pmatrix} S_\omega & 0 \\ 0 & S_\omega \end{pmatrix} \quad (7.2.6)$$

and  $\mathcal{U}_\omega$  characterizes the action of the object

$$\mathcal{U}_\omega = \begin{pmatrix} U_\omega^{11} & 0 & U_\omega^{12} & 0 \\ 0 & I & 0 & 0 \\ U_\omega^{21} & 0 & U_\omega^{22} & 0 \\ 0 & 0 & 0 & I \end{pmatrix} \quad (7.2.7)$$

where

$$U_{\omega}^{mn} = \begin{pmatrix} \alpha_{\omega\omega}^{mn} & \beta_{\omega\omega}^{mn} \\ \beta_{\omega\omega}^{mn*} & \alpha_{\omega\omega}^{mn*} \end{pmatrix}. \quad (7.2.8)$$

We want to emphasize that the general formalism developed here is valid for a wide class of quantum optical devices (objects), such as beamsplitters, single-mode squeezers, two-mode squeezers and cavities. In the next chapter, we will show that it generalizes to devices with time-dependent parameters, e.g., beamsplitters with time-dependent transmission coefficients. In this chapter, we mainly apply the formalism to the simplest case, a beamsplitter.

### 7.2.3 Circuit model for a uniformly accelerated mirror

The perfect moving mirror problem has been extensively studied for several decades. A perfect moving mirror provides a clear boundary for a quantum field, which vanishes along the mirror's trajectory. The standard method for calculating the radiation from a perfect moving mirror is to find the Bogoliubov transformation between the input and output modes by taking into account the Dirichlet boundary condition [BD82]. However a realistic mirror is not perfect but usually partially transparent, for which the Dirichlet boundary condition is not satisfied. In this chapter, we are interested in a uniformly accelerated imperfect mirror whose motion looks nontrivial for an inertial observer. Rather than use the standard method (which is still valid if appropriate boundary conditions are considered), we shall employ the circuit model developed in the previous subsection, leading to a much simpler way to attack this problem.

The idea is to work in the accelerated frame, in which the mirror is static and can be considered as a beamsplitter. Without loss of generality, we assume that the mirror uniformly accelerates in the right Rindler wedge. The beamsplitter transforms the right Rindler modes as

$$\begin{aligned} \hat{b}_{1\omega}^{IR} &= \cos \theta_{\omega} \hat{b}_{1\omega}^R - ie^{i\phi_{\omega}} \sin \theta_{\omega} \hat{b}_{2\omega}^R, \\ \hat{b}_{2\omega}^{IR} &= \cos \theta_{\omega} \hat{b}_{2\omega}^R - ie^{-i\phi_{\omega}} \sin \theta_{\omega} \hat{b}_{1\omega}^R, \end{aligned} \quad (7.2.9)$$

where  $\theta_\omega$  and  $\phi_\omega$  are frequency dependent. The relative phase shift  $ie^{\pm i\phi_\omega}$  ensures that the transformation is unitary. The intensity reflection and transmission coefficients of the beamsplitter are

$$R_\omega = \sin^2 \theta_\omega, \quad T_\omega = \cos^2 \theta_\omega.$$

By comparing Eqs. (7.2.9) and (7.2.2) we have

$$\begin{aligned} \alpha_{\omega\omega}^{11} &= \alpha_{\omega\omega}^{22} = \cos \theta_\omega, \\ \alpha_{\omega\omega}^{12} &= -\alpha_{\omega\omega}^{21*} = -ie^{i\phi_\omega} \sin \theta_\omega, \end{aligned}$$

and all  $\beta_{\omega\omega}^{mn}$  are zero. We can therefore express the action of the beamsplitter as

$$\mathcal{U}_\omega = \begin{pmatrix} I \cos \theta_\omega & 0 & Z \sin \theta_\omega & 0 \\ 0 & I & 0 & 0 \\ -Z^* \sin \theta_\omega & 0 & I \cos \theta_\omega & 0 \\ 0 & 0 & 0 & I \end{pmatrix}, \quad (7.2.10)$$

where  $I$  is the  $2 \times 2$  identity matrix and

$$Z = \begin{pmatrix} -ie^{i\phi_\omega} & 0 \\ 0 & ie^{-i\phi_\omega} \end{pmatrix}. \quad (7.2.11)$$

The explicit expressions for the transformation Eq. (7.2.5) can be calculated straightforwardly. We find

$$\begin{aligned} \hat{\mathbf{c}}'_{1\omega} &= \hat{\mathbf{c}}_{1\omega} [\cosh^2(r_\omega) \cos \theta_\omega - \sinh^2(r_\omega)] - \sigma_x \hat{\mathbf{d}}_{1\omega} \cosh(r_\omega) \sinh(r_\omega) (1 - \cos \theta_\omega) \\ &\quad + Z \hat{\mathbf{c}}_{2\omega} \cosh^2(r_\omega) \sin \theta_\omega + Z \sigma_x \hat{\mathbf{d}}_{2\omega} \cosh(r_\omega) \sinh(r_\omega) \sin \theta_\omega. \\ &= [\cosh^2(r_\omega) \cos \theta_\omega - \sinh^2(r_\omega)] \begin{pmatrix} \hat{c}_{1\omega} \\ \hat{c}_{1\omega}^\dagger \end{pmatrix} - \cosh(r_\omega) \sinh(r_\omega) (1 - \cos \theta_\omega) \begin{pmatrix} \hat{d}_{1\omega}^\dagger \\ \hat{d}_{1\omega} \end{pmatrix} \\ &\quad + \cosh^2(r_\omega) \sin \theta_\omega \begin{pmatrix} -ie^{i\phi_\omega} \hat{c}_{2\omega} \\ ie^{-i\phi_\omega} \hat{c}_{2\omega}^\dagger \end{pmatrix} + \cosh(r_\omega) \sinh(r_\omega) \sin \theta_\omega \begin{pmatrix} -ie^{i\phi_\omega} \hat{d}_{2\omega}^\dagger \\ ie^{-i\phi_\omega} \hat{d}_{2\omega} \end{pmatrix}, \end{aligned} \quad (7.2.12)$$

$$\begin{aligned} \hat{\mathbf{d}}'_{1\omega} &= \sigma_x \hat{\mathbf{c}}_{1\omega} \cosh(r_\omega) \sinh(r_\omega) (1 - \cos \theta_\omega) + \hat{\mathbf{d}}_{1\omega} [\cosh^2(r_\omega) - \sinh^2(r_\omega) \cos \theta_\omega] \\ &\quad - \sigma_x Z \hat{\mathbf{c}}_{2\omega} \cosh(r_\omega) \sinh(r_\omega) \sin \theta_\omega - \sigma_x Z \sigma_x \hat{\mathbf{d}}_{2\omega} \sinh^2(r_\omega) \sin \theta_\omega \\ &= \cosh(r_\omega) \sinh(r_\omega) (1 - \cos \theta_\omega) \begin{pmatrix} \hat{c}_{1\omega}^\dagger \\ \hat{c}_{1\omega} \end{pmatrix} + [\cosh^2(r_\omega) - \sinh^2(r_\omega) \cos \theta_\omega] \begin{pmatrix} \hat{d}_{1\omega} \\ \hat{d}_{1\omega}^\dagger \end{pmatrix} \\ &\quad - \cosh(r_\omega) \sinh(r_\omega) \sin \theta_\omega \begin{pmatrix} ie^{-i\phi_\omega} \hat{c}_{2\omega}^\dagger \\ -ie^{i\phi_\omega} \hat{c}_{2\omega} \end{pmatrix} - \sinh^2(r_\omega) \sin \theta_\omega \begin{pmatrix} ie^{-i\phi_\omega} \hat{d}_{2\omega} \\ -ie^{i\phi_\omega} \hat{d}_{2\omega}^\dagger \end{pmatrix}, \end{aligned} \quad (7.2.13)$$

$$\begin{aligned}
 \hat{\mathbf{c}}'_{2\omega} &= -Z^* \hat{\mathbf{c}}_{1\omega} \cosh^2(r_\omega) \sin \theta_\omega - Z^* \sigma_x \hat{\mathbf{d}}_{1\omega} \cosh(r_\omega) \sinh(r_\omega) \sin \theta_\omega \\
 &\quad + \hat{\mathbf{c}}_{2\omega} [\cosh^2(r_\omega) \cos \theta_\omega - \sinh^2(r_\omega)] - \sigma_x \hat{\mathbf{d}}_{2\omega} \cosh(r_\omega) \sinh(r_\omega) (1 - \cos \theta_\omega) \\
 &= \cosh^2(r_\omega) \sin \theta_\omega \begin{pmatrix} -ie^{-i\phi_\omega} \hat{\mathbf{c}}_{1\omega} \\ ie^{i\phi_\omega} \hat{\mathbf{c}}_{1\omega}^\dagger \end{pmatrix} + \cosh(r_\omega) \sinh(r_\omega) \sin \theta_\omega \begin{pmatrix} -ie^{-i\phi_\omega} \hat{\mathbf{d}}_{1\omega}^\dagger \\ ie^{i\phi_\omega} \hat{\mathbf{d}}_{1\omega} \end{pmatrix} \\
 &\quad + [\cosh^2(r_\omega) \cos \theta_\omega - \sinh^2(r_\omega)] \begin{pmatrix} \hat{\mathbf{c}}_{2\omega} \\ \hat{\mathbf{c}}_{2\omega}^\dagger \end{pmatrix} - \cosh(r_\omega) \sinh(r_\omega) (1 - \cos \theta_\omega) \begin{pmatrix} \hat{\mathbf{d}}_{2\omega}^\dagger \\ \hat{\mathbf{d}}_{2\omega} \end{pmatrix},
 \end{aligned} \tag{7.2.14}$$

$$\begin{aligned}
 \hat{\mathbf{d}}'_{2\omega} &= -\sigma_x Z^* \hat{\mathbf{c}}_{1\omega} \cosh(r_\omega) \sinh(r_\omega) \sin \theta_\omega + \sigma_x Z^* \sigma_x \hat{\mathbf{d}}_{1\omega} \sinh^2(r_\omega) \sin \theta_\omega \\
 &\quad + \sigma_x \hat{\mathbf{c}}_{2\omega} \cosh(r_\omega) \sinh(r_\omega) (1 - \cos \theta_\omega) + \hat{\mathbf{d}}_{2\omega} [\cosh^2(r_\omega) - \sinh^2(r_\omega) \cos \theta_\omega] \\
 &= -\cosh(r_\omega) \sinh(r_\omega) \sin \theta_\omega \begin{pmatrix} ie^{i\phi_\omega} \hat{\mathbf{c}}_{1\omega}^\dagger \\ -ie^{-i\phi_\omega} \hat{\mathbf{c}}_{1\omega} \end{pmatrix} - \sinh^2(r_\omega) \sin \theta_\omega \begin{pmatrix} ie^{i\phi_\omega} \hat{\mathbf{d}}_{1\omega} \\ -ie^{-i\phi_\omega} \hat{\mathbf{d}}_{1\omega}^\dagger \end{pmatrix} \\
 &\quad + \cosh(r_\omega) \sinh(r_\omega) (1 - \cos \theta_\omega) \begin{pmatrix} \hat{\mathbf{c}}_{2\omega}^\dagger \\ \hat{\mathbf{c}}_{2\omega} \end{pmatrix} + [\cosh^2(r_\omega) - \sinh^2(r_\omega) \cos \theta_\omega] \begin{pmatrix} \hat{\mathbf{d}}_{2\omega} \\ \hat{\mathbf{d}}_{2\omega}^\dagger \end{pmatrix}.
 \end{aligned} \tag{7.2.15}$$

With these transformations, it is easy to calculate the expectation value of the particle number of the output mode  $\hat{\mathbf{c}}'_{1\omega}$ ,

$$\begin{aligned}
 \langle 0_M | \hat{\mathbf{c}}_{1\omega}^\dagger \hat{\mathbf{c}}'_{1\omega} | 0_M \rangle &= 2(1 - \cos \theta_\omega) \cosh^2(r_\omega) \sinh^2(r_\omega) \delta(\omega - \omega') \\
 &= 2(1 - \cos \theta_\omega) \frac{e^{2\pi\omega/a}}{(e^{2\pi\omega/a} - 1)^2} \delta(\omega - \omega') \\
 &\equiv n(\omega) \delta(\omega - \omega').
 \end{aligned} \tag{7.2.16}$$

The corresponding expectation values for the other three outputs is the same as Eq. (7.2.16). Hence the number of Unruh particles in every output is generally not zero. The particle-number distribution is

$$n(\omega) = 2(1 - \cos \theta_\omega) \frac{e^{2\pi\omega/a}}{(e^{2\pi\omega/a} - 1)^2}, \tag{7.2.17}$$

depending on the transmission coefficient of the uniformly accelerated mirror. Note that  $n(\omega) = 0$  only when  $\theta_\omega = 0$ ; in other words when the mirror is completely transparent to the field mode with frequency  $\omega$ . We also note that the distribution of the output Unruh particles is not thermal.

## 7.3 Radiation from an eternally accelerated mirror

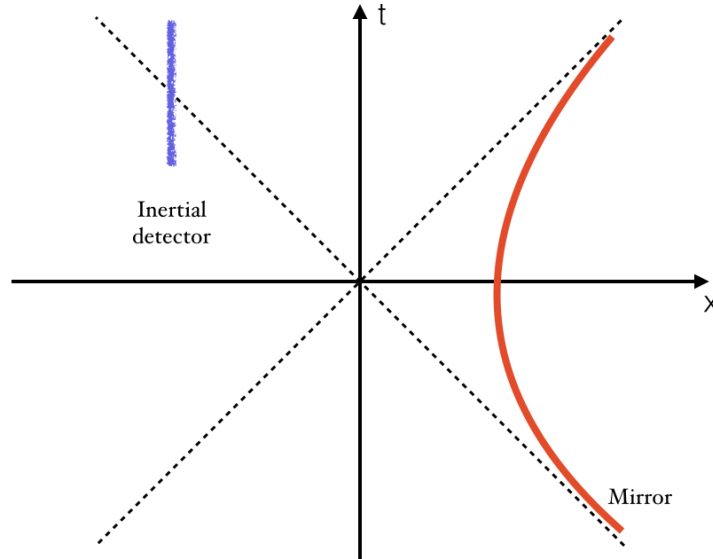


FIGURE 7.3: A uniformly accelerated mirror on the right Rindler wedge. An inertial detector is placed at an appropriate position to detect left-moving particles coming from the uniformly accelerated mirror.

### 7.3.1 Particle number flux

As an application of the quantum circuit model, we calculate the radiation flux from an eternally accelerated mirror. As shown in Fig. 7.3, an inertial detector is placed at an appropriate position to detect the left-moving particles radiated by the accelerated mirror. In the previous section, we have shown that the accelerated mirror radiates Unruh particles. However when considering the response of an inertial detector, it is more convenient to use Minkowski modes. The transformation from Unruh modes to Minkowski modes is given by Eq. (4.5.46). Since we only consider left-moving modes here, without introducing any confusion, we omit the subscript “1”. In realistic quantum optics experiments a detector normally detects localized wave packet modes. In order to take this into account we consider Gaussian wave packet modes defined as

$$\hat{a}(f) = \int_0^\infty dk f(k; k_0, \sigma, V_0) \hat{a}_k, \quad (7.3.1)$$

where

$$f(k; k_0, \sigma, V_0) = \left( \frac{1}{2\pi\sigma^2} \right)^{1/4} \exp \left\{ -\frac{(k - k_0)^2}{4\sigma^2} - ikV_0 \right\} \quad (7.3.2)$$

with  $k_0$ ,  $\sigma$  and  $V_0$  the central frequency, bandwidth and central position, respectively. In the narrow bandwidth limit ( $k_0 \gg \sigma$ ), the integration over  $k$  can be approximately calculated to a very good accuracy.

When  $k_0 \gg \sigma$ , the Gaussian wave packet  $f(k; k_0, \sigma, V_0)$  is significantly nonzero only for positive  $k$ , so the range of integration of  $k$  can be extended to  $(-\infty, \infty)$  without introducing large errors. Secondly, since  $f(k; k_0, \sigma, V_0)$  is well localized around  $k_0$ , those values of  $A_{k\omega}$  and  $B_{k\omega}$  only near  $k_0$  are relevant. Writing [DRW13]

$$\frac{1}{\sqrt{k}} \left( \frac{k}{a} \right)^{i\omega/a} \approx \frac{1}{\sqrt{k_0}} e^{i\frac{\omega}{k_0} \frac{k}{a}} e^{i\frac{\omega}{a} [\ln(\frac{k_0}{a}) - 1]} \quad (7.3.3)$$

and then expanding  $A_{k\omega}$  and  $B_{k\omega}$  around  $k_0$  yields

$$\begin{aligned} A_{f\omega} \equiv \int_0^\infty dk f(k) A_{k\omega} &\approx i \sqrt{\frac{\sigma}{\pi\omega k_0}} \left( \frac{1}{2\pi} \right)^{1/4} \sqrt{2 \sinh(\pi\omega/a)} \Gamma(1 - i\omega/a) e^{i\frac{\omega}{a} \ln(\frac{k_0}{a})} e^{-ik_0 V_0} \\ &\times \exp \left\{ -\frac{\sigma^2(\omega/a - k_0 V_0)^2}{k_0^2} \right\}, \end{aligned} \quad (7.3.4)$$

$$\begin{aligned} B_{f\omega} \equiv \int_0^\infty dk f(k) B_{k\omega} &\approx -i \sqrt{\frac{\sigma}{\pi\omega k_0}} \left( \frac{1}{2\pi} \right)^{1/4} \sqrt{2 \sinh(\pi\omega/a)} \Gamma(1 + i\omega/a) e^{-i\frac{\omega}{a} \ln(\frac{k_0}{a})} e^{-ik_0 V_0} \\ &\times \exp \left\{ -\frac{\sigma^2(\omega/a + k_0 V_0)^2}{k_0^2} \right\} \end{aligned} \quad (7.3.5)$$

up to first order in  $k - k_0$ . Using Eq. (7.2.16) and

$$|\Gamma(1 - i\omega/a)|^2 = |\Gamma(1 + i\omega/a)|^2 = \frac{\pi\omega/a}{\sinh(\pi\omega/a)} \quad (7.3.6)$$

the expectation value  $N(f) = \langle 0_M | \hat{a}^\dagger(f) \hat{a}(f) | 0_M \rangle$  of the Gaussian mode particle number is

$$\begin{aligned}
N(f) &= \int d\omega \int d\omega' \langle 0_M | (A_{f\omega}^* \hat{c}_\omega^\dagger + B_{f\omega}^* \hat{d}_\omega^\dagger) (A_{f\omega'} \hat{c}'_{\omega'} + B_{f\omega'} \hat{d}'_{\omega'}) | 0_M \rangle \\
&= 2 \int d\omega (|A_{f\omega}|^2 + |B_{f\omega}|^2) (1 - \cos \theta_\omega) \frac{e^{2\pi\omega/a}}{(e^{2\pi\omega/a} - 1)^2}, \\
&= \sqrt{\frac{8}{\pi}} \frac{\sigma}{k_0} \int_0^\infty d\Omega \left\{ \exp \left[ -\frac{2\sigma^2(\Omega - k_0 V_0)^2}{k_0^2} \right] + \exp \left[ -\frac{2\sigma^2(\Omega + k_0 V_0)^2}{k_0^2} \right] \right\} \\
&\quad \times (1 - \cos \theta_\Omega) \frac{e^{2\pi\Omega}}{(e^{2\pi\Omega} - 1)^2}, \tag{7.3.7}
\end{aligned}$$

where  $\Omega = \omega/a$  is the dimensionless Rindler frequency.

Two special cases are of particular interest. Consider first that the mirror is completely transparent for all modes, that is  $\cos^2 \theta_\omega = 1$ . From Eq. (7.3.7), the particle number vanishes,  $N(f) = 0$ . This is not surprising because a completely transparent mirror does nothing to the Minkowski vacuum. The second case is that the mirror is perfect for all modes, that is,  $\cos^2 \theta_\omega = 0$ . When  $\Omega \rightarrow 0$ ,  $(e^{2\pi\Omega} - 1)^{-2} \sim \Omega^{-2}$  and all other factors in the integrand of Eq. (7.3.7) are finite. Therefore, the particle number  $N(f)$  is divergent.

This infrared divergence occurs because we naively assume that the mirror accelerates for an infinitely long time, which seems physically unreasonable. In the framework of the self-interaction model, the mirror is switched on and off so that one obtains finite particle flux [OP01]. In our circuit model, we could also switch on and off the mirror. However instead we shall use a simpler method of regularization. The idea is to directly introduce a low frequency cutoff for the mirror, that is, the mirror is completely transparent for low-frequency field modes. The mechanism for a physical mirror to reflect electromagnetic waves is that the atoms consisting of the mirror absorb electromagnetic waves and then reemit them again. If the wavelength of the electromagnetic wave is very long, the response time of the mirror is very long. Hence if the mirror accelerates for a finite time, it cannot respond to Rindler modes with characteristic oscillation period longer than the accelerating time.

In this sense, introducing a low-frequency cutoff is equivalent to switching on and off the mirror. In higher dimensional spacetime, e.g.,  $(1+3)$ -dimensional spacetime, there is another reason justifying a low-frequency cutoff. A physical mirror with finite size cannot reflect field modes whose wavelengths are much larger than its size. This infrared divergence is not due to the pathological character of a massless scalar field in  $(1+1)$ -dimensional spacetime [Col73]; it also appears in higher dimensional spacetime [FS99] if the mirror is accelerated for an infinitely long time. If we assume that the reflectivity  $R_\omega$  of the mirror is a power law of  $\omega$

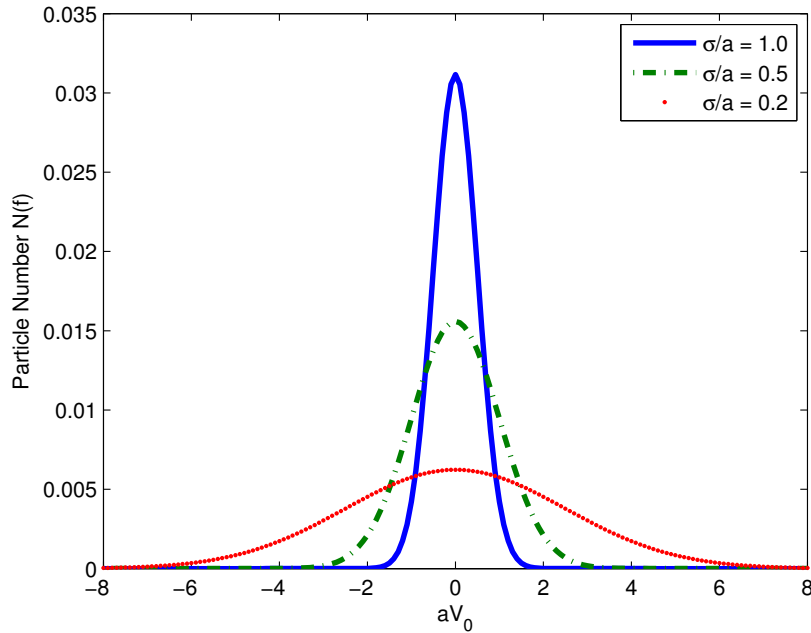


FIGURE 7.4: Particle number versus central position of the Gaussian wave packet:  $k_0/a = 20$ ,  $ag = 10$ . For larger bandwidth (narrower wave packet in time domain), the particle number distribution is narrower, showing that particles are localized around the past event horizon.

as  $\omega \rightarrow 0$  ( $R_\omega \sim \omega^\gamma$ ) then in order to obtain finite particle number we must have  $\gamma > 1$ . As a concrete example, we choose

$$R_\omega = \sin^2 \theta_\omega = \frac{g^2 \omega^2}{1 + g^2 \omega^2}, \quad (7.3.8)$$

where  $g$  is a parameter characterizing the low-frequency cutoff. Fig. 7.4 shows the particle number  $N(f)$  versus the central position of the Gaussian wave packet. We can see that the particle-number distribution is symmetric with respect to  $V_0 = 0$ . In addition, for larger bandwidth (narrower wave packet in time domain), the distribution is more localized around

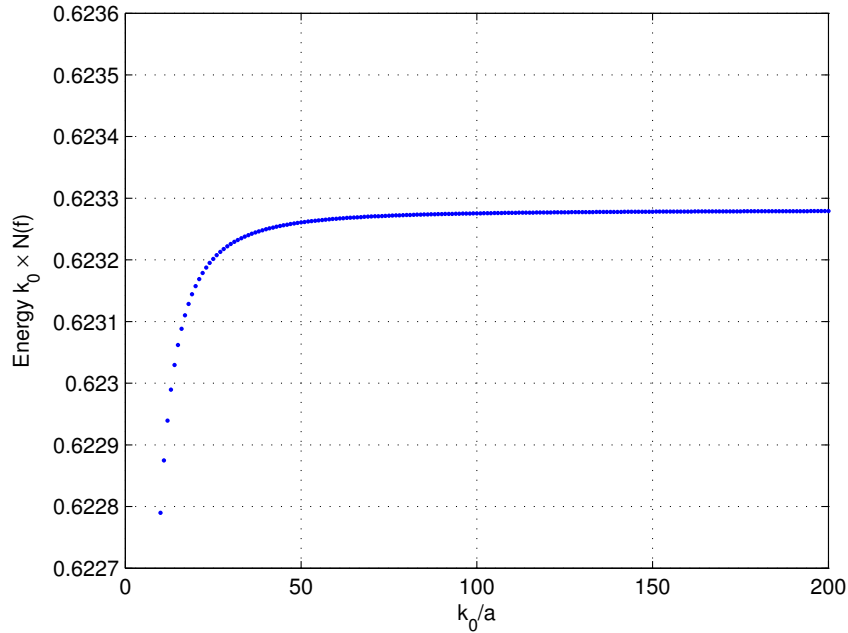


FIGURE 7.5: Energy of the wave packets versus the central frequency:  $\sigma/a = 1.0$ ,  $aV_0 = 0$ ,  $ag = 10$ . The energy is almost constant in the high central frequency limit.

$V_0 = 0$ . These two facts indicate that the particle flux radiated by the uniformly accelerated mirror is well localized around the past horizon  $V_0 = 0$ . Since the mirror starts to accelerate in the distant past, that means the mirror only radiates particles when it starts accelerating. It radiates no particles when it is uniformly accelerating.

### 7.3.2 Total energy flux

Since we are considering a narrow bandwidth Gaussian wave packet mode with central frequency  $k_0$ , the energy of the field in this wave packet mode can be approximated as  $k_0 N(f)$ , which is finite. It is interesting to know how much energy was emitted by the uniformly accelerated mirror. This can be calculated by integrating the energy in each wave packet mode for all  $k_0$ .

In the large  $k_0$  limit, we can derive an analytically approximate expression for the particle number  $N(f)$ . From Eq. (7.3.7), one expects that the term in the braces has two peaks at  $k_0 V_0$  and  $-k_0 V_0$ . If  $k_0$  is large then the peaks are far away from the origin. However,

the factor  $\frac{e^{2\pi\Omega}}{(e^{2\pi\Omega}-1)^2}$  exponentially decays for large  $\Omega$  so that it strongly suppresses one of the Gaussian peaks. Therefore, the main contribution to the integration is from the low frequency. We Taylor expand the term in the braces to second order,

$$\exp\left[-\frac{2\sigma^2(\Omega - k_0V_0)^2}{k_0^2}\right] + \exp\left[-\frac{2\sigma^2(\Omega + k_0V_0)^2}{k_0^2}\right] \approx 2e^{-2\sigma^2V_0^2} + \frac{4\sigma^2\Omega^2}{k_0^2}(4\sigma^2V_0^2 - 1)e^{-2\sigma^2V_0^2}.$$

In order to get an analytic expression, we introduce a sharp low frequency cutoff instead of the smooth cutoff Eq. (7.3.8):  $R_\omega = 1$  for  $\Omega \geq \epsilon$  and zero for  $0 < \Omega < \epsilon$ . Therefore we have  $1 - \cos\theta_\Omega = 1$  for  $\Omega \geq \epsilon$  and zero for  $0 < \Omega < \epsilon$ . The particle number  $N(f)$  can be approximated as

$$\begin{aligned} N(f) &\approx 4\sqrt{\frac{2}{\pi}}\frac{\sigma}{k_0}e^{-2\sigma^2V_0^2}\left[\int_\epsilon^\infty d\Omega\frac{e^{2\pi\Omega}}{(e^{2\pi\Omega}-1)^2} + \frac{2\sigma^2}{k_0^2}(4\sigma^2V_0^2 - 1)\int_\epsilon^\infty d\Omega\frac{\Omega^2e^{2\pi\Omega}}{(e^{2\pi\Omega}-1)^2}\right] \\ &\approx \left(\frac{2}{\pi}\right)^{3/2}\left(\frac{\sigma}{k_0}\right)e^{-2\sigma^2V_0^2}\left[\frac{1}{e^{2\pi\epsilon}-1} + \frac{2\sigma^2}{k_0^2}(4\sigma^2V_0^2 - 1)\left(\frac{1}{12} - \frac{\epsilon^2}{2\pi}\right)\right]. \end{aligned} \quad (7.3.9)$$

Comparison with direct numerical calculation shows that Eq. (7.3.9) is a very good approximation when  $\epsilon$  is small. We can see that the particle number is dependent on the low frequency cutoff  $\epsilon$ . The first term of Eq. (7.3.9) is proportional to  $\frac{1}{e^{2\pi\epsilon}-1}$  which is divergent when  $\epsilon \rightarrow 0$ . Furthermore, in the high central frequency limit  $k_0 \rightarrow \infty$ , the leading order term of  $N(f)$  is proportional to  $\frac{1}{k_0}$ , yielding the relationship  $E(f) \approx k_0N(f) \sim \mathcal{O}(1)$  for the energy of the wave packet.

A numerical result shown in Fig. 7.5 for smooth cutoff verifies the analytical result, namely, the energy in a wave packet tends to be a constant in the large  $k_0$  limit. Therefore, adding up the energy of all wave packets yields a divergent result. This ultraviolet divergence arises as a consequence of the physically unrealistic assumption that the mirror is accelerated eternally, so that it appears to any inertial observers when they cross the past horizon. This ultraviolet divergence can be removed by smoothly switching on the mirror [OP01], or by considering an accelerated mirror whose acceleration was slowly increased from zero. For a switch-on timescale of  $\Delta T$ , the particle number is suppressed for wave packets with central frequency  $k_0 > \frac{1}{\Delta T}$  while it remains the same for wave packets with central frequency  $k_0 < \frac{1}{\Delta T}$ . Therefore Eq. (7.3.7) is not applicable to wave packets with very high central

frequency because it does not take into account physical initial conditions. In next chapter, we are going to study interactions that are turned on and off, so that the energy divergence problem can be resolved.

## 7.4 Squeezing from accelerated mirrors

The two-mode squeezing process is a well-known mechanism for generating particles from the vacuum. Examples of two-mode squeezing include non-degenerate parametric amplification [BR04] and the Unruh effect [Unr76]. In the Unruh effect only one of the modes is observed locally. Hence, although the two output modes are entangled with each other, so that the composite state is a pure state, the locally observed state appears thermal. Another important mechanism is the single-mode squeezing process, for which the locally observed state is squeezed and pure; degenerate parametric amplification is an example [BR04]. It is possible that a particle generation process is the combination of the two, which we now show is the case for the uniformly accelerated mirror. Using the quantum circuit model for the uniformly accelerated mirror, it is very easy to show that the wave packet mode is locally squeezed at some quadrature phase depending on the central frequency and central position of the wave packet.

Using Eqs. (7.2.12)-(7.2.15), it is straightforward to calculate the expectation values of the products of two Unruh operators in the Minkowski vacuum state.

$$\begin{aligned}
\langle 0_M | \hat{c}'_{m\omega} \hat{d}'_{m\omega'} | 0_M \rangle &= \langle 0_M | \hat{d}'_{m\omega} \hat{c}'_{m\omega'} | 0_M \rangle = \langle 0_M | \hat{c}'_{m\omega} \hat{d}'_{m\omega'} | 0_M \rangle = \langle 0_M | \hat{d}'_{m\omega} \hat{c}'_{m\omega'} | 0_M \rangle \\
&= -(1 - \cos \theta_\omega) \cosh(r_\omega) \sinh(r_\omega) \left[ \sinh^2(r_\omega) + \cosh^2(r_\omega) \right] \delta(\omega - \omega'),
\end{aligned} \tag{7.4.1}$$

$$\begin{aligned}
\langle 0_M | \hat{c}'_{1\omega} \hat{d}'_{2\omega'} | 0_M \rangle &= \langle 0_M | \hat{d}'_{2\omega} \hat{c}'_{1\omega'} | 0_M \rangle = \langle 0_M | \hat{c}'_{1\omega} \hat{d}'_{2\omega'} | 0_M \rangle^* = \langle 0_M | \hat{d}'_{2\omega} \hat{c}'_{1\omega'} | 0_M \rangle^* \\
&= ie^{i\varphi_\omega} \sin \theta_\omega \cosh(r_\omega) \sinh(r_\omega) \delta(\omega - \omega'),
\end{aligned} \tag{7.4.2}$$

$$\begin{aligned}
 \langle 0_M | \hat{c}'_{2\omega} \hat{d}'_{1\omega'} | 0_M \rangle &= \langle 0_M | \hat{d}'_{1\omega} \hat{c}'_{2\omega'} | 0_M \rangle = \langle 0_M | \hat{c}'_{2\omega} \hat{d}'_{1\omega'} | 0_M \rangle^* = \langle 0_M | \hat{d}'_{1\omega} \hat{c}'_{2\omega'} | 0_M \rangle^* \\
 &= -ie^{-i\varphi_\omega} \sin \theta_\omega \cosh(r_\omega) \sinh(r_\omega) \delta(\omega - \omega'), \tag{7.4.3}
 \end{aligned}$$

with others zero and here  $m = 1, 2$ . We can see that the left-moving Unruh  $c'$  modes and  $d'$  modes are correlated. This is consistent with the pair production of Unruh quanta by linear scattering of Rindler quanta discussed in [MP96]. Furthermore, the left-moving Unruh modes are also correlated to the right-moving Unruh modes, as shown by Eqs. (7.4.2) and (7.4.3). From the perspective of an inertial observer, however, the Unruh modes highly oscillate when close to the horizon, so it is not clear what kind of physical detector can respond to the Unruh quanta and how to witness the correlations between the Unruh modes. We thus transform the Unruh modes to localized Minkowski modes to take into account the response of an inertial detector. While, according to Eqs. (7.4.2) and (7.4.3), it is expected that the left-moving and right-moving Minkowski modes are correlated, we mainly focus on left-moving Minkowski modes here.

### 7.4.1 Narrow bandwidth detector mode

We first consider left-moving and narrow bandwidth ( $k_0 \gg \sigma$ ) Gaussian wave packet modes. using Eqs. (4.5.46), (7.3.1), (7.3.4), (7.3.5) and (7.4.1), we have

$$\begin{aligned}
 \langle 0_M | \hat{a}(f) \hat{a}(f) | 0_M \rangle &= \int dk \int dk' f(k) f(k') \int d\omega \int d\omega' [A_{k\omega} B_{k'\omega'} \langle 0_M | \hat{c}'_\omega \hat{d}'_{\omega'} | 0_M \rangle \\
 &\quad + B_{k\omega} A_{k'\omega'} \langle 0_M | \hat{d}'_\omega \hat{c}'_{\omega'} | 0_M \rangle] \\
 &= -\sqrt{\frac{8}{\pi}} \frac{\sigma}{k_0} e^{-2ik_0 V_0} \int_0^\infty d\Omega \exp \left[ -\frac{\sigma^2 (\Omega - k_0 V_0)^2}{k_0^2} \right] \\
 &\quad \times \exp \left[ -\frac{\sigma^2 (\Omega + k_0 V_0)^2}{k_0^2} \right] (1 - \cos \theta_\Omega) e^{\pi\Omega} \frac{e^{2\pi\Omega} + 1}{(e^{2\pi\Omega} - 1)^2}. \tag{7.4.4}
 \end{aligned}$$

The quadrature observable of the localized wave packet mode  $\hat{a}(f)$  is defined as

$$\hat{X}(\phi) \equiv \hat{a}(f) e^{-i\phi} + \hat{a}^\dagger(f) e^{i\phi}, \tag{7.4.5}$$

where  $\phi$  is the quadrature phase. From Eqs. (7.3.7) and (7.4.4), we find that for a narrow bandwidth Gaussian wave packet the variance is

$$\begin{aligned}
& (\Delta X(\phi))^2 \\
&= 1 + 2\langle 0_M | \hat{a}^\dagger(f) \hat{a}(f) | 0_M \rangle + 2 \operatorname{Re} \left[ \langle 0_M | \hat{a}(f) \hat{a}(f) | 0_M \rangle e^{-2i\phi} \right] \\
&= 1 + 4\sqrt{\frac{2}{\pi}} \frac{\sigma}{k_0} \int_0^\infty d\Omega \left\{ \exp \left[ -\frac{2\sigma^2(\Omega - k_0 V_0)^2}{k_0^2} \right] + \exp \left[ -\frac{2\sigma^2(\Omega + k_0 V_0)^2}{k_0^2} \right] \right\} \\
&\quad \times (1 - \cos \theta_\Omega) \frac{e^{2\pi\Omega}}{(e^{2\pi\Omega} - 1)^2} - 4\sqrt{\frac{2}{\pi}} \frac{\sigma}{k_0} \cos(2\phi + 2k_0 V_0) \int_0^\infty d\Omega \exp \left[ -\frac{\sigma^2(\Omega - k_0 V_0)^2}{k_0^2} \right] \\
&\quad \times \exp \left[ -\frac{\sigma^2(\Omega + k_0 V_0)^2}{k_0^2} \right] (1 - \cos \theta_\Omega) e^{\pi\Omega} \frac{e^{2\pi\Omega} + 1}{(e^{2\pi\Omega} - 1)^2}, \tag{7.4.6}
\end{aligned}$$

where we have used the fact that in the Minkowski vacuum state,  $\langle 0_M | \hat{X}(\phi) | 0_M \rangle = 0$ . The variance of the wave packet mode could be smaller than one if the third term of Eq. (7.4.6) is larger than the second term. In order to show that squeezing is possible, we consider a Gaussian wave packet centered at  $V_0 = 0$ . Eq. (7.4.6) considerably simplifies, yielding

$$(\Delta X^{min})^2 = 1 - 4\sqrt{\frac{2}{\pi}} \frac{\sigma}{k_0} \int_0^\infty d\Omega \exp \left( -\frac{2\sigma^2\Omega^2}{k_0^2} \right) \times (1 - \cos \theta_\Omega) \frac{e^{\pi\Omega}}{(e^{\pi\Omega} + 1)^2} < 1 \tag{7.4.7}$$

for the minimum of  $(\Delta X(\phi))^2$ , which is at  $\phi = 0$ .

The variance of the quadrature beats the quantum shot noise, showing that the Gaussian wave packet mode is squeezed. When the center of the Gaussian wave packet is away from the past horizon  $V_0 = 0$ , the mode is squeezed at a different quadrature phase angle. According to Eq. (7.4.6), the minimum of the variance is reached when  $\phi_s + k_0 V_0 = 0$  is satisfied, that is

$$\phi_s = -k_0 V_0. \tag{7.4.8}$$

The squeezing phase angle  $\phi_s$  depends on both the central frequency and central position of the Gaussian wave packet. Other than the rotation of the squeezing phase angle, the squeezing amplitude decreases when the center of the wave packet is away from the past horizon. Fig. 7.6 shows the minimum variance of various wave packet modes (different central position and bandwidth), where the condition (7.4.8) has been satisfied.

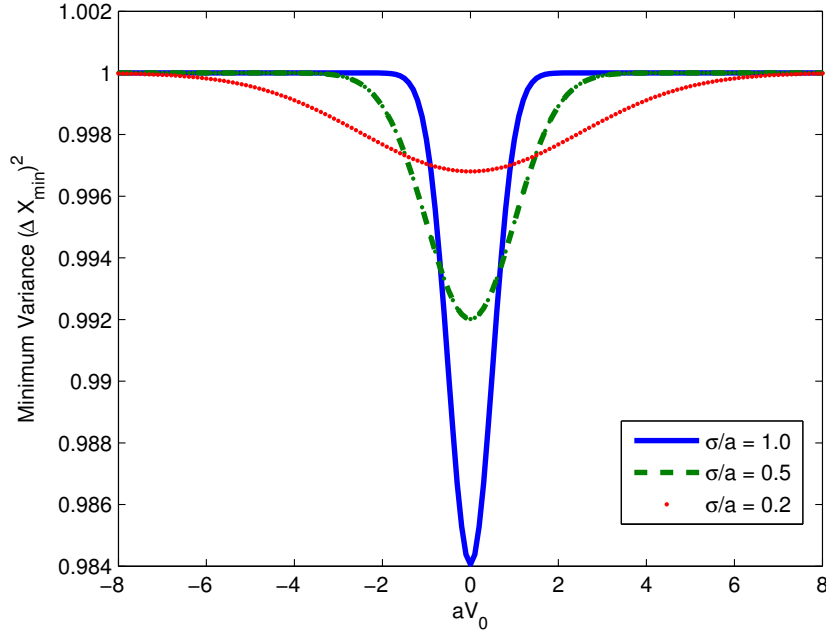


FIGURE 7.6: Minimum variance versus central position of the Gaussian wave packet:  $k_0/a = 20$ ,  $ag = 10$ . Maximum squeezing is achieved when the wave packet centres on the past horizon  $V_0 = 0$ . The squeezing is stronger for larger bandwidth wave packets.

### 7.4.2 Broad bandwidth detector mode

From Fig. 7.6 we see that the squeezing is stronger for a larger bandwidth Gaussian wave packet, which implies that different single-frequency Minkowski modes are also correlated. This can be verified if we replace  $f(k)$  in Eq. (7.4.4) by a Dirac delta function  $\delta(k - k_0)$ . In order to show that significant squeezing can be achieved, we consider a broad bandwidth wave packet mode. We introduce a specific example of a broad bandwidth localized detector mode and calculate its expectation of particle number and variance. The broad bandwidth wave packet is defined as

$$g(k; k_0, \sigma, V_0) = \mathcal{N} \sqrt{k} \exp \left\{ -\frac{(k - k_0)^2}{4\sigma^2} - ikV_0 \right\} \quad (7.4.9)$$

where  $\sqrt{k}$  is introduced to kill the low frequency tail.  $\mathcal{N}$  is the normalization factor

$$\mathcal{N} = \left\{ \sigma^2 e^{-\frac{k_0^2}{2\sigma^2}} + \sqrt{\frac{\pi}{2}} k_0 \sigma \left[ 1 + \operatorname{erf} \left( \frac{k_0}{\sqrt{2}\sigma} \right) \right] \right\}^{-1/2}, \quad (7.4.10)$$

where  $\operatorname{erf}(z)$  is the Error function. When  $k_0 \gg \sigma$ ,  $g(k)$  reduces to the usual Gaussian wave packet  $f(k)$ . When  $k_0 \lesssim \sigma$ ,  $g(k)$  is no longer a Gaussian wave packet and generally  $k_0$  does

not play the role as the central frequency of the wave packet. According to Eqs. (4.5.32) and (4.5.37), we find

$$\int_0^\infty dk g(k)A_{k\omega} = \frac{i\mathcal{N}\sqrt{a}\sqrt{2}\sinh\pi\Omega}{2\pi\sqrt{\Omega}}\Gamma(1-i\Omega)\left(\frac{2\sigma}{a}\right)^{i\Omega}e^{-\frac{k_0^2}{4\sigma^2}}\mathcal{I}_A(\Omega), \quad (7.4.11)$$

$$\int_0^\infty dk g(k)B_{k\omega} = -\frac{i\mathcal{N}\sqrt{a}\sqrt{2}\sinh\pi\Omega}{2\pi\sqrt{\Omega}}\Gamma(1+i\Omega)\left(\frac{2\sigma}{a}\right)^{-i\Omega}e^{-\frac{k_0^2}{4\sigma^2}}\mathcal{I}_B(\Omega), \quad (7.4.12)$$

where  $\mathcal{I}_A(\Omega)$  and  $\mathcal{I}_B(\Omega)$  are

$$\begin{aligned} \mathcal{I}_A &\equiv \frac{1}{a}(k_0 - 2i\sigma^2V_0)\Gamma\left(1 + \frac{i\Omega}{2}\right) {}_1F_1\left(1 + \frac{i\Omega}{2}, \frac{3}{2}, \frac{(k_0 - 2i\sigma^2V_0)^2}{4\sigma^2}\right) \\ &\quad + \frac{\sigma}{a}\Gamma\left(\frac{1}{2} + \frac{i\Omega}{2}\right) {}_1F_1\left(\frac{1}{2} + \frac{i\Omega}{2}, \frac{1}{2}, \frac{(k_0 - 2i\sigma^2V_0)^2}{4\sigma^2}\right), \end{aligned}$$

$$\begin{aligned} \mathcal{I}_B &\equiv \frac{1}{a}(k_0 - 2i\sigma^2V_0)\Gamma\left(1 - \frac{i\Omega}{2}\right) {}_1F_1\left(1 - \frac{i\Omega}{2}, \frac{3}{2}, \frac{(k_0 - 2i\sigma^2V_0)^2}{4\sigma^2}\right) \\ &\quad + \frac{\sigma}{a}\Gamma\left(\frac{1}{2} - \frac{i\Omega}{2}\right) {}_1F_1\left(\frac{1}{2} - \frac{i\Omega}{2}, \frac{1}{2}, \frac{(k_0 - 2i\sigma^2V_0)^2}{4\sigma^2}\right), \end{aligned}$$

with  ${}_1F_1(b, c, z)$  the generalized Hypergeometric function [NIS]. The particle number in this localized wave packet detector mode is

$$N(g) = \frac{(a\mathcal{N})^2}{\pi}e^{-\frac{k_0^2}{2\sigma^2}} \int d\Omega (|\mathcal{I}_A|^2 + |\mathcal{I}_B|^2)(1 - \cos\theta_\Omega) \frac{e^{2\pi\Omega}}{(e^{2\pi\Omega} - 1)^2} \quad (7.4.13)$$

and

$$\langle 0_M | \hat{a}(g) \hat{a}(g) | 0_M \rangle = -\frac{(a\mathcal{N})^2}{\pi}e^{-\frac{k_0^2}{2\sigma^2}} \int d\Omega \mathcal{I}_A \mathcal{I}_B (1 - \cos\theta_\Omega) e^{\pi\Omega} \frac{e^{2\pi\Omega} + 1}{(e^{2\pi\Omega} - 1)^2}. \quad (7.4.14)$$

Therefore the variance of the wave packet is

$$\begin{aligned} (\Delta X(\phi))^2 &= 1 + 2N(g) + 2 \operatorname{Re}[\langle 0_M | \hat{a}(g) \hat{a}(g) | 0_M \rangle e^{-2i\phi}] \\ &= 1 + \frac{2(a\mathcal{N})^2}{\pi}e^{-\frac{k_0^2}{2\sigma^2}} \int d\Omega (1 - \cos\theta_\Omega) \frac{e^{2\pi\Omega}}{(e^{2\pi\Omega} - 1)^2} \left[ |\mathcal{I}_A|^2 + |\mathcal{I}_B|^2 \right. \\ &\quad \left. - 2 \cosh(\pi\Omega) \operatorname{Re}\left(\mathcal{I}_A \mathcal{I}_B e^{-2i\phi}\right) \right]. \end{aligned} \quad (7.4.15)$$

Fig. 7.7 shows the minimum variance of the broadband wave packet modes centred on the past horizon. About 14% squeezing can be attained as we increase the bandwidth. For a very large bandwidth wave packet mode (such as a broad bandwidth top-hat mode), we find that the minimum variance approaches but never exceeds 50%. We also note that when  $\cos(2\phi + 2k_0V_0) = -1$ , the variance is maximal and larger than unity.

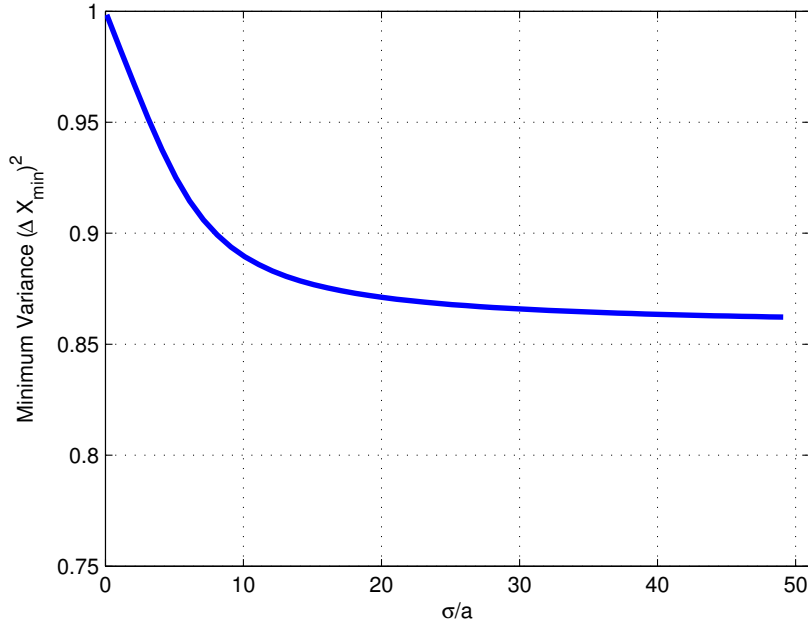


FIGURE 7.7: Minimum variance of broad bandwidth wave packet modes (Eq. (7.4.9)) centred on the past horizon:  $k_0/a = 20$ ,  $ag = 10$ . Stronger squeezing is achieved for larger bandwidth wave packet mode.

### 7.4.3 Ratio of single-mode squeezing

Both a single-mode squeezed state and one mode of a two-mode squeezed state contain particles. However it is possible for a single-mode squeezed state to be pure (and hence separable) whilst one mode of a two-mode squeezed state is mixed due to its entanglement with the other mode. Thus (given the same particle number) the presence of single-mode squeezing indicates a greater level of purity and separability from other modes than would be the case if there were only two mode squeezing. Given this relationship it is interesting to ask what proportion of the particle number in the detected mode is due to single-mode squeezing and how much is due to two-mode squeezing. The contribution by pure single-mode squeezing to the particle number can be estimated as

$$N_{ps} = \frac{1}{2} \left( V_{min} + \frac{1}{V_{min}} - 2 \right) \quad (7.4.16)$$

where  $V_{min} = (\Delta X^{min})^2$  is the minimum variance. The ratio

$$\eta = \frac{N_{ps}}{N} \quad (7.4.17)$$

characterizes how important the single-mode squeezing is as compare to correlations with other field modes. Here  $N$  is the total particle number of the detected mode. For a pure single-mode squeezed state one can verify that  $\eta = 1$ . Fig. 7.8 shows the portion of particle number from single-mode squeezing is small (up to  $\sim 3\%$ ) but not negligible. Note that for a very large bandwidth top-hat detection mode,  $\eta$  can climb as high as 7%.

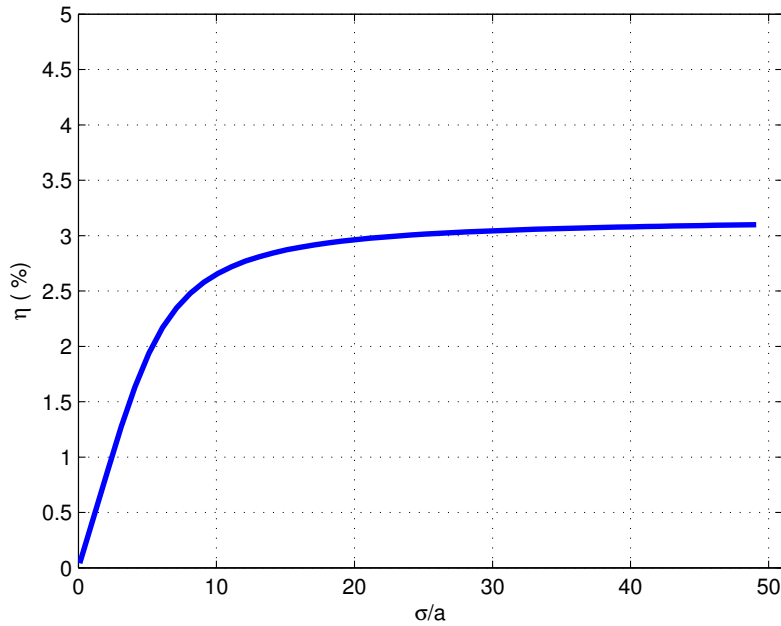


FIGURE 7.8: Portion of particle number from single-mode squeezing for broad bandwidth wave packet modes (Eq. (7.4.9)) centering on the past horizon:  $k_0/a = 20$ ,  $ag = 10$ .

#### 7.4.4 Origin of single-mode squeezing

According to the quantum circuit model, it is easy to understand the origin of the local squeezing. In Fig. 7.2, after passing through the mirror the left-moving Rindler mode  $\hat{b}'_\omega$  in the right Rindler wedge is in thermal state, as well as the left-moving Rindler mode  $\hat{b}^L_\omega$  in the  $L$  wedge. The entanglement between  $\hat{b}'_\omega$  and  $\hat{b}^L_\omega$  depends on the transmission coefficient of the mirror. If the mirror is completely transparent, they are perfectly entangled; while if the mirror is perfect, the entanglement is completely severed. The Rindler modes  $\hat{b}'_\omega$  and  $\hat{b}^L_\omega$  further pass through a two-mode antisqueezer  $S_\omega^{-1}$ , ending up with two Unruh modes  $\hat{c}'_\omega$  and  $\hat{d}'_\omega$ , which are also entangled. The amount of entanglement between  $\hat{c}'_\omega$  and  $\hat{d}'_\omega$  depends on

the amount of entanglement between  $\hat{b}_\omega^R$  and  $\hat{b}_\omega^L$ . If  $\hat{b}_\omega^R$  and  $\hat{b}_\omega^L$  are perfectly entangled, there is no entanglement between  $\hat{c}'_\omega$  and  $\hat{d}'_\omega$ ; otherwise,  $\hat{c}'_\omega$  and  $\hat{d}'_\omega$  are partially entangled. From Eq. (4.5.46), the Minkowski mode  $\hat{a}_k$  is a linear combination of the Unruh modes  $\hat{c}'_\omega$  and  $\hat{d}'_\omega$ . It is a general result in quantum optics that a linear combination of entangled modes would produce single-mode squeezing, e.g., a 50 : 50 beamsplitter transforms a two-mode squeezed state into single-mode squeezed state in each output mode. Therefore, the Minkowski mode  $\hat{a}_k$  is squeezed.

It is clear that the local squeezing is closely related to the correlations across the horizon. If the mirror is transparent ( $\cos \theta_\Omega = 1$ ), the correlations across the horizon are preserved and there is no local squeezing. When one uses a partially transmitting mirror ( $\cos \theta_\Omega < 1$ ) to sever the correlations across the horizon, local squeezing is inevitably produced according to Eq. (7.4.6). Furthermore, there may be other ways to sever the correlations across the horizon, for example by using two uniformly accelerated Unruh-DeWitt detectors in left and right Rindler wedges [MS06, SMM15].

## 7.5 Squeezed Firewall ?

Recently three assertions about black hole evaporation were shown to be mutually inconsistent [AMPS13]: (i) Hawking radiation is a unitary process, (ii) low energy effective field theory is valid near the event horizon, and (iii) an infalling observer encounters nothing unusual at the horizon. One of the proposed solutions to this paradox is that the infalling observer burns up at the horizon. A black hole firewall forms at the horizon for an old black hole and the correlations across the horizon are severed.

Recently this firewall state was modeled for a Rindler horizon in Minkowski spacetime by severing correlations across the horizon. The correlations across the horizon are severed by requiring the Wightman function to be zero, disregarding the underlying dynamics. Furthermore, a low-frequency cutoff in the Wightman function was introduced, implying that correlations between high-frequency modes are cut whilst correlations between low-frequency

modes are preserved. The response of an Unruh-DeWitt detector was seen to be finite [Lou14], leading to the author's conclusion of a finite firewall.

We propose that a uniformly accelerated mirror is a possible mechanism for generating a Rindler firewall. From the quantum circuit model we can see that the accelerated mirror acts as a pair of scissors cutting the correlations across the past horizon. If the mirror is perfect, the correlations across the horizon are completely severed and the particle flux along the horizon is divergent. This is a hot firewall, destroying everything that crosses it. However, if the mirror is not perfect but transparent for low-frequency modes, the high-frequency correlations are cut while low-frequency correlations are preserved, and the particle flux in a localized wave packet mode along the horizon is finite, similar to the warm firewall proposed by Louko [Lou14]. In Sec. 7.4, we showed that the radiation field from the accelerated mirror is locally squeezed, which implies that the Rindler firewall is locally squeezed. It seems that local squeezing is a general property of a Rindler firewall because in order to form a firewall one has to cut the correlations across the horizon, which inevitably generates local squeezing.

Is a black hole firewall locally squeezed? Black hole firewalls are introduced in order to preserve the unitarity of black hole evolution [AMPS13, BP13]. For an old black hole, the late time Hawking radiation should be correlated with early time Hawking radiation but not with the degrees of freedom inside the event horizon. The correlations across the horizon are severed during the evaporation. According to the arguments for the Rindler firewall, it is reasonable to conjecture that the black hole firewalls are also locally squeezed. In addition, if the local squeezing is strong enough, black hole firewalls do not have to be entangled with other unknown systems.

## 7.6 Summary

We have developed a quantum circuit formalism to describe unitary interactions between a uniformly accelerated object and the quantum fields. The key point is to work in the accelerated frame where the object is stationary and couples only to Rindler modes in one

of the Rindler wedges. If the initial state of the quantum fields is given in the inertial frame and the response of inertial detectors is considered, we have to transform modes from the inertial frame to the accelerated frame, which turns out to be a two-mode squeezing operation if we consider Unruh modes instead of Minkowski modes in the inertial frame. We thus can construct a quantum circuit using two-mode squeezers and devices depending on the interaction of the object with the Rindler modes.

As an example, we studied a uniformly accelerated mirror. In the accelerated frame, the mirror is stationary and is simply a beamsplitter with frequency dependent reflection coefficient. The input-output relation of a beamsplitter is well known and is widely used in quantum optics [BR04]. The quantum circuit for the uniformly accelerated mirror is shown in Fig. 7.2. As an application, we calculated the radiation flux from an eternally accelerating mirror in the Minkowski vacuum. We found that the particles are localized around the horizon and the particle number in a localized wave packet mode is divergent if no low frequency regularization is introduced. Our results are consistent with earlier results obtained using different methods [FS99, OP01]. The infrared divergence occurs due to the ideal assumption that the mirror accelerates for an infinitely long time. We emphasize that the infrared divergence is not due to the particular pathological character of a massless scalar field in  $(1 + 1)$ -dimensional spacetime [Col73] because it also appears in higher dimensional spacetime [FS99]. We regularize the radiation flux by introducing a low-frequency cutoff for the mirror, that is, the mirror is completely transparent for low frequency field modes. Physically, this is equivalent to having the mirror interact with the field for a finite time. After regularizing the infrared divergence, the particle number of a localized wave packet mode is finite. However the energy of the wave packet mode does not decay as the central frequency increases, in turn implying that the total energy of the radiation flux is infinite. This ultraviolet divergence arises because of the naive assumption that the mirror is accelerated eternally so that it appears to inertial observers when they cross the past horizon. If the mirror slowly increased its acceleration or was switched on smoothly, the number of high frequency particles would be suppressed, removing this ultraviolet divergence. Using perturbation theory it is straightforward to show that the energy flux is finite if the mirror

is smoothly turned on and off [OP01].

A further application of our circuit model would be in the study of a uniformly accelerated cavity. Previous work on this topic [AM03, DFR11, BFL12] studied how the quantum states stored inside a perfect cavity are affected by uniform acceleration. While Unruh-Davies radiation [Unr76, Dav75] cannot affect the field modes inside a perfect cavity, it can affect field modes inside an imperfect one. Because the circuit model is designed to study an imperfect uniformly accelerated mirror, we believe that by generalizing the model from one mirror to two mirrors, one can study the interaction between Unruh-Davies radiation and the field modes inside an imperfect cavity.

One limitation of our circuit model is that it is only suitable for studying hyperbolic trajectories in Minkowski spacetime; more general trajectories are not straightforwardly incorporated. One might expect this to severely limit the utility of the circuit model because physically it is not possible to accelerate a mirror for an infinitely long time. However our use of the transparency term shows that we can turn on and off the mirror so that it is transparent in the distant past and distant future. This could be used to model a mirror that initially undergoes inertial motion, accelerates for a finite period of time, and then returns to inertial motion. We will leave this topic for future work.

We find that the radiation flux from the uniformly accelerated mirror is locally squeezed. To the best of our knowledge, the contribution of local squeezing to the generation of particles by a moving mirror has not been discussed previously. The squeezing angle depends on the central frequency and position of the localized detector mode function. Maximum squeezing occurs when the detector mode function centers on the horizon. It is clear from the circuit model that the local squeezing is related to the correlations across the horizon. When the mirror is completely transparent, the correlations across the horizon are preserved and there is no squeezing. When the mirror completely reflects a Rindler mode with a particular frequency, it destroys the correlation across the horizon and generates some squeezing in the Minkowski mode. It therefore provides a mechanism for transferring the correlations across

the horizon to the squeezing of the radiation flux on the horizon.

Recently, Louko [Lou14] proposed a Rindler firewall state by severing the correlations across the horizon by hand and claimed that the response of a particle detector is finite. It was subsequently shown that entanglement survives this Rindler firewall [MML15]. Our calculation suggests that one way of generating a Rindler firewall is to uniformly accelerate a mirror. We conjecture that if the firewall is formed in an old black hole, the radiation flux at the horizon could be locally squeezed as the price of severing the entanglement across the event horizon. In addition, the black hole firewall may not need to be highly entangled with other systems [Sus16] because the local squeezing may be enough to account for the particle flux on the horizon.

# 8

## Quantum Circuit Model for Non-inertial Objects: Accelerated Squeezer

### 8.1 Introduction

In this chapter, we continue to discuss the quantum circuit model for uniformly accelerated objects. In Chapter 7, we have introduced a general formalism to study uniformly accelerated objects, but we have mainly focused on a special case where the interaction does not mix different frequency Rindler modes. This means we can draw a quantum circuit for every single frequency mode, as shown by Fig. 7.2. The decoupling of different frequency modes is the consequence of time independent interactions: no turning on and turning off. Although we can obtain finite particle number and energy in a localized wave packet detector mode by introducing a low frequency cutoff for an accelerated mirror, the total energy of the

radiation from the accelerated mirror is divergent. The energy divergence is due to the unphysical initial conditions imposed on the uniformly accelerated mirror and can be resolved by introducing turning on and off the interactions [OP01].

We are now going to generalize the circuit for time independent interactions to a circuit for time dependent interactions. Generally, time dependent interactions will create particles because they inevitably mix in negative frequency modes, e.g., due to suddenly changing the reflectivity of a static mirror [BL15]. However, if the switching process is smooth and slow enough, the particle creation effect can be neglected. In this chapter, we assume that the turning on and off of the interactions is realized by making the objects only act on a localized wave packet mode. The wave packet has a finite bandwidth and localized in time. We find that by making the accelerated objects act on a localized wave packet mode, the energy divergence problem can be resolved.

Using this circuit model for time dependent interactions, we study a uniformly accelerated single-mode squeezer. Suppose that the initial state of the field is the Minkowski vacuum. A uniformly accelerated observer would see thermal radiation with Unruh temperature  $T_U = a/2\pi$ , the well known Unruh effect [Unr76]. A uniformly accelerated single-mode squeezer in the right Rindler wedge thus squeezes the thermal state and the output is a squeezed thermal state as observed by a uniformly accelerated observer. Unexpectedly, we find that the output state as viewed by an inertial observer is not a pure state. We thus conclude that the whole process can not be described by a unitary operator. Because of the equivalence principle there is a strong relationship between gravity and acceleration [MTW73], so our finding may have important implications for the black hole information paradox.

In this chapter, we first discuss the circuit for a uniformly accelerated object that acts on a narrow bandwidth wave packet mode in Section 8.2. We then generalize this to a circuit for any localized wave packet mode in Section 8.3. Finally, we study the output state from a uniformly accelerated single-mode squeezer as viewed by inertial observers using homodyne detection in Section 8.4. The relevant manuscript is in preparation.

## 8.2 Accelerated objects acting on narrow bandwidth modes

### 8.2.1 Circuit for a single narrow bandwidth mode

In quantization of fields in free space, continuum frequency modes are usually used, which are normalized to a delta function. As we have discussed in Section 3.1.1, it is possible to introduce a set of discrete, complete and orthonormal wave packet modes, with which the field operator can be expanded. The localized wave packet operator is defined by Eq. (3.1.4) and the inverse relation is given by Eq. (3.1.5).

Now consider a wave packet mode in the right Rindler wedge, the localized Rindler operator is defined as

$$\hat{b}_{mg}^R = \int d\omega g(\omega) \hat{b}_{m\omega}^R, \quad (8.2.1)$$

where  $g(\omega)$  is a localized wave packet and  $m = 1, 2$ , represent left and right moving modes respectively. In this section we assume that  $g(\omega)$  is a narrow bandwidth wave packet with central frequency  $\omega_0$ . Using the relation between the Rindler operators and Unruh operators (4.5.45),

$$\begin{aligned} \hat{b}_{mg}^R &= \int d\omega g(\omega) \cosh(r_\omega) \hat{c}_{m\omega} + \int d\omega g(\omega) \sinh(r_\omega) \hat{d}_{m\omega}^\dagger \\ &\approx \cosh(r_0) \int d\omega g(\omega) \hat{c}_{m\omega} + \sinh(r_0) \int d\omega g(\omega) \hat{d}_{m\omega}^\dagger \\ &\approx \cosh(r_0) \hat{c}_{mg} + \sinh(r_0) \hat{d}_{mg^*}^\dagger, \end{aligned} \quad (8.2.2)$$

where  $\tanh(r_0) = e^{-\pi\omega_0/a}$  and we have defined localized Unruh operators

$$\hat{c}_{mg} \equiv \int d\omega g(\omega) \hat{c}_{m\omega}, \quad \hat{d}_{mg^*} \equiv \int d\omega g^*(\omega) \hat{d}_{m\omega}. \quad (8.2.3)$$

The corresponding localized Rindler operator in the left Rindler wedge is

$$\hat{b}_{mg^*}^L = \cosh(r_0) \hat{d}_{mg^*} + \sinh(r_0) \hat{c}_{mg}^\dagger. \quad (8.2.4)$$

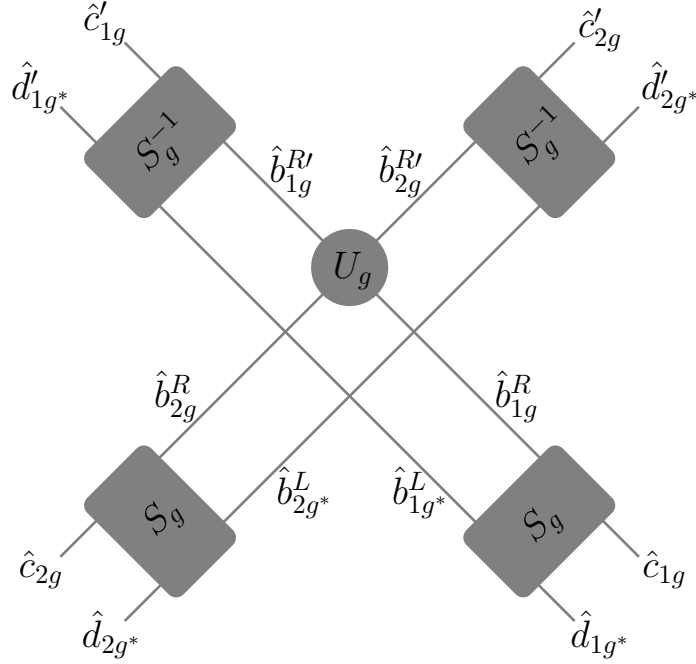


FIGURE 8.1: Quantum circuit for a narrow bandwidth wave packet mode.

The inverse of Eqs. (8.2.2) and (8.2.4) can be easily obtained,

$$\begin{aligned}
 \hat{c}_{mg} &= \cosh(r_0)\hat{b}_{mg}^R - \sinh(r_0)\hat{b}_{mg*}^{L\dagger}, \\
 \hat{d}_{mg*} &= \cosh(r_0)\hat{b}_{mg*}^L - \sinh(r_0)\hat{b}_{mg}^{R\dagger}.
 \end{aligned} \tag{8.2.5}$$

If the accelerated object acts only on a narrow bandwidth wave packet mode, that is, the unitary operator  $\hat{U}_g$  representing the interaction is constructed from  $\hat{b}_{1g}^R$  and  $\hat{b}_{2g}^R$ , then we can draw a circuit for the single narrow bandwidth mode, as shown in Fig. 8.1. From Eqs. (8.2.2), (8.2.4) and (8.2.5), we can derive the input-output relation for the localized wave packet Unruh modes,

$$\begin{aligned}
 \hat{c}'_{mg} &= \hat{c}_{mg} + \cosh(r_0)(\hat{U}_g^\dagger \hat{b}_{mg}^R \hat{U}_g - \hat{b}_{mg}^R), \\
 \hat{d}'_{mg*} &= \hat{d}_{mg*} - \sinh(r_0)(\hat{U}_g^\dagger \hat{b}_{mg}^{R\dagger} \hat{U}_g - \hat{b}_{mg}^{R\dagger}).
 \end{aligned} \tag{8.2.6}$$

Note that all other wave packet modes that are orthogonal to  $g(\omega)$  are not affected by the accelerated objects. Assume that the wave packets orthogonal to  $g(\omega)$  are denoted as  $g_{\perp i}(\omega)$  with  $i = 1, 2, \dots$ . According to the relation between the single frequency modes and the wave

packet modes, Eq. (3.1.5), the single frequency output Unruh operators can be written as

$$\begin{aligned}
\hat{c}'_{m\omega} &= g^*(\omega)\hat{c}'_{mg} + \sum_i g^*_{\perp i}(\omega) \hat{c}'_{mg_{\perp i}} = g^*(\omega)\hat{c}'_{mg} + \sum_i g^*_{\perp i}(\omega) \hat{c}_{mg_{\perp i}}, \\
&= \hat{c}_{m\omega} + g^*(\omega)(\hat{c}'_{mg} - \hat{c}_{mg}) \\
&= \hat{c}_{m\omega} + g^*(\omega) \cosh(r_0)(\hat{U}_g^\dagger \hat{b}_{mg}^R \hat{U}_g - \hat{b}_{mg}^R),
\end{aligned} \tag{8.2.7}$$

$$\begin{aligned}
\hat{d}'_{m\omega} &= g(\omega)\hat{d}'_{mg^*} + \sum_i g_{\perp i}(\omega) \hat{d}'_{mg^*_{\perp i}} = g(\omega)\hat{d}'_{mg^*} + \sum_i g_{\perp i}(\omega) \hat{d}_{mg^*_{\perp i}}, \\
&= \hat{d}_{m\omega} + g(\omega)(\hat{d}'_{mg^*} - \hat{d}_{mg^*}) \\
&= \hat{d}_{m\omega} - g(\omega) \sinh(r_0)(\hat{U}_g^\dagger \hat{b}_{mg}^{R\dagger} \hat{U}_g - \hat{b}_{mg}^{R\dagger}).
\end{aligned} \tag{8.2.8}$$

### 8.2.2 Uniformly accelerated mirror

We are now going to revisit the accelerated mirror problem. We assume that the mirror only reflects a localized wave packet mode characterized by  $g(\omega)$ . The unitary operator  $\hat{U}_g$  is chosen to be

$$\hat{U}_g = \exp \left\{ \theta (\hat{b}_{1g}^{R\dagger} \hat{b}_{2g}^R - \hat{b}_{1g}^R \hat{b}_{2g}^{R\dagger}) \right\} \tag{8.2.9}$$

so that

$$\begin{aligned}
\hat{b}_{1g}^{R'} &= \hat{U}_g^\dagger \hat{b}_{1g}^R \hat{U}_g = \cos \theta \hat{b}_{1g}^R + \sin \theta \hat{b}_{2g}^R, \\
\hat{b}_{2g}^{R'} &= \hat{U}_g^\dagger \hat{b}_{2g}^R \hat{U}_g = \cos \theta \hat{b}_{2g}^R - \sin \theta \hat{b}_{1g}^R.
\end{aligned} \tag{8.2.10}$$

Substituting this unitary operator into Eq. (8.2.6), we can find the input-output relations for the circuit Fig. 8.1.

$$\begin{aligned}
\hat{c}'_{1g} &= [1 + (\cos \theta - 1) \cosh^2(r_0)] \hat{c}_{1g} + (\cos \theta - 1) \cosh(r_0) \sinh(r_0) \hat{d}_{1g^*}^\dagger + \sin \theta \cosh^2(r_0) \hat{c}_{2g}, \\
&\quad + \sin \theta \cosh(r_0) \sinh(r_0) \hat{d}_{2g^*}^\dagger,
\end{aligned} \tag{8.2.11}$$

$$\begin{aligned}
\hat{d}'_{1g^*} &= [1 - (\cos \theta - 1) \sinh^2(r_0)] \hat{d}_{1g^*} - (\cos \theta - 1) \cosh(r_0) \sinh(r_0) \hat{c}_{1g}^\dagger - \sin \theta \sinh^2(r_0) \hat{d}_{2g^*} \\
&\quad - \sin \theta \cosh(r_0) \sinh(r_0) \hat{c}_{2g}^\dagger,
\end{aligned} \tag{8.2.12}$$

$$\begin{aligned}\hat{c}'_{2g} &= [1 + (\cos\theta - 1)\cosh^2(r_0)]\hat{c}_{2g} + (\cos\theta - 1)\cosh(r_0)\sinh(r_0)\hat{d}_{2g}^\dagger - \sin\theta\cosh^2(r_0)\hat{c}_{1g}, \\ &\quad - \sin\theta\cosh(r_0)\sinh(r_0)\hat{d}_{1g}^\dagger,\end{aligned}\quad (8.2.13)$$

$$\begin{aligned}\hat{d}'_{2g^*} &= [1 - (\cos\theta - 1)\sinh^2(r_0)]\hat{d}_{2g^*} - (\cos\theta - 1)\cosh(r_0)\sinh(r_0)\hat{c}_{2g}^\dagger + \sin\theta\sinh^2(r_0)\hat{d}_{1g^*} \\ &\quad + \sin\theta\cosh(r_0)\sinh(r_0)\hat{c}_{1g}^\dagger.\end{aligned}\quad (8.2.14)$$

If the initial state is the Minkowski vacuum, we can derive the nonzero vacuum expectation values of the products of two output Unruh operators straightforwardly,

$$\begin{aligned}\langle 0_M | \hat{c}'_{1g} \hat{c}'_{1g} | 0_M \rangle &= \langle 0_M | \hat{d}'_{1g^*} \hat{d}'_{1g^*} | 0_M \rangle = \langle 0_M | \hat{c}'_{2g} \hat{c}'_{2g} | 0_M \rangle = \langle 0_M | \hat{d}'_{2g^*} \hat{d}'_{2g^*} | 0_M \rangle \\ &= 2(1 - \cos\theta)\cosh^2(r_0)\sinh^2(r_0),\end{aligned}\quad (8.2.15)$$

$$\begin{aligned}\langle 0_M | \hat{c}'_{1g} \hat{d}'_{1g^*} | 0_M \rangle &= \langle 0_M | \hat{c}'_{1g} \hat{d}'_{1g^*} | 0_M \rangle = \langle 0_M | \hat{c}'_{2g} \hat{d}'_{2g^*} | 0_M \rangle = \langle 0_M | \hat{c}'_{2g} \hat{d}'_{2g^*} | 0_M \rangle \\ &= -(1 - \cos\theta)\cosh(r_0)\sinh(r_0)[\cosh^2(r_0) + \sinh^2(r_0)],\end{aligned}\quad (8.2.16)$$

$$\begin{aligned}\langle 0_M | \hat{c}'_{1g} \hat{d}'_{2g^*} | 0_M \rangle &= \langle 0_M | \hat{c}'_{1g} \hat{d}'_{2g^*} | 0_M \rangle = -\langle 0_M | \hat{c}'_{2g} \hat{d}'_{1g^*} | 0_M \rangle = -\langle 0_M | \hat{c}'_{2g} \hat{d}'_{1g^*} | 0_M \rangle \\ &= \sin\theta\cosh(r_0)\sinh(r_0).\end{aligned}\quad (8.2.17)$$

Using the relation between the single frequency modes and the localized wave packet modes, Eq. (8.2.7), we have

$$\begin{aligned}\langle 0_M | \hat{c}'_{1\omega} \hat{c}'_{1\omega'} | 0_M \rangle &= \langle 0_M | \hat{c}'_{2\omega} \hat{c}'_{2\omega'} | 0_M \rangle = g(\omega)g^*(\omega')\langle 0_M | \hat{c}'_{1g} \hat{c}'_{1g} | 0_M \rangle, \\ \langle 0_M | \hat{d}'_{1\omega} \hat{d}'_{1\omega'} | 0_M \rangle &= \langle 0_M | \hat{d}'_{2\omega} \hat{d}'_{2\omega'} | 0_M \rangle = g^*(\omega)g(\omega')\langle 0_M | \hat{d}'_{1g^*} \hat{d}'_{1g^*} | 0_M \rangle, \\ \langle 0_M | \hat{c}'_{1\omega} \hat{d}'_{1\omega'} | 0_M \rangle &= \langle 0_M | \hat{c}'_{2\omega} \hat{d}'_{2\omega'} | 0_M \rangle = g^*(\omega)g(\omega')\langle 0_M | \hat{c}'_{1g} \hat{d}'_{1g^*} | 0_M \rangle, \\ \langle 0_M | \hat{c}'_{1\omega} \hat{d}'_{2\omega'} | 0_M \rangle &= \langle 0_M | \hat{c}'_{2\omega} \hat{d}'_{2\omega'} | 0_M \rangle = g(\omega)g^*(\omega')\langle 0_M | \hat{c}'_{1g} \hat{d}'_{1g^*} | 0_M \rangle, \\ \langle 0_M | \hat{c}'_{1\omega} \hat{d}'_{2\omega'} | 0_M \rangle &= -\langle 0_M | \hat{c}'_{2\omega} \hat{d}'_{1\omega'} | 0_M \rangle = g^*(\omega)g(\omega')\langle 0_M | \hat{c}'_{1g} \hat{d}'_{2g^*} | 0_M \rangle, \\ \langle 0_M | \hat{c}'_{1\omega} \hat{d}'_{2\omega'} | 0_M \rangle &= -\langle 0_M | \hat{c}'_{2\omega} \hat{d}'_{1\omega'} | 0_M \rangle = g(\omega)g^*(\omega')\langle 0_M | \hat{c}'_{1g} \hat{d}'_{2g^*} | 0_M \rangle.\end{aligned}\quad (8.2.18)$$

Suppose that inertial detectors detect a left-moving localized wave packet Minkowski mode  $\hat{a}_1(f) = \int_0^\infty dk f(k)\hat{a}_{1k}$ , where  $f(k)$  is an arbitrary wave packet. The expectation value of

the particle number  $N_1(f) = \langle 0_M | \hat{a}_1^\dagger(f) \hat{a}_1(f) | 0_M \rangle$  in the Gaussian wave packet mode is

$$\begin{aligned}
N_1(f) &= \int d\omega \int d\omega' \langle 0_M | (A_{f\omega}^* \hat{c}_{1\omega}^\dagger + B_{f\omega}^* \hat{d}_{1\omega}^\dagger) (A_{f\omega'} \hat{c}'_{1\omega'} + B_{f\omega'} \hat{d}'_{1\omega'}) | 0_M \rangle \\
&= \int d\omega \int d\omega' \left[ A_{f\omega}^* A_{f\omega'} g(\omega) g^*(\omega') + B_{f\omega}^* B_{f\omega'} g^*(\omega) g(\omega') \right] \langle 0_M | \hat{c}'_{1g}^\dagger \hat{c}'_{1g} | 0_M \rangle \\
&= 2(1 - \cos \theta) \cosh^2(r_0) \sinh^2(r_0) (|A_{fg}|^2 + |B_{fg}|^2), \tag{8.2.19}
\end{aligned}$$

where the  $A_{fg}$  and  $B_{fg}$  are defined as

$$\begin{aligned}
A_{fg} &= \int d\omega A_{f\omega} g^*(\omega) = \int dk \int d\omega f(k) A_{k\omega} g^*(\omega), \\
B_{fg} &= \int d\omega B_{f\omega} g(\omega) = \int dk \int d\omega f(k) B_{k\omega} g(\omega). \tag{8.2.20}
\end{aligned}$$

The expectation value of the square of  $\hat{a}_1(f)$  is

$$\begin{aligned}
\langle 0_M | \hat{a}_1(f) \hat{a}_1(f) | 0_M \rangle &= \int d\omega \int d\omega' [A_{f\omega} B_{f\omega'} \langle 0_M | \hat{c}'_{1\omega} \hat{d}'_{1\omega'} | 0_M \rangle + B_{f\omega} A_{f\omega'} \langle 0_M | \hat{d}'_{1\omega} \hat{c}'_{1\omega'} | 0_M \rangle] \\
&= 2A_{fg} B_{fg} \langle 0_M | \hat{c}'_{1g} \hat{d}'_{1g^*} | 0_M \rangle \\
&= -2(1 - \cos \theta) \cosh(r_0) \sinh(r_0) [\cosh^2(r_0) + \sinh^2(r_0)] A_{fg} B_{fg}. \tag{8.2.21}
\end{aligned}$$

The variance of the quadrature amplitude  $\hat{X}_1(\phi) \equiv \hat{a}_1(f) e^{-i\phi} + \hat{a}_1^\dagger(f) e^{i\phi}$  is

$$\begin{aligned}
(\Delta X_1(\phi))^2 &= 1 + 2N_1(f) + 2 \operatorname{Re} [\langle 0_M | \hat{a}_1(f) \hat{a}_1(f) | 0_M \rangle e^{-2i\phi}] \\
&= 1 - 4(1 - \cos \theta) \cosh(r_0) \sinh(r_0) [\cosh^2(r_0) + \sinh^2(r_0)] \operatorname{Re}(A_{fg} B_{fg} e^{-2i\phi}) \\
&\quad + 4(1 - \cos \theta) \cosh^2(r_0) \sinh^2(r_0) (|A_{fg}|^2 + |B_{fg}|^2). \tag{8.2.22}
\end{aligned}$$

We see that the particle number and quadrature variance depend on the overlap integrals  $A_{fg}$  and  $B_{fg}$ . For any give  $f(k)$  and narrow bandwidth  $g(\omega)$ , they can be calculated numerically. In the case that  $f(k)$  is a very narrow bandwidth Gaussian wave packet,  $A_{f\omega}$  and  $B_{f\omega}$  can be approximated by Eqs. (7.3.4) and (7.3.5), respectively. Assume that  $g(\omega)$  is also a narrow bandwidth Gaussian wave packet

$$g(\omega) = \left( \frac{1}{2\pi\delta^2} \right)^{1/4} \exp \left\{ -\frac{(\omega - \omega_0)^2}{4\delta^2} \right\} e^{-i\omega v_c} \tag{8.2.23}$$

where  $\omega_0$  is the central frequency,  $\delta$  is the bandwidth, satisfying  $\omega_0 \gg \delta$ .  $v_c$  is the central position of the Gaussian mode in the Rindler frame. Analytical approximation can be obtained in two limiting cases: the central frequency of  $g(\omega)$  is large and is small.

**High central frequency limit**—When the central frequency of  $g(\omega)$  is large, namely,  $\Omega = \omega_0/a \gg 1$ , the Gamma function  $\Gamma(1 + i\Omega)$  can be approximated as [AS72]

$$\Gamma(1 + i\Omega) \approx \sqrt{\frac{\pi\Omega}{\sinh(\pi\Omega)}} e^{i\Omega \ln(\Omega) - i\Omega + i\pi/4}. \quad (8.2.24)$$

Substituting the Gamma function into the overlap integrals Eq. (8.2.20), we have

$$\begin{aligned} A_{fg} &\approx 2\sqrt{\frac{\sigma\delta}{ak_0}} e^{-ik_0V_0 + i\pi/4} \exp\left\{-i\frac{\omega_0}{a} \left[\ln\left(\frac{\omega_0}{ek_0}\right) - av_c\right]\right\} \exp\left\{-\frac{\sigma^2(\omega_0/a - k_0V_0)^2}{k_0^2}\right\} \\ &\quad \times \exp\left\{-(\delta/a)^2 \left[\ln\left(\frac{\omega_0}{ek_0}\right) - av_c\right]^2\right\}, \\ &\approx 2\sqrt{\frac{\sigma\delta}{ak_0}} e^{-ik_0V_0 + i\pi/4} \exp\left\{-i\frac{\omega_0}{a} \ln\left(\frac{\omega_0}{ek_0aV_c}\right)\right\} \exp\left\{-\frac{\sigma^2(\omega_0/a - k_0V_0)^2}{k_0^2}\right\} \\ &\quad \times \exp\left\{-(\delta/a)^2 \ln^2\left(\frac{\omega_0}{ek_0aV_c}\right)\right\}, \end{aligned} \quad (8.2.25)$$

$$\begin{aligned} B_{fg} &\approx 2\sqrt{\frac{\sigma\delta}{ak_0}} e^{-ik_0V_0 - i\pi/4} \exp\left\{i\frac{\omega_0}{a} \left[\ln\left(\frac{\omega_0}{ek_0}\right) - av_c\right]\right\} \exp\left\{-\frac{\sigma^2(\omega_0/a + k_0V_0)^2}{k_0^2}\right\} \\ &\quad \times \exp\left\{-(\delta/a)^2 \left[\ln\left(\frac{\omega_0}{ek_0}\right) - av_c\right]^2\right\}, \\ &\approx 2\sqrt{\frac{\sigma\delta}{ak_0}} e^{-ik_0V_0 - i\pi/4} \exp\left\{i\frac{\omega_0}{a} \ln\left(\frac{\omega_0}{ek_0aV_c}\right)\right\} \exp\left\{-\frac{\sigma^2(\omega_0/a + k_0V_0)^2}{k_0^2}\right\} \\ &\quad \times \exp\left\{-(\delta/a)^2 \ln^2\left(\frac{\omega_0}{ek_0aV_c}\right)\right\}. \end{aligned} \quad (8.2.26)$$

Here  $V_c$  is the central position of the wave packet  $g(\omega)$  in terms of the Minkowski coordinates, satisfying  $aV_c = e^{av_c}$ . If we define

$$\begin{aligned} \mathcal{E}^- &\equiv \exp\left[-\frac{2\sigma^2(\omega_0/a - k_0V_0)^2}{k_0^2}\right], \\ \mathcal{E}^+ &\equiv \exp\left[-\frac{2\sigma^2(\omega_0/a + k_0V_0)^2}{k_0^2}\right], \\ \Theta_h &\equiv 2\frac{\omega_0}{a} \ln\left(\frac{\omega_0}{ek_0aV_c}\right), \end{aligned}$$

The overlap integrals  $A_{fg}$  and  $B_{fg}$  can be written in a compact way,

$$\begin{aligned} A_{fg} &\approx 2\sqrt{\frac{\sigma\delta}{ak_0}} e^{-ik_0V_0+i\pi/4} e^{-i\Theta_h/2} \sqrt{\mathcal{E}^-} e^{-\frac{\delta^2\Theta_h^2}{4\omega_0^2}}, \\ B_{fg} &\approx 2\sqrt{\frac{\sigma\delta}{ak_0}} e^{-ik_0V_0-i\pi/4} e^{i\Theta_h/2} \sqrt{\mathcal{E}^+} e^{-\frac{\delta^2\Theta_h^2}{4\omega_0^2}}. \end{aligned} \quad (8.2.27)$$

Therefore, the particle number and variance can be rewritten as

$$N_1(f) \approx (1 - \cos\theta) \sinh^2(2r_0) (\mathcal{E}^- + \mathcal{E}^+) \left( \frac{2\sigma\delta}{ak_0} \right) \exp\left( -\frac{\delta^2\Theta_h^2}{2\omega_0^2} \right), \quad (8.2.28)$$

$$\begin{aligned} (\Delta X_1(\phi))^2 &\approx 1 + (1 - \cos\theta) \sinh(2r_0) \left( \frac{4\sigma\delta}{ak_0} \right) \exp\left( -\frac{\delta^2\Theta_h^2}{2\omega_0^2} \right) \left[ (\mathcal{E}^- + \mathcal{E}^+) \sinh(2r_0) \right. \\ &\quad \left. - 2\sqrt{\mathcal{E}^+\mathcal{E}^-} \cosh(2r_0) \cos(2k_0V_0 + 2\phi) \right]. \end{aligned} \quad (8.2.29)$$

Figs. 8.2 and 8.3 show the particle number and minimal quadrature variance of a Gaussian wave packet detector mode. Note that the particle number and the amount of single-mode squeezing is smaller than that for an accelerated mirror with time independent interactions, see Figs. 7.4 and 7.6.

In Chapter 7, we encountered the energy divergence problem. We now show that the energy divergence problem can be resolved by making the mirror only act on a localized wave packet mode, namely, the interaction is turned on and off. When the central frequency of the detector wave packet is large,  $k_0 \rightarrow \infty$ ,  $\mathcal{E}^\pm \rightarrow e^{-2\sigma^2V_0^2}$  and  $\Theta_h \rightarrow -\infty$ . From Eq. (8.2.28) we can see that the number of high energy particles is strongly suppressed by the factor  $e^{-\delta^2\Theta_h^2/4\omega_0^2}$ . Therefore we expect that the total energy radiated by the accelerated mirror is finite. Fig. 8.4 shows the energy,  $k_0N_1(f)$ , of the field in a detector wave packet mode  $f(k)$ . One can see that the energy decreases as the central frequency  $k_0$  increases, contrary to Fig. 7.5.

Furthermore, the introduction of switching on and off of the interaction also suppresses the number of low frequency particles. When  $k_0 \rightarrow 0$ ,  $\Theta_h \rightarrow \infty$ , so that  $e^{-\delta^2\Theta_h^2/4\omega_0^2} \rightarrow 0$ . This

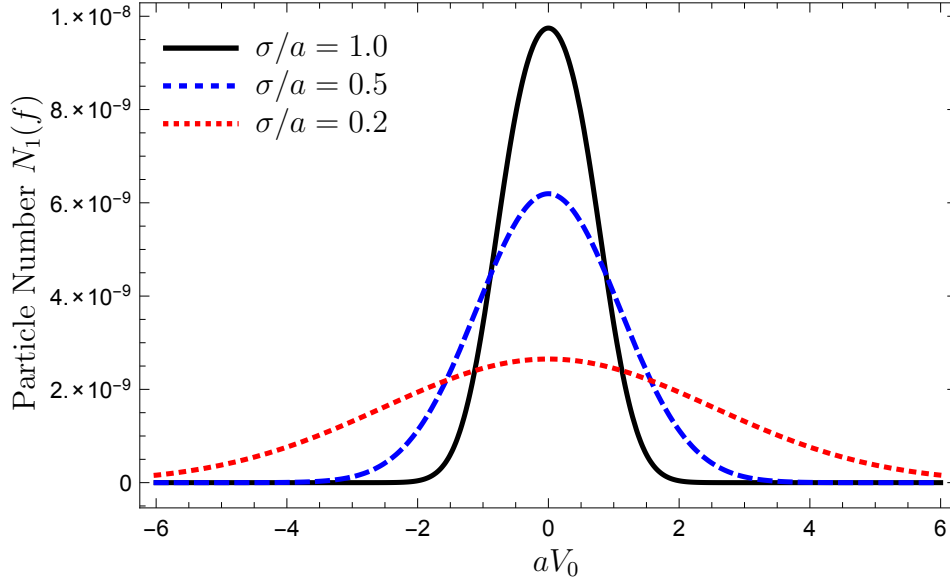


FIGURE 8.2: Particle number versus central position of the detector mode. Central frequency of the detector mode is  $k_0/a = 20$ . Parameters for the wave packet  $g(\omega)$  are  $\omega_0/a = 8.0$ ,  $\delta/a = 0.2$ ,  $aV_c = 1.0$ , and  $\theta$  is chosen to be  $\theta = \pi/2$ .

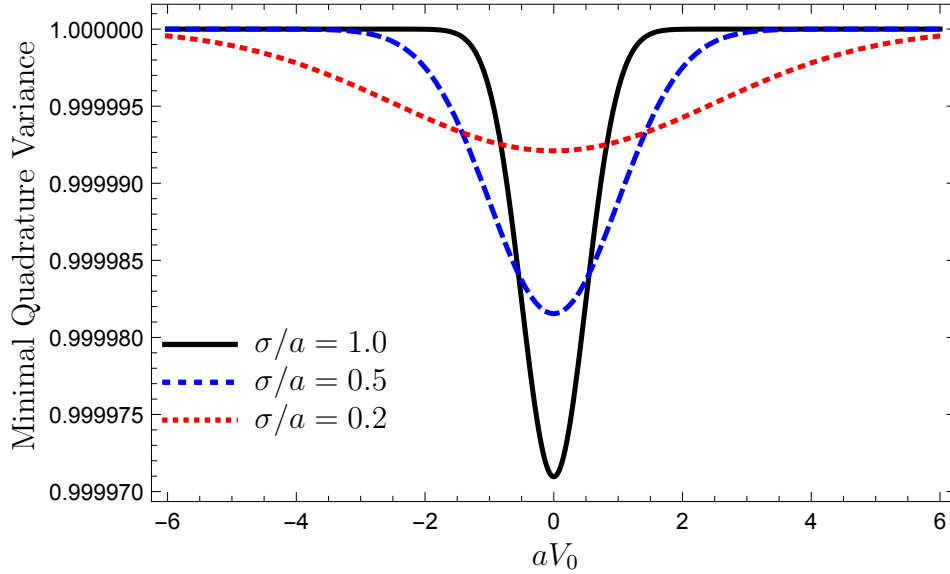


FIGURE 8.3: Minimal quadrature variance versus central position of the detector mode. Central frequency of the detector mode is  $k_0/a = 20$ . Parameters for the wave packet  $g(\omega)$  are  $\omega_0/a = 8.0$ ,  $\delta/a = 0.2$ ,  $aV_c = 1.0$ , and  $\theta$  is chosen to be  $\theta = \pi/2$ .

is expected because a finite duration of interaction does not produce very low frequency particles.

**Low central frequency limit** – When the central frequency of  $g(\omega)$  is small, namely,

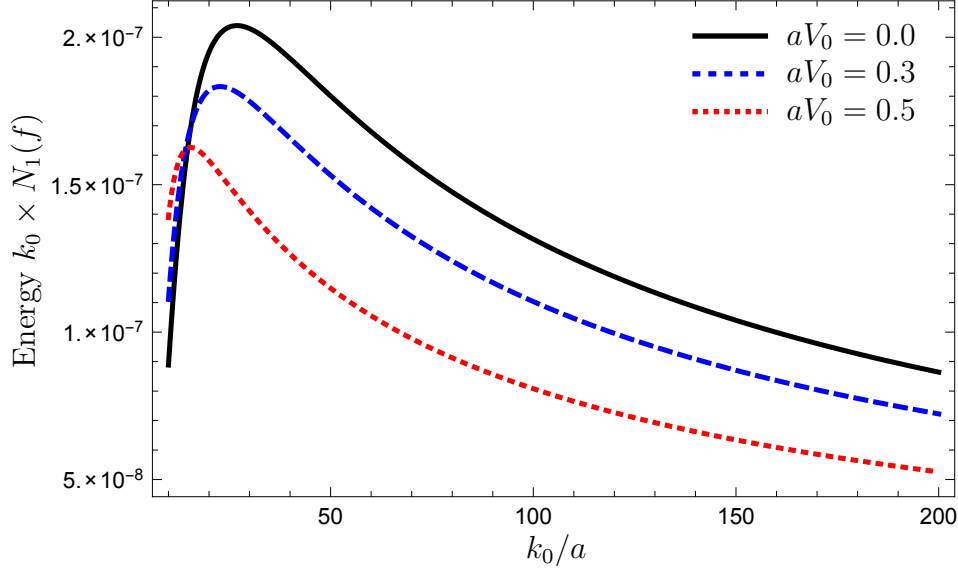


FIGURE 8.4: Energy of the fields versus central frequency of the detector mode. Bandwidth of the detector mode is  $\sigma/a = 1.0$ . Parameters for the wave packet  $g(\omega)$  are  $\omega_0/a = 8.0$ ,  $\delta/a = 0.2$ ,  $aV_c = 1.0$ , and  $\theta$  is chosen to be  $\theta = \pi/2$ .

$\Omega_0 \equiv \omega_0/a \ll 1$ , the Gamma function can be approximated as [AS72]

$$\Gamma(1 + i\Omega) \approx 1 - i\gamma\Omega \approx e^{-i\gamma\Omega}, \quad (8.2.30)$$

where  $\gamma$  is the Euler constant,  $\gamma \approx 0.577$ . If we define

$$\Theta_l \equiv 2\Omega_0 \ln(e^\gamma k_0 V_c), \quad (8.2.31)$$

the overlap integrals  $A_{fg}$  and  $B_{fg}$  can be approximated as

$$\begin{aligned} A_{fg} &\approx 2\sqrt{\frac{\sigma\delta}{ak_0}} e^{-ik_0 V_0} e^{i\Theta_l/2} \sqrt{\mathcal{E}^-} e^{-\frac{\delta^2 \Theta_l^2}{4\omega_0^2}}, \\ B_{fg} &\approx 2\sqrt{\frac{\sigma\delta}{ak_0}} e^{-ik_0 V_0} e^{-i\Theta_l/2} \sqrt{\mathcal{E}^+} e^{-\frac{\delta^2 \Theta_l^2}{4\omega_0^2}}. \end{aligned} \quad (8.2.32)$$

Therefore, the particle number and variance are

$$N_1(f) \approx (1 - \cos\theta) \sinh^2(2r_0) (\mathcal{E}^- + \mathcal{E}^+) \left(\frac{2\sigma\delta}{ak_0}\right) \exp\left(-\frac{\delta^2 \Theta_l^2}{2\omega_0^2}\right), \quad (8.2.33)$$

$$\begin{aligned} (\Delta X_1(\phi))^2 &\approx 1 + (1 - \cos\theta) \sinh(2r_0) \left(\frac{4\sigma\delta}{ak_0}\right) \exp\left(-\frac{\delta^2 \Theta_l^2}{2\omega_0^2}\right) \left[ (\mathcal{E}^- + \mathcal{E}^+) \sinh(2r_0) \right. \\ &\quad \left. - 2\sqrt{\mathcal{E}^+ \mathcal{E}^-} \cosh(2r_0) \cos(2k_0 V_0 + 2\phi) \right]. \end{aligned} \quad (8.2.34)$$

When the central frequency of the detector mode is large,  $k_0 \rightarrow \infty$ ,  $\Theta_l \rightarrow \infty$ . From Eq. (8.2.33) we see that the number of high frequency particles is suppressed by the factor  $e^{-\delta^2 \Theta_l^2 / 4\omega_0^2}$ . Therefore the total energy radiated by the mirror is finite. When  $k_0 \rightarrow 0$ ,  $\Theta_l \rightarrow -\infty$  so that  $e^{-\delta^2 \Theta_l^2 / 4\omega_0^2} \rightarrow 0$ . The number of low frequency particles is also suppressed.

### 8.3 Accelerated objects acting on arbitrary single mode

In the previous section, we used the narrow bandwidth approximation for the wave packet  $g(\omega)$ ,  $\omega_0/\delta \gg 1$ , and obtained a quite simple circuit model (Fig. 8.1) for a uniformly accelerated object that acts on a single wave packet mode. In this section, we are going to construct a circuit that is valid for arbitrary wave packets  $g(\omega)$ . For an arbitrary wave packet mode, especially a broadband mode, the action of the two-mode squeezers and two-modes anti-squeezers cannot be described simply by a single mode. We thus need to work out the transformation from Rindler modes to Unruh modes frequency by frequency. In the Rindler frame, the unitary  $\hat{U}_g$  acts on a single wave packet mode. The input-output relation for the single wave packet Rindler mode is determined by  $\hat{U}_g$ . Our first step is the find the input-output relations from the single frequency Rindler modes. The second step is to derive the input-output relations of the Unruh modes using the transformations between single frequency Rindler modes and single frequency Unruh modes. For simplicity, we only consider left-moving modes in the  $(1 + 1)$ -dimensional spacetime. The relevant circuit is shown in Fig. 8.5.

Suppose that  $g(\omega)$  is the wave packet that we are interested in and its corresponding localized Rindler operator is  $\hat{b}_g^R$ ;  $g_{\perp i}(\omega)$  are the wave packets that are orthogonal to  $g(\omega)$  and their corresponding localized Rindler operators are  $\hat{b}_{g_{\perp i}}^R$ . The uniformly accelerated unitary  $\hat{U}_g$  only acts on  $\hat{b}_g^R$ , that is,

$$\hat{U}_g^\dagger \hat{b}_g^R \hat{U}_g = \hat{b}_g^{R'}, \quad \hat{U}_g^\dagger \hat{b}_{g_{\perp i}}^R \hat{U}_g = \hat{b}_{g_{\perp i}}^R. \quad (8.3.1)$$

According to the relation between the single frequency modes and the wave packet modes,

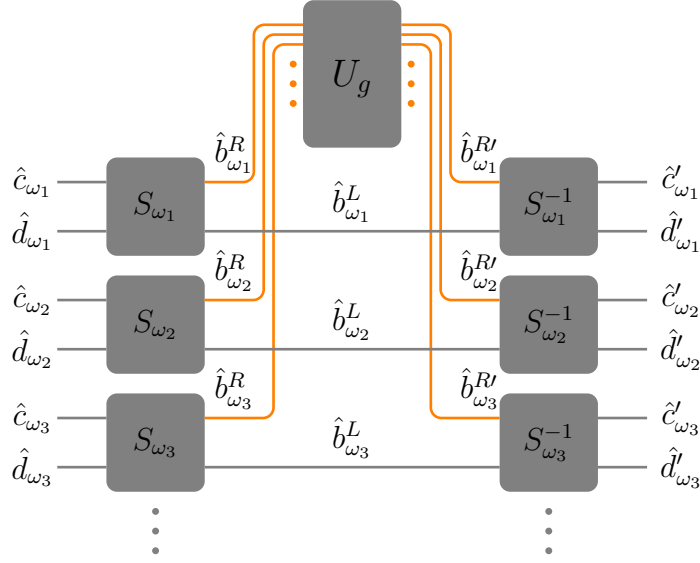


FIGURE 8.5: Circuit for a uniformly accelerated object. Rindler modes in the right Rindler wedge interact with the object, which is represented by the unitary operator  $\hat{U}_g$ , while Rindler modes in the left Rindler wedge remain unaffected. The time dependent interactions mix different frequency Rindler modes.

Eq. (3.1.5), we have

$$\hat{b}_{\omega}^R = g^*(\omega)\hat{b}_g^R + \sum_i g_{\perp i}(\omega)\hat{b}_{g_{\perp i}}^R. \quad (8.3.2)$$

Therefore the action of the unitary  $\hat{U}_g$  toward the single frequency Rindler operator is

$$\begin{aligned} \hat{b}_{\omega}^{R'} &= \hat{U}_g^\dagger \hat{b}_{\omega}^R \hat{U}_g = \hat{U}_g^\dagger \left[ g^*(\omega)\hat{b}_g^R + \sum_i g_{\perp i}(\omega)\hat{b}_{g_{\perp i}}^R \right] \hat{U}_g \\ &= g^*(\omega)\hat{U}_g^\dagger \hat{b}_g^R \hat{U}_g + \sum_i g_{\perp i}(\omega)\hat{b}_{g_{\perp i}}^R \\ &= \hat{b}_{\omega}^R + g^*(\omega)(\hat{U}_g^\dagger \hat{b}_g^R \hat{U}_g - \hat{b}_g^R). \end{aligned} \quad (8.3.3)$$

By using the relations between the single frequency Rindler modes and Unruh modes, we find

$$\begin{aligned} \hat{c}'_{\omega} &= \cosh(r_{\omega})\hat{b}_{\omega}^{R'} - \sinh(r_{\omega})\hat{b}_{\omega}^{L'\dagger} \\ &= \cosh(r_{\omega})\hat{b}_{\omega}^R - \sinh(r_{\omega})\hat{b}_{\omega}^{L\dagger} + g^*(\omega)\cosh(r_{\omega})(\hat{U}_g^\dagger \hat{b}_g^R \hat{U}_g - \hat{b}_g^R) \\ &= \hat{c}_{\omega} + g^*(\omega)\cosh(r_{\omega})(\hat{U}_g^\dagger \hat{b}_g^R \hat{U}_g - \hat{b}_g^R), \end{aligned} \quad (8.3.4)$$

$$\begin{aligned} \hat{d}'_{\omega} &= \cosh(r_{\omega})\hat{b}_{\omega}^{L'} - \sinh(r_{\omega})\hat{b}_{\omega}^{R'\dagger} \\ &= \cosh(r_{\omega})\hat{b}_{\omega}^L - \sinh(r_{\omega})\hat{b}_{\omega}^{R\dagger} - g(\omega)\sinh(r_{\omega})(\hat{U}_g^\dagger \hat{b}_g^{R\dagger} \hat{U}_g - \hat{b}_g^{R\dagger}) \\ &= \hat{d}_{\omega} - g(\omega)\sinh(r_{\omega})(\hat{U}_g^\dagger \hat{b}_g^{R\dagger} \hat{U}_g - \hat{b}_g^{R\dagger}). \end{aligned} \quad (8.3.5)$$

These input-output relations are valid for any wave packet mode  $g(\omega)$ . In the narrow bandwidth limit,  $\cosh(r_\omega)$  and  $\sinh(r_\omega)$  can be replaced by  $\cosh(r_0)$  and  $\sinh(r_0)$ , so Eqs. (8.3.4) and (8.3.5) go back to Eq. (8.2.7). To have a complete input-output relation for Unruh modes, one has to express  $\hat{b}_g^R$  in Eqs. (8.3.4) and (8.3.5) in terms of the input Unruh operators, which is straightforward. In the following we are going to discuss three examples that only takes into account left-moving modes. Generalization to include both left-moving and right-moving modes is straightforward.

### 8.3.1 Accelerated displacement

Suppose that  $\hat{U}_g$  represents a single mode displacement operator,  $\hat{U}_g = \hat{D}_g(\alpha) = \exp(\alpha \hat{b}_g^{R\dagger} - \alpha^* \hat{b}_g^R)$ , where  $\alpha$  is a complex number. It is easy to show that [BR04]

$$\hat{D}_g^\dagger(\alpha) \hat{b}_g^R \hat{D}_g(\alpha) = \hat{b}_g^R + \alpha. \quad (8.3.6)$$

From Eq. (8.3.3) we get the input-output relation for single frequency Rindler modes,

$$\hat{b}_\omega^{R'} = \hat{b}_\omega^R + \alpha g^*(\omega). \quad (8.3.7)$$

The input-output relations for single frequency Unruh modes can be obtained from Eqs. (8.3.4) and (8.3.5),

$$\begin{aligned} \hat{c}'_\omega &= \hat{c}_\omega + \alpha g^*(\omega) \cosh(r_\omega), \\ \hat{d}'_\omega &= \hat{d}_\omega - \alpha^* g(\omega) \sinh(r_\omega). \end{aligned} \quad (8.3.8)$$

This shows that a displacement to the Rindler mode results in a displacement to the Unruh modes. So if the initial state of the field is Minkowski vacuum, the states in the output Unruh modes  $\hat{c}'_\omega$  and  $\hat{d}'_\omega$  are coherent states, with frequency dependent displacement amplitudes. We can further look at the input-output relation for Minkowski modes. From the relations between the Unruh modes and Minkowski modes, Eq. (4.5.46), we have

$$\begin{aligned} \hat{a}'_k &= \int d\omega (A_{k\omega} \hat{c}'_\omega + B_{k\omega} \hat{d}'_\omega) \\ &= \int d\omega (A_{k\omega} \hat{c}_\omega + B_{k\omega} \hat{d}_\omega) + \alpha \int d\omega A_{k\omega} g^*(\omega) \cosh(r_\omega) - \alpha^* \int d\omega B_{k\omega} g(\omega) \sinh(r_\omega) \\ &= \hat{a}_k + \alpha \int d\omega A_{k\omega} g^*(\omega) \cosh(r_\omega) - \alpha^* \int d\omega B_{k\omega} g(\omega) \sinh(r_\omega). \end{aligned} \quad (8.3.9)$$

It is evident that the Minkowski modes are also displaced, with frequency dependent displacement amplitude. If the initial state of the field is the Minkowski vacuum, the output state as observed by inertial observers would be a coherent state. The expectation value of the total Minkowski particle number is

$$\int dk \langle 0_M | \hat{a}'_k \hat{a}'_k | 0_M \rangle = |\alpha|^2 (\mathcal{I}_c + \mathcal{I}_s), \quad (8.3.10)$$

where  $\mathcal{I}_c$  and  $\mathcal{I}_s$  are defined as

$$\mathcal{I}_c = \int d\omega |g(\omega)|^2 \cosh^2(r_\omega), \quad \mathcal{I}_s = \int d\omega |g(\omega)|^2 \sinh^2(r_\omega). \quad (8.3.11)$$

Since both  $\cosh^2(r_\omega)$  and  $\sinh^2(r_\omega)$  are proportional to  $1/\omega$  when  $\omega \rightarrow 0$ , one has to introduce a low frequency cutoff in  $g(\omega)$  in order  $\mathcal{I}_c$  and  $\mathcal{I}_s$  are finite, e.g.,  $g(\omega) \sim \sqrt{\omega}$  when  $\omega \rightarrow 0$ .

### 8.3.2 Accelerated phase shifter

Suppose that  $\hat{U}_g$  represents a single mode phase shift operator,  $\hat{U}_g = \exp(i\phi \hat{b}_g^R \hat{b}_g^R)$ . Substituting this unitary into Eq. (8.3.3), we get the input-output relation for the Rindler modes,

$$\hat{b}_\omega^{R'} = \hat{b}_\omega^R + (e^{i\phi} - 1)g^*(\omega)\hat{b}_g^R = \hat{b}_\omega^R + (e^{i\phi} - 1)g^*(\omega) \int d\omega' g(\omega') \hat{b}_{\omega'}^R. \quad (8.3.12)$$

The input-output relations for single frequency Unruh modes can be obtained from Eqs. (8.3.4) and (8.3.5),

$$\begin{aligned} \hat{c}'_\omega &= \hat{c}_\omega + (e^{i\phi} - 1)g^*(\omega) \cosh(r_\omega) \int_0^\infty d\omega' g(\omega') [\cosh(r_{\omega'})\hat{c}_{\omega'} + \sinh(r_{\omega'})\hat{d}'_{\omega'}], \\ \hat{d}'_\omega &= \hat{d}_\omega - (e^{-i\phi} - 1)g(\omega) \sinh(r_\omega) \int_0^\infty d\omega' g^*(\omega') [\cosh(r_{\omega'})\hat{c}'_{\omega'} + \sinh(r_{\omega'})\hat{d}_{\omega'}]. \end{aligned} \quad (8.3.13)$$

Assume that the initial state of the field is the Minkowski vacuum. The vacuum expectation values of the products of two output Unruh operators can be calculated straightforwardly.

$$\begin{aligned} \langle 0_M | \hat{c}'_\omega \hat{c}'_{\omega'} | 0_M \rangle &= g(\omega)g^*(\omega') \cosh(r_\omega) \cosh(r_{\omega'}) |e^{i\phi} - 1|^2 \mathcal{I}_s, \\ \langle 0_M | \hat{d}'_\omega \hat{d}'_{\omega'} | 0_M \rangle &= g^*(\omega)g(\omega') \sinh(r_\omega) \sinh(r_{\omega'}) |e^{i\phi} - 1|^2 \mathcal{I}_c, \\ \langle 0_M | \hat{c}'_\omega \hat{d}'_{\omega'} | 0_M \rangle &= -g(\omega)g^*(\omega') \cosh(r_\omega) \cosh(r_{\omega'}) [(e^{-i\phi} - 1) + |e^{i\phi} - 1|^2 \mathcal{I}_c], \end{aligned} \quad (8.3.14)$$

and others are either zero or can be derived from the above results.

### 8.3.3 Accelerated single-mode squeezer

Suppose that  $\hat{U}_g$  represents a single-mode squeezing operator,  $\hat{U}_g = \hat{S}_1(r)$ ,

$$\hat{S}_1(r) = \exp \left\{ \frac{r}{2} (\hat{b}_g^{R\dagger})^2 - \frac{r}{2} (\hat{b}_g^R)^2 \right\}, \quad (8.3.15)$$

where  $r$  is the squeezing factor and is assumed to be real. It can be shown that

$$\hat{S}_1(r) \hat{b}_g^R \hat{S}_1(r) = \cosh r \hat{b}_g^R + \sinh r \hat{b}_g^{R\dagger}. \quad (8.3.16)$$

Substituting this into Eq. (8.3.3), we get the input-output relation for the Rindler modes,

$$\hat{b}_\omega^{R'} = \hat{b}_\omega^R + g^*(\omega) \left[ (\cosh r - 1) \int d\omega' g(\omega') \hat{b}_{\omega'}^R + \sinh r \int d\omega' g^*(\omega') \hat{b}_{\omega'}^{R\dagger} \right]. \quad (8.3.17)$$

The input-output relations for single frequency Unruh modes can be obtained from Eqs. (8.3.4) and (8.3.5),

$$\begin{aligned} \hat{c}'_\omega &= \hat{c}_\omega + g^*(\omega) \cosh(r_\omega) \left\{ (\cosh r - 1) \int d\omega' g(\omega') [\hat{c}_{\omega'} \cosh(r_{\omega'}) + \hat{d}_{\omega'}^\dagger \sinh(r_{\omega'})] \right. \\ &\quad \left. + \sinh r \int d\omega' g^*(\omega') [\hat{c}_{\omega'}^\dagger \cosh(r_{\omega'}) + \hat{d}_{\omega'} \sinh(r_{\omega'})] \right\}, \\ \hat{d}'_\omega &= \hat{d}_\omega - g(\omega) \sinh(r_\omega) \left\{ (\cosh r - 1) \int d\omega' g^*(\omega') [\hat{c}_{\omega'}^\dagger \cosh(r_{\omega'}) + \hat{d}_{\omega'} \sinh(r_{\omega'})] \right. \\ &\quad \left. + \sinh r \int d\omega' g(\omega') [\hat{c}_{\omega'} \cosh(r_{\omega'}) + \hat{d}_{\omega'}^\dagger \sinh(r_{\omega'})] \right\}. \end{aligned} \quad (8.3.18)$$

The vacuum expectation values of the products of two output Unruh operators can be calculated straightforwardly from Eq. (8.3.18).

$$\begin{aligned} \langle 0_M | \hat{c}'_\omega \hat{c}'_{\omega'} | 0_M \rangle &= g(\omega) g^*(\omega') \cosh(r_\omega) \cosh(r_{\omega'}) E_c, \\ \langle 0_M | \hat{d}'_\omega \hat{d}'_{\omega'} | 0_M \rangle &= g^*(\omega) g(\omega') \sinh(r_\omega) \sinh(r_{\omega'}) E_d, \\ \langle 0_M | \hat{c}'_\omega \hat{c}'_{\omega'} | 0_M \rangle &= g^*(\omega) g^*(\omega') \cosh(r_\omega) \cosh(r_{\omega'}) E_{cc}, \\ \langle 0_M | \hat{d}'_\omega \hat{d}'_{\omega'} | 0_M \rangle &= g(\omega) g(\omega') \sinh(r_\omega) \sinh(r_{\omega'}) E_{dd}, \\ \langle 0_M | \hat{c}'_\omega \hat{d}'_{\omega'} | 0_M \rangle &= g^*(\omega) g(\omega') \cosh(r_\omega) \sinh(r_{\omega'}) E_{cd}, \\ \langle 0_M | \hat{c}'_\omega \hat{d}'_{\omega'} | 0_M \rangle &= g(\omega) g(\omega') \cosh(r_\omega) \sinh(r_{\omega'}) \bar{E}_{cd}. \end{aligned} \quad (8.3.19)$$

where

$$\begin{aligned}
E_c &= \mathcal{I}_s(\cosh r - 1)^2 + \mathcal{I}_c \sinh^2 r = [(\cosh r - 1)^2 + \sinh^2 r] \mathcal{I}_c - (\cosh r - 1)^2, \\
E_d &= \mathcal{I}_c(\cosh r - 1)^2 + \mathcal{I}_s \sinh^2 r = [(\cosh r - 1)^2 + \sinh^2 r] \mathcal{I}_c - \sinh^2 r, \\
E_{cc} &= \sinh r [(\mathcal{I}_c + \mathcal{I}_s)(\cosh r - 1) + 1] = \sinh r [(2\mathcal{I}_c - 1)(\cosh r - 1) + 1], \\
E_{dd} &= \sinh r [(\mathcal{I}_c + \mathcal{I}_s)(\cosh r - 1) - 1] = \sinh r [(2\mathcal{I}_c - 1)(\cosh r - 1) - 1], \\
E_{cd} &= -\cosh r(\cosh r - 1)(\mathcal{I}_c + \mathcal{I}_s) = -\cosh r(\cosh r - 1)(2\mathcal{I}_c - 1), \\
\bar{E}_{cd} &= -\sinh r(\cosh r - 1)(\mathcal{I}_c + \mathcal{I}_s) = -\sinh r(\cosh r - 1)(2\mathcal{I}_c - 1), \tag{8.3.20}
\end{aligned}$$

## 8.4 Decoherence in non-inertial frames

In the above section, we have constructed a quantum circuit for a uniformly accelerated object that acts on an arbitrary wave packet mode. The interaction is unitary in the accelerated frame, so it can be represented by a unitary operator  $\hat{U}_g$ . A question of particular interest is whether this process can be described by a unitary operator in the perspective of inertial observers. This question can be answered by checking the purity of the output state, given that the input state is pure. In this section, we are going to investigate the purity of the output state as observed by inertial observers by using the homodyne detection, given that the input is the Minkowski vacuum.

Unitary evolution is one of the fundamental assumptions of quantum mechanics. An initial pure state of an isolated quantum system always evolves into another pure state. The situation is not as simple when we consider non-inertial, relativistic frames of reference. For example, the transformation between the description of the quantum vacuum state as seen by inertial observers and the description of the same state by uniformly accelerated observers is not strictly unitary. Nevertheless it is still assumed that in transforming between reference frames pure states will always evolve to pure states provided that the entire space-time is included. Consider an inertial observer who constantly observes a massless field prepared in the Minkowski vacuum state. By definition they will observe no particles. However, according to the Unruh/Davies effect [Unr76, Dav75], a uniformly accelerating observer who

constantly observes the same field will see thermal radiation (Unruh radiation), and hence will count particles. The vacuum state is pure whilst a thermal state is mixed, seemingly implying a non-unitary evolution. The resolution is that a single accelerating observer is restricted to a section of space-time called a Rindler wedge. By introducing a second, mirror image accelerated observer we find that the thermal state can be purified into a two-mode squeezed state [UW84, Lee86, Tak86] and unitarity is restored.

We consider accelerated quantum systems in flat space, however we set up the problem differently such that we explicitly start and end with global, inertial observers. In the intermediate region we allow interactions with an accelerated system. The specific problem we will analyse is summarized by the Penrose diagram [MTW73] in Fig. 8.6. An object uniformly accelerates in the right Rindler wedge (black curve). Interactions with a massless scalar field are unitarily turned on and off during its lifetime (shaded region) such that it interacts with a single spatio-temporal mode in the accelerated (Rindler) coordinates. In the past null infinity  $\mathcal{I}^-$ , the initial state of the field is set to be the Minkowski vacuum. For simplicity we consider a 1+1 theory in which the right and left moving fields are decoupled. We assume the right moving field modes are unaffected by the accelerating object. The output state of the left moving field modes in the future null infinity  $\mathcal{I}^+$  is detected by inertial, Minkowski detectors. Here the inertial detectors are those detectors that can detect the overall output state of the scalar field. From Fig. 8.6 one can easily see that there are no particles before and after the interaction, a consequence of causality. We assume that the inertial detectors are turned on for all times (at least at the spacetime points that are connected to the shaded interaction region by null rays) and detect particles with all frequencies. Unexpectedly we find a decoherence effect that only affects non-classical quantum states and cannot be removed by appealing to inaccessible regions of space-time.

#### 8.4.1 Detection of the state

The Minkowski detectors are modelled by the Hermitian number operators,  $\hat{N}_k = \hat{a}_k^\dagger \hat{a}_k$ , where  $\hat{a}_k$  ( $\hat{a}_k^\dagger$ ) are the Minkowski field annihilation (creation) operators for wave-number  $k$ .

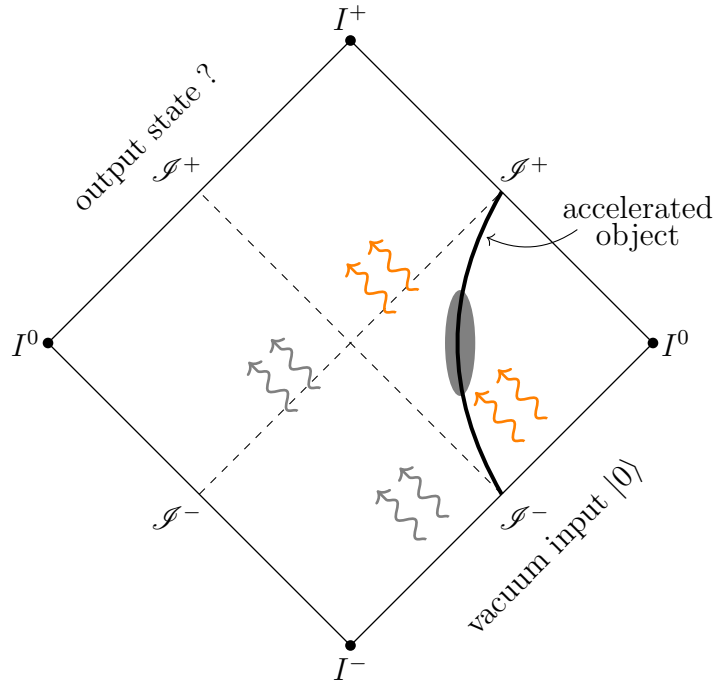


FIGURE 8.6: Penrose diagram of Minkowski spacetime.  $I^0$  is the spatial infinity,  $I^-$  and  $I^+$  are the past and future infinities,  $\mathcal{S}^-$  and  $\mathcal{S}^+$  are the past and future null infinities. A uniformly accelerated object follows the black worldline. Interactions between the accelerated object and the field are localized in Rindler time, represented by the shaded region.

The frequencies  $|k|$  are with respect to the proper time of the inertial reference frame under consideration. The excitation probability of an ideal, inertial, 2-level system of resonant frequency  $|k|$ , coupled weakly to the field, is proportional to  $\langle \hat{N}_k \rangle$  [SZ97]. We can model a finite bandwidth detector via the operator  $\hat{N}_{\Delta k} = \int_{k_o - \Delta k}^{k_o + \Delta k} dk \hat{a}_k^\dagger \hat{a}_k$ . If the bandwidth of the detector is much larger than that of the mode under consideration then we can extend the limits of integration to  $\pm\infty$  and so define  $\hat{N} = \int dk \hat{a}_k^\dagger \hat{a}_k$ . Note that by definition  $\langle 0 | \hat{N} | 0 \rangle = 0$  for the Minkowski vacuum state,  $|0\rangle$ .

In order to characterize the state of a particular field mode we use homodyne tomography [LR09]. In homodyne tomography, the Wigner function of the state is reconstructed from measurements of the moments of quadrature amplitudes via homodyne detection. For Gaussian states it is sufficient to measure and analyse only the first and second order moments [WPGP<sup>+</sup>12]. In homodyne detection [BR04], a weak signal field and a strong local oscillator are coherently combined and measured with broad-band detection as discussed

above. For simplicity and to stay within the 1+1, scalar field paradigm, we specifically use self-homodyne detection here. In self-homodyne detection, the signal field is displaced by a strong local oscillator directly, and the output field is detected. Assume that the signal field mode operator is  $\hat{a} = \int dk f(k) \hat{a}_k$  and the local oscillator is a strong coherent state  $|\alpha\rangle$ , prepared in the same field mode (characterized by  $f(k)$ ) with  $\alpha$  a complex number,  $\alpha = |\alpha|e^{i\phi}$ , and  $|\alpha| \gg 1$ . The photon number operator can be shown to be

$$\hat{N}(\phi) \approx |\alpha|^2 + |\alpha| \hat{X}(\phi) \quad (8.4.1)$$

where  $\hat{X}(\phi) = \hat{a}e^{-i\phi} + \hat{a}^\dagger e^{i\phi}$  is the quadrature amplitude of the signal field and a term not multiplied by  $|\alpha|$  has been neglected as small. As a reference we can also consider the operator

$$\hat{N}_0 \approx |\alpha|^2 + |\alpha| \hat{X}_v \quad (8.4.2)$$

representing the situation where the signal is not imposed and so  $\hat{v}$  represents the mode when it is prepared in the vacuum state. Hence the average quadrature amplitude of the field is given by

$$\langle \hat{X}(\phi) \rangle = \frac{\langle \hat{N}(\phi) \rangle - \langle \hat{N}_0 \rangle}{\sqrt{\langle \hat{N}_0 \rangle}} \quad (8.4.3)$$

where we have used  $\langle \hat{X}_v \rangle = 0$ . Its variance is given by

$$(\Delta X(\phi))^2 = \frac{(\Delta N(\phi))^2}{\langle \hat{N}_0 \rangle}. \quad (8.4.4)$$

For the Gaussian states considered here this will be sufficient to completely characterize them.

### 8.4.2 Accelerated self-homodyne detection

We wish to apply this technique to the output state from the interactions between a uniformly accelerated object and the scalar field. In order to do this we need to match the mode shape of the local oscillator to that of the output signal field. However, the mode shape of the signal is distorted due to the acceleration of the object. It is difficult for an inertial observer to construct a local oscillator with this distorted mode shape. We avoid this complication

by assuming that the local oscillator is also imposed in the accelerated frame in a matching mode to the signal.

In Section 8.3, we have constructed a general circuit (Fig. 8.5) for a uniformly accelerated object that acts on an arbitrary Rindler wave packet mode. The input-output relations for Unruh modes are given by Eqs. (8.3.4) and (8.3.5). However, The Unruh operators [Unr76] are only a useful mathematical stepping stone between the accelerated and inertial reference frames. In order to represent our inertial detection scheme, we need to construct the Minkowski modes,  $\hat{a}_k$ , from the output Unruh modes – this final step is not represented by a circuit.

In the circuit 8.5,  $\hat{U}_g$  is an arbitrary unitary operator. We assume that  $\hat{U}_g = \hat{\mathcal{S}}_g$  creates the quantum signal we wish to analyse, as shown in Fig. 8.7(a). To achieve self-homodyne detection, a displacement (local oscillator) is added after the signal operator, namely, the unitary operator  $\hat{U}_g = \hat{D}_g(\alpha)\hat{\mathcal{S}}_g$ , as shown in Fig. 8.7(b).  $\hat{D}_g(\alpha) = \exp(\alpha\hat{b}_g^{R\dagger} - \alpha^*\hat{b}_g^R)$  produces the local oscillator for self-homodyne detection, where  $\alpha = |\alpha|e^{i\phi}$  is a complex number. In the following, we assume that  $|\alpha| \gg 1$ . Note that the mode shape of the local oscillator should perfectly match the mode shape of the signal operator. At first glance, it seems problematic to use an accelerated local oscillator, because we want to know the output state as observed by inertial observers. The use of accelerated local oscillator can be justified by noticing that a uniformly accelerated displacement also creates a coherent state as observed by inertial observers, as shown in Section 8.3.1. Therefore, a uniformly accelerated local oscillator is also an inertial local oscillator.

The total Minkowski particle number operator,  $\hat{N} = \int dk \hat{a}_k^\dagger \hat{a}_k$ , is obtained by using Eq. (4.5.46),

$$\begin{aligned} \hat{N} &= \int dk \int d\omega_1 \int d\omega_2 (A_{k\omega_1}^* \hat{c}_{\omega_1}^\dagger + B_{k\omega_1}^* \hat{d}_{\omega_1}^\dagger) (A_{k\omega_2} \hat{c}_{\omega_2} + B_{k\omega_2} \hat{d}_{\omega_2}) \\ &= \int d\omega (\hat{c}_\omega^\dagger \hat{c}_\omega + \hat{d}_\omega^\dagger \hat{d}_\omega), \end{aligned} \quad (8.4.5)$$

where we have used  $\int dk A_{k\omega} A_{k\omega'}^* = \delta(\omega - \omega')$  and  $\int dk A_{k\omega} A_{k\omega'} = 0$ . This tells us that the

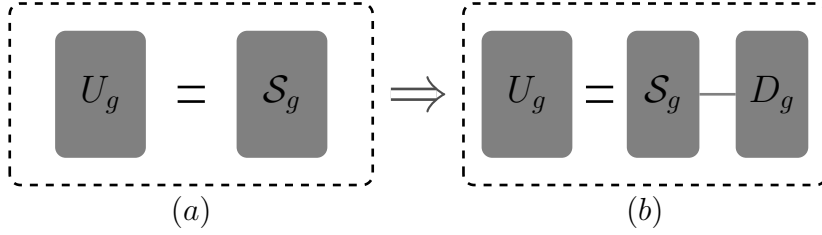


FIGURE 8.7: Self-homodyne detection. (a) A signal unitary  $\hat{S}_g$  generates quantum signals that we are going to analyze. (b) A displacement is added after the signal unitary  $\hat{S}_g$  to realize homodyne detection. The mode shape of the displacement is perfectly matched to that of the signal unitary.

total number of Minkowski particles is the same as the total number of Unruh particles. The conservation of particle number is expected because the Bogoliubov transformation Eq. (4.5.46) does not mix negative frequency modes. The square of the total particle number operator is

$$\hat{N}^2 = \int d\omega_1 \int d\omega_2 (\hat{c}'_{\omega_1} \hat{c}'_{\omega_1} \hat{c}'_{\omega_2} \hat{c}'_{\omega_2} + \hat{d}'_{\omega_1} \hat{d}'_{\omega_1} \hat{d}'_{\omega_2} \hat{d}'_{\omega_2} + \hat{c}'_{\omega_1} \hat{c}'_{\omega_1} \hat{d}'_{\omega_2} \hat{d}'_{\omega_2} + \hat{d}'_{\omega_1} \hat{d}'_{\omega_1} \hat{c}'_{\omega_2} \hat{c}'_{\omega_2}). \quad (8.4.6)$$

A full computation of the vacuum expectation value of  $\hat{N}^2$  is straightforward but usually tedious. However, when the amplitude of displacement is large ( $|\alpha| \gg 1$ ), it is adequate to only keep terms of order  $|\alpha|^4$  and  $|\alpha|^2$  as per the approximation leading to equations (8.4.3) and (8.4.4).

### 8.4.3 Classical signals

We first consider preparing a classical signal on the accelerated mode. In particular, we generate a classical signal by displacing the Rindler mode  $\hat{b}_g^R$  with an amplitude  $\beta$ . This produces a coherent state, the “most classical” quantum state. The operator that creates this signal is  $\hat{S}_g = \hat{D}_g(\beta)$ , with  $|\beta| \ll |\alpha|$ . The expectation value and variance of the quadrature amplitudes as observed by the inertial detectors are

$$\begin{aligned} X_\beta(\phi) &= \sqrt{2\mathcal{I}_c - 1}(\beta e^{-i\phi} + \beta^* e^{i\phi}), \\ V_\beta(\phi) &= 1, \end{aligned} \quad (8.4.7)$$

where  $\mathcal{I}_c = \int d\omega |g(\omega)|^2 \cosh^2 r_\omega$ . Equation (8.4.7) characterises a pure coherent state. Therefore, displacing a Rindler mode generates a coherent state with amplitude  $(\sqrt{2\mathcal{I}_c - 1})\beta$  as

viewed by an inertial observer. This is consistent with the results obtained in Section 8.3.1.. As expected the overall evolution is from a pure state to a pure state.

#### 8.4.4 Quantum signals

A more interesting scenario is that a uniformly accelerated single-mode squeezer squeezes the thermal state in the right Rindler wedge. The single-mode squeezing operator  $\hat{S}_1(r)$  is defined as [BR04]

$$\hat{S}_1(r) = \exp \left\{ \frac{r}{2} (\hat{b}_g^{R\dagger})^2 - \frac{r}{2} (\hat{b}_g^R)^2 \right\}, \quad (8.4.8)$$

where  $r$  is the squeezing factor and is assumed to be real. The operator that creates quantum signals is  $\hat{\mathcal{S}}_g = \hat{S}_1(r)$  so that the unitary  $\hat{U}_g = \hat{D}_g(\alpha)\hat{\mathcal{S}}_1(r)$ .

In the perspective of an accelerated observer, the output state is basically a squeezed thermal state. Define the quadrature amplitude of the localized Rindler wave packet mode  $\hat{b}_g^{R'}$  as  $\hat{X}_g^R(\phi) = \hat{b}_g^{R'} e^{-i\phi} + \hat{b}_g^{R\dagger} e^{i\phi}$ . It can be shown that  $\langle 0 | \hat{X}_g^R(\phi) | 0 \rangle = 0$ , and the variance of the quadrature amplitude is

$$(\Delta X_g^R(\phi))^2 = (2\mathcal{I}_c - 1) [\cosh(2r) + \sinh(2r) \cos(2\phi)]. \quad (8.4.9)$$

The maximum and minimum variances are obtained when  $\phi = 0$  and  $\phi = \pi/2$ , respectively. An important quantity that characterizes the purity of a state is the product of the maximum and minimum quadrature variances. If the product is unity then the state is pure, whilst if the product is greater than unity then the state is mixed. From Eq. (8.4.9), we find

$$(\Delta X_g^R(0) \Delta X_g^R(\pi/2))^2 = (2\mathcal{I}_c - 1)^2. \quad (8.4.10)$$

We see that the product of the maximum and minimum variances is always greater than unity, implying that the state observed by an accelerated observer is mixed. This is expected because the accelerated observer in the right Rindler wedge can not access the correlations with the left Rindler wedge.

We are now going to find out the output state as observed by inertial observers. By substituting  $\hat{U}_g = \hat{D}_g(\alpha)\hat{\mathcal{S}}_1(r)$  into Eqs. (8.3.4) and (8.3.5) one can derive the input-output

relations for Unruh modes,

$$\begin{aligned}\hat{c}'_{\omega} &= \hat{c}_{\omega} + g^*(\omega) \cosh r_{\omega} [\hat{b}_g^R (\cosh r - 1) + \hat{b}_g^{R\dagger} \sinh r + \alpha], \\ \hat{d}'_{\omega} &= \hat{d}_{\omega} - g(\omega) \sinh r_{\omega} [\hat{b}_g^{R\dagger} (\cosh r - 1) + \hat{b}_g^R \sinh r + \alpha^*].\end{aligned}\quad (8.4.11)$$

The localized Rindler operator  $\hat{b}_g^R$  can be expressed in terms of the input Unruh operators by using the transformations between the Rindler and Unruh modes. Eq. (8.4.11) becomes

$$\begin{aligned}\hat{c}'_{\omega} &= \hat{c}_{\omega} + g^*(\omega) \cosh r_{\omega} \left[ (\cosh r - 1) \int d\omega' g(\omega') (\hat{c}_{\omega'} \cosh r_{\omega'} + \hat{d}_{\omega'}^{\dagger} \sinh r_{\omega'}) \right. \\ &\quad \left. + \sinh r \int d\omega' g^*(\omega') (\hat{c}_{\omega'}^{\dagger} \cosh r_{\omega'} + \hat{d}_{\omega'} \sinh r_{\omega'}) + \alpha \right], \\ \hat{d}'_{\omega} &= \hat{d}_{\omega} - g(\omega) \sinh r_{\omega} \left[ (\cosh r - 1) \int d\omega' g^*(\omega') (\hat{c}_{\omega'}^{\dagger} \cosh r_{\omega'} + \hat{d}_{\omega'} \sinh r_{\omega'}) \right. \\ &\quad \left. + \sinh r \int d\omega' g(\omega') (\hat{c}_{\omega'} \cosh r_{\omega'} + \hat{d}_{\omega'}^{\dagger} \sinh r_{\omega'}) + \alpha^* \right].\end{aligned}\quad (8.4.12)$$

It is now straightforward to calculate the vacuum expectation values of the product of two output Unruh operators.

$$\begin{aligned}\langle 0_M | \hat{c}'_{\omega} \hat{c}'_{\omega'} | 0_M \rangle &= g(\omega) g^*(\omega') \cosh r_{\omega} \cosh r_{\omega'} (E_c + |\alpha|^2), \\ \langle 0_M | \hat{d}'_{\omega} \hat{d}'_{\omega'} | 0_M \rangle &= g^*(\omega) g(\omega') \sinh r_{\omega} \sinh r_{\omega'} (E_d + |\alpha|^2), \\ \langle 0_M | \hat{c}'_{\omega} \hat{c}'_{\omega'} | 0_M \rangle &= g^*(\omega) g^*(\omega') \cosh r_{\omega} \cosh r_{\omega'} (E_{cc} + \alpha^2), \\ \langle 0_M | \hat{d}'_{\omega} \hat{d}'_{\omega'} | 0_M \rangle &= g(\omega) g(\omega') \sinh r_{\omega} \sinh r_{\omega'} (E_{dd} + \alpha^{*2}), \\ \langle 0_M | \hat{c}'_{\omega} \hat{d}'_{\omega'} | 0_M \rangle &= g^*(\omega) g(\omega') \cosh r_{\omega} \sinh r_{\omega'} (E_{cd} - |\alpha|^2), \\ \langle 0_M | \hat{c}'_{\omega}^{\dagger} \hat{d}'_{\omega'} | 0_M \rangle &= g(\omega) g(\omega') \cosh r_{\omega} \sinh r_{\omega'} (\bar{E}_{cd} - \alpha^{*2}),\end{aligned}\quad (8.4.13)$$

where  $E_c, E_d, E_{cc}, E_{dd}, E_{cd}$  and  $\bar{E}_{cd}$  are given by Eq. (8.3.20). From equations (8.4.5) and (8.4.6), the vacuum expectation value of the total Minkowski particle number is

$$\langle 0_M | \hat{N} | 0_M \rangle = |\alpha|^2 (\mathcal{I}_c + \mathcal{I}_s) + (\mathcal{I}_c E_c + \mathcal{I}_s E_d) \quad (8.4.14)$$

and the variance of total Minkowski particle number is

$$\begin{aligned}
(\Delta N)^2 &= \langle 0_M | \hat{N}^2 | 0_M \rangle - \langle 0_M | \hat{N} | 0_M \rangle^2 \\
&= |\alpha|^2 (\mathcal{I}_c + \mathcal{I}_s) + 2|\alpha|^2 (\mathcal{I}_c^2 E_c + \mathcal{I}_s^2 E_d) + \mathcal{I}_c^2 (\alpha^2 E_{cc}^* + \alpha^{*2} E_{cc}) + \mathcal{I}_s^2 (\alpha^2 E_{dd} + \alpha^{*2} E_{dd}^*) \\
&\quad - 2|\alpha|^2 \mathcal{I}_c \mathcal{I}_s (E_{cd} + E_{cd}^*) - 2\mathcal{I}_c \mathcal{I}_s (\alpha^2 \bar{E}_{cd} + \alpha^{*2} \bar{E}_{cd}^*) \\
&= |\alpha|^2 \left[ (\mathcal{I}_c + \mathcal{I}_s) + 2(\mathcal{I}_c^2 E_c + \mathcal{I}_s^2 E_d) + 2\mathcal{I}_c^2 E_{cc} \cos(2\phi) + 2\mathcal{I}_s^2 E_{dd} \cos(2\phi) - 4\mathcal{I}_c \mathcal{I}_s E_{cd} \right. \\
&\quad \left. - 4\mathcal{I}_c \mathcal{I}_s \bar{E}_{cd} \cos(2\phi) \right], \tag{8.4.15}
\end{aligned}$$

where  $\phi$  is the displacement phase. In the homodyne detection, normalizing the variance of the particle number using the strength of the local oscillator gives the variance of the quadrature amplitude [BR04]. Here the strength of the local oscillator is  $\sim |\alpha|^2 (\mathcal{I}_c + \mathcal{I}_s)$ , so the variance of quadrature amplitude is

$$\begin{aligned}
V(\phi) &= \frac{(\Delta N)^2}{|\alpha|^2 (\mathcal{I}_c + \mathcal{I}_s)} \\
&= \cosh(2r) + 4\mathcal{I}_c (\mathcal{I}_c - 1) (\cosh 2r - 2 \cosh r + 1) \\
&\quad + 2 \sinh r [(2\mathcal{I}_c - 1)^2 \cosh r - 4\mathcal{I}_c (\mathcal{I}_c - 1)] \cos(2\phi). \tag{8.4.16}
\end{aligned}$$

The maximum and minimum variances are obtained when  $\phi = 0$  and  $\phi = \pi/2$ , respectively.

$$\begin{aligned}
V_{\max} &= e^{2r} + 4\mathcal{I}_c (\mathcal{I}_c - 1) (e^r - 1)^2, \\
V_{\min} &= e^{-2r} + 4\mathcal{I}_c (\mathcal{I}_c - 1) (e^{-r} - 1)^2. \tag{8.4.17}
\end{aligned}$$

It is evident from equations (8.4.16) and (8.4.17) that noises are added onto the variance of the original single-mode squeezed state. The amount of additional noises depends on the squeezing factor  $r$  and  $\mathcal{I}_c$ . A question of particular interest is whether the final state is a pure state or not. For Gaussian states, the criteria for purity is that the product of maximum and minimum variances is unity [BR04]. From equation (8.4.17) we find the product of the minimum and maximum variances is

$$V_{\max} V_{\min} = 1 + 16\mathcal{I}_c (\mathcal{I}_c - 1) (\cosh r - 1) \cosh r + 64\mathcal{I}_c^2 (\mathcal{I}_c - 1)^2 (\cosh r - 1)^2 \tag{8.4.18}$$

We can see that the product is always greater than one unless  $r = 0$  or  $\mathcal{I}_c = 1$ . This is our main result. Unexpectedly, the inertial observer sees a decoherence effect that in general takes the initial pure state to a mixed state.

The case of  $r = 0$  means the accelerated object does nothing so that the output state is the Minkowski vacuum.  $\mathcal{I}_c$  can be approximated as  $\mathcal{I}_c \approx e^{2\pi\omega_0/a}/(e^{2\pi\omega_0/a} - 1)$  when  $g(\omega)$  is a very narrow bandwidth wave packet with central frequency  $\omega_0$ . When  $2\pi\omega_0/a \rightarrow \infty$ ,  $\mathcal{I}_c \rightarrow 1$  so that  $V_{\min} \rightarrow e^{-2r}$  and  $V_{\max} \rightarrow e^{2r}$ . This corresponds to a single-mode squeezed vacuum state, which is pure. The above limit could happen in two cases. The first is that the central frequency  $\omega_0$  is fixed while  $a \rightarrow 0$ . This means the single-mode squeezer tends to be static in an inertial frame. It thus produces the standard single-mode squeezed vacuum state. The second case is that  $a$  is fixed and finite, while  $\omega_0 \rightarrow \infty$ . It is well known that a uniformly accelerated observer experiences a thermal radiation with temperature  $T_U = \frac{a}{2\pi}$  in the Minkowski vacuum [Unr76]. The spectral distribution of the thermal radiation follows the Planck's law, which exponentially decays in the high frequency limit. Or equivalently, the high frequency tail of a thermal state looks almost like a vacuum. Therefore the single-mode squeezer that squeezes the high frequency tail of the Unruh radiation produces a squeezed vacuum state. Overall, when the Unruh effect is not significant, a uniformly accelerated single-mode squeezer produces the standard single-mode squeezed vacuum state. Otherwise, the product of the minimum and maximum variances is greater than one (see Fig. 8.8), indicating that the output state is mixed.

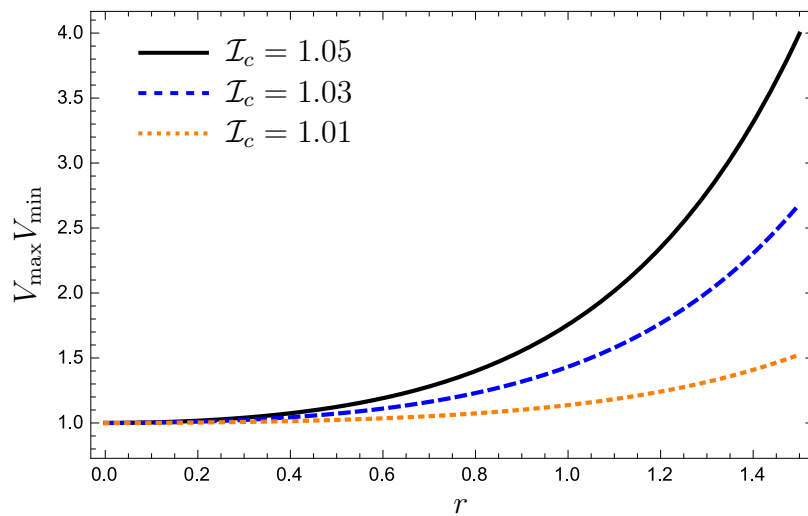


FIGURE 8.8: Product of maximum and minimum quadrature variances.

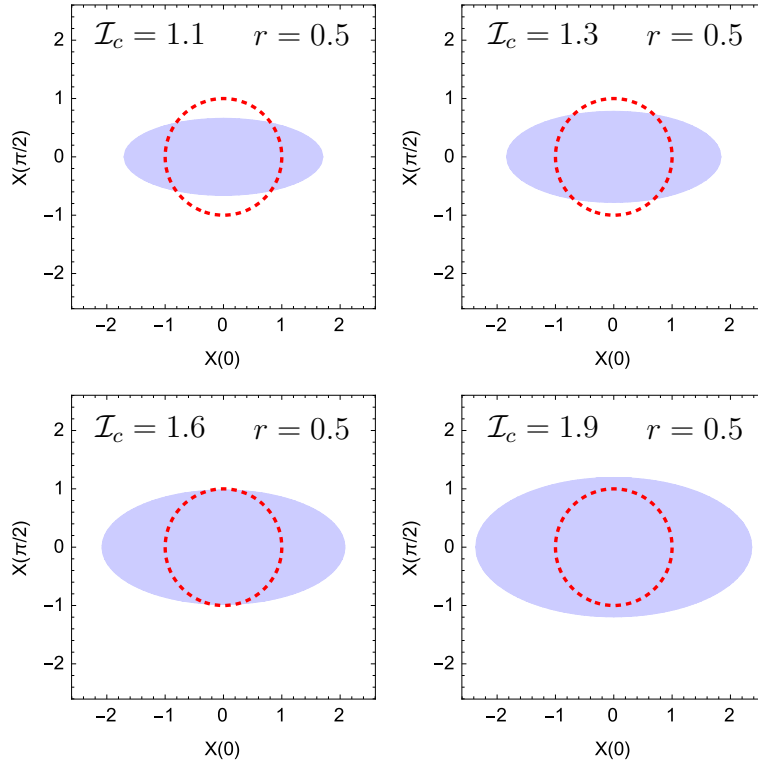


FIGURE 8.9: Phase space representation of quadrature in the final state. The red dashed circle represents the vacuum shot noise, and the blue shaded ellipse represents the quadrature variance of the output state. For fixed single-mode squeezing factor ( $r = 0.5$ ), the minimum quadrature variance is below the vacuum shot noise for small  $\mathcal{I}_c$ , indicating the output state is a squeezed state. While for large enough  $\mathcal{I}_c$ , the minimum quadrature variance surpasses the vacuum shot noise, showing that squeezing is destroyed.

As the Unruh effect in the Rindler frame becomes more pronounced, the decoherence in the Minkowski frame becomes stronger. Eventually squeezing disappears and the final state becomes classical in the sense that coherent state superpositions are removed and the state becomes decomposable into a mixture of coherent states. Fig. 8.9 shows an example of the phase space representation of the quadrature amplitude. For a given squeezing factor, the minimal variance  $V_{\min}$  increases as  $\mathcal{I}_c$  increases and eventually exceeds one, the vacuum shot noise. When  $\mathcal{I}_c < \frac{1}{2}(1 + \sqrt{1 + \coth(r/2)})$ , the minimum quadrature variance  $V_{\min}$  is smaller than one, indicating that the final state is still a squeezed state but with reduced amount of squeezing. When  $\mathcal{I}_c > \frac{1}{2}(1 + \sqrt{1 + \coth(r/2)})$ , the squeezing disappears. In the narrow bandwidth limit, we use the approximate relation between  $\mathcal{I}_c$  and  $\omega_0$  to find the distribution of minimum quadrature variance in terms of  $r$  and  $\omega_0$ , as shown in Fig. 8.10. A critical

curve, which is determined by

$$\frac{2\pi\omega_0}{a} = \ln \left( \frac{\sqrt{1 + \coth(r/2)} + 1}{\sqrt{1 + \coth(r/2)} - 1} \right), \quad (8.4.19)$$

separates the squeezing region and no squeezing region. When  $r \rightarrow \infty$ ,  $2\pi\omega_0/a \rightarrow 2 \ln(\sqrt{2} + 1) \approx 1.763$ . Below this value, one can always make the output state classical by increasing the single-mode squeezing factor  $r$ .

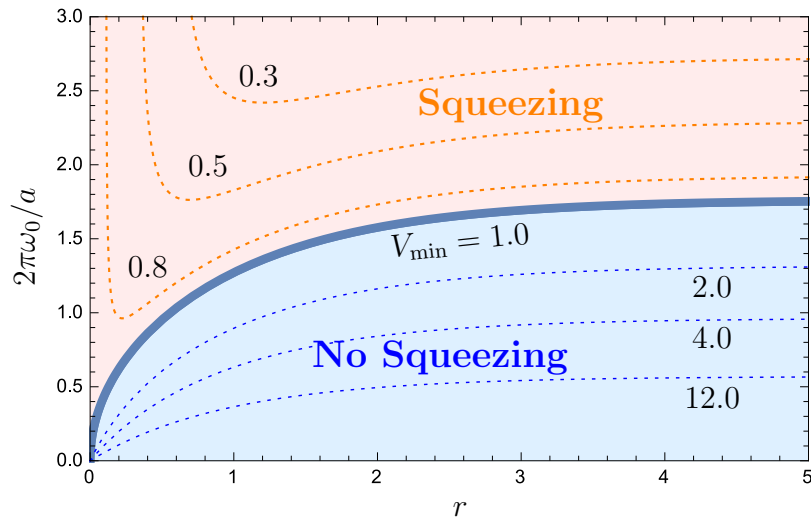


FIGURE 8.10: Distribution of minimum quadrature variance of the output state as a function of single-mode squeezing factor  $r$  and the central frequency  $\omega_0$  in the narrow bandwidth limit. A critical curve along which  $V_{\min} = 1.0$  separates the squeezing region and no squeezing region. In the squeezing region  $V_{\min} < 1.0$ , while in the no squeezing region  $V_{\min} > 1.0$ .

### 8.4.5 Connection to black hole information paradox

The decoherence effect we describe here is a previously unnoticed consequence of the transformation from the bipartite Hilbert space of the Rindler and Unruh modes, to the single Hilbert space of the Minkowski modes. Notice that in Eq. (8.4.5) any phase relationship between the left and right Unruh modes is lost in the construction of the Minkowski number operator. This means that interactions which lead to entanglement between the left and right Unruh modes, as occurs with the accelerated squeezer, will in general appear as decoherence with respect to measurements by inertial observers. Nevertheless, notice that the interaction with the accelerated squeezer is reversible in principle in the sense that the

Rindler mode can be unsqueezed by a second accelerated squeezer, thus returning the field to the Minkowski vacuum state. The accelerations required to generate this decoherence effect are well beyond those that can be produced in the lab. However, such accelerations do occur naturally in many regions of the universe. We also note that simulation of these effects using optical squeezing is possible with current technology and could allow an experimental investigation of the decoherence effect described here.

Because of the equivalence principle there is a strong relationship between gravity and acceleration [MTW73]. The analogous situation to Unruh radiation in curved space-time is that of thermal radiation from black holes (Hawking radiation) [Haw75]. In this case regaining unitarity is not straightforward because the analogue of the mirror image Rindler wedge lies behind the black hole event horizon and so is inaccessible. Given that in the far future the black hole is expected to completely evaporate, this leads to the black hole information paradox [Haw76]. In spite of many attempts [STU93, StHW94, Mat05, HPS16, BMT], a completely satisfactory resolution of this problem has not been found [AMPS13, BP13].

We believe the decoherence effect discussed in this section has significance for understanding quantum effects in gravitational systems. For example, our system can be viewed as a crude toy model for the creation and eventual evaporation of a black hole. We begin in the far past in a pure Minkowski vacuum state, before the formation of the black-hole. In the intermediate epoch accelerated observers, representing observers close to the black-hole, interact with the field modes. Finally in the far-future the black-hole has evaporated leaving flat space, however the field is left in a mixed state with respect to inertial observers. This may indicate a new direction for understanding the black-hole information paradox.

## 8.5 Summary

In this chapter, we discuss time dependent interactions between a uniform accelerated object and a massless quantum field. The switching on and off of the interactions is realized by making the accelerated objects only act on a localized Rindler wave packet mode. We first

constructed a circuit for narrow bandwidth Rindler wave packet modes and then generalized it to arbitrary wave packet modes. One of the advantages of this method is that it resolves the energy divergence problem we encountered in Chapter 7. Based on this circuit model, we focus on the problem of a uniformly accelerated single-mode squeezer. The most interesting discovery is that the output state from a uniformly accelerated single-mode squeezer becomes mixed as observed by inertial observers, given that the input state is pure. This decoherence effect may have important implications for the black hole information paradox.

# 9

## Particle Creation from Gravitational Perturbations Around Schwarzschild Black Holes

### 9.1 Introduction

Particle creation in curved spacetimes is a fundamental phenomenon and is a very important research topic in quantum field theory in curved spacetime [BD82, Wal94, PT09]. It usually occurs in highly dynamical spacetimes. In the very early universe, initial quantum fluctuations of curvature can be amplified by the exponentially expanding universe to form tiny perturbations on the background spacetime [MFB92], which play a crucial role in explaining the origin of the anisotropies of the cosmic microwave background (CMB) and the formation

of the large scale structure of the observed universe. Primordial gravitational waves are also expected to be generated in the early universe and their detection is one of the main targets of modern astrophysics. In addition to dynamical spacetimes, stationary or static spacetimes can also create quantum particles. Well-known examples include superradiance from a rotating black hole [Zel72, Mis72, Unr74], Unruh-Davies [Unr76, Dav75] radiation observed by a uniformly accelerated observer, and Hawking radiation from a Schwarzschild black hole [Haw75]. Although Hawking particles were observed in an analogue system recently [Ste16], detection of Hawking radiation from a real black hole remains elusive because the temperature of an astrophysical black hole ( $10^{-8}$  K) is much lower than the temperature of the CMB ( $\sim 2.7$  K).

One question of particular interest is whether gravitational waves (ripples of spacetime) can create quantum particles. Generally a dynamical spacetime generates particles, however it has been shown that particle creation by plane gravitational waves is forbidden [Gib75, Des75, GV91, Sor00]. A similar statement is applied to the electromagnetic waves: electron-positron pairs cannot be produced by plane electromagnetic waves, no matter how strong we make the electromagnetic field [Sch51]. If electron-positron pairs were created, momentum conservation would be violated. Pair production of electron and positron is possible if a nucleus is introduced to balance the momentum [Hub06]. In the gravitational wave case, one would expect that an analog to the nucleus, e.g., a black hole, has to be introduced to allow particle creation. From the theoretical perspective, it is very important and necessary to study this issue in details to determine whether and to what degree gravitational perturbations in a black hole spacetime can create particles. Recently, gravitational waves from the coalescence of two black holes were directly detected by the Laser Interferometer Gravitational-Wave Observatory (LIGO) [ea16b, ea16a]. The observed gravitational waves reveal dramatic change of spacetime when two black holes merge into one and carry away a huge amount of energy from the binary black hole system. If the gravitational perturbations can create particles, e.g., photons, they would travel along with the gravitational waves. These particles could be detected if the particle creation efficiency is high enough. So from the observational perspective, it is important to have a thorough study of this question.

In this chapter we address this question. Instead of studying the whole process of the coalescence of two black holes, a very complicated situation requiring numerical relativity [Leh01], we study the final stage of merging, where the ring-down is dominant. In particular, we are interested in the effects of the gravitational quasi-normal modes (QNMs) of a black hole, which have been extensively studied for decades [Nol99, KS99, BCS09, KZ11] and analytical techniques can be applied. We consider a massless Hermitian scalar field that propagates in the Schwarzschild background spacetime with quasi-normal perturbations. The scalar field is assumed to be minimally coupled with the spacetime. The coupling can be divided into two parts: coupling with Schwarzschild background spacetime and the QNMs. The former is well studied, whilst the latter is less known and is the main content of this chapter. We derive the interaction Hamiltonian for the scalar field, which shows that the QNMs play the role of a multimode squeezer, familiar in quantum optics. The QNMs “squeeze” the initial state (vacuum or thermal state) of the scalar field and produce particles.

This chapter is organized as follows. In Sec. 9.2, we briefly review the quantization of a massless scalar field in the Schwarzschild background spacetime. In Sec. 9.3, we review the gravitational QNMs for Schwarzschild black holes and list some important results for our calculations. In Sec. 9.4, we study the coupling between the scalar field and the gravitational QNMs, and derive the interaction Hamiltonian for the scalar field, based on which we show that the gravitational perturbations around a Schwarzschild black hole create particles. The results of this chapter have been accepted for publication in [SHMR17a].

## 9.2 Scalar field in curved spacetimes

We consider a Hermitian massless scalar field  $\Phi$  that minimally couples to the curved spacetime with metric  $g_{\mu\nu}$ . The Lagrangian density for the scalar field is [BD82]

$$\mathcal{L} = \frac{1}{2} \sqrt{-g} g^{\mu\nu} (\partial_\mu \Phi)(\partial_\nu \Phi), \quad (9.2.1)$$

where  $g$  is the determinant of  $g_{\mu\nu}$ . We assume that the metric  $g_{\mu\nu}$  can be decomposed into the background part  $g_{B\mu\nu}$  and the perturbation part  $h_{\mu\nu}$ , namely,  $g_{\mu\nu} = g_{B\mu\nu} + h_{\mu\nu}$ . The background metric usually possesses some symmetries (time-translation invariance, rotational invariance etc.) and the dynamics of the scalar field on the background spacetime is well established. The perturbation  $h_{\mu\nu}$  is assumed to be small so that perturbation theory is applicable. Expanding the Lagrangian density Eq. (9.2.1) with respect to  $h_{\mu\nu}$  and keeping terms to first order, we find

$$\mathcal{L} = \mathcal{L}_0 + \mathcal{L}_1, \quad (9.2.2)$$

where the background part  $\mathcal{L}_0$  and perturbed part  $\mathcal{L}_1$  are

$$\begin{aligned} \mathcal{L}_0 &= \frac{1}{2} \sqrt{-g_B} g_B^{\mu\nu} (\partial_\mu \Phi) (\partial_\nu \Phi), \\ \mathcal{L}_1 &= \frac{1}{4} \sqrt{-g_B} (h^\alpha{}_\alpha g_B^{\mu\nu} - 2h^{\mu\nu}) (\partial_\mu \Phi) (\partial_\nu \Phi), \end{aligned}$$

with  $g_B$  the determinant of the background metric and  $h^\alpha{}_\alpha \equiv g_{B\alpha\beta} h^{\alpha\beta}$  the trace of the metric perturbation. Note that we use the convention:  $h^{\mu\nu} \equiv g_B^{\mu\alpha} g_B^{\nu\beta} h_{\alpha\beta}$ . In this chapter, we are concerned with the Schwarzschild background spacetime, for which the line element in the Schwarzschild coordinates  $(t, r, \theta, \phi)$  is

$$ds^2 = -f(r) dt^2 + \frac{1}{f(r)} dr^2 + r^2 (d\theta^2 + \sin^2 \theta d\phi^2), \quad (9.2.3)$$

where  $f(r) = 1 - \frac{2M}{r}$  and  $M$  is the mass of the Schwarzschild black hole.

The canonically conjugate field of  $\Phi$  is also decomposed into background part and perturbed part,

$$\Pi = \Pi_0 + \Pi_1, \quad (9.2.4)$$

where

$$\begin{aligned} \Pi_0 &= \frac{\partial \mathcal{L}_0}{\partial (\partial_t \Phi)} = \sqrt{-g_B} g_B^{tt} (\partial_t \Phi), \\ \Pi_1 &= \frac{\partial \mathcal{L}_1}{\partial (\partial_t \Phi)} = -\frac{1}{2} \sqrt{-g_B} [h^{t\nu} (\partial_\nu \Phi) - h^\alpha{}_\alpha g_B^{tt} (\partial_t \Phi)]. \end{aligned}$$

The Hamiltonian density is

$$\mathcal{H} = \mathcal{H}_0 + \mathcal{H}_1, \quad (9.2.5)$$

where

$$\mathcal{H}_0 = \Pi_0(\partial_t\Phi) - \mathcal{L}_0 = \frac{1}{2}\sqrt{-g_B}[g_B^{tt}(\partial_t\Phi)^2 - g_B^{ij}(\partial_i\Phi)(\partial_j\Phi)] \quad (9.2.6)$$

is the unperturbed Hamiltonian density and

$$\mathcal{H}_1 = \Pi_1(\partial_t\Phi) - \mathcal{L}_1 = -\frac{1}{2}\sqrt{-g_B}[h^{tt}(\partial_t\Phi)^2 - h^{ij}(\partial_i\Phi)(\partial_j\Phi)] + \frac{1}{2}h^\alpha{}_\alpha\mathcal{H}_0 \quad (9.2.7)$$

is the perturbed Hamiltonian density. For the Schwarzschild background spacetime,  $\sqrt{-g_B} = r^2 \sin\theta$ , so the perturbed Hamiltonian

$$\begin{aligned} H_1 = \int d^3x \mathcal{H}_1 = \frac{1}{2} \int_{2M}^\infty dr \int_{4\pi} d\Omega r^2 \left\{ -h^{tt}(\partial_t\Phi)^2 + h^{ij}(\partial_i\Phi)(\partial_j\Phi) \right. \\ \left. + \frac{1}{2}h^\alpha{}_\alpha [g_B^{tt}(\partial_t\Phi)^2 - g_B^{ij}(\partial_i\Phi)(\partial_j\Phi)] \right\} \end{aligned} \quad (9.2.8)$$

where  $d\Omega = \sin\theta d\theta d\phi$ .

The dynamics of the scalar field on the background spacetime is determined by the unperturbed Lagrangian density  $\mathcal{L}_0$ . The quantization of the scalar field has been discussed in details in Section 4.6.2. The difference here is that we only consider the scalar field in region I. The scalar field operator can be expanded as

$$\hat{\Phi} = \sum_{l=0}^{\infty} \sum_{m=-l}^l \int_0^\infty d\omega \left( \hat{a}_{\omega lm} u_{\omega lm}^{\text{up}} + \hat{b}_{\omega lm} u_{\omega lm}^{\text{in}} + \text{h.c.} \right), \quad (9.2.9)$$

where the superscript ‘‘I’’ has been omitted for simplicity. The operators  $\hat{a}_{\omega lm}$  and  $\hat{b}_{\omega lm}$  represent upcoming and ingoing modes, respectively. They satisfy the boson commutation relations

$$\begin{aligned} [\hat{a}_{\omega lm}, \hat{a}_{\omega' l' m'}^\dagger] &= \delta(\omega - \omega') \delta_{ll'} \delta_{mm'}, \\ [\hat{b}_{\omega lm}, \hat{b}_{\omega' l' m'}^\dagger] &= \delta(\omega - \omega') \delta_{ll'} \delta_{mm'}, \\ [\hat{a}_{\omega lm}, \hat{b}_{\omega' l' m'}^\dagger] &= [\hat{a}_{\omega lm}, \hat{b}_{\omega' l' m'}] = 0. \end{aligned} \quad (9.2.10)$$

### 9.3 Gravitational quasi-normal modes

A Schwarzschild black hole is a static and spherically symmetric spacetime that is described by the Schwarzschild metric Eq. (9.2.3). Taking this metric to be the background metric  $g_{B\mu\nu}$ , gravitational perturbations  $h_{\mu\nu} = g_{\mu\nu} - g_{B\mu\nu}$  can arise through various physical processes, such as a star falling into the black hole. The equations governing the evolution of the perturbations were first derived by Regge and Wheeler [RW57], Zerilli [Zer70] in the Regge-Wheeler-Zerilli (RWZ) gauge. Due to the time-translation and rotational invariance of the Schwarzschild metric, the perturbations can be decomposed into eigenmodes with definite frequency and angular momentum. Furthermore, they can be classified as two distinct types: odd-parity (or magnetic-parity) and even-parity (or electric-parity) perturbations.

In the RWZ gauge, the odd-parity perturbations are characterized by two functions  $\tilde{h}_0(r)$  and  $\tilde{h}_1(r)$ . The nonzero components of  $h_{\mu\nu}$  are

$$\begin{aligned} h_{tA}^{(o)} &= \tilde{h}_0(r)e^{-i\omega t} X_A^{lm}(\theta, \phi), \\ h_{rA}^{(o)} &= \tilde{h}_1(r)e^{-i\omega t} X_A^{lm}(\theta, \phi), \end{aligned} \tag{9.3.1}$$

where  $A = \{\theta, \phi\}$ . Here  $\omega$  is the frequency of the perturbations, and  $X_A^{lm}$  is the odd-parity vector spherical harmonic on the unit two-sphere [MP05],

$$X_\theta^{lm} = -\csc\theta Y_{,\phi}^{lm}, \quad X_\phi^{lm} = \sin\theta Y_{,\theta}^{lm}, \tag{9.3.2}$$

where  $Y^{lm}(\theta, \phi)$  are the scalar spherical harmonics. The two functions  $\tilde{h}_0(r)$  and  $\tilde{h}_1(r)$  are not independent and can be expressed in terms of a single scalar function  $Q(r)$  as [RW57]

$$\tilde{h}_0 = -\frac{f}{i\omega} \frac{d}{dr} (rQ), \quad \tilde{h}_1 = \frac{rQ}{f}. \tag{9.3.3}$$

The scalar function  $Q(r)$  satisfies the equation

$$-\frac{d^2 Q}{dr_*^2} + V_l^{(o)} Q = \omega^2 Q \tag{9.3.4}$$

where

$$V_l^{(o)}(r) = f(r) \left[ \frac{l(l+1)}{r^2} - \frac{6M}{r^3} \right] \tag{9.3.5}$$

is the odd-parity effective potential.

In the RWZ gauge, the even-parity perturbations are characterized by three functions:  $\tilde{H}_0(r)$ ,  $\tilde{H}_1(r)$  and  $\tilde{K}(r)$ . The nonzero components of  $h_{\mu\nu}$  are

$$\begin{aligned} h_{tt}^{(e)} &= f(r)\tilde{H}_0(r)e^{-i\omega t}Y^{lm}, \\ h_{tr}^{(e)} &= \tilde{H}_1(r)e^{-i\omega t}Y^{lm}, \\ h_{rr}^{(e)} &= \frac{\tilde{H}_0(r)}{f(r)}e^{-i\omega t}Y^{lm}, \\ h_{AB}^{(e)} &= r^2\Omega_{AB}\tilde{K}(r)e^{-i\omega t}Y^{lm}, \end{aligned} \quad (9.3.6)$$

where  $\Omega_{AB} = \text{diag}\{1, \sin^2\theta\}$  is the metric on the unit two-sphere.  $\tilde{H}_0(r)$ ,  $\tilde{H}_1(r)$  and  $\tilde{K}(r)$  can be expressed in terms of the Zerilli function  $Z(r)$  as [NZC<sup>+</sup>12]

$$\begin{aligned} \tilde{K} &= \left[ \frac{\lambda(\lambda+1)r^2 + 3\lambda Mr + 6M^2}{r^2(\lambda r + 3M)} \right] Z + \sqrt{f}Z_{,r}, \\ \tilde{H}_1 &= -i\omega \left[ \frac{\lambda r^2 - 3\lambda Mr - 3M^2}{(r-2M)(\lambda r + 3M)} \right] Z - i\omega r Z_{,r}, \\ \tilde{H}_0 &= \left[ \frac{\lambda r(r-2M) - \omega^2 r^4 + M(r-3M)}{(r-2M)(\lambda r + 3M)} \right] \tilde{K} + \left[ \frac{(\lambda+1)M - \omega^2 r^3}{i\omega r(\lambda r + 3M)} \right] \tilde{H}_1, \end{aligned} \quad (9.3.7)$$

where

$$\lambda = \frac{1}{2}(l-1)(l+2). \quad (9.3.8)$$

The Zerilli function satisfies the equation

$$-\frac{d^2 Z}{dr_*^2} + V_l^{(e)} Z = \omega^2 Z \quad (9.3.9)$$

with the even-parity effective potential

$$V_l^{(e)}(r) = f(r) \left[ \frac{2\lambda^2(\lambda+1)r^3 + 6\lambda^2 Mr^2 + 18\lambda M^2 r + 18M^3}{r^3(\lambda r + 3M)^2} \right]. \quad (9.3.10)$$

The boundary conditions for QNMs are that on the event horizon there is only ingoing mode,

$$Q(Z) \sim e^{-i\omega r_*}, \quad r_* \rightarrow -\infty \quad (r \rightarrow 2M) \quad (9.3.11)$$

and at the spatial infinity there is only outgoing mode,

$$Q(Z) \sim e^{i\omega r_*}, \quad r_* \rightarrow +\infty \quad (r \rightarrow +\infty). \quad (9.3.12)$$

The above boundary conditions imply that the perturbations are dissipative: waves can escape either to infinity or into the black hole. The frequencies of the QNMs are complex,

$$\omega = \omega_R - i\omega_I \quad (9.3.13)$$

where  $\omega_I$  is positive and characterizes the decay of the QNMs. For a Schwarzschild black hole, there is a discrete infinity of QNMs. The QNM frequencies depend on  $l$  and also an integer  $n$  called overtone number [SW85a, Lea85].

Based on the Newman-Penrose (NP) null-tetrad formalism [NP62], another approach has been developed to study gravitational perturbations in a Schwarzschild background [Pri72, BP73]. This more general method has been generalized to study neutrino, electromagnetic and gravitational perturbations in a Kerr background spacetime [Teu72, Teu73, PT73, TP74]. In this framework, gravitational perturbations are represented by two field quantities  $\psi_s$  with  $s = \pm 2$ , which are related to the Weyl scalars [NP62] and satisfy the Teukolsky's master equation [Teu72]. For the Schwarzschild case, one can take the limit  $a \rightarrow 0$  ( $a$  is the angular momentum per unit mass of the Kerr black hole) in the master equation to obtain the corresponding field equation for  $\psi_s$ . This quantity can be decomposed as

$$\psi_s = e^{-i\omega t} {}_s Y_{lm}(\theta, \phi) {}_s R_{\omega l}(r) \quad (9.3.14)$$

where  ${}_s Y_{lm}$  is the spin-weighted spherical harmonic [GMN<sup>+</sup>67],  ${}_s R_{\omega l}(r)$  is the radial function satisfying the equation [BP73]

$$\left\{ \Delta_r^{-s} \frac{d}{dr} \left( \Delta_r^{s+1} \frac{d}{dr} \right) + \left[ \frac{r^4 \omega^2 - 2isr^2(r-M)\omega}{\Delta_r} + 4is\omega r - (l-s)(l+s+1) \right] \right\} {}_s R_{\omega l}(r) = 0, \quad (9.3.15)$$

where  $\Delta_r = r(r-2M)$ . At large distance from the black hole, the asymptotic solutions of  ${}_s R_{\omega l}$  are

$${}_s R_{\omega l} \sim \frac{e^{-i\omega r^*}}{r}, \quad \text{and} \quad {}_s R_{\omega l} \sim \frac{e^{i\omega r^*}}{r^{2s+1}} \quad (9.3.16)$$

whereas very close to the event horizon

$${}_s R_{\omega l} \sim \Delta_r^{-s} e^{-i\omega r^*}, \quad \text{and} \quad {}_s R_{\omega l} \sim e^{i\omega r^*}. \quad (9.3.17)$$

For quasi-normal modes, the boundary conditions are: only outgoing modes at spatial infinity and ingoing modes on the future horizon,

$${}_sR_{\omega l} \sim \begin{cases} C_{\omega l} \Delta_r^{-s} e^{-i\omega r_*}, & r_* \rightarrow -\infty; \\ D_{\omega l} e^{i\omega r_*} / r^{2s+1}, & r_* \rightarrow +\infty. \end{cases} \quad (9.3.18)$$

where  $C_{\omega l}$  and  $D_{\omega l}$  are the amplitude of the QNM at the event horizon and spatial infinity, respectively.

The explicit expressions for the components of the metric perturbation  $h_{\mu\nu}$  are very important when considering the coupling between the gravitational perturbations and the quantum fields. Chrzanowski, Cohen and Kegeles (CCK) developed a procedure to reconstruct the metric perturbation  $h_{\mu\nu}$  in the *ingoing* and *outgoing* radiation gauges from the field quantity  $\psi_s$  [Chr75, CK74, KC79]. Roughly speaking, the CCK procedure consists of two steps. The first step is to relate the field quantity  $\psi_s$  to the so-called Hertz potential  $\Psi$ , which also satisfies the master equation with spin weight  $s = -2$ . The second step is to find the relation between  $h_{\mu\nu}$  and the Hertz potential  $\Psi$  [Chr75]. The first explicit calculation of the relation between the Hertz potential  $\Psi$  and  $\psi_s$  for the Schwarzschild black hole was done by Lousto and Whiting [LW02]. Generalization to the Kerr black hole was performed by Ori [Ori03], Yunes and Gonzalez [YG06].

In the ingoing and outgoing gauges, the trace of the metric perturbation  $h^\alpha{}_\alpha$  vanishes in the whole spacetime [Chr75]. In the ingoing gauge the perturbation  $h_{\mu\nu}$  is transverse at past null infinity and at the future horizon. Thus it is a suitable gauge to study the gravitational effects near the event horizon. While in the outgoing gauge,  $h_{\mu\nu}$  is transverse in the future null infinity and at the past horizon. It is therefore a suitable gauge for studying gravitational effects at spatial infinity, e.g., gravitational waves emitted by a black hole. Since it is reasonable to expect that the interaction between metric perturbations and quantum fields is strong near the event horizon, we therefore work in the ingoing radiation gauge throughout this chapter.

Following the CCK procedure, Nichols *et al.* [NZC<sup>+</sup>12] derived explicit expressions for the metric perturbation  $h_{\mu\nu}$  in the Schwarzschild background spacetime in the ingoing radiation gauge. For the odd(magnetic)-parity perturbations, the nonzero components are

$$\begin{aligned}
 h_{tA}^{(o)} &= -fh_{rA}^{(o)} = \frac{\sqrt{D}}{2f\sqrt{2l(l+1)}} \Re \left\{ \left[ \frac{d}{dr_*} - \left( i\omega + \frac{2f}{r} \right) \right] {}_{-2}R_{\omega l} ({}_{-1}Y_{lm}m_A + {}_1Y_{lm}m_A^*) e^{-i\omega t} \right\}, \\
 h_{AB}^{(o)} &= \frac{1}{f^2} \Re \left\{ \left[ (i\omega r^2 - M) \frac{d}{dr_*} - \left( \frac{1}{2}\mu^2 f - i\omega(-3r + 7M) - \omega^2 r^2 \right) \right] {}_{-2}R_{\omega l} \right. \\
 &\quad \left. \times ({}_{-2}Y_{lm}m_A m_B - {}_2Y_{lm}m_A^* m_B^*) e^{-i\omega t} \right\}, \tag{9.3.19}
 \end{aligned}$$

where  $D = (l+2)!/(l-2)!$ ,  $\mu^2 = (l-1)(l+2)$ ,  $\Re$  represents the real part of some function, and  $m_A = \frac{1}{\sqrt{2}}(1, i \sin \theta)$  is a vector on the unit-sphere with its index raised by the metric  $\Omega^{AB}$ . For even(electric)-parity perturbations,

$$\begin{aligned}
 h_{tt}^{(e)} &= -fh_{tr}^{(e)} = f^2 h_{rr}^{(e)} = -\frac{2\sqrt{D}}{r^2} \Re \left\{ {}_{-2}R_{\omega l} Y_{lm} e^{-i\omega t} \right\}, \\
 h_{tA}^{(e)} &= -fh_{rA}^{(e)} = \frac{\sqrt{D}}{2f\sqrt{2l(l+1)}} \Re \left\{ \left[ \frac{d}{dr_*} - \left( i\omega + \frac{2f}{r} \right) \right] {}_{-2}R_{\omega l} ({}_{-1}Y_{lm}m_A - {}_1Y_{lm}m_A^*) e^{-i\omega t} \right\}, \\
 h_{AB}^{(e)} &= \frac{1}{f^2} \Re \left\{ \left[ (i\omega r^2 - M) \frac{d}{dr_*} - \left( \frac{1}{2}\mu^2 f - i\omega(-3r + 7M) - \omega^2 r^2 \right) \right] {}_{-2}R_{\omega l} \right. \\
 &\quad \left. \times ({}_{-2}Y_{lm}m_A m_B + {}_2Y_{lm}m_A^* m_B^*) e^{-i\omega t} \right\}. \tag{9.3.20}
 \end{aligned}$$

Note that the metric perturbation in the ingoing radiation gauge is related to that in the RWZ gauge, Eqs. (9.3.1) and (9.3.6), by a gauge transformation.

## 9.4 Coupling between scalar field and odd-parity QNMs

In the absence of gravitational perturbations, the scalar field  $\Phi$  evolves freely on the Schwarzschild background spacetime. Its dynamics is dominated by the unperturbed Lagrangian density  $\mathcal{L}_0$ . If the Schwarzschild background spacetime is perturbed, the scalar field would couple to the gravitational perturbations. The dynamics of it is governed by the interaction Hamiltonian  $H_1$ , Eq. (9.2.8), as well. It is a general phenomenon that quantum particles are generated in a dynamical spacetime, e.g., the exponentially expanding universe [?, MFB92]. Our particular interest is in whether or not gravitational perturbations in a Schwarzschild

background can produce particles. It is well known that the plane gravitational waves do not produce particles [Gib75, Des75, GV91, Sor00]; Were it otherwise, momentum conservation would be violated. As we shall demonstrate, the situation is different for spherical perturbations. We will show that gravitational perturbations in a Schwarzschild background do generate scalar particles and that angular momentum is conserved in this process.

In order to know the state evolution of the scalar field, one needs to find the explicit expression for the interaction Hamiltonian  $\hat{H}_1$  (we restore a hat from now on to indicate that we consider a quantized scalar field) which contains first order terms of the components of the metric perturbation  $h_{\mu\nu}$ . An appropriate gauge can be chosen so that the interaction Hamiltonian  $\hat{H}_1$  takes a relatively simple form. Throughout this discussion we will work in the ingoing radiation gauge. There are several advantages of choosing this gauge. First, it is straightforward to generalize the calculations to the Kerr background case. Second, it is expected that the coupling between gravitational perturbations and the scalar field is strong around the event horizon so it is more convenient to use the ingoing radiation gauge. Third, the trace of the metric perturbation vanishes in this gauge,  $h^\alpha_\alpha = 0$ . Consequently Eq. (9.2.8) is simplified:

$$\hat{H}_1 = \frac{1}{2} \int_{2M}^{\infty} r^2 dr \int_{4\pi} d\Omega \left[ -h^{tt} (\partial_t \hat{\Phi})^2 + h^{rr} (\partial_r \hat{\Phi})^2 + 2h^{rA} (\partial_r \hat{\Phi})(\partial_A \hat{\Phi}) + h^{AB} (\partial_A \hat{\Phi})(\partial_B \hat{\Phi}) \right]. \quad (9.4.1)$$

where we have replaced  $x^i$  by  $\{r, A\}$ , with  $A, B = \{\theta, \phi\}$ . In what follows we will consider the effects of both odd-parity and even-parity QNMs with frequency  $\omega_0 = \omega_R - i\omega_I$  and angular momentum  $l_0, m_0$ .

### 9.4.1 Interaction Hamiltonian from odd-parity QNMs

For simplicity, we only consider the coupling between upcoming and upcoming modes, and neglect the superscript ‘‘up’’ without introducing any confusion. Couplings between upcoming and ingoing modes, ingoing and ingoing modes are also possible, which we leave for future work. Since for odd-parity perturbations,  $h_{tt}^{(o)} = h_{rr}^{(o)} = 0$ , the relevant terms in Eq.

(9.4.1) are  $(\partial_r \hat{\Phi})(\partial_A \hat{\Phi})$  and  $(\partial_A \hat{\Phi})(\partial_B \hat{\Phi})$ . Using the expansion of the scalar field operator, Eq. (9.2.9), and the explicit expression of the upcoming mode function, Eq. (4.6.5), we find

$$\begin{aligned} & (\partial_r \hat{\Phi})(\partial_A \hat{\Phi}) \\ &= \sum_{l,l'} \sum_{m,m'} \int d\omega \int d\omega' \frac{1}{4\pi\sqrt{\omega\omega'}} \left[ \hat{a}_{\omega lm} \hat{a}_{\omega' l' m'} e^{-i(\omega+\omega')t} \partial_r \left( \frac{R_{\omega l}}{r} \right) \left( \frac{R_{\omega' l'}}{r} \right) Y_{lm} (\partial_A Y_{l' m'}) \right. \\ & \quad \left. + \hat{a}_{\omega lm} \hat{a}_{\omega' l' m'}^\dagger e^{-i(\omega-\omega')t} \partial_r \left( \frac{R_{\omega l}}{r} \right) \left( \frac{R_{\omega' l'}}{r} \right) Y_{lm} (\partial_A Y_{l' m'}^*) + \text{h.c.} \right]. \end{aligned} \quad (9.4.2)$$

$$\begin{aligned} & (\partial_A \hat{\Phi})(\partial_B \hat{\Phi}) \\ &= \sum_{l,l'} \sum_{m,m'} \int d\omega \int d\omega' \frac{1}{4\pi\sqrt{\omega\omega'}} \left[ \hat{a}_{\omega lm} \hat{a}_{\omega' l' m'} e^{-i(\omega+\omega')t} \left( \frac{R_{\omega l}}{r} \right) \left( \frac{R_{\omega' l'}}{r} \right) (\partial_A Y_{lm}) (\partial_B Y_{l' m'}) \right. \\ & \quad \left. + \hat{a}_{\omega lm} \hat{a}_{\omega' l' m'}^\dagger e^{-i(\omega-\omega')t} \left( \frac{R_{\omega l}}{r} \right) \left( \frac{R_{\omega' l'}}{r} \right) (\partial_A Y_{lm}) (\partial_B Y_{l' m'}^*) + \text{h.c.} \right]. \end{aligned} \quad (9.4.3)$$

From Eq. (9.3.19) we see that  $h_{rA}^{(o)}$  and  $h_{AB}^{(o)}$  contain terms that are proportional to  $e^{-i\omega_0 t} = e^{-\omega_I t} e^{-i\omega_R t}$  and  $(e^{-i\omega_0 t})^* = e^{-\omega_I t} e^{i\omega_R t}$ . When multiplying with  $(\partial_r \hat{\Phi})(\partial_A \hat{\Phi})$  and  $(\partial_A \hat{\Phi})(\partial_B \hat{\Phi})$  we get terms containing factors

$$e^{\pm i(\omega_R - \omega - \omega')t}, \quad e^{\pm i(\omega_R + \omega + \omega')t}, \quad e^{\pm i(\omega_R + \omega - \omega')t}, \quad e^{\pm i(\omega_R - \omega + \omega')t}.$$

In the rotating-wave approximation, terms with the lowest frequency oscillations  $e^{\pm i(\omega_R - \omega - \omega')t}$  dominate over more highly oscillatory terms. This approximation ensures that the energy is approximately conserved,  $\omega_R \approx \omega + \omega'$ . Substituting Eqs. (9.3.19), (9.4.2) and (9.4.3) into Eq. (9.4.1) we have in this approximation

$$\begin{aligned} \hat{H}_1^{(o)} &\approx \frac{1}{16\pi} e^{-\omega_I t} \sum_{l,l'} \sum_{m,m'} \int d\omega \int d\omega' \frac{1}{\sqrt{\omega\omega'}} \left[ e^{-i(\omega_R - \omega - \omega')t} (\mathcal{I}_{r1} \mathcal{I}_{a1} + \mathcal{I}_{r2} \mathcal{I}_{a2}) \hat{a}_{\omega lm}^\dagger \hat{a}_{\omega' l' m'}^\dagger \right. \\ & \quad \left. + e^{i(\omega_R - \omega - \omega')t} (\mathcal{I}_{r1}^* \mathcal{I}_{a1}^* + \mathcal{I}_{r2}^* \mathcal{I}_{a2}^*) \hat{a}_{\omega lm} \hat{a}_{\omega' l' m'} \right], \end{aligned} \quad (9.4.4)$$

where  $\mathcal{I}_{r1}$  and  $\mathcal{I}_{r2}$  are the radial integrals,

$$\begin{aligned} \mathcal{I}_{r1} &= -\frac{\sqrt{D_0}}{\sqrt{2l_0(l_0+1)}} \int_{2M}^{\infty} dr \frac{1}{f} \left[ \frac{d}{dr_*} {}_{-2}R_{\omega_0 l_0} - \left( i\omega_0 + \frac{2f}{r} \right) {}_{-2}R_{\omega_0 l_0} \right] \partial_r \left( \frac{R_{\omega l}}{r} \right) \left( \frac{R_{\omega' l'}}{r} \right), \\ \mathcal{I}_{r2} &= \int_{2M}^{\infty} dr \frac{1}{r^2 f^2} \left[ (i\omega_0 r^2 - M) \frac{d}{dr_*} {}_{-2}R_{\omega_0 l_0} - \left( \frac{1}{2} \mu_0^2 f - i\omega_0(-3r + 7M) - \omega_0^2 r^2 \right) {}_{-2}R_{\omega_0 l_0} \right] \\ & \quad \times \left( \frac{R_{\omega l}}{r} \right) \left( \frac{R_{\omega' l'}}{r} \right), \end{aligned} \quad (9.4.5)$$

$\mathcal{I}_{a1}$  and  $\mathcal{I}_{a2}$  are the angular integrals,

$$\mathcal{I}_{a1}(l_0, m_0; l, m; l', m') = \int_{4\pi} d\Omega (-{}_1Y_{l_0 m_0} m^A + {}_1Y_{l_0 m_0} m^{A*}) Y_{lm}^* (\partial_A Y_{l'm'}^*), \quad (9.4.6)$$

$$\mathcal{I}_{a2}(l_0, m_0; l, m; l', m') = \int_{4\pi} d\Omega (-{}_2Y_{l_0 m_0} m^A m^B - {}_2Y_{l_0 m_0} m^{A*} m^{B*}) (\partial_A Y_{lm}^*) (\partial_B Y_{l'm'}^*). \quad (9.4.7)$$

Since the Hamiltonian (9.6.3) is quadratic in creation (and annihilation) operators, it is clear that it describes multimode squeezing. The quantity  $\mathcal{I}_{r1}\mathcal{I}_{a1} + \mathcal{I}_{r2}\mathcal{I}_{a2}$  plays the role of a phase matching function, the nonzero value of which would imply that the gravitational perturbations generate quantum particles.

### 9.4.2 Radial integral

It is difficult to find exactly analytic results for the radial integrals  $\mathcal{I}_{r1}$  and  $\mathcal{I}_{r2}$  because we do not have analytic solutions for  ${}_{-2}R_{\omega_0 l_0}$  and  $R_{\omega l}$ . One might expect they can be calculated numerically. It turns out that the calculation of the radial integrals is not trivial because of the peculiar property of the radial function of the QNMs. When  $r_* \rightarrow +\infty$  (spatial infinity), the integrands of  $\mathcal{I}_{r1}$  and  $\mathcal{I}_{r2}$  are both proportional to  $e^{i(\omega_0 - \omega - \omega')r_*}$  according to Eqs. (9.3.18) and (4.6.9); when  $r_* \rightarrow -\infty$  (event horizon), they are proportional to  $e^{-i(\omega_0 - \omega - \omega')r_*}$ . The QNM frequency is a complex number,  $\omega_0 = \omega_R - i\omega_I$ , so the integrands are proportional to  $e^{\omega_I r_*}$  when  $r_* \rightarrow +\infty$ , and  $e^{-\omega_I r_*}$  when  $r_* \rightarrow -\infty$ . Since  $\omega_I > 0$ , the integrands are divergent at the spatial infinity and on the event horizon, which implies the radial integrals are not well defined.

Leaver [Lea86] proposed a method to overcome this difficulty by exploiting the analyticity of the integrand in  $r_*$ . A new contour is chosen such that the integral along this contour is finite. Sun and Price [SP88] discussed in detail how to construct Leaver's contour by analytic continuation and restored a factor that is missed in [Lea86]. Similar techniques were also used by Yang *et al* [YZL15] to define the inner product of the radial function of the QNMs. In this thesis, we follow the method of Leaver (taking into account the missing factor) to regularize the radial integral to obtain a finite result. By using Leaver's method, the radial

integral can be in principle calculated numerically. In order to obtain an approximately analytic result, we assume that the main contribution to the integration is from the region near the event horizon, that is,  $r \sim 2M$ . This is because the coupling between the QNMs and scalar field near the horizon is expected to be stronger. This assumption can be also justified by looking at the asymptotic behaviour of the integrand along the contour at infinity, which is exponentially suppressed. To further simplify the result, we assume that the imaginary part of the QNM frequencies are small. This is rather a crude approximation because the imaginary part of the QNM frequencies of a Schwarzschild black hole are not so small. However this approximation is adequate for the purpose of this thesis.

Noting that  $r = 2M$  and  $r = \infty$  are two branch points, the branch cut can be chosen as a line perpendicular to the real  $r$  axis, starting at  $r = 2M$  and ending at  $r = \infty$ . It lies in the upper complex  $r$  plane if  $\omega_R - \omega - \omega' > 0$ , as shown in Fig. 9.1, and in the lower complex  $r$  plane if  $\omega_R - \omega - \omega' < 0$ . When  $\omega_R - \omega - \omega' > 0$ , the contour  $C$  begins at  $r = \infty$ , right next to the branch cut, moves downward to  $r = 2M$ , where it wraps and, left next to the branch cut, moves upward to  $r = \infty$ , as shown in Fig. 9.1. We refer to the region near  $r = 2M$  as the *in* region and the region around  $r = \infty$  as the *out* region, as schematically represented by the shaded region in Fig. 9.1. By analytically extending the integrands to the complex  $r$  plane we see that along the contour  $C$  the integrands exponentially decay in the *out* region, which can remove the formal divergence. In addition, the exponential decay of the integrands in the *out* region implies that the main contributions to the integrals are from the *in* region.

We describe in detail how to find the approximately analytic result for the radial integral  $\mathcal{I}_{r1}$ ; the result for  $\mathcal{I}_{r2}$  can be obtained in a similar way. At spatial infinity, by using Eqs.

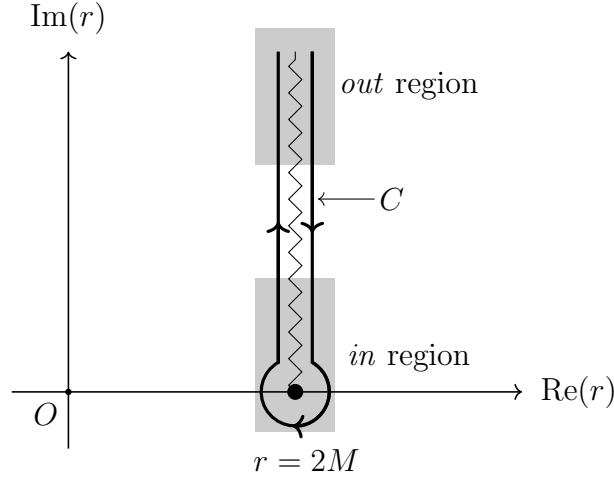


FIGURE 9.1: The contour  $C$  and branch cut for  $\omega_R - \omega - \omega' > 0$ . The two shaded regions are referred to as *in* (close to the horizon) and *out* (around  $r = \infty$ ) regions, respectively.

(9.3.18) and (4.6.9), the integrand of  $\mathcal{I}_{r_1}$  can be approximated as

$$\begin{aligned}
& \frac{1}{f} \left[ \left( \frac{d}{dr_*} - i\omega_0 - \frac{2f}{r} \right) {}_{-2}R_{\omega_0 l_0} \right] \frac{d}{dr} \left( \frac{R_{\omega l}^*}{r} \right) \left( \frac{R_{\omega' l'}^*}{r} \right) \\
& \approx -B_{\omega l}^* B_{\omega' l'}^* D_{\omega_0 l_0} \left( \frac{i\omega}{f} + \frac{1}{r} \right) e^{i(\omega_0 - \omega - \omega')r_*} \\
& \approx -\frac{B_{\omega l}^* B_{\omega' l'}^* D_{\omega_0 l_0}}{2M} \left[ i\Omega x (x-1)^{-1+i\Delta} + x^{-1} (x-1)^{i\Delta} \right] e^{i\Delta x}, \tag{9.4.8}
\end{aligned}$$

where we have defined dimensionless quantities  $x = r/2M$ ,  $\Delta = 2M(\omega_0 - \omega - \omega')$ ,  $\Omega = 2M\omega$ ,  $\Omega_0 = 2M\omega_0$ ,  $\Omega' = 2M\omega'$ . Near the event horizon, according to Eqs. (9.3.18) and (4.6.9), the integrand of  $\mathcal{I}_{r_1}$  can be approximated as

$$\begin{aligned}
& \frac{1}{f} \left[ \left( \frac{d}{dr_*} - i\omega_0 - \frac{2f}{r} \right) {}_{-2}R_{\omega_0 l_0} \right] \frac{d}{dr} \left( \frac{R_{\omega l}^*}{r} \right) \left( \frac{R_{\omega' l'}^*}{r} \right) \\
& \approx 2A_{\omega l}^* A_{\omega' l'}^* C_{\omega_0 l_0} \left[ x^{-1} (1 - i\Omega_0 x) (i\Omega x - 1) (x-1)^{1-i\Delta} + i\Omega (1 - i\Omega_0 x) (x-1)^{-i\Delta} \right] e^{-i\Delta x}, \tag{9.4.9}
\end{aligned}$$

where we have only kept the term proportional to  $e^{-i(\omega_0 - \omega - \omega')r_*}$  owing to the rotating wave approximation. As discussed before, the integration along the real axis is formally divergent. The integrands Eqs. (9.4.8) and (9.4.9) are analytically extended to the whole complex  $r$  plane. Along the contour  $C$  in the *out* region,  $e^{i\Delta x} \sim e^{-2M\omega_I|x|}$ , which means the integrand of  $\mathcal{I}_{r_1}$  exponentially decays. We therefore expect that the integral  $\mathcal{I}_{r_1}$  is finite along the contour

$C$ . Unfortunately, we cannot find an analytic expression for the integrand on the whole contour  $C$ . Numerical techniques need to be introduced to perform the contour integration. However, it may be possible that an approximate result can be obtained by using only the asymptotic behaviour of the integrand. Note that in the *out* region the integrand (9.4.8) exponentially decays and contributes very little to the total integral. Introducing another exponential decaying function in the *out* region would not introduce large deviation to the integral. We therefore replace Eq. (9.4.8) by Eq. (9.4.9) with the factor  $e^{-i\Delta x}$  replaced by  $e^{i\Delta x}$ . In the *in* region, the asymptotic expression for the integrand is Eq. (9.4.9) which dominates the contribution to the integral. We expect that most pairs of particles that are produced satisfy the energy conservation condition,  $\omega_R = \omega + \omega'$ , and furthermore the imaginary part of the QNM frequency is usually small. We thus can take the limit of  $i\Delta \sim 0$ , so that  $e^{-i\Delta x} \approx e^{i\Delta x}$ . The exponential factor  $e^{-i\Delta x}$  in Eq. (9.4.9) is replaced by  $e^{i\Delta x}$  and an approximate asymptotic expression is obtained. In a word, we approximate the original integrand by

$$\begin{aligned} & \frac{1}{f} \left[ \left( \frac{d}{dr_*} - i\omega_0 - \frac{2f}{r} \right) {}_{-2}R_{\omega_0 l_0} \right] \frac{d}{dr} \left( \frac{R_{\omega l}^*}{r} \right) \left( \frac{R_{\omega' l'}^*}{r} \right) \\ & \approx 2A_{\omega l}^* A_{\omega' l'}^* C_{\omega_0 l_0} \left[ x^{-1} (1 - i\Omega_0 x) (i\Omega x - 1) (x - 1)^{1-i\Delta} + i\Omega (1 - i\Omega_0 x) (x - 1)^{-i\Delta} \right] e^{i\Delta x} \end{aligned} \quad (9.4.10)$$

along the whole contour  $C$ . Obviously, this is a very crude approximation since we have ignored the behaviour of the integrand in the intermediate region. The validity of this approximation has to be verified by numerical calculation. However, we expect that this approximation provides a lower bound for the exact integral since near the horizon we replace an exponentially growing function by an exponentially decaying function. The advantage of this approximation is that we can obtain an analytic result for the radial integral  $\mathcal{I}_{r_1}$ .

From Eq. (9.4.10) we see that basically we need to calculate

$$\oint_C dx e^{i\Delta x} (x - 1)^{n_1 - i\Delta} x^{n_2} \quad (9.4.11)$$

where  $n_1, n_2$  are two integers,  $C$  is the contour we introduce, as shown in Fig. 9.1. Defining

a new variable  $u = i\Delta(x - 1)$ , we have [MF53]

$$\begin{aligned}
& \oint_C dx e^{i\Delta x} (x - 1)^{n_1 - i\Delta} x^{n_2} \\
&= (i\Delta)^{i\Delta - n_1 - 1} \oint_F du e^u u^{n_1 - i\Delta} \left(1 + \frac{u}{i\Delta}\right)^{n_2} \\
&= \frac{2\pi i (-1)^{n_1 + 1 - i\Delta} e^{i\Delta}}{\Gamma(-n_1 + i\Delta)} U(n_1 + 1 - i\Delta, n_1 + n_2 + 2 - i\Delta, -i\Delta), \tag{9.4.12}
\end{aligned}$$

where  $F$  is the contour illustrated by Morse and Feshbach's Fig. 5.1.2 [MF53],  $\Gamma(z)$  is the Gamma's function and  $U(a, c, z)$  is the confluent hypergeometric function [AS72]. Therefore the radial integral  $\mathcal{I}_{r1}$  can be approximated as

$$\begin{aligned}
\mathcal{I}_{r1} &\approx -\frac{8\pi M i \sqrt{D_0}}{\sqrt{2l_0(l_0 + 1)}} \frac{A_{\omega l}^* A_{\omega' l'}^* C_{\omega_0 l_0} e^{i\Delta}}{1 - e^{2\pi\Omega_0}} \left\{ \frac{(-1)^{2 - i\Delta}}{\Gamma(-1 + i\Delta)} \left[ \Omega\Omega_0 U(2 - i\Delta, 4 - i\Delta, -i\Delta) \right. \right. \\
&\quad \left. \left. + i(\Omega + \Omega_0) U(2 - i\Delta, 3 - i\Delta, -i\Delta) - U(2 - i\Delta, 2 - i\Delta, -i\Delta) \right] \right. \\
&\quad \left. + \frac{(-1)^{1 - i\Delta}}{\Gamma(i\Delta)} \left[ \Omega\Omega_0 U(1 - i\Delta, 3 - i\Delta, -i\Delta) + i\Omega U(1 - i\Delta, 2 - i\Delta, -i\Delta) \right] \right\} \\
&\approx -\frac{8\pi M i \sqrt{D_0}}{\sqrt{2l_0(l_0 + 1)}} A_{\omega l}^* A_{\omega' l'}^* e^{i\Delta} C_{\omega_0 l_0} \left\{ \frac{(i\Delta)^{i\Delta - 2}}{\Gamma(-1 + i\Delta)} \left[ -\frac{2\Omega\Omega_0}{i\Delta} + 2\Omega\Omega_0 + i(\Omega + \Omega_0) \right] \right. \\
&\quad \left. - \frac{(-1)^{2 - i\Delta}}{\Gamma(-1 + i\Delta)} U(2 - i\Delta, 2 - i\Delta, -i\Delta) + \frac{(i\Delta)^{i\Delta - 1}}{\Gamma(i\Delta)} \left( -\frac{\Omega\Omega_0}{i\Delta} + 2\Omega\Omega_0 + i\Omega \right) \right\}, \tag{9.4.13}
\end{aligned}$$

where we have used the fact that [NIS]

$$U(a, a + n + 1, z) = \frac{z^{-a}}{\Gamma(a)} \sum_{k=0}^n \binom{n}{k} \Gamma(a + k) z^{-k}, \tag{9.4.14}$$

with  $n = 0, 1, 2, \dots$ . In the limit of  $i\Delta \sim 0$ , from Eq. (9.4.13) we obtain the dominant term

$$\mathcal{I}_{r1} \approx -\frac{\sqrt{D_0}}{\sqrt{2l_0(l_0 + 1)}} \frac{16\pi i M \Omega \Omega_0}{(i\Delta)^2} \frac{A_{\omega l}^* A_{\omega' l'}^* C_{\omega_0 l_0}}{1 - e^{2\pi\Omega_0}}. \tag{9.4.15}$$

The calculation of the radial integral  $\mathcal{I}_{r2}$  is very similar and we put the details in Appendix A (Section 9.8.1). The dominant term of  $\mathcal{I}_{r2}$  in the limit of  $i\Delta \sim 0$  is

$$\mathcal{I}_{r2} \approx \frac{16\pi i M \Omega_0^2}{(i\Delta)^2} \frac{A_{\omega l}^* A_{\omega' l'}^* C_{\omega_0 l_0}}{1 - e^{2\pi\Omega_0}}. \tag{9.4.16}$$

### 9.4.3 Angular integral

In order to calculate the the angular integrals  $\mathcal{I}_{a1}$  and  $\mathcal{I}_{a2}$ , we need to know the explicit expressions for the spin weighted spherical harmonics  ${}_{\pm 1}Y_{lm}$  and  ${}_{\pm 2}Y_{lm}$ . The spin weighted spherical harmonics  ${}_sY_{lm}$  for integers  $s, l, m$  is defined from the spherical harmonics  $Y_{lm}$  [GMN<sup>+</sup>67],

$${}_sY_{lm} = \begin{cases} \sqrt{\frac{(l-s)!}{(l+s)!}} \bar{\partial}^s Y_{lm}, & 0 \leq s \leq l; \\ \sqrt{\frac{(l+s)!}{(l-s)!}} (-1)^s \bar{\partial}^{-s} Y_{lm}, & -l \leq s \leq 0, \end{cases} \quad (9.4.17)$$

where  $\bar{\partial}$  and  $\bar{\partial}$  are the spin-raising and spin-lowering operators, respectively. Assume that  $\eta$  is a quantity of spin-weight  $s$ , then  $\bar{\partial}\eta$  is a quantity of spin-weight  $s + 1$ ,

$$\bar{\partial}\eta \equiv -(\sin \theta)^s \left( \frac{\partial}{\partial \theta} + \frac{i}{\sin \theta} \frac{\partial}{\partial \phi} \right) [(\sin \theta)^{-s} \eta]; \quad (9.4.18)$$

and  $\bar{\partial}\eta$  is a quantity of spin-weight  $s - 1$ ,

$$\bar{\partial}\eta \equiv -(\sin \theta)^{-s} \left( \frac{\partial}{\partial \theta} - \frac{i}{\sin \theta} \frac{\partial}{\partial \phi} \right) [(\sin \theta)^s \eta]. \quad (9.4.19)$$

According to the definition (9.4.17), we derive in detail the explicit expressions for  ${}_{\pm 1}Y_{lm}$  and  ${}_{\pm 2}Y_{lm}$  in Appendix B (Section 9.8.2). In terms of associated Legendre functions  $P_l^m(\cos \theta)$ , we find

$${}_{\pm 1}Y_{lm} = \frac{1}{2} (-1)^m \sqrt{\frac{2l+1}{4\pi} \frac{(l-1)! (l-m)!}{(l+1)! (l+m)!}} \left( \mp P_l^{m+1} \pm c_{lm}^2 P_l^{m-1} + \frac{2m}{\sin \theta} P_l^m \right) e^{im\phi}, \quad (9.4.20)$$

$$\begin{aligned} {}_{\pm 2}Y_{lm} &= \frac{1}{4} (-1)^m \sqrt{\frac{2l+1}{4\pi} \frac{(l-2)! (l-m)!}{(l+2)! (l+m)!}} \left[ P_l^{m+2} + c_{lm}^2 c_{l,m-1}^2 P_l^{m-2} - 2 \left( \cot \theta \pm \frac{2m}{\sin \theta} \right) P_l^{m+1} \right. \\ &\quad \left. + 2 \left( \cot \theta \pm \frac{2m}{\sin \theta} \right) c_{lm}^2 P_l^{m-1} + \left( -c_{lm}^2 - c_{l,m+1}^2 + \frac{4m^2}{\sin^2 \theta} \pm \frac{8m \cot \theta}{\sin \theta} \right) P_l^m \right] e^{im\phi}, \end{aligned} \quad (9.4.21)$$

where  $c_{lm} = \sqrt{(l+m)(l-m+1)}$ . Eqs. (9.8.20) and (9.8.21) can be further transformed to eliminate the trigonometric functions by using the recurrence properties of the associated Legendre functions [AS72]. Finally, the calculation of the angular integral is reduced to the evaluation of the integrals of the products of three associated Legendre functions,

$$\mathcal{I}_{P3}(l_1, m_1; l_2, m_2; l_3, m_3) = \int_{-1}^1 d\mu P_{l_1}^{m_1}(\mu) P_{l_2}^{m_2}(\mu) P_{l_3}^{m_3}(\mu). \quad (9.4.22)$$

where  $\mu \equiv \cos \theta$ . The integral  $\mathcal{I}_{P_3}$  has an analytic result and is shown in Appendix C (Section 9.8.3). Therefore, the angular integrals can always be calculated although the calculation is tedious in the general case.

For simplicity we consider a special case where the angular momentum of the QNMs along the  $z$  direction is zero, that is,  $m_0 = 0$ . This simplifies the calculation a lot and is sufficient to demonstrate quantum particle generation by the QNMs. It is easy to show that, if we let  $m = 0$  in Eqs. (9.8.20) and (9.8.21),

$$\pm_1 Y_{l0} = \mp \sqrt{\frac{2l+1}{4\pi} \frac{(l-1)!}{(l+1)!}} P_l^1, \quad (9.4.23)$$

$$\pm_2 Y_{l0} = \sqrt{\frac{2l+1}{4\pi} \frac{(l-2)!}{(l+2)!}} P_l^2. \quad (9.4.24)$$

We thus immediately find

$$\mathcal{I}_{a1} = \sqrt{2} \int d\Omega \, {}_{-1}Y_{l_0 0} Y_{lm}^* \left( \frac{i}{\sin \theta} \partial_\phi Y_{l'm'}^* \right), \quad (9.4.25)$$

$$\mathcal{I}_{a2} = \int d\Omega \, {}_{-2}Y_{l_0 0} \left[ (\partial_\theta Y_{lm}^*) \left( \frac{i}{\sin \theta} \partial_\phi Y_{l'm'}^* \right) + \left( \frac{i}{\sin \theta} \partial_\phi Y_{lm}^* \right) (\partial_\theta Y_{l'm'}^*) \right]. \quad (9.4.26)$$

The integration over  $\phi$  gives rise to a  $\delta$ -function  $\delta_{m', -m}$ , which implies that the produced pair of particles have opposite angular momentum along the  $z$  direction. This is not surprising given that  $m_0 = 0$  and is an illustration of the angular momentum conservation in the particle production process.

Using the recurrence properties

$$\begin{aligned} \partial_\theta P_l^m &= \frac{1}{2} [P_l^{m+1} - (l+m)(l-m+1)P_l^{m-1}], \\ \frac{m}{\sin \theta} P_l^m &= -\frac{1}{2} [P_{l-1}^{m+1} + (l+m)(l+m-1)P_{l-1}^{m-1}] \end{aligned}$$

of the associated Legendre function, the angular integral  $\mathcal{I}_{a1}$  and  $\mathcal{I}_{a2}$  becomes

$$\mathcal{I}_{a1} = -\sqrt{2}\pi \delta_{m', -m} \mathcal{K}_{l_0 1}^{lm l' m'} \int_{-1}^1 d\mu \, P_{l_0}^1 P_l^m [P_{l'-1}^{m'+1} + (l' + m')(l' + m' - 1)P_{l'-1}^{m'-1}], \quad (9.4.27)$$

$$\begin{aligned}
 \mathcal{I}_{a2} = & -\frac{\pi}{2} \delta_{m', -m} \mathcal{K}_{l_0 2}^{lm'l'm'} \int_{-1}^1 d\mu P_{l_0}^2 \left\{ [P_l^{m+1} - (l+m)(l-m+1)P_l^{m-1}] \right. \\
 & \times [P_{l'-1}^{m'+1} + (l'+m')(l'+m'-1)P_{l'-1}^{m'-1}] \\
 & \left. + [P_{l-1}^{m+1} + (l+m)(l+m-1)P_{l-1}^{m-1}] [P_{l'}^{m'+1} - (l'+m')(l'-m'+1)P_{l'}^{m'-1}] \right\},
 \end{aligned} \tag{9.4.28}$$

where the factor  $\mathcal{K}_{LM}^{lm'l'm'}$  is defined as

$$\mathcal{K}_{LM}^{lm'l'm'} = \sqrt{\frac{(2L+1)(2l+1)(2l'+1)(L-M)!(l-m)!(l'-m')!}{(4\pi)^3 (L+M)!(l+m)!(l'+m')!}} \tag{9.4.29}$$

Now  $\mathcal{I}_{a1}$  and  $\mathcal{I}_{a2}$  can be explicitly calculated by using the result of  $\mathcal{I}_{P3}(l_1, m_1; l_2, m_2; l_3, m_3)$ . As an example, we calculate the angular integrals  $\mathcal{I}_{a1}$  and  $\mathcal{I}_{a2}$  for a QNM with angular momentum  $(l_0, m_0) = (2, 0)$  and a pair of scalar particles, the first of which with angular momentum  $(l, m) = (1, 1)$  and the other  $(l', -1)$ . We find that the particle  $(1, 1)$  only couples with those particles with  $l' = 2$ , namely, the only nonzero  $\mathcal{I}_{a1}$  and  $\mathcal{I}_{a2}$  are

$$\mathcal{I}_{a1}(2, 0; 1, 1; 2, -1) = -\frac{1}{2} \sqrt{\frac{3}{\pi}}, \quad \mathcal{I}_{a2}(2, 0; 1, 1; 2, -1) = \sqrt{\frac{3}{2\pi}}. \tag{9.4.30}$$

## 9.5 QNM as multimode squeezer

In the last two subsections, we have analytically calculated the angular integrals, and derived approximately analytic expressions for the radial integrals for odd-parity QNMs. We thus can obtain the interaction Hamiltonian  $\hat{H}_1^{(o)}$ , which dominates the evolution of the scalar field. Given the approximate results we will estimate the strength of the coupling between the QNMs and the scalar field. The time evolution operator is

$$\hat{U}^{(o)} = \hat{T} \exp \left\{ -i \int_0^\infty dt \hat{H}_1^{(o)}(t) \right\}, \tag{9.5.1}$$

where  $\hat{T}$  is the time ordering operator. In the weak-coupling regime [WLBR06], the time ordering is not important so that we can approximate the time evolution operator as

$$\hat{U}^{(o)} \approx \exp \left\{ -i \int_0^\infty dt \hat{H}_1^{(o)}(t) \right\}, \tag{9.5.2}$$

and the integration over  $t$  can be directly evaluated. Using the integration

$$\int_0^\infty dt e^{-\omega t} e^{-i(\omega_R - \omega - \omega')t} = \frac{1}{i[(\omega_R - \omega - \omega') - i\omega_I]}, \quad (9.5.3)$$

we have

$$\begin{aligned} \hat{U}^{(o)} &= \bigotimes_{lm} \bigotimes_{l'm'} \hat{U}_{lm'l'm'}^{(o)}, \\ \hat{U}_{lm'l'm'}^{(o)} &\approx \exp \left\{ -i \int d\omega \int d\omega' \left[ \mathcal{F}_{lm'l'm'}^{(o)}(\omega, \omega') \hat{a}_{\omega lm}^\dagger \hat{a}_{\omega' l'm'}^\dagger + \text{h.c.} \right] \right\} \end{aligned} \quad (9.5.4)$$

where

$$\mathcal{F}_{lm'l'm'}^{(o)}(\omega, \omega') = \frac{4iM^3 A_{\omega l}^* A_{\omega' l'm'}^* C_{\omega_0 l_0}}{\sqrt{\Omega \Omega'} (1 - e^{2\pi \Omega_0})} \frac{1}{(i\Delta)^3} \left[ \Omega_0^2 \mathcal{I}_{a2} - \frac{\sqrt{D_0}}{\sqrt{2l_0(l_0 + 1)}} \Omega \Omega_0 \mathcal{I}_{a1} \right]. \quad (9.5.5)$$

It is evident that Eq. (9.5.4) represents a multimode squeezing operator and  $\mathcal{F}_{lm'l'm'}^{(o)}(\omega, \omega')$  is known as the joint frequency distribution. Eq. (9.5.5) shows that the joint frequency distribution  $\mathcal{F}_{lm'l'm'}^{(o)}(\omega, \omega')$  is not zero, indicating that there would be scalar particle creation. If the initial state of the scalar field is a vacuum state (the Boulware vacuum), the QNMs would squeeze the vacuum and produce a squeezed vacuum state; if the initial state is a thermal state, e.g., Hawking thermal radiation, the QNMs would squeeze the Hawking thermal radiation and amplify it. In a word, the presence of QNMs would squeeze any state of the scalar field, amplify it and produce scalar particles. The energy of producing particle is from the QNMs. This is the main conclusion of this chapter.

In Eq. (9.5.5),  $A_{\omega l}$  is the reflection amplitude (see Eq. (4.6.9)) of the upcoming scalar field mode determined by the effective potential, Eq. (4.6.7). Fig. 9.2 shows the effective potential of the scalar field for several low angular quantum number  $l$ . For a given  $l$ , the effective potential peaks around  $r_* = 2M$  with its maximum depending on  $l$ , higher for bigger  $l$ . Unfortunately, there is no analytic expression for the reflection amplitude, however, we can infer the qualitative behaviour of  $A_{\omega l}$ . If the frequency of the field mode is lower than the maximum of the effective potential, most of the field mode is reflected; whilst if the frequency is higher than the peak of the effective potential, the field mode almost penetrates through the potential. Fig. 9.3 shows the numerical results of the reflection coefficients,  $|A_{\omega l}|^2$ .

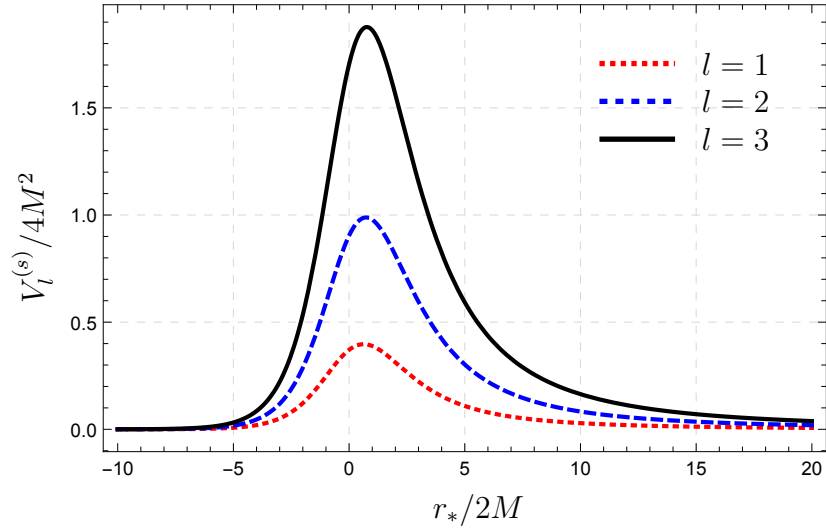


FIGURE 9.2: The effective potential for scalar field modes.

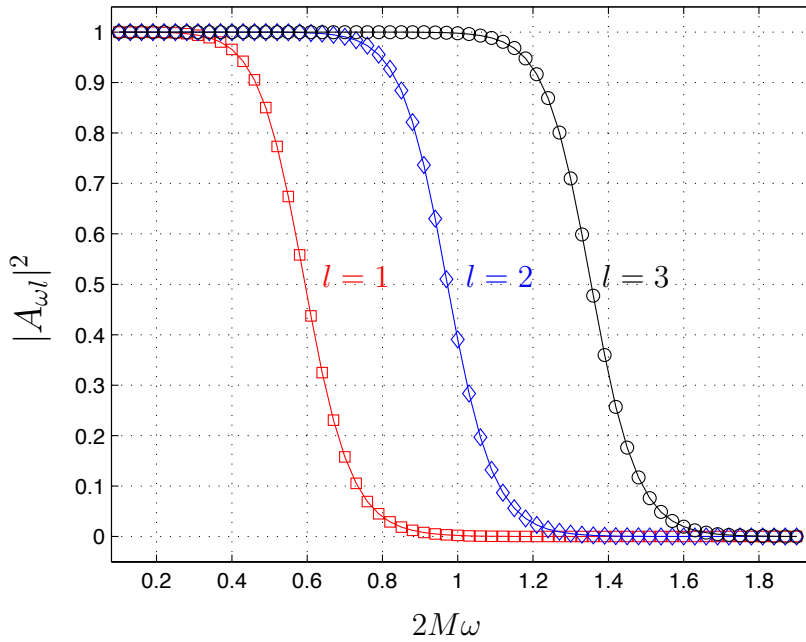


FIGURE 9.3: Reflection coefficient for the scalar field modes.

After knowing the behaviour of the reflection amplitude, we can study the behaviour of the joint frequency distribution. The factor  $\Delta$  is defined as

$$\Delta \equiv 2M(\omega_0 - \omega - \omega') = (\Omega_R - \Omega - \Omega') - i\Omega_I, \quad (9.5.6)$$

where  $\Omega_R = 2M\omega_R$ ,  $\Omega_I = 2M\omega_I$ . Therefore we have

$$\frac{1}{|\Delta|^3} = \frac{1}{[(\Omega_R - \Omega - \Omega')^2 + \Omega_I^2]^{3/2}}. \quad (9.5.7)$$

This is a distribution with respect to  $\Omega$  and  $\Omega'$  that peaks along the line  $\Omega + \Omega' = \Omega_R$ , the maximum of which is  $1/\Omega_I^3$ . Here  $\Omega_R - \Omega - \Omega'$  can be considered as the frequency detuning, and  $\Omega_I$  can be considered as the decay rate which also characterizes the width of the distribution Eq. (9.5.7). If  $\Omega_I$  is small, the distribution Eq. (9.5.7) is nonzero only for  $\Omega + \Omega' \approx \Omega_R$ . This is an indication of energy conservation: the sum of the frequencies of the pair of scalar particles should be equal to the real part of the QNM frequency. Figs. 9.4 and 9.5 show an example of the absolute value of the joint frequency distribution,  $|\mathcal{F}_{lm'l'}^{(o)}(\omega, \omega')|$ . We can see that basically  $|\mathcal{F}_{lm'l'}^{(o)}(\omega, \omega')|$  follows the energy-conservation line  $\Omega + \Omega' \approx \Omega_R$ . The high frequency part is suppressed by the reflection amplitude  $A_{\omega l}$ ; while in the low frequency regime,  $|A_{\omega l}|$  is almost one and the factor  $1/\sqrt{\Omega\Omega'}$  dominates. The latter is annoying because that means the joint frequency distribution is divergent at  $\Omega = 0$  or  $\Omega' = 0$ . At the current stage, we assume that there exists a low frequency cutoff so that the joint frequency distribution is finite. We leave this for future work and do not worry about the low frequency behaviour here.

We can compute a crude estimate of the maximum of the joint frequency distribution. Assume that in Eq. (9.5.5),  $\Omega \sim \Omega' \sim \Omega_R/2$ ,  $|A_{\omega l}| \sim |A_{\omega' l'}| \sim 1/\sqrt{2}$  and the contribution from the angular integral part is at the order of unity, we find

$$|\mathcal{F}_{lm'l'}^{(o)}|_{\max} \sim 4M^3 \left(\frac{\Omega_R}{\Omega_I}\right) \left(\frac{1}{\Omega_I^2}\right) \frac{|C_{\omega_0 l_0}|}{|1 - e^{2\pi(\Omega_R - i\Omega_I)}|}. \quad (9.5.8)$$

This is an approximate relation between the squeezing amplitude (or the strength of coupling) and various parameters of the black hole and QNM. Here  $\Omega_R$  is the resonance frequency of the QNM and  $\Omega_I$  characterizes the decay rate. If we make an analogy with an optical cavity [BR04],  $\Omega_R/\Omega_I$  can be considered as the quality factor of the QNM. We see that the squeezing amplitude is proportional to the cube of the black hole mass, the amplitude of the QNM at the event horizon, the quality factor of the QNM, and is inversely proportional to the square of the decay rate. This means the strength of coupling is stronger for longer lasting

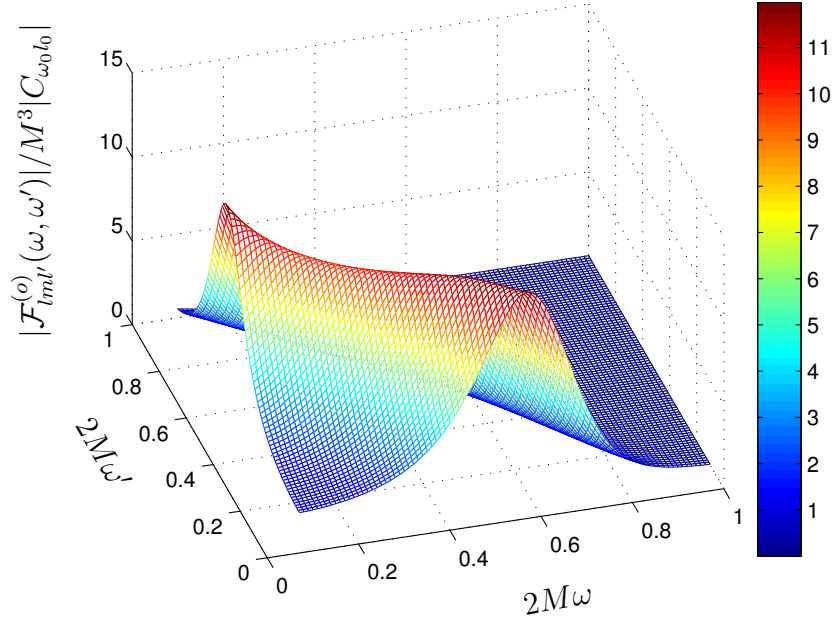


FIGURE 9.4: Modulus of the joint frequency distribution. QNM:  $\Omega_R = 0.7474, \Omega_I = 0.178, (l_0, m_0) = (2, 0)$ . Scalar particle one:  $(l, m) = (1, 1)$ ; scalar particle two:  $(l', m') = (2, -1)$ .

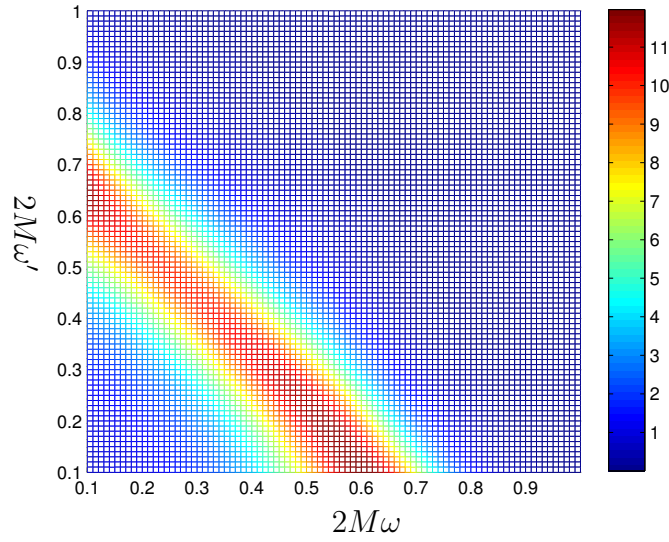


FIGURE 9.5: Density plot of the modulus of the joint frequency distribution. QNM:  $\Omega_R = 0.7474, \Omega_I = 0.178, (l_0, m_0) = (2, 0)$ . Scalar particle one:  $(l, m) = (1, 1)$ ; scalar particle two:  $(l', m') = (2, -1)$ .

QNMs, larger amplitude of QNMs and bigger black holes. However for Schwarzschild black holes the QNMs decay very fast and the least damping QNM is the fundamental QNM for which the overtone number is  $n = 0$  [BCS09]. For example, for the fundamental QNM of

$(l_0, m_0) = (2, 0)$ ,  $\Omega_R = 0.7474$  and  $\Omega_I = 0.178$  [BCS09]. Substituting these into Eq. (9.5.8), we find

$$|\mathcal{F}_{lm'l'}^{(o)}|_{\max} \sim 5M^3 |C_{\omega_0 l_0}|. \quad (9.5.9)$$

## 9.6 Coupling between scalar field and even-parity QNMs

The procedure to evaluate the coupling between the scalar field and the even-parity QNMs is similar. For the even-parity perturbations,  $h_{tt}^{(e)} \neq 0$ ,  $h_{rr}^{(e)} \neq 0$ , so we also need  $(\partial_t \hat{\Phi})(\partial_t \hat{\Phi})$  and  $(\partial_r \hat{\Phi})(\partial_r \hat{\Phi})$  in Eq. (9.4.1), which is

$$\begin{aligned} & (\partial_t \hat{\Phi})(\partial_t \hat{\Phi}) \\ = & \sum_{l=0}^{\infty} \sum_{l'=0}^{\infty} \sum_{m=-l}^l \sum_{m'=-l'}^{l'} \int d\omega \int d\omega' \frac{1}{4\pi\sqrt{\omega\omega'}} \left[ -\omega\omega' \hat{a}_{\omega lm} \hat{a}_{\omega' l' m'} e^{-i(\omega+\omega')t} \left(\frac{R_{\omega l}}{r}\right) \left(\frac{R_{\omega' l'}}{r}\right) Y_{lm} Y_{l'm'} \right. \\ & \left. + \omega\omega' \hat{a}_{\omega lm} \hat{a}_{\omega' l' m'}^\dagger e^{-i(\omega-\omega')t} \left(\frac{R_{\omega l}}{r}\right) \left(\frac{R_{\omega' l'}}{r}\right) Y_{lm} Y_{l'm'}^* + \text{h.c.} \right]. \end{aligned} \quad (9.6.1)$$

$$\begin{aligned} & (\partial_r \hat{\Phi})(\partial_r \hat{\Phi}) \\ = & \sum_{l=0}^{\infty} \sum_{l'=0}^{\infty} \sum_{m=-l}^l \sum_{m'=-l'}^{l'} \int d\omega \int d\omega' \frac{1}{4\pi\sqrt{\omega\omega'}} \left[ \hat{a}_{\omega lm} \hat{a}_{\omega' l' m'} e^{-i(\omega+\omega')t} \partial_r \left(\frac{R_{\omega l}}{r}\right) \partial_r \left(\frac{R_{\omega' l'}}{r}\right) Y_{lm} Y_{l'm'} \right. \\ & \left. + \hat{a}_{\omega lm} \hat{a}_{\omega' l' m'}^\dagger e^{-i(\omega-\omega')t} \partial_r \left(\frac{R_{\omega l}}{r}\right) \partial_r \left(\frac{R_{\omega' l'}}{r}\right) Y_{lm} Y_{l'm'}^* + \text{h.c.} \right]. \end{aligned} \quad (9.6.2)$$

Substituting Eqs. (9.3.20) and Eq. (9.2.9) into Eq. (9.4.1), and taking into account the rotating wave approximation, we have

$$\begin{aligned} \hat{H}_1^{(e)} \approx & \frac{1}{16\pi} e^{-\omega_I t} \sum_{l,l'} \sum_{m,m'} \int d\omega \int d\omega' \frac{1}{\sqrt{\omega\omega'}} \left\{ e^{-i(\omega_R - \omega - \omega')t} \hat{a}_{\omega lm}^\dagger \hat{a}_{\omega' l' m'}^\dagger [(\mathcal{I}_{r3} + \mathcal{I}_{r4}) \mathcal{I}_{a3} \right. \\ & \left. + \mathcal{I}_{r1} \mathcal{I}_{a4} + \mathcal{I}_{r2} \mathcal{I}_{a5}] + \text{h.c.} \right\}, \end{aligned} \quad (9.6.3)$$

where the radial integrals  $\mathcal{I}_{r1}$  and  $\mathcal{I}_{r2}$  are defined in the last section, Eq. (9.4.5),  $\mathcal{I}_{r3}$  and  $\mathcal{I}_{r4}$  are

$$\mathcal{I}_{r3} = -\omega\omega' \sqrt{D_0} \int_{2M}^{\infty} dr \frac{1}{f^2} {}_{-2}R_{\omega_0 l_0} \left(\frac{R_{\omega l}}{r}\right) \left(\frac{R_{\omega' l'}}{r}\right), \quad (9.6.4)$$

$$\mathcal{I}_{r4} = -\sqrt{D_0} \int_{2M}^{\infty} dr {}_{-2}R_{\omega_0 l_0} \partial_r \left(\frac{R_{\omega l}}{r}\right) \partial_r \left(\frac{R_{\omega' l'}}{r}\right). \quad (9.6.5)$$

The angular integrals  $\mathcal{I}_{a3}$ ,  $\mathcal{I}_{a4}$ ,  $\mathcal{I}_{a5}$  are

$$\mathcal{I}_{a3}(l_0, m_0; l, m; l', m') = \int_{4\pi} d\Omega Y_{l_0 m_0} Y_{lm}^* Y_{l'm'}^*, \quad (9.6.6)$$

$$\mathcal{I}_{a4}(l_0, m_0; l, m; l', m') = \int_{4\pi} d\Omega (-{}_1Y_{l_0 m_0} m^A - {}_1Y_{l_0 m_0} m^{A*}) Y_{lm}^* (\partial_A Y_{l'm'}^*), \quad (9.6.7)$$

$$\mathcal{I}_{a5}(l_0, m_0; l, m; l', m') = \int_{4\pi} d\Omega (-{}_2Y_{l_0 m_0} m^A m^B + {}_2Y_{l_0 m_0} m^{A*} m^{B*}) (\partial_A Y_{lm}^*) (\partial_B Y_{l'm'}^*). \quad (9.6.8)$$

The radial integral  $\mathcal{I}_{r3}$  and  $\mathcal{I}_{r4}$  can be calculated similarly to that for  $\mathcal{I}_{r1}$ ; details are in Appendix A (Section 9.8.1). In the limit  $i\Delta \sim 0$ , we find

$$\mathcal{I}_{r3} \approx -\mathcal{I}_{r4} \approx -\frac{8\pi i \sqrt{D_0} M \Omega \Omega' A_{\omega l}^* A_{\omega' l'}^* C_{\omega_0 l_0}}{(i\Delta)^2 (1 - e^{2\pi\Omega_0})}. \quad (9.6.9)$$

This implies  $\mathcal{I}_{r3} + \mathcal{I}_{r4} \approx 0$ .

It turns out that  $\mathcal{I}_{a3}$  can be easily obtained and expressed in terms of the 3- $j$  symbols,

$$\mathcal{I}_{a3} = (-1)^{m_0} \sqrt{\frac{(2l_0 + 1)(2l + 1)(2l' + 1)}{4\pi}} \begin{pmatrix} l & l' & l_0 \\ 0 & 0 & 0 \end{pmatrix} \begin{pmatrix} l & l' & l_0 \\ -m & -m' & m_0 \end{pmatrix}, \quad (9.6.10)$$

which is zero when  $m_0 \neq m + m'$ . Taking into account the property of the 3- $j$  symbols,  $\mathcal{I}_{a3}$  vanishes when  $l_0 + l + l'$  is an odd integer. If we consider the special case where the angular momentum of the quasi-normal modes along the  $z$  direction is zero, that is  $m_0 = 0$ , the calculation of the other angular integrals can be simplified. We have

$$\mathcal{I}_{a4} = \sqrt{2} \int d\Omega {}_{-1}Y_{l_0 0} Y_{lm}^* (\partial_\theta Y_{l'm'}^*), \quad (9.6.11)$$

$$\mathcal{I}_{a5} = \int d\Omega {}_{-2}Y_{l_0 0} \left[ (\partial_\theta Y_{lm}^*) (\partial_\theta Y_{l'm'}^*) + \left( \frac{i}{\sin \theta} \partial_\phi Y_{lm}^* \right) \left( \frac{i}{\sin \theta} \partial_\phi Y_{l'm'}^* \right) \right]. \quad (9.6.12)$$

Using the recurrence properties of the associated Legendre function as before, the angular integral  $\mathcal{I}_{a4}$  and  $\mathcal{I}_{a5}$  become

$$\mathcal{I}_{a4} = \sqrt{2\pi} \delta_{m', -m} \mathcal{K}_{l_0 1}^{lm l' m'} \int_{-1}^1 d\mu P_{l_0}^1 P_l^m [P_{l'}^{m'+1} - (l' + m')(l' - m' + 1) P_{l'}^{m'-1}], \quad (9.6.13)$$

	$l' = 1$	$l' = 3$
$\mathcal{I}_{a4}(2, 0; 1, 1; l', -1)$	$\frac{1}{2}\sqrt{\frac{3}{5\pi}}$	$-4\sqrt{\frac{6}{35\pi}}$
$\mathcal{I}_{a5}(2, 0; 1, 1; l', -1)$	$\sqrt{\frac{3}{10\pi}}$	$2\sqrt{\frac{3}{35\pi}}$

TABLE 9.1: Nonzero  $\mathcal{I}_{a4}$  and  $\mathcal{I}_{a5}$  for a QNM  $(l_0, m_0) = (2, 0)$  and a pair of scalar particles:  $(l, m) = (1, 1)$  and  $(l', -1)$ .

$$\begin{aligned}
\mathcal{I}_{a5} = & \frac{\pi}{2} \delta_{m', -m} \mathcal{K}_{l_0 2}^{lm'l'm'} \int_{-1}^1 d\mu P_{l_0}^2 \left\{ [P_l^{m+1} - (l+m)(l-m+1)P_l^{m-1}] \right. \\
& \times [P_{l'}^{m'+1} - (l'+m')(l'-m'+1)P_{l'}^{m'-1}] \\
& \left. + [P_{l-1}^{m+1} + (l+m)(l+m-1)P_{l-1}^{m-1}] [P_{l'-1}^{m'+1} + (l'+m')(l'+m'-1)P_{l'-1}^{m'-1}] \right\},
\end{aligned} \tag{9.6.14}$$

where the factor  $\mathcal{K}_{LM}^{lm'l'm'}$  is by Eq. (9.4.29). As an example, we calculate the angular integrals  $\mathcal{I}_{a4}$  and  $\mathcal{I}_{a5}$  for a QNM with angular momentum  $(l_0, m_0) = (2, 0)$  and a pair of scalar particles, the first of which with angular momentum  $(l, m) = (1, 1)$  and the other  $(l', -1)$ . We find that the only nonzero  $\mathcal{I}_{a4}$  and  $\mathcal{I}_{a5}$  are for  $l' = 1$  and  $l' = 3$ , as shown in Table 9.1.

The time evolution operator is

$$\hat{U}^{(e)} = \hat{T} \exp \left\{ -i \int_0^\infty dt \hat{H}_1^{(e)}(t) \right\}, \tag{9.6.15}$$

where  $\hat{T}$  is the time ordering operator. In the low downconversion regime [WLBR06], the time ordering is not important so that we can approximate the time evolution operator as

$$\hat{U}^{(e)} \approx \exp \left\{ -i \int_0^\infty dt \hat{H}_1^{(e)}(t) \right\}, \tag{9.6.16}$$

and the integration over  $t$  can be directly evaluated. we find

$$\begin{aligned}
\hat{U}^{(e)} &= \bigotimes_{lm} \bigotimes_{l'} \hat{U}_{lm'l'}^{(e)}, \\
\hat{U}_{lm'l'}^{(e)} &\approx \exp \left\{ -i \int d\omega \int d\omega' \left[ \mathcal{F}_{lm'l'}^{(e)}(\omega, \omega') \hat{a}_{\omega lm}^\dagger \hat{a}_{\omega' l', -m}^\dagger + \text{h.c.} \right] \right\}
\end{aligned} \tag{9.6.17}$$

where the joint frequency distribution is

$$\mathcal{F}_{lm'l'}^{(e)}(\omega, \omega') = \frac{4iM^3 A_{\omega l}^* A_{\omega' l'}^* C_{\omega_0 l_0}}{\sqrt{\Omega \Omega'} (1 - e^{2\pi \Omega_0})} \frac{1}{(i\Delta)^3} \left[ \Omega_0^2 \mathcal{I}_{a5} - \frac{\sqrt{D_0}}{\sqrt{2l_0(l_0+1)}} \Omega \Omega_0 \mathcal{I}_{a4} \right]. \tag{9.6.18}$$

It is evident that the joint frequency distribution  $\mathcal{F}_{lm'l'}^{(e)}(\omega, \omega')$  for coupling between the scalar field and the even-parity QNM is nonzero, showing that there would be scalar particle creation. Figs. 9.6 and 9.7 show an example of the joint frequency distribution.

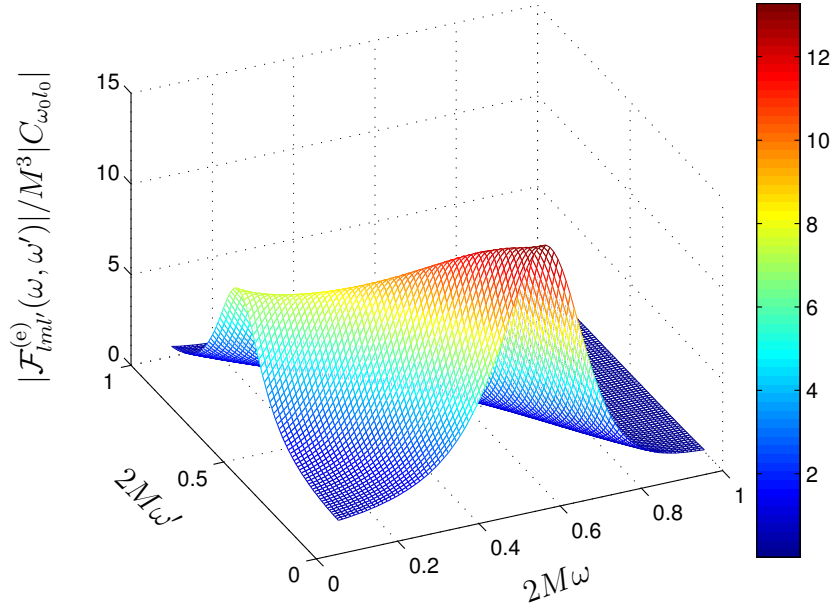


FIGURE 9.6: Modulus of the joint frequency distribution for even-parity QNMs. QNM:  $\Omega_R = 0.7474, \Omega_I = 0.178, (l_0, m_0) = (2, 0)$ . Scalar particle one:  $(l, m) = (1, 1)$ ; scalar particle two:  $(l', m') = (3, -1)$ .

## 9.7 Summary

In this chapter, we studied the coupling between the gravitational QNMs of a Schwarzschild black hole and a massless scalar field, and showed that scalar particles can be produced by the gravitational perturbations. This is contrary to the plane gravitational wave case where particle creation is forbidden due to the violation of momentum conservation. In the Schwarzschild black hole case, the total angular momentum of the QNMs and the pair of particles is conserved. In arriving at the above conclusion, we explicitly derived the interaction Hamiltonian for the scalar field which shows that the QNMs play the role as a multimode squeezer. The QNMs squeeze the initial state of the scalar field and produce particles. If the initial state of the scalar field is a vacuum state (Boulware vacuum), then

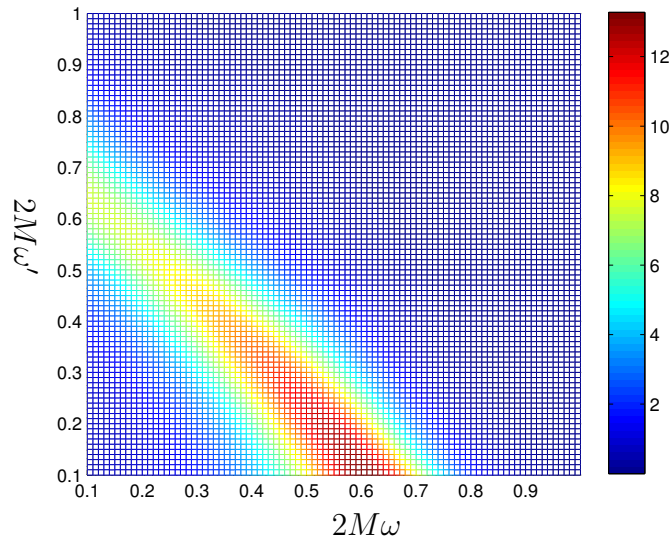


FIGURE 9.7: Density plot of the modulus of the joint frequency distribution for even-parity QNMs. QNM:  $\Omega_R = 0.7474, \Omega_I = 0.178, (l_0, m_0) = (2, 0)$ . Scalar particle one:  $(l, m) = (1, 1)$ ; scalar particle two:  $(l', m') = (3, -1)$ .

the final state is a squeezed vacuum state, indicating that the QNMs amplify the vacuum fluctuations and create particles. If initially there exists Hawking radiation, a thermal state with temperature proportional to the surface gravity of the black hole, the QNMs would squeeze the Hawking radiation and amplify it. A recent study [AK] shows that the Unruh radiation can be modulated by non-uniform acceleration, which implies, according to the equivalence principle, that the Hawking radiation could be modulated by infalling matters. In this chapter we explicitly show that the presence of gravitational perturbations results in coupling between different Hawking particles, and therefore may build correlations between them, modifying the thermal characteristic. In the realistic astrophysical situations, the temperature of the CMB is higher than the Hawking temperature, so it is expected that the amplification of the CMB around a black hole by the QNMs is more significant than the amplification of the Hawking radiation.

How significant the amplification is depends on the squeezing amplitude. We showed that the squeezing amplitude is proportional to the amplitude of the QNMs, which is reasonable because larger gravitational perturbations would create more particles. In addition, the maximal squeezing amplitude is proportional to the cube of the black hole mass and the real

part of the QNMs frequency, and is inversely proportional to the cube of the imaginary part of the QNMs frequency. This implies that for given amplitude of the QNMs a larger black hole would create more particles. Furthermore, the particle creation efficiency is higher for lower decaying QNMs. For Schwarzschild black holes, the damping of the QNMs is fast. The least damping mode has  $2M\omega_I = 0.178$ . For extreme Kerr black holes, there exists QNMs with very small damping rate, called Zero-Damping modes [YZZ<sup>+</sup>13]. We expect that our result is qualitatively correct for the Kerr black holes, which implies the particle creation by gravitational perturbations around an extreme Kerr black hole is much more efficient than Schwarzschild black holes. We leave this topic for future work.

## 9.8 Appendix

### 9.8.1 Appendix A: Radial integrals $\mathcal{I}_{r2}$ , $\mathcal{I}_{r3}$ and $\mathcal{I}_{r4}$

The evaluation of  $\mathcal{I}_{r2}$  is very similar to that of  $\mathcal{I}_{r1}$ . At spatial infinity ( $r \rightarrow \infty$ ), according to Eqs. (9.3.18) and (4.6.9), the integrand of  $\mathcal{I}_{r2}$  can be approximated as

$$\begin{aligned} & \frac{1}{r^2 f^2} \left[ (i\omega_0 r^2 - M) \frac{d}{dr_*} - \left( \frac{1}{2} \mu_0^2 f - i\omega_0(-3r + 7M) - \omega_0^2 r^2 \right) \right] {}_{-2}R_{\omega_0 l_0} \left( \frac{R_{\omega l}^*}{r} \right) \left( \frac{R_{\omega' l'}}{r} \right) \\ & \approx B_{\omega l}^* B_{\omega' l'}^* D_{\omega_0 l_0} \left[ \frac{3i\omega_0}{f} \left( 1 - \frac{1}{f} \right) + \frac{6iM\omega_0}{r f^2} - \frac{\mu_0^2}{2rf} - \frac{3M}{r^2 f} \right] e^{i(\omega_0 - \omega - \omega')r_*} \\ & \approx \frac{1}{2M} B_{\omega l}^* B_{\omega' l'}^* D_{\omega_0 l_0} \left[ 3i\Omega_0 x (x-1)^{-2+i\Delta} - \frac{1}{2} \mu_0^2 (x-1)^{-1+i\Delta} - \frac{3}{2} x^{-1} (x-1)^{-1+i\Delta} \right] e^{i\Delta x}. \end{aligned} \tag{9.8.1}$$

The dominant term is  $e^{i\Delta x}/x$  when  $x$  is large. Near the event horizon ( $r \rightarrow 2M$ ), according to Eqs. (9.3.18) and (4.6.9), the integrand of  $\mathcal{I}_{r2}$  can be approximated as

$$\begin{aligned} & \frac{1}{r^2 f^2} \left[ (i\omega_0 r^2 - M) \frac{d}{dr_*} - \left( \frac{1}{2} \mu_0^2 f - i\omega_0(-3r + 7M) - \omega_0^2 r^2 \right) \right] {}_{-2}R_{\omega_0 l_0} \left( \frac{R_{\omega l}^*}{r} \right) \left( \frac{R_{\omega' l'}}{r} \right) \\ & \approx A_{\omega l}^* A_{\omega' l'}^* C_{\omega_0 l_0} \left[ 2\omega_0^2 r^2 + i\omega_0 r + 4iM\omega_0 - \frac{1}{2} \mu_0^2 f - \frac{4M}{r} + \frac{4M^2}{r^2} \right] e^{-i(\omega_0 - \omega - \omega')r_*} \\ & \approx A_{\omega l}^* A_{\omega' l'}^* C_{\omega_0 l_0} \left[ (2\Omega_0^2 x^2 + i\Omega_0 x + 2i\Omega_0 - 2x^{-1} + x^{-2})(x-1)^{-i\Delta} - \frac{1}{2} \mu_0^2 x^{-1} (x-1)^{1-i\Delta} \right] \\ & \quad \times e^{-i\Delta x}. \end{aligned} \tag{9.8.2}$$

By using the same approximation that leads to Eq. (9.4.10), we obtain an approximate expression for the integrand of  $\mathcal{I}_{r2}$  along the whole contour  $C$ ,

$$\begin{aligned} & \frac{1}{r^2 f^2} \left[ (i\omega_0 r^2 - M) \frac{d}{dr_*} - \left( \frac{1}{2} \mu_0^2 f - i\omega_0(-3r + 7M) - \omega_0^2 r^2 \right) \right] {}_{-2}R_{\omega_0 l_0} \left( \frac{R_{\omega l}^*}{r} \right) \left( \frac{R_{\omega' l'}^*}{r} \right) \\ & \approx A_{\omega l}^* A_{\omega' l'}^* C_{\omega_0 l_0} \left[ (2\Omega_0^2 x^2 + i\Omega_0 x + 2i\Omega_0 - 2x^{-1} + x^{-2})(x-1)^{-i\Delta} - \frac{1}{2} \mu_0^2 x^{-1} (x-1)^{1-i\Delta} \right] \\ & \quad \times e^{i\Delta x}. \end{aligned} \quad (9.8.3)$$

We can see that in the *out* region along the contour  $C$ , the dominant term in Eq. (9.8.3) is  $x^2 e^{i\Delta x}$ , which is greater than the dominant term in Eq. (9.8.1),  $e^{i\Delta x}/x$ . However, these two terms are both exponentially suppressed so that their contribution to the total integration is small. We therefore expect that this approximation only introduces a small error. The main contribution to the integration comes from the *in* region where  $x$  is not large. In the limit of  $i\Delta \sim 0$ , which is the case that we are mostly interested in,  $e^{-i\Delta x} \approx e^{i\Delta x}$ . We therefore expect that Eq. (9.8.3) is a good approximation to Eq. (9.8.2) in the *in* region. Note that we replace an exponential growing function by an exponentially decaying function in the *in* region, the final result provides a lower bound for the exact radial integral  $\mathcal{I}_{r2}$ . Using Eq. (9.4.12) we have

$$\begin{aligned} \mathcal{I}_{r2} & \approx 4\pi M i \frac{A_{\omega l}^* A_{\omega' l'}^* C_{\omega_0 l_0} e^{i\Delta}}{1 - e^{2\pi\Omega_0}} \left\{ \frac{(-1)^{1-i\Delta}}{\Gamma(i\Delta)} \left[ 2\Omega_0^2 U(1-i\Delta, 4-i\Delta, -i\Delta) \right. \right. \\ & \quad \left. \left. + i\Omega_0 U(1-i\Delta, 3-i\Delta, -i\Delta) + 2i\Omega_0 U(1-i\Delta, 2-i\Delta, -i\Delta) + U(1-i\Delta, -i\Delta, -i\Delta) \right. \right. \\ & \quad \left. \left. - 2U(1-i\Delta, 1-i\Delta, -i\Delta) \right] - \frac{(-1)^{2-i\Delta}}{2\Gamma(-1+i\Delta)} \mu_0^2 U(2-i\Delta, 2-i\Delta, -i\Delta) \right\} \\ & \approx 4\pi M i \frac{A_{\omega l}^* A_{\omega' l'}^* C_{\omega_0 l_0} e^{i\Delta}}{1 - e^{2\pi\Omega_0}} \left\{ \frac{(i\Delta)^{i\Delta-1}}{\Gamma(i\Delta)} \left[ \frac{4\Omega_0^2}{(i\Delta)^2} - \frac{i\Omega_0 + 10\Omega_0^2}{i\Delta} + 8\Omega_0^2 + 4i\Omega_0 \right] \right. \\ & \quad \left. - \frac{(-1)^{1-i\Delta}}{\Gamma(i\Delta)} \left[ 2U(1-i\Delta, 1-i\Delta, -i\Delta) - U(1-i\Delta, -i\Delta, -i\Delta) \right] \right. \\ & \quad \left. - \frac{(-1)^{2-i\Delta}}{2\Gamma(-1+i\Delta)} \mu_0^2 U(2-i\Delta, 2-i\Delta, -i\Delta) \right\}. \end{aligned} \quad (9.8.4)$$

The dominant term in the limit of  $i\Delta \sim 0$  is

$$\mathcal{I}_{r2} \approx \frac{16\pi i M \Omega_0^2}{(i\Delta)^2} \frac{A_{\omega l}^* A_{\omega' l'}^* C_{\omega_0 l_0}}{1 - e^{2\pi\Omega_0}}. \quad (9.8.5)$$

At spatial infinity ( $r \rightarrow \infty$ ), the integrand of  $\mathcal{I}_{r3}$  can be approximated as

$$\frac{1}{f^2} {}_{-2}R_{\omega_0 l_0} \left( \frac{R_{\omega l}^*}{r} \right) \left( \frac{R_{\omega' l'}^*}{r} \right) \approx 2M B_{\omega l}^* B_{\omega' l'}^* D_{\omega_0 l_0} x^3 (x-1)^{-2+i\Delta} e^{i\Delta x}. \quad (9.8.6)$$

The dominant term is  $x e^{i\Delta x}$  when  $x$  is large. Near the event horizon ( $r \rightarrow 2M$ ), the the integrand of  $\mathcal{I}_{r3}$  can be approximated as

$$\frac{1}{f^2} {}_{-2}R_{\omega_0 l_0} \left( \frac{R_{\omega l}^*}{r} \right) \left( \frac{R_{\omega' l'}^*}{r} \right) \approx 4M^2 A_{\omega l}^* A_{\omega' l'}^* C_{\omega_0 l_0} x^2 (x-1)^{-i\Delta} e^{-i\Delta x}. \quad (9.8.7)$$

By using the same approximation as before, we obtain an approximate expression for the integrand of  $\mathcal{I}_{r3}$  along the whole contour  $C$ ,

$$\frac{1}{f^2} {}_{-2}R_{\omega_0 l_0} \left( \frac{R_{\omega l}^*}{r} \right) \left( \frac{R_{\omega' l'}^*}{r} \right) \approx 4M^2 A_{\omega l}^* A_{\omega' l'}^* C_{\omega_0 l_0} x^2 (x-1)^{-i\Delta} e^{i\Delta x}. \quad (9.8.8)$$

Using Eq. (9.4.12) we have

$$\begin{aligned} \mathcal{I}_{r3} &\approx -4\pi i \sqrt{D_0} M \Omega \Omega' \frac{A_{\omega l}^* A_{\omega' l'}^* C_{\omega_0 l_0} e^{i\Delta}}{1 - e^{2\pi\Omega_0}} \frac{(-1)^{1-i\Delta}}{\Gamma(i\Delta)} U(1-i\Delta, 4-i\Delta, -i\Delta) \\ &\approx -4\pi i \sqrt{D_0} M \Omega \Omega' \frac{A_{\omega l}^* A_{\omega' l'}^* C_{\omega_0 l_0} e^{i\Delta}}{1 - e^{2\pi\Omega_0}} \frac{(i\Delta)^{i\Delta-1}}{\Gamma(i\Delta)} \left[ 4 - \frac{5}{i\Delta} + \frac{2}{(i\Delta)^2} \right]. \end{aligned} \quad (9.8.9)$$

The dominant term in the limit of  $i\Delta \sim 0$  is

$$\mathcal{I}_{r3} \approx -\frac{8\pi i \sqrt{D_0} M \Omega \Omega' A_{\omega l}^* A_{\omega' l'}^* C_{\omega_0 l_0}}{(i\Delta)^2} \frac{1}{1 - e^{2\pi\Omega_0}}. \quad (9.8.10)$$

At spatial infinity ( $r \rightarrow \infty$ ), the integrand of  $\mathcal{I}_{r4}$  can be approximated as

$$\begin{aligned} {}_{-2}R_{\omega_0 l_0} \frac{d}{dr} \left( \frac{R_{\omega l}^*}{r} \right) \frac{d}{dr} \left( \frac{R_{\omega' l'}^*}{r} \right) &\approx \frac{1}{2M} B_{\omega l}^* B_{\omega' l'}^* D_{\omega_0 l_0} \left[ -\Omega \Omega' x^3 (x-1)^{-2} + x^{-1} \right. \\ &\quad \left. + i(\Omega + \Omega') x (x-1)^{-1} \right] (x-1)^{i\Delta} e^{i\Delta x}. \end{aligned} \quad (9.8.11)$$

Near the event horizon ( $r \rightarrow 2M$ ), the the integrand of  $\mathcal{I}_{r4}$  can be approximated as

$$\begin{aligned} {}_{-2}R_{\omega_0 l_0} \frac{d}{dr} \left( \frac{R_{\omega l}^*}{r} \right) \frac{d}{dr} \left( \frac{R_{\omega' l'}^*}{r} \right) &\approx -A_{\omega l}^* A_{\omega' l'}^* C_{\omega_0 l_0} \left[ \Omega \Omega' x^2 + i(\Omega + \Omega') (x-1) \right. \\ &\quad \left. - x^{-2} (x-1)^2 \right] (x-1)^{-i\Delta} e^{-i\Delta x}. \end{aligned} \quad (9.8.12)$$

By analytically extending Eqs. (9.8.11) and (9.8.12) to the complex  $r$  plane and using the same approximation as before, we obtain an approximate expression for the integrand of  $\mathcal{I}_{r3}$

along the whole contour  $C$ ,

$$\begin{aligned}
-2R_{\omega_0 l_0} \frac{d}{dr} \left( \frac{R_{\omega l}^*}{r} \right) \frac{d}{dr} \left( \frac{R_{\omega' l'}}{r} \right) &\approx -A_{\omega l}^* A_{\omega' l'}^* C_{\omega_0 l_0} [\Omega \Omega' x^2 + i(\Omega + \Omega')(x - 1) \\
&\quad - x^{-2}(x - 1)^2] (x - 1)^{-i\Delta} e^{i\Delta x}. \tag{9.8.13}
\end{aligned}$$

Using Eq. (9.4.12) we have

$$\begin{aligned}
\mathcal{I}_{r4} &\approx 4\pi M i \sqrt{D_0} \frac{A_{\omega l}^* A_{\omega' l'}^* C_{\omega_0 l_0} e^{i\Delta}}{1 - e^{2\pi\Omega_0}} \left\{ \frac{(-1)^{1-i\Delta}}{\Gamma(i\Delta)} \Omega \Omega' U(1 - i\Delta, 4 - i\Delta, -i\Delta) \right. \\
&\quad \left. + \frac{(-1)^{2-i\Delta}}{\Gamma(-1 + i\Delta)} i(\Omega + \Omega') U(2 - i\Delta, 2 - i\Delta, -i\Delta) - \frac{(-1)^{3-i\Delta}}{\Gamma(-2 + i\Delta)} U(3 - i\Delta, 2 - i\Delta, -i\Delta) \right\} \\
&\approx 4\pi M i \sqrt{D_0} \frac{A_{\omega l}^* A_{\omega' l'}^* C_{\omega_0 l_0} e^{i\Delta}}{1 - e^{2\pi\Omega_0}} \left\{ \frac{(i\Delta)^{i\Delta-1}}{\Gamma(i\Delta)} \Omega \Omega' \left[ 4 - \frac{5}{i\Delta} + \frac{2}{(i\Delta)^2} \right] \right. \\
&\quad \left. + \frac{(-1)^{2-i\Delta}}{\Gamma(-1 + i\Delta)} i(\Omega + \Omega') U(2 - i\Delta, 2 - i\Delta, -i\Delta) - \frac{(-1)^{3-i\Delta}}{\Gamma(-2 + i\Delta)} U(3 - i\Delta, 2 - i\Delta, -i\Delta) \right\}. \tag{9.8.14}
\end{aligned}$$

The dominant term in the limit of  $i\Delta \sim 0$  is

$$\mathcal{I}_{r4} \approx \frac{8\pi i \sqrt{D_0} M \Omega \Omega' A_{\omega l}^* A_{\omega' l'}^* C_{\omega_0 l_0}}{(i\Delta)^2 (1 - e^{2\pi\Omega_0})}. \tag{9.8.15}$$

## 9.8.2 Appendix B: Spin-weighted spherical harmonics

If we define two differential operators  $\hat{S}_{\pm}$  as

$$\hat{S}_{\pm} \equiv - \left( \frac{\partial}{\partial \theta} \pm \frac{i}{\sin \theta} \frac{\partial}{\partial \phi} \right), \tag{9.8.16}$$

then the action of  $\bar{\partial}$  (spin-raising operator) and  $\bar{\partial}$  (spin-lowering operator) on  $\eta$ , which is a quantity of spin weight  $s$ , can be written as

$$\begin{aligned}
\bar{\partial} \eta &= \hat{S}_+ \eta + s \cot \theta \eta, \\
\bar{\partial} \eta &= \hat{S}_+ \eta - s \cot \theta \eta. \tag{9.8.17}
\end{aligned}$$

According to the definition of the spin-weighted spherical harmonics (9.4.17), we find for  $s = \pm 1$

$${}_{\pm 1} Y_{lm} = \pm \sqrt{\frac{(l-1)!}{(l+1)!}} \hat{S}_{\pm} Y_{lm} \tag{9.8.18}$$

and for  $s = \pm 2$

$$\begin{aligned} {}_{\pm 2}Y_{lm} &= \sqrt{\frac{(l-2)!}{(l+2)!}} (\hat{S}_{\pm}^2 + \cot \theta \hat{S}_{\pm}) Y_{lm} \\ &= \sqrt{\frac{(l-2)!}{(l+2)!}} \left[ \partial_{\theta}^2 - \cot \theta \partial_{\theta} \pm \frac{2i}{\sin \theta} (\partial_{\theta} - \cot \theta) \partial_{\phi} - \frac{1}{\sin^2 \theta} \partial_{\phi}^2 \right] Y_{lm} \end{aligned} \quad (9.8.19)$$

since  $Y_{lm}$  is of spin-weight 0. Taking into account the definition of the spherical harmonics,

$$Y_{lm}(\theta, \phi) = (-1)^m \sqrt{\frac{(2l+1)(l-m)!}{4\pi(l+m)!}} P_l^m(\cos \theta) e^{im\phi},$$

and the recurrence relation for the associated Legendre function

$$\partial_{\theta} P_l^m = \frac{1}{2} [P_l^{m+1} - (l+m)(l-m+1)P_l^{m-1}],$$

we obtain the explicit expressions for the  $s = \pm 1, \pm 2$  spin-weighted spherical harmonics in terms of Legendre function,

$${}_{\pm 1}Y_{lm} = \frac{1}{2} (-1)^m \sqrt{\frac{2l+1}{4\pi} \frac{(l-1)!(l-m)!}{(l+1)!(l+m)!}} \left( \mp P_l^{m+1} \pm c_{lm}^2 P_l^{m-1} + \frac{2m}{\sin \theta} P_l^m \right) e^{im\phi}, \quad (9.8.20)$$

$$\begin{aligned} {}_{\pm 2}Y_{lm} &= \frac{1}{4} (-1)^m \sqrt{\frac{2l+1}{4\pi} \frac{(l-2)!(l-m)!}{(l+2)!(l+m)!}} \left[ P_l^{m+2} + c_{lm}^2 c_{l,m-1}^2 P_l^{m-2} - 2 \left( \cot \theta \pm \frac{2m}{\sin \theta} \right) P_l^{m+1} \right. \\ &\quad \left. + 2 \left( \cot \theta \pm \frac{2m}{\sin \theta} \right) c_{lm}^2 P_l^{m-1} + \left( -c_{lm}^2 - c_{l,m+1}^2 + \frac{4m^2}{\sin^2 \theta} \pm \frac{8m \cot \theta}{\sin \theta} \right) P_l^m \right] e^{im\phi}, \end{aligned} \quad (9.8.21)$$

where  $c_{lm} = \sqrt{(l+m)(l-m+1)}$ .

### 9.8.3 Appendix C: Integrals of the products of three Legendre Functions

We need the overlap integrals of three associated Legendre functions in order to finish the angular integrals,

$$\mathcal{I}_{P_3}(l_1, m_1; l_2, m_2; l_3, m_3) \equiv \int_{-1}^1 d\mu P_{l_1}^{m_1}(\mu) P_{l_2}^{m_2}(\mu) P_{l_3}^{m_3}(\mu). \quad (9.8.22)$$

This was done by Mavromatis and Alassar [MA99], albeit with a phase error in their result. Dong and Lemus [DL02] restudied the problem and found an expression for  $\mathcal{I}_{P_3}$  with positive  $m_1, m_2$  and  $m_3$ . Here we correct the phase error in [MA99] and give an expression that is valid for all values of  $m_1, m_2$  and  $m_3$ .

$$\begin{aligned}
& \mathcal{I}_{P_3}(l_1, m_1; l_2, m_2; l_3, m_3) \\
= & \frac{(|\Delta m|)! (-1)^{m_1+m_2+\min\{m_1+m_2, m_3\}}}{2^{|\Delta m|+2} \Gamma(|\Delta m|) K_{l_1 m_1} K_{l_2 m_2} K_{l_3 m_3}} \sum_L \sum_{L'} (2L+1)(2L'+1) \\
& \times \begin{pmatrix} l_1 & l_2 & L \\ 0 & 0 & 0 \end{pmatrix} \begin{pmatrix} l_1 & l_2 & L \\ m_1 & m_2 & -m_1 - m_2 \end{pmatrix} \begin{pmatrix} L & l_3 & L' \\ 0 & 0 & 0 \end{pmatrix} \begin{pmatrix} L & l_3 & L' \\ -m_1 - m_2 & m_3 & -\Delta m \end{pmatrix} \\
& \times \frac{[1 + (-1)^{L'+|\Delta m|}] \Gamma(L'/2) \Gamma((L' - |\Delta m| + 1)/2)}{K_{L', |\Delta m|} \Gamma((L' + |\Delta m| + 2)/2) \Gamma((L' + 3)/2)}, \tag{9.8.23}
\end{aligned}$$

where we have defined  $\Delta m = m_3 - m_1 - m_2$ ,  $K_{lm} = \sqrt{(l-m)!/(l+m)!}$ .  $\min\{a, b\}$  represents the minimal value of  $a$  and  $b$ ,  $|l_1 - l_2| \leq L \leq l_1 + l_2$  and  $|L - l_3| \leq L' \leq L + l_3$ .



# 10

## Conclusion and Future Outlook

### 10.1 Summary

In this thesis, we investigated how relativistic quantum field effects help to realize quantum information tasks, and how concepts and techniques in quantum information science help to deepen our understanding of quantum effects in non-inertial frames and gravitational fields. The main results are summarized as follows.

#### 10.1.1 Spacetime diamonds

We showed that the state of a massless field confined within a finite spacetime diamond is a thermal state in the Minkowski vacuum, with temperature inversely proportional to the size of the diamond. An Unruh-DeWitt detector with appropriate energy scaling responds to

this thermal state. We further studied time-like entanglement between fields within different diamonds. It is expected that entanglement exists between various diamonds in order that the composite state is pure. We found that the entanglement is dominant between adjacent diamonds and decays when two diamonds move apart.

### 10.1.2 Quantum communication with accelerated observers

We studied two types of quantum communication with a uniformly accelerated observer: the sender is an inertial observer and another accelerated observer, respectively. In both cases, the sender prepare a small coherent state as signal and a large coherent state as local oscillator, the accelerated receiver performs homodyne detection using the local oscillator they detect. In the case where the sender is inertial, we find that under some special conditions the accelerated observer cannot detect substantial low frequency particles regardless of his proper acceleration, in contrast with the general viewpoint that the accelerated observer sees large amounts of low frequency particles if their acceleration is large. We also show that the Unruh frequency provides a natural low frequency cutoff both for quantum limited classical communication and quantum communication between the inertial observer and uniformly accelerated observer. In the case where the sender is another uniformly accelerated observer, we explicitly calculated the normalized output signal and the normalized variance in the high central frequency and narrow bandwidth limit. It is surprising that they are almost the same as in the case where the sender is inertial. We thus conclude that the output of the homodyne detection as performed by an accelerated observer does not strongly depend on the motion of the senders. Instead, it reflects the unique properties of the horizon of the receiver.

### 10.1.3 Quantum circuit model for uniformly accelerated objects

We constructed a non-perturbative quantum circuit model to describe the interactions between uniformly accelerated objects and quantum fields. We first considered time independent interactions in the accelerated frame, for which a circuit can be drawn for every single frequency Rindler mode. As a first application of the circuit model, the radiation flux from an accelerated mirror was calculated. We found that a pulse of particles is located around

the past horizon and the radiation field is locally squeezed. The local squeezing found here is related to cutting the correlations across the past horizon.

We then generalized the circuit model for time independent interactions to a circuit model for time dependent interactions. The time dependent interactions are realized by making the accelerated objects only act on a localized wave packet mode. By using this more general circuit, we studied the output field from an accelerated single-mode squeezer, given that the initial state is the Minkowski vacuum. Unexpectedly, we found that the output state of the field as observed by inertial observers is mixed, although the input state is pure. The decoherence effect we describe here is a previously unnoticed consequence of the transformation from the bipartite Hilbert space of the Rindler and Unruh modes, to the single Hilbert space of the Minkowski modes. Because of the equivalence principle there is a strong relationship between gravity and acceleration. Our finding may indicate a new direction for understanding the black hole information paradox.

#### 10.1.4 Squeezed black holes

We studied the coupling between the gravitational perturbations, QNMs, of a Schwarzschild black hole and a massless scalar field, and showed that scalar particles can be produced by the gravitational QNMs. The gravitational QNMs play the role as a multimode squeezer, squeezing any initial state of the scalar field and creating scalar particles. How significant the particle creation effect is depends on the squeezing amplitude. We showed that the squeezing amplitude is proportional to the amplitude of the QNMs, which is reasonable because larger gravitational perturbations would create more particles. In addition, the maximal squeezing amplitude is proportional to the cube of the black hole mass and the real part of the QNMs frequency, and is inversely proportional to the cube of the imaginary part of the QNMs frequency.

## 10.2 Future work and outlook

Several further studies based on works in this thesis are summarized in the following.

### 10.2.1 Spacetime diamonds

We have derived the Bogoliubov transformations between the diamond modes and the Minkowski modes in  $(1 + 1)$ -dimensional spacetime. Future work would be to derive the similar Bogoliubov transformations in  $(1 + 3)$ -dimensional spacetime, although we are confident that the result is the same by looking at the response of an energy scaled Unruh-deWitt detector in  $(1 + 3)$ -dimensional spacetime. The more important and challenging future work is to explore how to conceive a detector with appropriate energy scaling so that we can detect the diamond temperature and extract the time-like or space-like entanglement. At microwave frequencies, the artificial absorbers such as superconducting qubits [ZKSS10, ZSK<sup>+</sup>11] are possible. At optical frequencies, standard techniques such as electro-optic or acousto-optic modulation are also possible but could be very challenging.

### 10.2.2 Quantum communication with accelerated observers

For the quantum communication between two accelerated observers, we derived general expressions for the normalized output signal and the variance, and discussed a special case where the central frequency is high and the bandwidth is narrow. A thorough numerical investigation for other cases could be useful. By comparing the results of such an investigation with that of an inertial sender, we could have a more convincing conclusion that whether the normalized output signal and the variance are independent of the motion of the sender.

Due to the strong relation between acceleration and gravity, it is interesting to generalize this type of quantum communication protocols to the black hole horizon case. For example, one can consider a scenario where a freely falling observer (inertial) sends a coherent signal and local oscillator to a stationary observer (accelerated) outside the black hole, who then performs homodyne detection. These kinds of studies may tell us some unique properties of

the black hole horizon.

### 10.2.3 Quantum circuit model for uniformly accelerated objects

We have considered a uniformly accelerated single-mode squeezer that only acts on left-moving modes. It is interesting to study a uniformly accelerated two-mode squeezer that couples both the left-moving and right-moving modes. The two-mode squeezer produces entanglement between the left-moving and right-moving Rindler modes. In the perspective of the inertial observers, the entanglement between the left-moving and right-moving fields may disappear. If this is the case, the accelerated motion can also induce decoherence of entanglement.

The second future work is to generalize these calculations to the black hole case. Due to the strong relationship between acceleration and gravity, it is expected the decoherence effect also happens if the Hawking thermal radiation is squeezed. Results from Chapter 9 show that the gravitational perturbations, QNMs, around a black hole play the role as a multimode squeezer. So the presence of gravitational perturbations around a black hole would induce decoherence of the state, as well as entanglement, as observed by a freely falling observer.

### 10.2.4 Squeezed black holes

A number of future directions could be explored in relation to particle production from gravitational waves around a black hole. First could be to input some appropriate values for various parameters to estimate how many particles can be produced by the ring down that has been observed by LIGO. Other than the ring down stage, the inspiral and merger stages can also produce particles although this calculation is beyond the scope of our current work. In fact, the particle number from the ring down stage provides only a lower bound (could be a very small fraction) for the total particle number from the coalescence of two black holes. For the first LIGO event, the gravitational waves carried away energy of about three solar masses. It would be interesting to see how much of this energy would have been converted into photons (modelled by massless scalar particles) and whether these photons

can be detected.

The second work to do is to consider QNMs of Kerr black holes. There exists very slow damping QNMs for the extreme Kerr black holes [YZZ<sup>+</sup>13]. The nonlinear coupling between these slow damping QNMs can produce gravitational turbulence [YZL15]. We have shown that the squeezing amplitude is inversely proportional to the cube of the damping rate of the QNMs of Schwarzschild black holes. It is reasonable to expect that this result may be qualitatively correct for the QNMs of Kerr black holes. It is thus necessary to find the exact relation between the squeezing amplitude and the damping rate of the Kerr black hole QNMs. If our expectation is correct, we then would have a very efficient particle creation mechanism.

The most interesting future work is to study the effects of quantized metric perturbations on quantum fields. Effort has been expended to relate the spectrum of QNMs to the quantization of the area of the black hole event horizon [Mag08]. Up to now, the QNMs are treated classically and represent classical metric perturbations to the black holes. The metric perturbations can also result in perturbations to the event horizon [ABB<sup>+</sup>95, CPS09]. We can quantize the QNMs to obtain a quantum theory describing the interactions between the quantum fields and the quantized metric fluctuations [TS10], or the quantized fluctuations of event horizon. When the black hole emits a Hawking particle, the event horizon is no longer stationary and some quantum fluctuations are induced. When quantum fluctuations of the event horizon interact with other Hawking particles, correlations between different Hawking particles can be built up. It is important to study this mechanism of building correlations within Hawking particles, since it may help to understand the black hole information paradox and ultimately provide clues for the final form of a theory of quantum gravity.

## References

- [AAF10] M. Aspachs, G. Adesso, and I. Fuentes. Optimal quantum estimation of the Unruh-Hawking effect. *Phys. Rev. Lett.*, 105:151301, 2010.
- [ABB<sup>+</sup>95] P. Anninos, D. Bernstein, S. Brandt, J. Libson, J. Masso, E. Seidel, L. Smarr, W. Suen, and P. Walker. Dynamics of apparent and event horizons. *Phys. Rev. Lett.*, 74:630, 1995.
- [ABS<sup>+</sup>14] M. Ahmadi, D. E. Bruschi, C. Sabin, G. Adesso, and I. Fuentes. Relativistic quantum metrology: Exploiting relativity to improve quantum measurement technologies. *Sci. Rep.*, 4(4996), 2014.
- [AFSMT06] P. M. Alsing, I. Fuentes-Schuller, R. B. Mann, and T. E. Tessier. Entanglement of Dirac fields in noninertial frames. *Phys. Rev. A*, 74:032326, 2006.
- [AK] A. Ahmadzadegan and A. Kempf. Strong Transient Modulation of Horizon Radiation. *arXiv:1702.00472*.
- [AM03] P. M. Alsing and G. J. Milburn. Teleportation with a uniformly accelerated partner. *Phys. Rev. Lett.*, 91:180404, 2003.
- [AMPS13] A. Almheiri, D. Marolf, J. Polchinski, and J. Scully. Black holes: complementarity or firewalls? *J. High Energy Phys.*, 02:062, 2013.
- [AS72] M. Abramowitz and I. A. Stegun. *Handbook of Mathematical Functions with Formulas, Graphs and Mathematical Tables*. Dover, New York, 1972.

- [BB84] C. H. Bennett and G. Brassard. Quantum cryptography: public key distribution and coin tossing. *Proceeding of IEEE International Conference on Computers Systems and Signal Processing*, 1984.
- [BBC<sup>+</sup>93] C. H. Bennett, G. Brassard, C. Crepeau, R. Jozsa, A. Peres, and W. K. Wootters. Teleporting an unknown quantum state via dual classical and Einstein-Podolsky-Rosen channels. *Phys. Rev. Lett.*, 70:1895, 1993.
- [BCS09] E. Berti, V. Cardoso, and A. O. Starinets. Quasinormal modes of black holes and black branes. *Class. Quantum Grav.*, 26:163001, 2009.
- [BD82] N. D. Birrell and P. C. W. Davies. *Quantum fields in curved space*. Cambridge University Press, 1982.
- [BDU<sup>+</sup>14] D. E. Bruschi, A. Datta, R. Ursin, T. C. Ralph, and I. Fuentes. Quantum estimation of the Schwarzschild spacetime parameters of the earth. *Phys. Rev. D*, 90:124001, 2014.
- [BFL12] D. E. Bruschi, I. Fuentes, and J. Louko. Voyage to alpha centauri: Entanglement degradation of cavity modes due to motion. *Phys. Rev. D*, 85:061701(R), 2012.
- [BFSS06] J. L. Ball, I. Fuentes-Schuller, and F. P. Schuller. Entanglement in an expanding spacetime. *Phys. Lett. A*, 359:550, 2006.
- [Bir23] G. D. Birkhoff. *Relativity and Modern Physics*. Cambridge, Massachusetts: Harvard University Press, 1923.
- [BK72] G. F. Belinfante and B. Kolman. *A Survey of Lie Groups and Lie Algebras with Applications and Computational Methods*. SIAM, Philadelphia, 1972.
- [BKC<sup>+</sup>06] A. Belyanin, V. V. Kocharovskiy, F. Capasso, E. Fry, M. S. Zubairy, and M. O. Scully. Quantum Electrodynamics of accelerated atoms in free space and in cavities. *Phys. Rev. A*, 74:023807, 2006.

- [BL83] J. S. Bell and J. M. Leinaas. Electrons as accelerated thermometers. *Nucl. Phys. B*, 212:131, 1983.
- [BL15] E. Brown and J. Louko. Smooth and sharp creation of a Dirichlet wall in 1+1 quantum field theory: how singular is the sharp creation limit? *J. High Energy Phys.*, 08:061, 2015.
- [BLPS90] K. J. Blow, R. Loudon, S. J. D. Phoenix, and T. J. Shepherd. Continuum fields in quantum optics. *Phys. Rev. A*, 42:4102, 1990.
- [BMT] V. Baccetti, R. B. Mann, and D. R. Terno. Role of evaporation in gravitational collapse. *arXiv:1610.07839*.
- [Bou75] D. G. Boulware. Quantum field theory in Schwarzschild and Rindler space. *Phys. Rev. D*, 11:1404, 1975.
- [BP73] J. M. Bardeen and W. H. Press. Radiation fields in the Schwarzschild background. *J. Math. Phys.*, 14:7, 1973.
- [BP13] S. L. Braunstein and S. Pirandola. Better late than never: Information retrieval from black holes. *Phys. Rev. Lett.*, 110:101301, 2013.
- [BR04] H. A. Bachor and T. C. Ralph. *A Guide to Experiments in Quantum Optics*. Wiley-VCH, Weinheim, 2004.
- [BW92] C. H. Bennett and S. J. Wiesner. Communication via one- and two-particle operators on Einstein-Podolsky-Rosen states. *Phys. Rev. Lett.*, 69:2881, 1992.
- [Car04] S. M. Carroll. *Spacetime and Geometry: An introduction to general relativity*. Addison Wesley, 2004.
- [CF77] S. M. Christensen and S. A. Fulling. Trace anomalies and the Hawking effect. *Phys. Rev. D*, 15:2088, 1977.
- [CGH<sup>+</sup>96] R. M. Corless, G. H. Gonnet, D. E. G. Hare, D. J. Jeffrey, and D. E. Knuth. On the Lambert W function. *Advances in Computational Mathematics*, 5:329–359, 1996.

- [CH74] B. J. Carr and S. W. Hawking. Black holes in the early universe. *Mon. Not. Roy. Astro. Soc.*, 168:399, 1974.
- [CHM08] L. C. B. Crispino, A. Higuchi, and G. E. A. Matsas. The Unruh effect and its application. *Rev. Mod. Phys.*, 80:787, 2008.
- [Chr75] P. L. Chrzanowski. Vector potential and metric perturbations of a rotating black hole. *Phys. Rev. D*, 11:2042, 1975.
- [CK74] J. M. Cohen and L. S. Kegeles. Electromagnetic fields in curved spaces: A constructive procedure. *Phys. Rev. D*, 10:1070, 1974.
- [Col73] S. R. Coleman. There are no Goldstone bosons in two dimensions. *Commun. Math. Phys.*, 31:259–264, 1973.
- [CP48] H. B. G. Casimir and D. Polder. The influence of retardation on the London-van der Waals forces. *Phys. Rev.*, 73:360, 1948.
- [CPS09] M. I. Cohen, H. P. Pfeiffer, and M. A. Scheel. Revisiting event horizon finders. *Class. Quantum Grav.*, 26:035005, 2009.
- [CR94] A. Connes and C. Rovelli. Von Neumann algebra automorphisms and time-thermodynamics relation in generally covariant quantum theories. *Class. Quantum Grav.*, 11:2899–2917, 1994.
- [CT99] P. Chen and T. Tajima. Testing Unruh radiation with ultraintense lasers. *Phys. Rev. Lett.*, 83:256, 1999.
- [CW87] R. D. Carlitz and R. S. Willey. Reflections on moving mirrors. *Phys. Rev. D*, 36:2327, 1987.
- [Dat09] A. Datta. Quantum discord between relatively accelerated observers. *Phys. Rev. A*, 80:052304, 2009.
- [Dav75] P. C. W. Davies. Scalar production in Schwarzschild and Rindler metrics. *J. Phys. A*, 8:609, 1975.

- [DDMM13] A. Dragan, J. Doukas, and E. Martin-Martinez. Localized detection of quantum entanglement through the event horizon. *Phys. Rev. A*, 87:052326, 2013.
- [DDMMB13] A. Dragan, J. Doukas, E. Martin-Martinez, and D. E. Bruschi. Localized projective measurement of a quantum field in non-inertial frames. *Class. Quantum Grav.*, 30:235006, 2013.
- [Des75] S. Deser. Plane waves do not polarize the vacuum. *J. Phys. A: Math. Gen.*, 8:1972, 1975.
- [DeW79] B. S. DeWitt. *General Relativity: An Einstein Centenary Survey*. Cambridge University Press, Cambridge, England, 1979.
- [DF77] P. C. W. Davies and S. A. Fulling. Radiation from moving mirrors and from black holes. *Proc. R. Soc. Lond. A*, 356:237–257, 1977.
- [DFR11] T. G. Downes, I. Fuentes, and T. C. Ralph. Entangling moving cavities in noninertial frames. *Phys. Rev. Lett.*, 106:210502, 2011.
- [Dir27] P. A. Dirac. The quantum theory of the emission and absorption of radiation. *Proc. R. Soc. London, Ser. A*, 114:243, 1927.
- [DL02] S. Dong and R. Lemus. The overlap integral of three associated Legendre polynomials. *Appl. Math. Lett.*, 15:541, 2002.
- [DRW13] T. G. Downes, T. C. Ralph, and N. Walk. Quantum communication with an accelerated partner. *Phys. Rev. A*, 87:012327, 2013.
- [ea16a] B. P. Abbott et al. Gw151226: Observation of gravitational waves from a 22-solar-mass binary black hole coalescence. *Phys. Rev. Lett.*, 116:241103, 2016.
- [ea16b] B. P. Abbott et al. Observation of gravitational waves from a binary black hole merger. *Phys. Rev. Lett.*, 116:061102, 2016.

- [Ein05] A. Einstein. On the electrodynamics of moving bodies. *Ann. Phys. Leipz.*, 17:891, 1905.
- [Eke91] A. K. Ekert. Quantum cryptography based on Bell's theorem. *Phys. Rev. Lett.*, 67:661, 1991.
- [FD76] S. A. Fulling and P. C. W. Davies. Radiation from a moving mirror in two dimensional space-time: conformal anomaly. *Proc. R. Soc. Lond. A*, 348:393–414, 1976.
- [FLT<sup>+</sup>13] N. Friis, A. R. Lee, K. Troung, C. Sabin, E. Solano, G. Johansson, and I. Fuentes. Relativistic quantum teleportation with superconducting circuits. *Phys. Rev. Lett.*, 110:113602, 2013.
- [FM<sup>+</sup>10] I. Fuentes, R. B. Mann, E. Martin-Martinez, and S. Moradi. Entanglement of Dirac fields in an expanding spacetime. *Phys. Rev. D*, 82:045030, 2010.
- [FS79] V. P. Frolov and E. M. Serebriany. Quantum effects in systems with accelerated mirrors. *J. Phys. A: Math. Gen.*, 12:3205, 1979.
- [FS80] V. P. Frolov and E. M. Serebriany. Quantum effects in systems with accelerated mirrors. II. electromagnetic field. *J. Phys. A: Math. Gen.*, 13:3205, 1980.
- [FS99] V. P. Frolov and D. Singh. Quantum effects in the presence of expanding semi-transparent spherical mirrors. *Class. Quantum Grav.*, 16:3693, 1999.
- [FSM05] I. Fuentes-Schuller and R. B. Mann. Alice falls into a black hole: entanglement in noninertial frames. *Phys. Rev. Lett.*, 95:120404, 2005.
- [Ful73] S. A. Fulling. Nonuniqueness of canonical field quantization in Riemannian space-time. *Phys. Rev. D*, 7:2850, 1973.
- [Gib75] G. W. Gibbons. Quantized field propagating in plane-wave spacetimes. *Commun. Math. Phys.*, 45:191, 1975.

- [GLM04] V. Giovannetti, S. Lloyd, and L. Maccone. Quantum-enhanced measurements: Beating the standard quantum limit. *Science*, 306:1330, 2004.
- [GLM06] V. Giovannetti, S. Lloyd, and L. Maccone. Quantum metrology. *Phys. Rev. Lett.*, 96:010401, 2006.
- [GMN<sup>+</sup>67] J. N. Goldberg, A. J. Macfarlane, E. T. Newman, F. Rohrlich, and E. C. G. Sudarshan. Spin-s Spherical Harmonics and  $\delta$ . *J. Math. Phys.*, 8:2155, 1967.
- [Gol65] H. Goldstein. *Classical Mechanics*. Pearson Education India, 1965.
- [GRKD17] P. T. Grochowski, G. Rajchel, F. Kialka, and A. Dragan. Effect of relativistic acceleration on continuous variable quantum teleportation and dense coding. *Phys. Rev. D*, 95:105005, 2017.
- [Gro86] P. G. Grove. On the detection of particle and energy fluxes in two dimensions. *Class. Quantum Grav.*, 3:793, 1986.
- [GV91] J. Garriga and E. Verdaguer. Scattering of quantum particles by gravitational plane waves. *Phys. Rev. D*, 43:391, 1991.
- [Haa12] R. Haag. *Local quantum physics: Fields, particles, algebras*. Springer Science and Business Media, 2012.
- [Har03] J. B. Hartle. *Gravity: An Introduction to Einstein's General Relativity*. San Francisco: Addison-Wesley, 2003.
- [Haw75] S. W. Hawking. Particle creation by black holes. *J. Math. Phys.*, 43:199, 1975.
- [Haw76] S. W. Hawking. Breakdown of predictability in gravitational collapse. *Phys. Rev. D*, 14:2460, 1976.
- [HE73] S. W. Hawking and G. F. R. Ellis. *The Large Scale Structure of Space-Time*. Cambridge: Cambridge University Press, 1973.

- [HH76] J. B. Hartle and S. W. Hawking. Path-integral derivation of black-hole radiance. *Phys. Rev. D*, 13:2188, 1976.
- [HLO14] L. Hodgkinson, J. Louko, and A. C. Ottewill. Static detectors and circular-geodesic detectors on the Schwarzschild black hole. *Phys. Rev. D*, 89:104002, 2014.
- [Hol98] A. S. Holevo. The capacity of the quantum channel with general signal states. *IEEE Transactions on Information Theory*, 44:269–273, 1998.
- [HP07] P. Hayden and J. Preskill. Black holes as mirrors: quantum information in random subsystems. *J. High Energy Phys.*, 09:120, 2007.
- [HPS16] S. W. Hawking, M. J. Perry, and A. Strominger. Soft hair on black holes. *Phys. Rev. Lett.*, 116:231301, 2016.
- [HSU15] M. Hotta, R. Schutzhold, and W. G. Unruh. Partner particles for moving mirror radiation and black hole evaporation. *Phys. Rev. D*, 91:124060, 2015.
- [Hub06] J. H. Hubbell. Electron-positron pair production by photons: a historical overview. *Radiation Physics and Chemistry*, 75:614, 2006.
- [IOS13] D. Ida, T. Okamoto, and M. Saito. Modular theory for operator algebra in a bounded region of space-time and quantum entanglement. *Prog. Theor. Exp. Phys.*, 083E03, 2013.
- [IZ06] C. Itzykson and J. B. Zuber. *Quantum field theory*. Courier Corporation, 2006.
- [Jac75] J. D. Jackson. *Electrodynamics*. Wiley-VCH Verlag GmbH and Co. KGaA, 1975.
- [JMMK15] R. H. Jonsson, E. Martin-Martinez, and A. Kempf. Information transmission without energy exchange. *Phys. Rev. Lett.*, 114:110505, 2015.
- [Kay15] B. S. Kay. Instability of enclosed horizons. *Gen. Relativ. Gravit.*, 47:31, 2015.

- [KC79] L. S. Kegeles and J. M. Cohen. Constructive procedure for perturbations of spacetimes. *Phys. Rev. D*, 19:1641, 1979.
- [KL16] B. S. Kay and U. Lupo. Non-existence of isometry-invariant Hadamard states for a Kruskal black hole in a box and for massless fields on  $1 + 1$  Minkowski spacetime with a uniformly accelerating mirror. *Class. Quantum Grav.*, 33:215001, 2016.
- [KMN<sup>+</sup>07] P. Kok, W. J. Munro, K. Nemoto, T. C. Ralph, J. P. Dowling, and G. J. Milburn. Linear optical quantum computing with photonic qubits. *Rev. Mod. Phys.*, 79:135, 2007.
- [KR16] S. P. Kish and T. C. Ralph. Estimating spacetime parameters with a quantum probe in a lossy environment. *Phys. Rev. D*, 93:105013, 2016.
- [KS99] K. D. Kokkotas and B. G. Schmidt. Quasi-normal modes of stars and black holes. *Living Review in Relativity*, 2:2, 1999.
- [KZ11] R. A. Konoplya and A. Zhidenko. Quasinormal modes of black holes: From astrophysics to string theory. *Rev. Mod. Phys.*, 83:793, 2011.
- [Lea85] E. W. Leaver. An analytic representation for the quasinormal modes of Kerr black holes. *Proc. R. Soc. Lond. A*, 402:285, 1985.
- [Lea86] E. W. Leaver. Spectral decomposition of the perturbation response of the Schwarzschild geometry. *Phys. Rev. D*, 34:384, 1986.
- [Lee86] T. D. Lee. Are black holes black bodies? *Nucl. Phys.*, B264:437, 1986.
- [Leh01] L. Lehner. Numerical relativity: a review. *Class. Quantum Grav.*, 18:R25, 2001.
- [LH10] S. Y. Lin and B. L. Hu. Entanglement creation between two causally disconnected objects. *Phys. Rev. D*, 81:045019, 2010.

- [Llo97] S. Lloyd. Capacity of the noisy quantum channel. *Phys. Rev. A*, 55:1613, 1997.
- [LM99] J. Louko and D. Marolf. Single-exterior black holes and the ADS-CFT conjecture. *Phys. Rev. D*, 59:066002, 1999.
- [Lou14] J. Louko. Unruh-DeWitt detector response across a Rindler firewall is finite. *J. High Energy Phys.*, 09:141, 2014.
- [LPHH13] P. Lahteenmaki, G. S. Paraoanu, J. Hassel, and P. J. Hakonen. Dynamical Casimir effect in a Josephson metamaterial. *Proc. Natl. Acad. Sci. U.S.A.*, 110:4234, 2013.
- [LR09] A. I. Lvovsky and M. G. Raymer. Continuous-variable optical quantum-state tomography. *Rev. Mod. Phys.*, 81:299, 2009.
- [LW02] C. O. Lousto and B. F. Whiting. Reconstruction of black hole metric perturbations from the Weyl curvature. *Phys. Rev. D*, 66:024026, 2002.
- [MA99] H. A. Mavromatis and R. S. Alassar. A generalized formula for the integral of three associated Legendre polynomials. *Appl. Math. Lett.*, 12:101, 1999.
- [Mag08] M. Maggiore. Physical interpretation of the spectrum of black hole quasinormal modes. *Phys. Rev. Lett.*, 100:141301, 2008.
- [Mat05] S. D. Mathur. The fuzzball proposal for black holes: an elementary review. *Fortschr. Phys.*, 53:793, 2005.
- [MBF14] M. Ahmadi, D. E. Bruschi, and I. Fuentes. Quantum metrology for relativistic quantum fields. *Phys. Rev. D*, 89:065028, 2014.
- [MF53] P. M. Morse and H. Feshbach. *Methods of Theoretical Physics*. McGraw-Hill, New York, 1953.
- [MFB92] V. F. Mukhanov, H. A. Feldman, and R. H. Brandenberger. Theory of cosmological perturbations. *Phys. Rep.*, 215:203, 1992.

- [Mil72] W. Miller. *Symmetry Groups and Their Applications*. Academic, New York, 1972.
- [Mis72] C. W. Misner. Interpretation of gravitational-wave observations. *Phys. Rev. Lett.*, 28:994, 1972.
- [MMGL10] E. Martin-Martinez, L. J. Garay, and J. Leon. Unveiling quantum entanglement degradation near a Schwarzschild black hole. *Phys. Rev. D*, 82:064006, 2010.
- [MML15] E. Martin-Martinez and J. Louko. (1+1) D calculation provides evidence that quantum entanglement survives a firewall. *Phys. Rev. Lett.*, 115:031301, 2015.
- [MMM12] E. Martin-Martinez and N. C. Menicucci. Cosmological quantum entanglement. *Class. Quantum Grav.*, 29:224003, 2012.
- [Moo70] G. T. Moore. Quantum theory of the electromagnetic field in a variable-length one-dimensional cavity. *J. Math. Phys.*, 11:2679, 1970.
- [MP96] S. Massar and R. Parentani. From vacuum fluctuations to radiation. I. accelerated detectors. *Phys. Rev. D*, 54:7426, 1996.
- [MP05] K. Martel and E. Poisson. Gravitational perturbations of the Schwarzschild spacetime: A practical covariant and gauge-invariant formalism. *Phys. Rev. D*, 71:104003, 2005.
- [MR03] P. Martinetti and C. Rovelli. Diamond’s temperature: Unruh effect for bounded trajectories and thermal time hypothesis. *Class. Quantum Grav.*, 20(4919-4931), 2003.
- [MS98] J. Maldacena and A. Strominger.  $AD\text{S}_3$  black holes and a stringy exclusion principle. *J. High Energy Phys.*, 9812:005, 1998.
- [MS06] S. Massar and P. Spindel. Einstein-Podolsky-Rosen correlations between two uniformly accelerated oscillators. *Phys. Rev. D*, 74:085031, 2006.

- [MTW73] C. W. Misner, K. Thorne, and J. A. Wheeler. *Gravitation*. Freeman, San Francisco, 1973.
- [NC00] M. A. Nielsen and I. L. Chuang. *Quantum Computation and Quantum Information*. Cambridge University Press India, 2000.
- [NIS] *NIST Digital Library of Mathematical Functions*, <http://dlmf.nist.gov>.
- [Nol99] H. P. Nollert. Quasinormal modes: the characteristic 'sound' of black holes and neutron stars. *Class. Quantum Grav.*, 16:R159, 1999.
- [NP62] E. Newman and R. Penrose. An approach to gravitational radiation by a method of spin coefficients. *J. Math. Phys.*, 3:566, 1962.
- [NZC<sup>+</sup>12] D. A. Nichols, A. Zimmerman, Y. Chen, G. Lovelace, K. D. Matthews, R. Owen, F. Zhang, and K. S. Thorne. Visualizing spacetime curvature via frame-drag vortexes and tidal tendexes. III. quasinormal pulsations of Schwarzschild and Kerr black holes. *Phys. Rev. D*, 86:104028, 2012.
- [OP01] N. Obadia and R. Parentani. Notes on moving mirrors. *Phys. Rev. D*, 64:044019, 2001.
- [OP03a] N. Obadia and R. Parentani. Uniformly accelerated mirrors. I. mean fluxes. *Phys. Rev. D*, 67:024021, 2003.
- [OP03b] N. Obadia and R. Parentani. Uniformly accelerated mirrors. II. quantum correlations. *Phys. Rev. D*, 67:024022, 2003.
- [OR11] S. J. Olson and Timothy C. Ralph. Entanglement between the future and he past in the quantum vacuum. *Phys. Rev. Lett.*, 106:110404, 2011.
- [OR12] S. J. Olson and T. C. Ralph. Extraction of timelike entanglement from the quantum vacuum. *Phys. Rev. A*, 85:012306, 2012.
- [Ori03] A. Ori. Reconstruction of inhomogeneous metric perturbations and electromagnetic four-potential in Kerr spacetime. *Phys. Rev. D*, 67:124010, 2003.

- [OV39] J. R. Oppenheimer and G. M. Volkoff. On massive neutron cores. *Phys. Rev.*, 55:374, 1939.
- [Pag76] D. N. Page. Particle emission rates from a black hole: Massless particles from an uncharged, nonrotating hole. *Phys. Rev. D*, 13:198, 1976.
- [Par68] L. Parker. Particle creation in expanding universes. *Phys. Rev. Lett.*, 21:562, 1968.
- [Par75] L. Parker. Probability distribution of particles created by a black hole. *Phys. Rev. D*, 12:1519, 1975.
- [PJ08] Q. Pan and J. Jing. Hawking radiation, entanglement, and teleportation in the background of an asymptotically flat static black hole. *Phys. Rev. D*, 78:065015, 2008.
- [Pre98] J. Preskill. *Lecture notes for physics 229: Quantum information and computation*. California Institute of Technology, 1998.
- [Pri72] R. H. Price. Nonspherical perturbations of relativistic gravitational collapse. II. integer-spin, zero-rest-mass fields. *Phys. Rev. D*, 5:2439, 1972.
- [PS95] M. E. Peskin and D. V. Schroeder. *An Introduction to Quantum Field Theory*. Addison-Wesley, New York, 1995.
- [PT73] W. H. Press and S. A. Teukolsky. Perturbations of a rotating black hole. II. dynamical stability of the Kerr metric. *Astrophys. J.*, 185:649, 1973.
- [PT04] A. Peres and D. R. Terno. Quantum information and relativity. *Rev. Mod. Phys.*, 76:93, 2004.
- [PT09] L. Parker and D. Toms. *Quantum field theory in curved spacetime: quantized fields and gravity*. Cambridge University Press, 2009.
- [RCR05] A. Retzker, J. I. Cirac, and B. Reznik. Detecting vacuum entanglement in a linear ion trap. *Phys. Rev. Lett.*, 94:050504, 2005.

- [RL98] T. C. Ralph and P. K. Lam. Teleportation with bright squeezed light. *Phys. Rev. Lett.*, 81:5668, 1998.
- [Rog88] J. Rogers. Detector for the temperaturelike effect of acceleration. *Phys. Rev. Lett.*, 61:2113, 1988.
- [RRS05] B. Reznik, A. Retzker, and J. Silman. Violating Bell’s inequalities in vacuum. *Phys. Rev. A*, 71:042104, 2005.
- [RW57] T. Regge and J. A. Wheeler. Stability of a Schwarzschild singularity. *Phys. Rev.*, 108:1063, 1957.
- [RW15] T. C. Ralph and N. Walk. Quantum key distribution without sending a quantum signal. *New Journal of Physics*, 17:063008, 2015.
- [Sak85] J. J. Sakurai. *Modern Quantum Mechanics*. Addison-Wesley, Redwood City, CA, 1985.
- [Sch16] K. Schwarzschild. On the gravitational field of a mass point according to Einstein’s theory. *Sitzungsber. Preuss. Akad. Wiss. Berlin (Math. Phys.)*, 7:189–196, 1916.
- [Sch51] J. Schwinger. On gauge invariance and vacuum polarization. *Phys. Rev.*, 82:664, 1951.
- [Sch95] B. Schumacher. Quantum coding. *Phys. Rev. A*, 51:2738, 1995.
- [SHMR17a] D. Su, C. T. M. Ho, R. B. Mann, and T. C. Ralph. Black hole squeezers. *Phys. Rev. D*, accepted for publication, 2017.
- [SHMR17b] D. Su, C. T. M. Ho, R. B. Mann, and T. C. Ralph. Quantum circuit model for non-inertial objects: a uniformly accelerated mirror. *New Journal of Physics*, 19:063017, 2017.
- [Sho94] P. W. Shor. Algorithms for quantum computations: discrete logarithms and factoring. *Proceedings of the 35th Annual Symposium on Foundations of Computer Science*, pages 124–134, 1994.

- [Sho95] P. W. Shor. Scheme for reducing decoherence in quantum computer memory. *Phys. Rev. A*, 52:R2493(R), 1995.
- [SKB<sup>+</sup>03] M. O. Scully, V. V. Kocharovsky, A. Belyanin, E. Fry, and F. Capasso. Enhancing acceleration radiation from ground-state atoms via cavity quantum Electrodynamics. *Phys. Rev. Lett.*, 91:243004, 2003.
- [SM09] G. V. Steeg and N. C. Menicucci. Entangling power of an expanding universe. *Phys. Rev. D*, 79:044027, 2009.
- [SMM15] G. Salton, R. B. Mann, and N. Menicucci. Acceleration-assisted entanglement harvesting and rangefinding. *New Journal of Physics*, 17:035001, 2015.
- [Sor00] F. Sorge. Do gravitational waves create particles? *Class. Quantum Grav.*, 17:4655, 2000.
- [SP88] Yonghe Sun and Richard H. Price. Excitation of quasinormal ringing of a Schwarzschild black hole. *Phys. Rev. D*, 38:1040, 1988.
- [SPdRMM12] C. Sabin, B. Peropadre, M. del Rey, and E. Martin-Martinez. Extracting past-future vacuum correlations using circuit QED. *Phys. Rev. Lett.*, 109:033602, 2012.
- [SR14] D. Su and T. C. Ralph. Quantum communication in the presence of a horizon. *Phys. Rev. D*, 90:084022, 2014.
- [SR16] D. Su and T. C. Ralph. Spacetime diamonds. *Phys. Rev. D*, 93:044023, 2016.
- [SSH06] R. Schutzhold, G. Schaller, and D. Habs. Signatures of the Unruh effect from electrons accelerated by ultrastrong laser fields. *Phys. Rev. Lett.*, 97:121302, 2006.
- [Ste16] J. Steinhauer. Observation of quantum Hawking radiation and its entanglement in an analogue black hole. *Nat. Phys.*, 12:959, 2016.

- [StHW94] C. R. Stephens, G. 't Hooft, and B. F. Whiting. Black hole evaporation without information loss. *Class. Quantum Grav.*, 11:621, 1994.
- [STU93] L. Susskind, L. Thorlacius, and J. Uglum. The stretched horizon and black hole complementarity. *Phys. Rev. D*, 48:3743, 1993.
- [Sus16] L. Susskind. ER = EPR, GHZ, and the consistency of quantum measurements. *Fortschr. Phys.*, 64:72–83, 2016.
- [SW85a] B. F. Schutz and C. M. Will. Black hole normal modes: a semianalytic approach. *Astrophys. J. Lett.*, 291:L33, 1985.
- [SW85b] S. J. Summers and R. Werner. The vacuum violates Bell's inequalities. *Phys. Lett. A*, 110:257, 1985.
- [SW87] S. J. Summers and R. Werner. Bell's inequalities and quantum field theory. II. Bell's inequalities are maximally violated in the vacuum. *J. Math. Phys.*, 28:2448, 1987.
- [SW97] B. Schumacher and M. D. Westmoreland. Sending classical information via noisy quantum channels. *Phys. Rev. A*, 56:131, 1997.
- [SZ97] M. O. Scully and M. S. Zubairy. *Quantum Optics*. Cambridge University Press, 1997.
- [Tak86] S. Takagi. Vacuum noise and stress induced by uniform acceleration: Hawking-Unruh effect in Rindler manifold of arbitrary dimension. *Prog. Theor. Phys.*, 88:1–142, 1986.
- [Teu72] S. A. Teukolsky. Rotating black holes: Separable wave equations for gravitational and electromagnetic perturbations. *Phys. Rev. Lett.*, 29:1114, 1972.
- [Teu73] S. A. Teukolsky. Perturbations of a rotating black hole. I. fundamental equations for gravitational, electromagnetic, and neutrino-field perturbations. *Astrophys. J.*, 185:635, 1973.

- [Tol39] R. C. Tolman. Static solution of Einstein's field equations for spheres of fluid. *Phys. Rev.*, 55:364, 1939.
- [TP74] S. A. Teukolsky and W. H. Press. Perturbations of a rotating black hole. III - interaction of the hole with gravitational and electromagnetic radiation. *Astrophys. J.*, 193:443, 1974.
- [Tru85] D. R. Truax. Baker-Cambell-Hausdorff relations and unitary of  $SU(2)$  and  $SU(1,1)$  squeeze operator. *Phys. Rev. D*, 31:1988, 1985.
- [TS10] T. Takahashi and J. Soda. Hawking radiation from fluctuating black holes. *Class. Quantum Grav.*, 27:175008, 2010.
- [Tsv95] A. M. Tsvelik. *Quantum Field Theory in Condensed Matter Physics*. Cambridge University Press, 1995.
- [Unr74] W. G. Unruh. Second quantization in the Kerr metric. *Phys. Rev. D*, 10:3194, 1974.
- [Unr76] W. G. Unruh. Notes on black-hole evaporation. *Phys. Rev. D*, 14:870, 1976.
- [Unr92] W. G. Unruh. Thermal bath and decoherence of Rindler spacetimes. *Phys. Rev. D*, 46:3271, 1992.
- [UW84] W. G. Unruh and R. M. Wald. What happens when an accelerating observer detects a Rindler particle. *Phys. Rev. D*, 29:1047, 1984.
- [Wal75] R. M. Wald. On particle creation by black holes. *Commun. Math. Phys.*, 45:9–34, 1975.
- [Wal85] W. R. Walker. Particle and energy creation by moving mirrors. *Phys. Rev. D*, 31:767, 1985.
- [Wal94] R. M. Wald. *Quantum field theory in curved spacetime and black hole thermodynamics*. University of Chicago Press, 1994.

- [Wei72] S. Weinberg. *Gravitation and Cosmology: principles and applications of the general theory of relativity*. New York: Willy, 1972.
- [Wei95] S. Weinberg. *The quantum theory of fields*. Cambridge University Press, 1995.
- [Wil93] F. Wilczek. Quantum purity at a small price: Easing a black hole paradox. *arXiv:hep-th/9302096*, 1993.
- [WJP<sup>+</sup>11] C. M. Wilson, G. Johansson, A. Pourkabirian, M. Simoen, J. R. Johansson, T. Duty, F. Nori, and P. Delsing. Observation of the dynamical Casimir effect in a superconducting circuit. *Nature (London)*, 479:376, 2011.
- [WLBR06] W. Wasilewski, A. I. Lvovsky, K. Banaszek, and C. Radzewicz. Pulsed squeezed light: Simultaneous squeezing of multiple modes. *Phys. Rev. A*, 73:063819, 2006.
- [WM07] D. F. Walls and G. J. Milburn. *Quantum Optics*. Springer Science and Business Media, 2007.
- [WND96] J. G. Williams, X. X. Newhall, and J. O. Dickey. Relativity parameters determined from lunar laser ranging. *Phys. Rev. D*, 53:6730, 1996.
- [WPGP<sup>+</sup>12] C. Weedbrook, S. Pirandola, R. Garcia-Patron, N. J. Cerf, T. C. Ralph, J. H. Shapiro, and S. Lloyd. Gaussian quantum information. *Rev. Mod. Phys.*, 84:621, 2012.
- [YG06] N. Yunes and J. Gonzalez. Metric of a tidally perturbed spinning black hole. *Phys. Rev. D*, 73:024010, 2006.
- [YZL15] H. Yang, A. Zimmerman, and L. Lehner. Turbulent black holes. *Phys. Rev. Lett.*, 114:081101, 2015.
- [YZZ<sup>+</sup>13] H. Yang, A. Zimmerman, A. Zenginoglu, F. Zhang, E. Berti, and Y. Chen. Quasinormal modes of nearly extremal Kerr spacetimes: Spectrum bifurcation and power-law ringdown. *Phys. Rev. D*, 88:044047, 2013.

- 
- [Zee10] A. Zee. *Quantum field theory in a nutshell*. Princeton university press, 2010.
- [Zel72] I. A. B. Zel'dovich. Amplification of cylindrical electromagnetic waves reflected from a rotating body. *Soviet Physics-JETP*, 35:1085, 1972.
- [Zer70] F. J. Zerilli. Gravitational field of a particle falling in a Schwarzschild geometry analyzed in tensor harmonics. *Phys. Rev. D*, 2:2141, 1970.
- [ZKSS10] X. Zhu, A. Kemp, S. Saito, and K. Semba. Coherent operation of a gap-tunable flux qubit. *Appl. Phys. Lett.*, 97:102503, 2010.
- [ZSK<sup>+</sup>11] X. Zhu, S. Saito, A. Kemp, K. Kakuyanagi, S. Karimoto, H. Nakano, W. J. Munro, Y. Tokura, M. S. Everitt, K. Nemoto, M. Kasu, N. Mizuochi, and K. Semba. Coherent coupling of a superconducting flux qubit to an electron spin ensemble in diamond. *Nature*, 478:221, 2011.